THE ROLE OF A HIGHLY CONSERVED MAJOR FACILITATOR SUPERFAMILY MEMBER IN *DROSOPHILA* EMBRYONIC MACROPHAGE INVASION

by

Katarína Valošková

June, 2019

A thesis presented to the
Graduate School
of the
Institute of Science and Technology Austria, Klosterneuburg, Austria
in partial fulfillment of the requirements
for the degree of
Doctor of Philosophy

The dissertation of Katarína Valošková, titled The role of a highly conserved major facilitator superfamily member in *Drosophila* embryonic macrophage migration, is approved by:

Supervisor: Daria Siekhaus, IST Austria, Klosterneuburg, Austria

Signature: _____

Committee Member: Michael Sixt, IST Austria, Klosterneuburg, Austria

Signature: _____

Committee Member: Katja Brückner, University of California San Francisco, San Francisco, USA

Signature: _____

Exam Chair: Jiří Friml, IST Austria, Klosterneuburg, Austria

Signature: _____

Signed page is on the file

IST Austria Thesis, ISSN:2663-337X

I hereby declare that this dissertation is my own work and that it does not contain other people's work without this being so stated; this thesis does not contain my previous work without this being stated, and the bibliography contains all the literature that I used in writing the dissertation.

I declare that this is a true copy of my thesis, including any final revisions, as approved by my thesis committee, and that this thesis has not been submitted for a higher degree to any other university or institution.

I certify that any republication of materials presented in this thesis has been approved by the relevant publishers and co-authors.

Signature: _____

Katarína Valošková

June 7, 2019

Signed page is on the file

Abstract

Invasive migration plays a crucial role not only during development and homeostasis but also in pathological states, such as tumor metastasis. *Drosophila* macrophage migration into the extended germband is an interesting system to study invasive migration. It carries similarities to immune cell transmigration and cancer cell invasion, therefore studying this process could also bring new understanding of invasion in higher organisms. In our work, we uncover a highly conserved member of the major facilitator family that plays a role in tissue invasion through regulation of glycosylation on a subgroup of proteins and/or by aiding the precise timing of DN-Cadherin downregulation.

Aberrant display of the truncated core1 O-glycan T-antigen is a common feature of human cancer cells that correlates with metastasis. Here we show that T-antigen in *Drosophila melanogaster* macrophages is involved in their developmentally programmed tissue invasion. Higher macrophage T-antigen levels require an atypical major facilitator superfamily (MFS) member that we named Minerva which enables macrophage dissemination and invasion. We characterize for the first time the T and Tn glycoform O-glycoproteome of the *Drosophila melanogaster* embryo, and determine that Minerva increases the presence of T-antigen on proteins in pathways previously linked to cancer, most strongly on the sulfhydryl oxidase Qsox1 which we show is required for macrophage tissue entry. Minerva's vertebrate ortholog, MFSD1, rescues the *minerva* mutant's migration and T-antigen glycosylation defects. We thus identify a key conserved regulator that orchestrates O-glycosylation on a protein subset to activate a program governing migration steps important for both development and cancer metastasis.

Acknowledgments

First of all, I would like to thank to my supervisor Daria Siekhaus for giving me opportunity to work in her group on this project and for support and mentoring I was getting from her in last years. I would like to thank as well to all current and former members of Siekhaus group who created good and supportive working environment, starting with people who are co-authors of the work in Chapter 3. Mainly, I would like to thank my colleague Julia Biebl for her not only scientific support and creative research ideas she has shared.

I would like to also thank to my committee members Michael Sixt and Katja Brückner who, although being quite geographically distant and/or having high work load, always found time to meet and discuss my results, gave me useful advices and asked important questions. My acknowledgement also belongs to our collaborators, Henrik Clausen, Sergey Y. Vakhrushev and Ida S.B. Larsen for data discussion as well as to members of our bioimaging facility who provided not only support during data acquisition but also in the process of analysis.

Last, but not least, I would like to thank to my family, mainly to my husband, for their endless support, understanding and patience during my whole study.

This work was supported by DOC fellowship from Austrian Academy of Science.

About the Author

Katarína Valošková completed a BSc in Biology and an MSc in Genetics at the Comenius University in Bratislava, Slovakia, before joining IST Austria in September 2012 and Siekhaus group in spring 2013. Her main research interests include regulation of cell migration and the role of glycosylation in it. Katarína received DOC fellowship in 2014. During her PhD studies, she has presented her research results in the EMBO workshop “Glycosylation in the Golgi complex” in Vico Equense 2016 and in Joint Meeting of German and Israeli Societies of Developmental Biology, Vienna, 2019. Katarína is a first co-author on the paper “A conserved major facilitator superfamily member orchestrates a subset of O-glycosylation to aid macrophage tissue invasion” published in eLife.

List of Publications Appearing in Thesis

1. Gyoergy, A., Roblek, M., Ratheesh, A., Valoskova, K., Belyaeva, V., Wachner, S., Matsubayashi, Y., Sánchez-Sánchez, B.J., Stramer, B., and Siekhaus, D.E. (2018). Tools Allowing Independent Visualization and Genetic Manipulation of *Drosophila* melanogaster Macrophages and Surrounding Tissues. G3 (Bethesda). *8*, 845–857.
2. Valoskova, K.*, Biebl, J.*, Roblek M., Emtenani S., Gyoergy A., Misova M., Ratheesh A., Reis-Rodrigues, P., Shkarina K., Larsen, I.S.B., Vakhrushev S.Y., Clausen, H., Siekhaus, D.E. (2019). A conserved major facilitator superfamily member orchestrates a subset of O-glycosylation to aid macrophage tissue invasion. eLife. *8. pii:* e41801.

* these authors contributed equally

Table of Contents

List of Figures

List of Tables

List of Symbols/Abbreviations

BDGP	Berkeley *Drosophila* Genome Project
BLAST	Basic Local Alignment Search Tool
BMP	bone morphogenetic protein
BPA	*Bauhinia purpurea* agglutinin
C1GalT	Core 1 Galactosyltransferase
CAT	collective to ameboid transition
Cnx99A	Calnexin 99A
Col4a1	Collagen type IV alpha 1
ConA	Concanavalin A
Cwo	Clock-work orange
DBA	*Dolichos biflorus* agglutinin
DE-Cad	*Drosophila* E-Cadherin
Dhc64C	Dynein heavy chain 64C
DN-Cad	*Drosophila* E-Cadherin
Dp1	Dodeca-satellite binding protein 1
DPiM	*Drosophila* Protein Interaction Map
Dpp	Decapentaplegic
Dtg	Dpp target gene
ECM	extracellular matrix
EGF	Epidermal growth factor
EMT	epithelial to mesenchymal transition
ER	endoplasmatic reticulum
Frc	Fringe connection
Fuc	fucose
Gal	galactose
GalNAc	N-acetylgalactosamine
GCM	Glial cells missing
GFP	green fluorescent protein
Glc	glucose
GlcA	glucuronic acid
GlcAT	glucuronyltransferase
GlcNAc	N-acetylglucosamine
GMAP	Golgi microtubule-associated protein
GP210	Glycoprotein 210 kDa
GS-I	*Griffonia simplicifolia* agglutinin I
GS-II	*Griffonia simplicifolia* agglutinin II
HA	hemagglutinin
HPA	*Helix pomatia* agglutinin
If	Inflated
ItgaPS	Integrin alpha PS
Itgbn	Integrin betanu subunit
Lan	Laminin

LPA	*Limulus polyphenus* agglutinin
Man	mannose
MAT	mesenchymal to ameboid transition
Mew	Multiple edematous wings
MFS	major facilitator superfamily
MFSD1	Major facilitator superfamily domain containing 1
mmMFSD1	*mus musculus* MFSD1
MPA	Maclura pomifera agglutinin
Mrva	Minerva
MT	metallothionein
Mys	myospheroid
Ndg	Nidogen
Qsox1	Quiescin sulfhydryl oxidase 1
PNA	peanut agglutinin
ppGalNAcT	Polypeptide α-N-acetylgalactosaminyltransferase
PVR	PDGF- and VEGF-receptor related
RNA	ribonucleic acid
RNAi	RNA interference
SBA	Soybean agglutinin
Scb	Scab
Ser	serine
Shot	Short stop
Thr	threonine
Trol	Terribly reduced optic lobes
UDP	uridine-5'-diphosphate
UEA-I	*Ulex europaeus* agglutinin
Ush	U-shaped
VDRC	Vienna *Drosophila* Resource Center
Vkg	Viking
vnc	ventral nerve cord
Wb	Wingblister
WB	western blot
WGA	wheat germ agglutinin
Xyl	xylose

Chapter 1: Introduction

Regulation of cell migration by glycosylation and adhesion to the components of extracellular matrix (ECM)

Cell migration is crucial for many physiological processes such as organismal development, tissue homeostasis, wound healing or inflammation but at the same time it plays a critical role in cancer metastasis. Therefore, gaining as deep understanding as is possible of this dynamic and very adaptive process has been a top of priority of many researchers. In this introduction, I will try to summarize the basics of the current knowledge of the regulation of directed cell migration with a focus on migration modes that are relevant for the later described project: namely the invasive migration of metastatic cells and immune cell transmigration, glycosylation as a regulator of (invasive) migration and the role of the ECM and adhesion to it.

To migrate persistently and in directed manner in response to an external stimulus, a migrating cell requires an internal program to generate forces in a specific direction to move the cell forward (Mak et al., 2016). The classical image that is based mainly on *in vitro* studies with cells plated on 2D substrates describes actin-driven protrusions at the front and myosin-driven detachment at the rear (Lauffenburger and Horwitz, 1996). A combination of protrusions and firm adhesions at the cell front and contractions and detachment at the rear makes the cell to move forward (Mak et al., 2016). Protrusions are driven by the polymerization of actin filaments, namely the addition of monomeric G actin at the barbed end of F actin. This is activated mainly by Cdc42 and Rac1 signaling at the leading edge by nucleation promoting factors like Wasp/Wave and Arp2/3 (Kraynov et al., 2000; Ma et al., 1998; Machesky and Insall, 1998; Mak et al., 2016; Mullins et al., 1998; Pankov et al., 2005). At the rear of the cell, RhoA activates contractile forces from myosin II motors that in combination with the turnover of old adhesions lead to forward movement (Mak et al., 2016). However, in 3D migration, many components may be altered as well as their interaction and the exact mechanism is context dependent (Petrie and Yamada, 2016).

Regulation of transmigration of immune cells

Getting to the site of inflammation is a key process of high importance for the organism. At the same time, the whole process has to be tightly regulated to prevent prolonged or incorrectly localized inflammation and the associated pathology. In this part, I will shortly describe the transmigration of immune cells and compare them with our model system, hemocyte invasion into the extended germband.

Getting to the site of inflammation actually consists of a sequence of adhesive steps in which leukocytes:

1. attach to the vessel wall
2. locomote along the wall to the endothelial borders
3. traverse the endothelium and the subendothelial basement membrane
4. migrate through the interstitial tissue (Muller, 2013).

Transendothelial migration mainly happens at the boundaries between endothelial cells and therefore is called paracellular transmigration. Later, a more rare migration through the endothelial cellular body, so called transcellular migration, was discovered (Carman and Springer, 2008).

Leukocytes passively move in the blood stream so the first step is to capture them. To do so, contact with the blood vessel has to occur which is enhanced by a local decrease in blood streaming at the site of inflammation (Muller, 2013). Inflammatory reactions induce the release of pathogen-associated molecular pattern from microorganism or damage-associated molecular patterns from injured tissue cells. These stimulate resident components of the innate immune system and result in the secretion of cytokines that activate nearby endothelial cells (Vestweber, 2015). Therefore endothelial Ca^{2+}-dependent lectins, P- and E-selectins, are induced on the surface of endothelial cells (McEver, 2015). Selectins bind sialylated fucosylated carbohydrate residues of the Lewis x blood group family (Muller, 2013).

The subsequent process, associated with a high on and off binding rate of selectins, is called rolling, resulting in a slowing down of the immune cell movement or so called 'slow rolling' (Muller, 2013) that is mediated by E-selectin (Kunkel and Ley, 1996). This process allows further activation of leukocytes by chemokines and other proinflammatory agents on the surface of endothelial cells (Muller, 2013). Chemokines through their receptors activate leukocyte adhesion receptors – integrins (more details on integrin structure and function, see later) in so called 'inside-out' integrin activation (Ginsberg, 2014).

Activated integrins bind to a member of the immunoglobulin superfamily – ICAM1 and VCAM1- on endothelial cells which leads to the next step, arrest followed up by crawling (Dustin and Springer, 1988; Muller, 2013) in search for a nearby endothelial cell border. Binding of a leukocyte to ICAM1 and VCAM1 causes tyrosine dephosphorylation in the cytoplasmic domain of the VE-Cadherin and therefore allows opening of endothelial junctions (Shaw et al., 2001; Vestweber, 2015).

While previous steps are reversible, the commitment to the next step means no return (Muller, 2013). The whole process is regulated by a big set of receptors expressed on the surface of endothelial cells, and in the case of the more common paracellular migration, on endothelial cell contacts: JAMA-C, ESAM, PECAM1, ICAM2, CD99, PVR (Nasdala et al., 2002; Schenkel et al., 2002; Vestweber, 2015; Woodfin et al., 2011, 2009). Diapedesis itself is a sequential process (Schenkel et al., 2002), consisting of the following steps: luminal association with endothelial cells apically of endothelial cell junctions (ICAM2), engagement between junctions (JAMA), accumulation between endothelial cells and the basement membrane (PECAM1 and CD99). (Vestweber, 2015)

Once the basal side of the endothelial cell is reached, leukocytes have to dissociate and cross the basement membrane. This process is not so deeply studied as previous steps. Neutrophils and monocytes migrate through areas in the basement membrane of the least resistance - where collagen IV and laminin 10 are expressed at relatively low density. (Muller, 2013; Voisin et al., 2009; Wang et al., 2006).

In our model system, no blood stream occurs, therefore the first steps are different as hemocytes need to delaminate from head mesoderm rather than being captured from the flow. Based on BLAST analysis, there are no known P- and E-selectins in *Drosophila* genome. However, the following up processes carry some similarities to above described transendothelial migration:

1. The involvement of integrins – hemocyte migration into the extended germband is also integrin-dependent process (Siekhaus et al., 2010)
2. TNF signaling – as TNF signaling is one of the signals for extravasation, the tissue where hemocytes enter is also 'getting ready' for their entrance thanks to TNF signaling (Ratheesh et al., 2018a)
3. Interaction with ECM - although *Drosophila* stage 11/12 embryos do not have formed basement membrane (Matsubayashi et al., 2017), hemocytes have to interact with ECM components that are already deposited on their path (Ratheesh et al., 2018a; Sánchez-Sánchez et al., 2017) as well as they deposit it on their own (Fessler and Fessler, 1989; Matsubayashi et al., 2017; Ratheesh et al., 2018a). As it is shown also in this work, this ECM components actually influence their migration.

Properties and regulation of metastasis

Metastasis is a very complex, diverse and inefficient process. It is a multistep process that involves:

1. Local infiltration of tumor cells into the surrounding tissue
2. Transendothelial migration into the vessels
3. Survival in circulatory system
4. Extravasation
5. Proliferation in the competent organ leading to colonization (van Zijl et al., 2011)

Metastases account for the majority of cancer deaths (Chambers et al., 2002), therefore they are potential therapeutic target. In this part of the introduction, I will shortly described the initial step(s) of metastasis – on the invasion of tumor cells in its surroundings as it might be similar to our model system.

Metastasis is a very diverse process, demonstrated already on the first step: invasion into surrounding tissues. Cancer cells can invade either collectively (in sheets or clusters) (Rørth, 2009) or as single cells (mesenchymal or amoeboid cells) (van Zijl et al., 2011). To do so, they commonly undergo phenotypical conversions, such as an epithelial to mesenchymal transition (EMT) (Nieto et al., 2016), a collective to amoeboid transition (CAT) (Krakhmal et al., 2015) and a mesenchymal to amoeboid transition (MAT) (Wolf et al., 2003).

Collective cell migration is migration of a whole group of cells. A moving cell group has a leading edge/front that resembles mesenchymal cells and followers that are more tightly packed. Leading cells use integrins to adhere and perform proteolytic degradation of the extracellular matrix (Krakhmal et al., 2015). Collective migration is connected to EMT, although there is an ongoing discussion about role of EMT in cancer progression (Fischer et al., 2015; Zheng et al., 2015).

The execution of EMT in cancer is not homogeneous, therefore EMT should be seen as a spectrum of intermediate states (Nieto et al., 2016). On a molecular level, EMT means a loss of an epithelial character and a gain of a mesenchymal program, e.g. downregulation or loss of E-cadherin and subsequent upregulation of vimentin and N-Cadherin (so called cadherin switch) (van Zijl et al., 2011). This leads to an enhanced motility of cancer cells (Yilmaz and Christofori, 2010). This transition is induced by transcription factors, such as twist and snail (Nieto et al.,

2016). At the secondary site, an opposite transition (mesenchymal to epithelial) allows colonization (van Zijl et al., 2011).

Due to its heterogenic character, it is difficult to compare cancer cell invasion and invasion of hemocytes into the extended germband. It is still not confirmed whether hemocytes migrate into the germband collectively. It was observed that they form a stream (Siekhaus et al., 2010) that resembles the initial steps of metastasis but whether it is a classical collective migration including defined leading cell(s) is not clear. Similar to collective migration of metastatic cells, hemocytes use integrins (Siekhaus et al., 2010). There is also a change in the expression of cadherins, however DN-Cadherin is actually downregulated (see Chapter 2). However, whether there are similarities between our system and the initial steps of metastasis that would allow the translation of results from *Drosophila* to human carcinogenesis has to be tested experimentally and this testing is in progress in our group.

Migration can be regulated on different levels. Intracellularly, through the regulation of the cytoskeleton, the regulation of signaling, protein phosphorylation or the general transcriptome/ proteome. It can also be regulated by signals coming from outside, such as signaling molecules or the properties of the surroundings. I would like to discuss two regulators relevant for the following work – protein glycosylation that can be inside or on the surface of the cell but also on its surroundings and the extracellular matrix (ECM) and adhesion connected to it.

Protein glycosylation

Protein glycosylation is a common posttranslational modification in which different types of sugars are added on a protein in the endoplasmatic reticulum (ER) and/or in the Golgi apparatus. The most common types of protein glycosylation are N- and O-glycosylation. On the top of these two main types of glycosylation, a lot of unusual and rare forms of glycosylation exists. Thirteen naturally occurring aminoacids contain various functional groups in their side chains that present potential sites for glycosylation, unusual N-bonds (amido group on Arginine, Lysine, Tryptophan and Histidine) or O-bonds (hydroxyl group on the Tyrosine, Hydroxyproline or Hydroxylysine), as well as C- and S-bound glycans (Lafite and Daniellou, 2012).

N-glycosylation in eukaryotes starts on the cytoplasmic side of the ER by the assembly of a precursor bound to the dolichol that serves as a carrier. After the precursor is made, dolichol is translocated and the rest of glycosylation happens in the lumen of the ER and Golgi apparatus (Burda and Aebi, 1999). First, the whole precursor is transferred to the amido group of an asparagine in a protein (Bhagavan, 2002). The glycosylation site is context dependent, the typical sequence being NxS/T X≠P site (Aebi, 2013). After the addition of the precursor, the sugar chain is trimmed and extended/modified by a toolkit of enzymes as it is passing through the ER and Golgi apparatus (Bhagavan, 2002).

In contrast to N-glycosylation, O-glycosylation can be initiated in the ER (except O-GalNAc and O-Xyl) but occurs mainly in the Golgi (with some exceptions, e.g. O-GlcNAc glycosylation on cytoplasmic and nuclear proteins) and therefore on folded proteins (Comer and Hart, 2000; Roth, 1984). O-glycosylation is not as easily predictable as N-glycosylation since a conserved sequence for O-glycosylation has not yet been identified. Some types of O-glycosylation happen on folded

proteins and therefore folding influences which sites are accessible (Christlet and Veluraja, 2001). O-glycosylation encompasses a broad group of different types of glycosylation in which sugar group is added on the hydroxyl group of a serine or threonine of a protein (Christlet and Veluraja, 2001; Steen et al., 1998). While O-GlcNAc glycosylation happens in the cytoplasm and nucleus results in the addition of a single sugar group per site (Copeland et al., 2013), the major types of O-glycosylation (O-Man, O-GalNAc, O-Fuc, O-Glc, O-GlcNAc, O-Xyl and Hyl O-Gal) occur in the ER but mainly in the Golgi (Joshi et al., 2018).

Protein glycosylation in insects

Glycosylation is a very complex type of modification that usually involves a lot of steps and therefore interpretation of the results, especially when working with mutants in the involved enzymes, is complicated. Therefore, there is a constant search for an easier system in which to study different types of glycosylation. On the one side, single-cloned mammalian cell lines offer the option of decreased (genetic) variability and together with CRISPR based approaches has already uncovered a lot (Narimatsu et al., 2018). However, the problem with a complex pattern of glycosylation remains. The attempt to overcome this problem is SimpleCell technology developed and already successfully used for studying O-GalNAc (Steentoft et al., 2013a; Vakhrushev et al., 2013). However, interpretation of how *in vitro* studies can predict results within an *in vivo* context is complicated and many times, it has been shown that an *in vivo* context changes even the substrate specificity of some enzymes and *in vivo*, many glycosyl-transferases are more restricted in what they actually modify e.g.(Breloy et al., 2016b; Kim et al., 2003). Therefore, an *in vivo* model with a simpler version of glycosylation would be very useful.

In general, insect glycosylation could be considered to be a simpler version of the mammalian one. In mammals, the complex N-glycans are the most common type of N-glycosylation. In *Drosophila*, truncated, paucimannosidic (Man_{1-3} $GlcNAc_2$) or oligomannosidic glycans (Man_{5-9} $GlcNAc_2$) are more common than complex N-glycans that make up only a minor fraction of the insect N-glycomes (1-20%) (Chung et al., 2017; Schiller et al., 2012). Another feature characteristic for insect N-glycosylation is the presence of up to two core fucose residues α-1,6-linked and α-1,3-linked, to the innermost GlcNAc (Chung et al., 2017; Fabini et al., 2001). The α-1,3-linked core fucose residue is typical for insect but not for humans (Chung et al., 2017).

A similar conclusion can be reached about insect O-glycosylation. Although 90% of detected O-glycoproteins are O-GalNAc (Aoki et al., 2008), except Hyl O-Gal, all types of O-glycosylation are conserved (Joshi et al., 2018). However, everything is 'reduced'- the number of genes involved in initiation is generally smaller and O-GalNAc as well as O-Man complex structures are fully missing (or have not been identified as of now) (Aoki et al., 2008). Sialylation of O-glycans was also never detected in *Drosophila*. However, this type of final modification seems to be functionally 'replaced' by addition of glucuronic acid (GlcA) that is also negatively charged and therefore could fulfill similar functions as sialic acid (Aoki and Tiemeyer, 2010a).

To sum up, *Drosophila* has a less complex glycosylation that usually happens with the assistance of less enzymes. Combined with the classical advantages of *Drosophila* as a model organism, I consider it to be an interesting model to study the role of glycosylation during cell migration and embryonic development. The existence of only shorter versions that are at least for O-GalNAc glycosylation more typical for cancer cells also opens the option of interpreting data from normal developmental regulation to the process of tumorigenesis and metastasis.

Mucin-type or O-GalNAc glycosylation

O-GalNAc glycosylation, or so called mucin-type as it is abundant on mucins, is initiated by the polypeptide α-N-acetylgalactosaminyltransferase (ppGalNAcT) that adds GalNAc in an α-configuration on Serine or Threonine residues (Sugiura et al., 1982; Tenno et al., 2007). From the first step on, O-GalNAc glycosylation is happening only in the Golgi apparatus (Roth, 1984) and therefore on folded proteins (with one exception, the GALA pathway, see later). The first formed structure is called Tn antigen (see Fig 1A, Chapter 2) which is further extended by Gal, GlcNAc or GalNAc to form core 1 (Galβ1-3GalNAcα1-O-Ser/Thr , also called T antigen), core 2, core 3, core 4 and core 5 that can be further modified by the addition of GlcNAc and Gal and terminally decorated by sialic acid, a sulfate group, GalNAc or Fuc (Fu et al., 2016; Ten Hagen et al., 2003a).

To synthesize core 1, a T-synthase adds Gal on GalNAcα1-O-Ser/Thr. In mammals, only one gene, *C1GalT1*, encodes T-synthase (Ju et al., 2002a, 2002b). The proper folding of C1GalT1 depends on Cosmc, a single protein chaperone (Ju and Cummings, 2002; Wang et al., 2010). In the case Cosmc is absent, there is no functional C1GalT1 produced in the ER and as the system is not redundant, there is no Core 1 and higher structures that depend on it (Wang et al., 2010).

On top of the previously mentioned enzymes, also core 3 β1,3-N-acetylglucosaminyl-transferase (core 3 β3GlcNAcT), which synthesizes core 3 structure and sialyltransferase ST6GalNAc-I are needed to synthesize the whole range of O-GalNAc structures in mammals (Fu et al., 2016).

In *Drosophila*, only short forms of O-GalNAc glycans were detected: Tn and T antigen. Sialylation of O-glycans in *Drosophila* was never confirmed but in contrast to mammals, T and Tn antigen can be glucuronylated (Aoki and Tiemeyer, 2010a; Ghosh, 2018; Repnikova et al., 2010). Mammals have at least 15 ppGalNAcTs (Ten Hagen et al., 2003a) while *Drosophila* has only around 9 of them (Tran et al., 2012). Surprisingly, C1GalT1 has more than one homolog in *Drosophila* although the exact number is not fully accepted and depends on how *in vitro* tests for specificity are set up (Correia et al., 2003; Lin et al., 2008; Müller et al., 2005). However, C1GalTA is probably the main T synthase as it shows an at least 150fold higher activity for the substrate compared to other tested transferases (Müller et al., 2005) and was proven to have the function also *in vivo* (Lin et al., 2008). Interestingly, in *Drosophila*, there is no Cosmc homolog and there is no indication that C1GalTA needs a specific chaperone for its proper folding.

O-GalNAc glycosylation in (invasive) migration and cancer progression

Both Tn and T antigen on the cell surface are associated with cancer cells and their increased aggressiveness although the mechanisms by which increased Tn or T antigens appear on the surface and how they influence cells are independent (Fu et al., 2016).

Tn antigen in connection with cancer cells was described for the first time in 1974 by Springer et al. who detected it on the majority of breast carcinomas (Fu et al., 2016; Springer et al., 1974). Later, it was associated with other tumors as well, e.g. colon, ovary or prostate tumors (Inoue et al., 1991; Itzkowitz et al., 1989; Kuwabara et al., 1997). Due to a similar structure and biosynthesis pathway, Tn and its sialylated version, sTn, are always overexpressed in the tumors at the same time (Fu et al., 2016). The exact role of Tn antigen is still unclear. Some studies point out that Tn antigen is bound by C-type macrophage galactose binding lectin (MGL) that is expressed in dendritic cells and macrophages. This way the tumor might escape

immunosurveillance (Higashi et al., 2002; Napoletano et al., 2007; Saeland et al., 2007; van Vliet et al., 2013).

T antigen was also described by Springer et al. as an oncofetal antigen, just one year later than Tn antigen (Fu et al., 2016; Springer et al., 1975). The classical and intensively studied protein extensively decorated by T antigen in cancer cells is Mucin1 (MUC1) (Nath and Mukherjee, 2014). T antigen is able to mobilize Galectin-3 to the surface of endothelial cells and therefore mediate cancer cell adhesion to the endothelium (Glinsky et al., 2000). This way T antigen could play a role in the metastatic spreading of cancer cells, consistent with observations that T antigen is a bad prognosis marker (Baldus et al., 2000; MacLean and Longenecker, 1991; Schindlbeck et al., 2005; Springer, 1997; Summers et al., 1983).

Overexpression of Tn and sTn antigen is in many cases connected to mutation in Cosmc (Ju et al., 2008) or hypermethylation of its promoter (Radhakrishnan et al., 2014). In this case, no functional C1GalT1 exists and therefore only shorter O-glycan forms, Tn and sTn antigens, are created. The other described mechanism of increased Tn antigen on tumors is the GALA pathway in which ppGalNAcTs are relocalized to the ER where they function on unfolded proteins (Gill et al., 2013). However, this mechanism leads only to slight if any change in T antigen (Chia et al., 2014). The presence of T antigen on the surface of cancer cells was recently connected with increased Golgi pH (Rivinoja et al., 2006). The current hypothesis assumes that an increased pH disturbs heterodimers between transferases, resulting in inefficient glycosylation and therefore truncated forms reaching the surface of the cells (Kellokumpu et al., 2016).

It was observed and described many times before that shorter forms of O-GalNAc glycans (Tn, sTn and T antigen) are associated with a bad prognosis and higher invasiveness of cancer cells (Baldus et al., 2000; MacLean and Longenecker, 1991; Schindlbeck et al., 2005; Springer, 1997; Summers et al., 1983). However, the exact mechanism is not fully understood. The discovery and initial analysis of the GALA pathway revealed one possible mechanism. *In vitro*, ER-localized ppGalNAcT1 increases adhesion to fibronectin and collagen and these cells are moving faster in a scratch wound-healing assay, thanks to bigger and more stable lamellipodia. These results were confirmed also *in vivo* in which ER-localized ppGalNAcT1 promotes efficient lung colonization (Gill et al., 2013). Therefore, one of the activities that is probably regulated by differential glycosylation in cancer cells is the adhesion/interaction with ECM components.

Extracellular matrix (ECM)

Effective cell motility requires cells to adapt to, interact with and potentially also modify their surroundings (Jacquemet et al., 2015) that consist of ECM and other cells. ECM is mainly composed of glycoproteins that assemble into a supramolecular structure, containing binding domains for growth factors and chemokines, allowing the establishment of complex adhesion surfaces and forming diffusion barriers (Mouw et al., 2014). Therefore, ECM components can be a support for the cells but also an active participant in signaling and thus regulating cell behavior. ECM structures are tissue or organ-specific (Mouw et al., 2014; Naba et al., 2012).

In general, the ECM can be divided into two groups/types: interstitial matrix and basement membrane (Hallmann et al., 2015). While the interstitial matrix consists of fibrillar collagens, mainly of Collagen I and some other minor components, depending on tissue type

(Hallmann et al., 2015; Mouw et al., 2014), the basement membrane is more biochemically variable and contains mainly laminins, Collagen type IV, heparin sulfate proteoglycans and nidogens (Hallmann et al., 2015; Yurchenco, 2011).

In our system (*Drosophila* embryos stage 11/12), ECM production is already on but the structure is not considered to be a basement membrane. The basement membrane was detected and defined in *Drosophila* embryos only shortly before embryo hatching (Matsubayashi et al., 2017). The components of an embryonic basement membrane are being laid to different extents by embryonic hemocytes (Fessler and Fessler, 1989; Matsubayashi et al., 2017; Ratheesh et al., 2018a), except Nidogen/entactin that is produced only by other tissues although hemocytes migrate through the places where Nidogen is deposited (Wolfstetter et al., 2019). The following nine molecules are the main components of *Drosophila* basement membrane, some of them being already known to play a role in the regulation of cell migration:

Collagen type IV

Two adjacent loci encode for type IV collagens (*col4a1* and *viking*) (Monson et al., 1982; Yasothornsrikul et al., 1997). Collagen IV is being produced and laid by hemocytes and the fat body (Matsubayashi et al., 2017). Collagen type IV plays a role in the structure of muscles; mutants in *col4a1* cause severe myopathy resulting in female sterility (Kelemen-Valkony et al., 2012). Hemocyte-deposited Vkg is important for proper development of Malpighian tubules through enhancing BMP signaling (Bunt et al., 2010). Interestingly, a recent study (Itoh et al., 2018) pointed out an indirect connection between O-GalNAc glycosylation and Vkg. Although they show that Vkg does not directly carry T antigen (the correct size band is not visible on a PNA blot), it can be pulled down using PNA and therefore interacts with T antigen-modified protein(s). Absent T antigen causes a partial loss of Vkg at the basement membrane on muscles (Itoh et al., 2018). However, whether and how Collagen IV subunits play a direct role in immune cell migration and invasion is not clear and would be interesting to address this question.

Laminins

Drosophila laminin is a disulfide-linked molecule consisting of three chains. It has a cross-shaped appearance and contains globular domains characteristic of vertebrate laminin with closely similar dimensions (Fessler et al., 1987). There are four genes in *Drosophila* encoding for laminins: *laminin A* (*lanA*), *wing blister* (*wb*), *laminin B1* (*lanB1*) *and laminin B2* (*lan B2*).

LanA is an α chain that has similarity to its vertebrate counterpart but the sequence that forms the short arm is quite different and longer (Garrison et al., 1991; Kusche-Gullberg et al., 1992). LanA expression appeared in embryonic mesoderm and later on is heavily produced by hemocytes (Kusche-Gullberg et al., 1992). LanA has a whole set of roles during *Drosophila* development, including proper development of the heart, somatic mesoderm and the gut in late-staged embryos (Yarnitzky and Volk, 1995) as well as axon pathfinding (García-Alonso et al., 1996). Full loss-of-function mutant are embryonically lethal (García-Alonso et al., 1996).

Wb is another α subunit that is also essential for embryonic viability (Martin et al., 1999). The mutant phenotypes in many cases overlap with phenotypes for *lanA* and *integrin* mutants (Martin et al., 1999). It was described to play a role in germband morphology and retraction (Martin et al., 1999; Schöck and Perrimon, 2003; Sorrosal et al., 2010) and wing development (Inoue and Hayashi, 2007).

LanB1 is a β chain that carries some similarities to its mouse counterpart, especially in its 13 EGF domains (Montell and Goodman, 1988). It regulates tissue migration during egg development (Díaz de la Loza et al., 2017), cardiac development and muscle attachment (Hollfelder et al., 2014). *LanB2* encodes a γ chain (Montell and Goodman, 1989). LanB2 plays a role in mesoderm development, muscle attachment (Wolfstetter and Holz, 2012), embryonic salivary gland development (Patel and Myat, 2013) and adhesion dependent cell spreading (Gotwals et al., 1994a).

While there are 2 genes encoding for α subunit, LanB1 is the only β chain of the laminin trimer and LanB2 the only γ chain. Therefore, there are only 2 forms of laminin trimer existing in *Drosophila*. Assembly of a *Drosophila* laminin trimer depends on the formation of disulfide bonds. While the β and γ chain form a stable dimer before the disulfide bond is made, the α subunit is not able to bind either monomeric β or γ, or the βγ dimer before the disulfide bond is made. Although *Drosophila* laminins form stable trimer, quite common detection of βγ dimer and monomeric α subunit in the medium of Kc167 cells was described (Kumagai et al., 1997).

Laminins play a crucial role in the assembly of the basal membrane (Urbano et al., 2009) and therefore influence a whole set of functions, including cell migration. In *Drosophila* embryonic hemocytes, Sánchez-Sánchez et al. described the role of hemocyte-produced laminins in their migration on the ventral nerve cord (vnc). Hemocytes in *lanB1* mutant embryos migrate slower and by stage 13, in contrast to control embryos, they do not cover the whole vnc. Using hemocyte transplantation, they proved that hemocyte-derived laminins are important for their directed migration (Sánchez-Sánchez et al., 2017).

Collagen XV/XVIII

Multiplexin encodes for the ColXV/XVIII homolog. It is a chondroitin sulfate proteoglycan (Momota et al., 2011). It is required for proper maintenance of the basal membrane and may be involved in establishing the wingless signaling gradients in *Drosophila* embryo (Momota et al., 2011) and polarized enhancement of Slit/Robo signaling at the heart lumen (Harpaz et al., 2013). To my knowledge, a role in the embryonic hemocytes was not described.

Perlecan

terribly reduced optic lobes (*trol*) locus encodes the *Drosophila* version of Perlecan (Voigt et al., 2002). It is known to play a role in the regulation of the activity of different types of stem cells (Voigt et al., 2002; You et al., 2014). In lymph glands, it influences the balance between proliferation and differentiation of blood progenitors (Grigorian et al., 2013). Similar to the mammalian Perlecan, Trol is a multidomain heparin sulphate proteoglycan that can influence cellular signaling by interacting with other ECM components, growth factors and receptors (Aviezer et al., 1994; Dragojlovic-Munther and Martinez-Agosto, 2013; Noonan et al., 1991; Voigt et al., 2002). The role in the invasive migration of embryonic hemocytes is not probable as based on *in situ* hybridization (Tomancak et al., 2007, 2002), *trol* is expressed only in late embryonic stages.

Nidogen

While mammals have 2 *Nidogen* genes (*Ndg1 and Ndg2*), *Drosophila* possesses only one *Nidogen/entactin* gene (Wolfstetter et al., 2019), that is poorly characterized, compared to other

ECM components. Nidogen is considered to be an 'ECM linker protein' that connects laminins and Collagen IV in basement membrane (Aumailley et al., 1993; Wolfstetter et al., 2019). Consistent with its function in mammals, *Drosophila* Nidogen was recently described to play a role in basement membrane stability and development of peripheral nervous system, demonstrated by crawling problems and decreased answer to vibrational stimuli (Wolfstetter et al., 2019).

ECM adhesion molecules: Integrins

Integrins are adhesion receptors consisting of α and β subunits with a large extracellular domain and a short cytoplasmic tail (Campbell and Humphries, 2011; Tamkun et al., 1986). Humans have 18 α and 8 β subunits that can assemble into 24 receptors with different binding properties (Barczyk et al., 2010; Ginsberg, 2014). The α subunit defines ligand specificity while the β subunit influences signaling pathway inside of the cell (Barczyk et al., 2010). An important feature of the majority of integrin receptors is their ability to bind a wide spectrum of ligands; additionally ECM components and other adhesion molecules can interact with the quite high variability of integrin receptors (Campbell and Humphries, 2011; Plow et al., 2000).

As integrins lack enzymatic activity, signaling is induced by the assembly of signaling complexes on the cytoplasmic face of the plasma membrane. Many integrins are not constitutively active; they are often expressed on cell surfaces in an inactive state, in which they do not bind ligands and do not signal. This allows rapid action when needed, for example during immune responses (Campbell and Humphries, 2011). It also allows temporal and spatial regulation of adhesion during cell migration (Lauffenburger and Horwitz, 1996). Signals from inside cells can increase the binding of integrin extracellular domains to ligands, a process called integrin activation (Ginsberg, 2014) which is achieved by either receptor clustering into oligomers or by conformational changes in the receptor that expose effector binding site (Shattil et al., 2010).

The first established molecular function of integrins was as a link between the ECM and cytoskeletal substituents, mainly actin (Geiger et al., 2009), but not exclusively (Bhattacharya et al., 2009). Some components of this mechanical linkage play a role also in integrin activation, e.g. talin (Barczyk et al., 2010). Integrins can also function as bi-directional signaling receptors involved in inside-out (namely the integrin activation, described above) and outside-in signaling. Outside-in signaling is triggered by conformational changes upon ligand binding. This activate complex and cell-specific signaling events (Barczyk et al., 2010; Gahmberg et al., 2009).

Integrins are essential cell adhesion proteins, not playing a role only in adhesion and migration but also influencing cell survival and apoptosis (Desgrosellier and Cheresh, 2010). In *Drosophila*, the variability is not so high as in mammals: *Drosophila* has 5 α and only 2 β subnits that are implicated in different biological functions:

Multiple edematous wings (mew)

Mew encodes an α subunit of integrin (α-PS1 integrin) that binds laminin (Gotwals et al., 1994b). It plays a role in many processes, e.g. wing development (Brabant et al., 1996), salivary gland and

myoblast migration (Jattani et al., 2009), the regulation of responses to Slit repellent signals (Stevens and Jacobs, 2002), maintenance of intestinal stem cells (Lin et al., 2013) or migration of the caudal visceral mesoderm (Urbano et al., 2011).

Inflated (If)

If is a gene encoding α subunit of integrin (α-PS2 integrin) that binds Wingblister, Thrombospondin and Tiggrin (Fogerty et al., 1994; Gotwals et al., 1994b; Pérez-Moreno et al., 2017). Originally, it was discovered in muscle attachment (Bogaert et al., 1987). It plays a role in the migration of border cells (Kókai et al., 2012) as well as hemocyte invasion into the extended germband (Siekhaus et al., 2010). It also has other (developmental) roles, including: axon guidance (Huang et al., 2007), salivary gland and myoblast migration (Jattani et al., 2009), maintenance of tracheal terminal branches (Levi et al., 2006), regulation of neuromuscular function (Wang et al., 2018) and wing development during puparization (Brabant et al., 1996).

Scab (Scb)

α-PS3 integrin is encoded in *Drosophila* by *scab*. It was discovered as a broad regulator of the movement and morphogenesis of tissues during development in *Drosophila* (Stark et al., 1997). After dimerization with Integrin βv, it is required for effective phagocytosis of apoptotic cells in *Drosophila* embryos and phagocytosis of *S. aureus* by larval hemocytes (Nonaka et al., 2013). It also functions in the nervous system where it regulates short-term memory (Grotewiel et al., 1998), synaptic morphology, transmission and plasticity (Rohrbough et al., 2000) and regulation of response to Slit repellent signals (Stevens and Jacobs, 2002).

Integrin alphaPS4 subunit (ItgaPS4) and Integrin alphaPS5 subunit (ItgaPS5)

The last 2 α subunits are not so deeply studied and seem to have redundant functions with Scb in the defining final length of an egg (Dinkins et al., 2008). *ItgaPS4* is used as a marker of lamellocytes (Makki et al., 2010).

Myospheroid (Mys)

Mys is a beta subunit of the integrin dimer (Bunch et al., 1992). It regulates migration of *Drosophila* hemocytes in two ways; by shaping the three-dimensional environment in which hemocytes migrate and by regulating the migration of hemocytes themselves (Comber et al., 2013). As it dimerizes with α subunits, many of its functions are identical with previously described subunits.

Integrin betanu subunit (Itgbn)

Itgbn encodes the second β subunit. It was originally described to be restricted in its expression to the midgut endoderm and its precursors during embryonic development (Yee and Hynes, 1993). It dimerizes with Scb to ensure effective phagocytosis of apoptotic cells in *Drosophila* embryos and phagocytosis of *S. aureus* by larval hemocytes (Nagaosa et al., 2011; Nonaka et al., 2013).

Glycosylation is one of the regulators of adhesion. Not only ECM components are usually highly glycosylated, integrins are a subject of regulation by both N- and O-glycosylation (Rogriguez et

al., 2018). Their abberant glycosylation may result in changes in cell behavior and properties. For example, terminal (hyper)sialylation interferes with cell attachment to Collagen IV and Fibronectin, therefore promoting migratory and invasive phenotypes (Dennis et al., 1982, Seales et al., 2005). In general, different types of glycosylation or their changes play very different roles in the regulation of cell signaling.

Different effects of regulation of cell signaling by glycosylation

Glycosylation is strongly context dependent and might have both inhibiting and enhancing effects on signaling as well as potentially modifying receptor-ligand interactions. While in the case of some types of integrin heterodimers, hypersialylation prevents ECM-integrin interaction (Dennis et al., 1982), in dendritic cells, polysialylation of CCR7 releases an autoinhibited conformation of CCL21 and allows its interaction with CCR7 and the ensuing signaling (Kiermaier et al., 2016).

Another good example of the inhibitory role of glycosylation is the classical target of O-GalNAc glycosylation – MUC1. MUC1 is a highly glycosylated single pass transmembrane protein (Nath and Mukherjee, 2014). Immediately after translation, it is autoproteolytically cleaved to a longer MUC1-N and a shorter MUC1-C (contains transmembrane domain) that stay associated through stable hydrogen bonds (Hattrup and Gendler, 2008). MUC1-N in normal conditions roughly doubles in size after full glycosylation but depending on tissue and physiological conditions, glycosylation might constitute up to 90% of the total weight of the protein (Nath and Mukherjee, 2014). In normal conditions, MUC1 contains mainly core 2 O-glycans while in some types of cancer cells, e.g. breast cancer, core 1 O-glycans and hypersialylation are present (Whitehouse et al., 1997, Brockhausen et al., 1995, Picco et al., 2010). This hypoglycosylation results in unmasking of the MUC1 peptide core and therefore cleavage of MUC1-N by extracellular proteases (Nath and Mukherjee, 2014), conformational changes in MUC1-C and hyperactivation of MAPK, P13K/Akt and Wnt signaling pathways (Hollingsworth and Swanson, 2004, Nath et al., 2013, Li et al., 1998). MUC1 hypoglycosylation has therefore broad effects on different cellular behaviors such as proliferation, tumor metabolism, invasion and metastasis, angiogenesis or chemoresistence (Nath and Mukherjee, 2014).

An intensively studied example of how O-glycosylation regulates receptor functions is in Notch signaling, a conserved pathway required for both proper development and homeostasis. Notch consists of the Notch extracellular domain (NECD) that binds to ligand and the intracellular domain (NICD) that moves into the nucleus to regulate transcription (Hori et al., 2013). Notch carries different types of glycosylation: mainly O-fucose, O-glucose and O-GlcNAc on its EGF repeats on NECD, but also O-GalNAc outside of EGF domains as well as some amount of N-glycosylation on NECD (Takeuchi and Haltiwanger, 2014, Boskovski et al., 2015).

The O-fucose on the EGF domains of NECD plays an important role in Notch signaling. The first enzyme discovered to be involved is Fringe that catalyzes futher elongation of O-fucose (Brückner et al., 2000). It depends on Fringe connection transporter activity (Goto et al., 2001; Selva et al., 2001, for more details see Chapter 2). Fringe increases Notch sensitivity to respond to one of its ligands, Delta (Brückner et al., 2000, Panin et al., 1997, Xu et al., 2007). However, the situation in the step before Fringe activity is different. The addition of fucose to serine or threonine is in *Drosophila* regulated by Ofut1 (Wang et al., 2001). Proper activity of Notch in

general requires the presence of Ofut1 but, interestingly, its overexpression has an inhibitory effect on Notch (Okajima and Irvine, 2002).

Also other types of O-glycosylation are important for Notch signaling (Takeuchi and Haltiwanger, 2014): for example, O-glucose is required for S2 cleavage during Notch activation (Acar et al., 2008), while its xylosyl extension seems to negatively regulate Notch (Lee et al., 2013). However, the function of other types of glycosylation like O-GlcNAc, O-GalNAc or N-glycosylation is not fully understood (Takeuchi and Haltiwanger, 2014).

This short summary highlights how diverse the functions of glycosylation can be on signaling from basic on and off to modulation of the activity and ligand preferences. Therefore, work with glycosylation always requires looking at the cell in whole complexity and not forgetting that while the glycosylation regulator activates one component of the pathway, it may modulate or inhibit something different that intersects with the pathway later and therefore result in very complicated effects (or phenotypes, in the case of mutant analysis). The work described in this thesis clearly demonstrates this.

Chapter 2: Potential players in invasive migration of embryonic macrophages of *Drosophila* melanogaster

Introduction

The *Drosophila* cell mediated immune system consists of 3 types of hemocytes (blood cells) (Evans et al., 2003; Honti et al., 2014; Parsons and Foley, 2016): plasmatocytes that have the ability to phagocytose (Franc et al., 1996; Nelson et al., 1994), crystal cells responsible for melanization (Ashida and Brey, 1995; Rizki and Rizki, 1959) and lamellocytes that encapsulate bigger objects (Rizki and Rizki, 1992). Embryonic hemocytes are born in the head mesoderm (Tepass et al., 1994), being defined already at the blastoderm stage (Holz et al., 2003). Embryonic hemocytes are specified by the transcription factor Serpent (Rehorn et al., 1996; Lebestky et al., 2000) belonging to the GATA transcription factor family (Crozatier and Meister, 2007). *Serpent* is expressed in other tissues as well (Rehorn et al., 1996), therefore other transcription factors are needed to define hemocytes: *glial cells missing* (*gcm/gcm2*) that is initially expressed in all prohemocytes but quickly downregulated in the precursor of crystal cells to allow expression of *lozenge* (Lebestky et al., 2000; Bataillé et al., 2005); Lozenge, a RUNX transcription factor, that interacts through a conserved domain with Serpent to induce crystal cell formation (Waltzer et al., 2003) and U-shaped (Ush), a member of the Friend-of-GATA multiple zinc-finger protein family that antagonizes the development of crystal cells (Fossett et al., 2001; 2003; Waltzer et al., 2002). Gcm plays an instructive role in plasmatocyte development (Bernardoni et al., 1997; Alfonso and Jones, 2002).

Drosophila plasmatocytes, in contrast to crystal cells, migrate out of the head on the following defined routes (Brückner et al., 2004; Cho et al., 2002; Ratheesh et al., 2015):

1. Towards the extended germband which they invade (Siekhaus et al., 2010) and where they support the development of Malpighian tubules by secreting extracellular matrix components (Bunt et al., 2010). Afterwards, they migrate along the ventral nerve cord (vnc)
2. On the vnc where they engulf apoptotic cells and are important for vnc condensation (Olofsson and Page, 2005; Sears, 2003). They later merge with plasmatocytes coming from the posterior vnc.
3. Along the dorsal vessel. This route has not been described yet to have an important developmental role but it participates in hemocyte spreading through the whole embryo (Ratheesh et al., 2015)

One of the above mentioned routes requires tissue invasion (Siekhaus et al., 2010). Plasmatocytes enter the extended germband at specific locations between ectoderm expressing DE-Cadherin and mesoderm expressing DN-Cadherin and then migrate along this interface (Ratheesh et al., 2018). Prior to plasmatocyte entry, the ectoderm and mesoderm are close neighbours, without a premade space but the tissue separates during plasmatocyte entry (Ratheesh et al., 2018). This is in contrast with migration on the vnc where experiments with injecting dextran revealed premade space for migration along the vnc (Evans et al., 2010). Migration towards and into the extended germband depends on integrin but does not seem to require degradation of the ECM (Siekhaus et al., 2010). Although the Laminin A is already

deposited, plasmatocytes migrate on it (Ratheesh et al., 2018) and it was shown that LanA is needed for the proper migration of hemocytes (Sánchez-Sánchez et al., 2017). This pathway demonstrates molecular similarities to the transmigration of vertebrate immune cells, such as the modulation of integrin affinity by small GTPases (Siekhaus et al., 2010).

Plasmatocyte migration is an interesting topic that could show us how tissue invasion is regulated and as it displays some similarities with the transmigration of vertebrate immune cells, it could potentially open new topics also in higher organisms. However, studying early steps of migration has been limited by the genetic tools available. Recently, our group published a paper (Gyoergy et al., 2018) with a toolkit that allows:

1. Study of the early steps of migration thanks to the fusion of the *srpHemo* promoter (Brückner et al., 2004) with 3xmCherry or 2xSuperfolder GFP
2. Specific modulation of 2 different types of tissues with tissue specific drivers thanks to the *srpHemoQF* system
3. Specific turning off the expression only in hemocytes by the *srpHemoGal80* system.

These tools enable early observation and deep characterization of prehemocytes and hemocytes and therefore allow us to understand and uncover important early molecular players as well as to dissect complicated phenotypes. The direct fusion containing flies are used also in this work, mainly in Chapter 3.

Plasmatocytes share similarities with vertebrate macrophages (Gold and Brückner, 2015) therefore I will address them as macrophages in this work.

Results

A secondary screen uncovered a gene with an effect specific for the invasive pathway

To analyze potential players in invasive migration, a screen was performed (data not shown), resulting in 26 positive hits. From those, we focused on a few conserved genes: 3 transporters - 2 members of the major facilitator superfamily (CG8602, Cln7) and 1 subunit of v-ATPase (Vha68-2), 1 protein predicted to bind histones (l((2)09851) and 1 protein known to be involved in circadian rhythms (cwo).

The major facilitator superfamily (MFS) is one of two (along with ABC transporters) transporter superfamilies that occur in all living organisms (Griffith et al., 1992; Pao et al., 1998). They are single-polypeptide secondary carriers capable of transporting only small solutes in response to chemiosmotic ion gradients (Pao et al., 1998). Members of this superfamily can transport a variety of substances (Madej and Kaback, 2013) and have very variable functions in different contexts, from lactose transport by the deeply studied lactose permease in *Escherichia coli* (Abramson et al., 2003; Yin et al., 2006), mediation of cellular responses to phosphate (Bergwitz et al., 2012) to embryo survival and fetal growth during pregnancy (Salker et al., 2017). CG8602 and Cln7 are predicted to be members of MFS, having the typical 12 transmembrane structure (Protter prediction, Fig 1A, B). MFS transporters most likely evolved from a two-transmembrane hairpin that was duplicated several times, resulting in the most common twelve-transmembane domain structure of MFS transporters (Reddy et al., 2012). CG8602 is an uncharacterized protein while CLN7 is predicted to function in the larval nervous system, being localized at the blood brain barrier (Mohammed et al., 2017). Both of them are highly conserved.

CG8602's mammalian ortholog is called MFSD1 and has 50% identity and 68% similarity. CLN7's homolog in humans is called MFSD8 and has 35% identity and 57% similarity.

The Vacuolar-type H^+-ATPase (V-ATPase) is a multicomponent complex that functions as a proton pumping rotary nano-motor (Marshansky and Futai, 2008). The importance of this complex is supported by the high degree of homology in its subunit composition and similarities in biochemical mechanisms that have been described from yeast to mammals (Smith et al., 2003). It consists of two parts. The cytoplasmic V_1 sector is composed of 8 different subunits and the transmembrane V_0 sector has of six different subunits (Fig 1C). Vacuolar-type ATPase's well-studied and widely accepted functions are in the acidification of endosomes and lysosomes as well as vesicular trafficking, especially in pH-dependent degradation (Marshansky and Futai, 2008). However, some studies such as (Williamson et al., 2010; Zoncu et al., 2011), showed that some subunits (V_0 subunit a1 in (Williamson et al., 2010), a few V_1 subunits in (Zoncu et al., 2011) may play pH-independent roles in different pathways. The existence of pH-independent and location/timing-specific functions is supported by the fact that many subunits are encoded by more than one gene and many of those genes are restricted in the location as well as the developmental timing of their expression (Allan et al., 2005).

Lethal (2) 09851 contains a WD40 repeat (Fig 1D) that is known to play a role in a protein complex formation (Jain and Pandey, 2018). It is predicted to bind histones and could play a role in transcriptional regulation but the real function remains undiscovered. *l(2) 09851* is a conserved gene; its human ortholog is called *grwd1* (glutamine rich WD repeat containing 1) with 53% identity and 66% similarity.

Clockwork orange (Cwo, Fig 1E) is a transcriptional regulator that plays a role in both the repression and activation of some genes (Richier et al., 2008). It was identified as a basic helix-loop-helix transcriptional repressor belonging to the Orange family (Kadener et al., 2007; Lim et al., 2007; Matsumoto et al., 2007). In adult flies, *cwo* is rhythmically expressed and directly regulated by Clock-Cycle (CLK–CYC) through canonical E-box sequences (Matsumoto et al., 2007). *cwo* mutants display reduced amplitude of molecular and behavioral rhythms with lengthened periods suggesting that it acts as a transcriptional and behavioral circadian rhythm amplifier (Lim et al., 2007). In addition, Cwo also forms its own negative feedback loop (Matsumoto et al., 2007). Based on the available data, Cwo acts preferentially in the late night to help terminate CLK–CYC-mediated transcription of direct target genes (Kadener et al., 2007).

To analyze the effect on tissue invasion of the downregulation of these genes, we used P element insertion mutants (*CG8602, cln7, vha68-2 and l(2) 09851*) or hemocyte-specific RNAi (*cwo*) and counted the number of macrophages entering the extended germband in early stage 12 embryos (up to a germband retraction of 41%). As shown in Fig 1F and G, there is a strong effect on migration into the extended germband in the *CG8602* mutant. This could not be explained by a decreased number of macrophages (Fig 1H) or a general migration effect (Fig 1I). Figure 1J and K show also a strong decrease in the number of macrophages in the germband in the *cln7* mutant but this gene seems to influence general migration as there is an effect on vnc as well (Fig 1L). Therefore we excluded this gene from futher analysis. We also excluded *l(2) 09851* that has a phenotype at early stage 12 (Fig 1Q, R) since homozygous embryos die at this stage hampering any further mutant analysis. *vha68-2* also displays a decreased number of macrophages entering the extended germband (figure 1M, N) with no effect on the total cell number (Fig 1O) and a mild effect on the vnc (Fig 1P). Hemocyte-specific *cwo* RNAi did not confirm

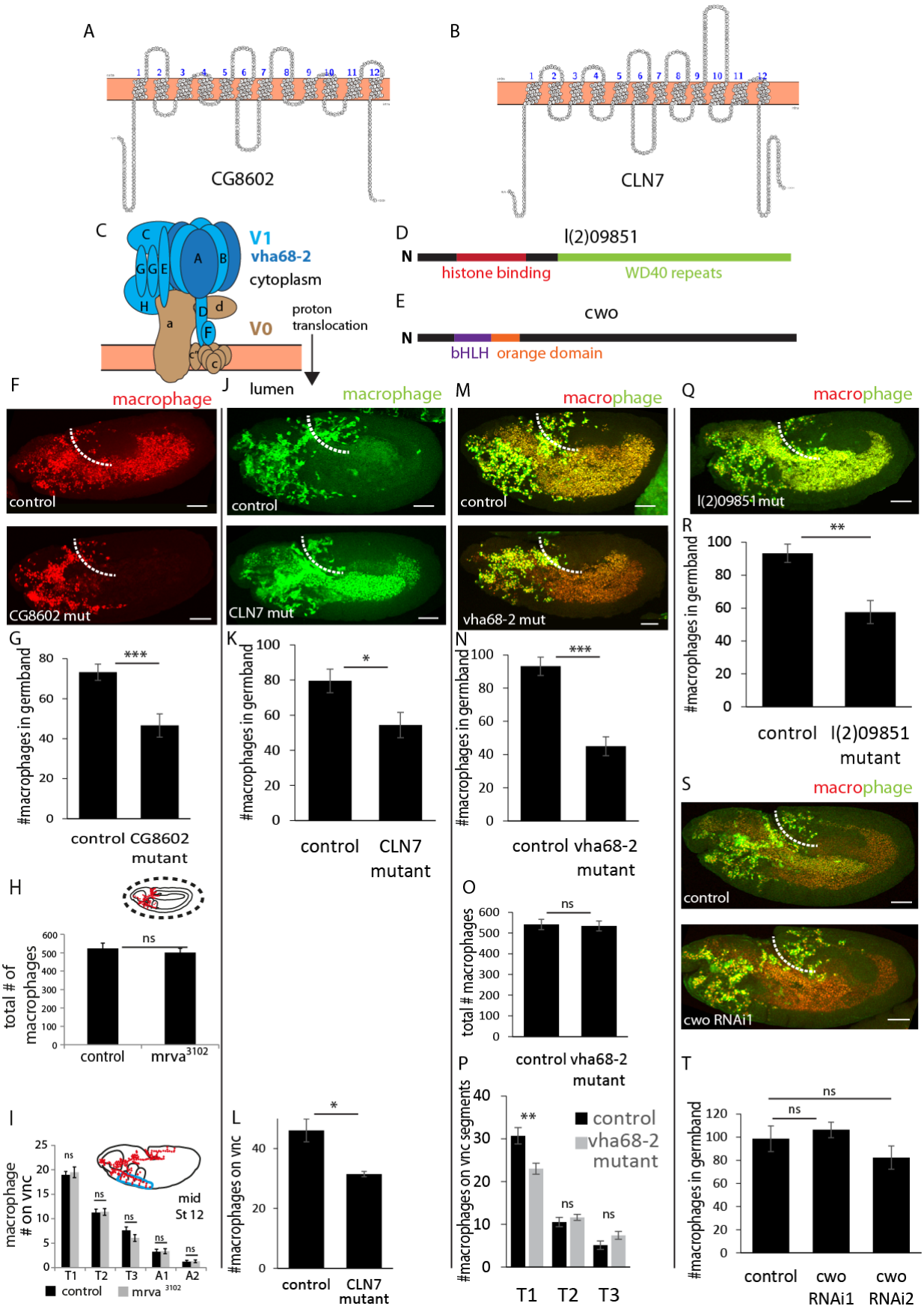
A
CG8602
B
CLN7
C
V1
vha68-2
cytoplasm
proton
translocation
V0
D
l(2)09851
N
histone binding
WD40 repeats
E
cwo
N
bHLH
orange domain
F
macrophage
control
CG8602 mut
G
#macrophages in germband
control
CG8602
mutant
H
total # of
macrophages
control
mrva3102
I
macrophage
on vnc
mid
St 12
T1
T2
T3
A1
A2
control
mrva 3102
J
lumen
macrophage
control
CLN7 mut
K
#macrophages in germband
control
CLN7
mutant
L
#macrophages on vnc
control
CLN7
mutant
M
macrophage
control
vha68-2 mut
N
#macrophages in germband
control
vha68-2
mutant
O
total # macrophages
control
vha68-2
mutant
P
#macrophages on vnc segments
control
vha68-2
mutant
T1
T2
T3
Q
macrophage
l(2)09851 mut
R
#macrophages in germband
control
l(2)09851
mutant
S
macrophage
control
cwo RNAi1
T
#macrophages in germband
control
cwo
RNAi1
cwo
RNAi2

Figure 1: Secondary screen uncovered CG8602 as a potential regulator of invasive migration
A-B: Prediction of (A) CG8602 and (B) Cln7 structure made by Protter **C:** Structure of v-ATPase protein complex – V1 subunit is blue, V0 subunit brown (modified from Smith et al., 2003) **D-E:** Structural prediction of (D) Lethal (2) 09851 and (E) cwo based on InterPro **F, J, M, Q, S**: Representative confocal images of early stage 12 embryos of controls and mutants of (F) *CG8602 (P{EP}CG86023102)*, (J) *CLN7 (P{SUPor-P}KG05284)*, (M) *vha68*-2 (*P{EP}Vha68-2EP2364*), (Q) *Lethal* (*2) 09851* (*P{EPgy2}l(2)09851EY06365*, for control see M) and (S) RNAi of *cwo*; **G, K, N, R, T**: Number of macrophages entering the extended germband in control and mutant of (G) *CG8602*, (K) *CLN7*, (N) *vha68-2*, (R*) Lethal (2) 09851* and (T) RNAi of *cwo (v106783, v42822*); **H, O:** Total number of macrophages in the whole embryo in control and mutant of (H) *CG8602* and (O) *vha68-2*. **I, L, P**: Macrophage number on different segments of the vnc in control and mutant of (I) *CG8602* and (P) *vha68-2* or (L) on the whole vnc in the control and mutant of *CLN7*.
Scale bar in F, J, M, Q, S is 50µm. Significance in G-I, K,L, N-P, R, T was analyzed by Student t-test.

a previously observed increase in macrophage numbers in the extended germband (Fig 1S, T). Therefore, we decided to focus on the only candidate from our selected list that has a specific effect on germband invasion – CG8602.

CG8602 potentially interacts with a sugar transporter, Frc

To understand the function of CG8602 in invasive migration, we took advantage of published data from a two-hybrid assay (Giot et al., 2003) and the *Drosophila* Protein Interaction Map (DPiM) initiative (Guruharsha et al., 2011) which tagged nearly 5000 *Drosophila* genes with FLAG-HA, expressed them in S2 R+ cells, and pulled down and analyzed interactors using mass spectrometry. CG8602 was one of the tagged genes. The list of proteins pulled down with CG8602 is in Table 1 (see the end of the chapter). From those, we chose 7 candidates that could be expressed in macrophages at stages 9-12 (UDP-galactose 4-epimerase; CG1444; Fringe connection, Ataxin 2; Dodeca-satellite binding protein 1; Surfeit 4; Walrus) and did a macrophage-specific RNAi screen on them. Our RNAi screen (data produced and evaluated by Kateryna Shkarina; statistics by KV) showed that 1 line for Frc, Ataxin-2, CG1444 and 2 lines for Dp1 have a decreased number of macrophages in the extended germband (fig 2A).

To see which protein(s) could interact with CG8602 to affect tissue invasion, we searched for those that phenocopy CG8602. Therefore we evaluated 2 RNAi lines per gene (CG1444, frc, dp1) not only for a germband phenotype but also for their vnc migration (Fig 2B) and total cell count (Fig 2C, data produced, evaluated and analyzed by Julia Biebl). Only one gene, *fringe connection*, phenocopies CG8602 while two others have significant changes in their total cell number (Dp1, CG1444, Fig 2C) and/or vnc (Dp1, Fig 2B) as well.

fringe connection (frc) is a gene encoding a transmembrane protein. It is characterized as a UDP-GlcA, UDP-GlcNAC and potentially UDP-xylose transporter (Goto et al., 2001; Selva et al., 2001) required for proper glycosylation. It brings in material for the proper function of a transferase called fringe (Goto et al., 2001; Selva et al., 2001) that is important for the glycosylation and therefore functionality of Notch (Irvine and Wieschaus, 1994; Moloney et al., 2000; Brückner et al., 2000).

To test whether Frc is a potential interactor of CG8602, we tested whether they are colocalized. Frc was previously shown to be localized in Golgi (Goto et al., 2001; Yano et al., 2005), with one study showing its very precise localization to medial Golgi (Yamamoto-Hino et al., 2012). Julia Biebl made a myc-tagged version of Frc and we also used the DPiM construct (FLAG-HA

Figure 2

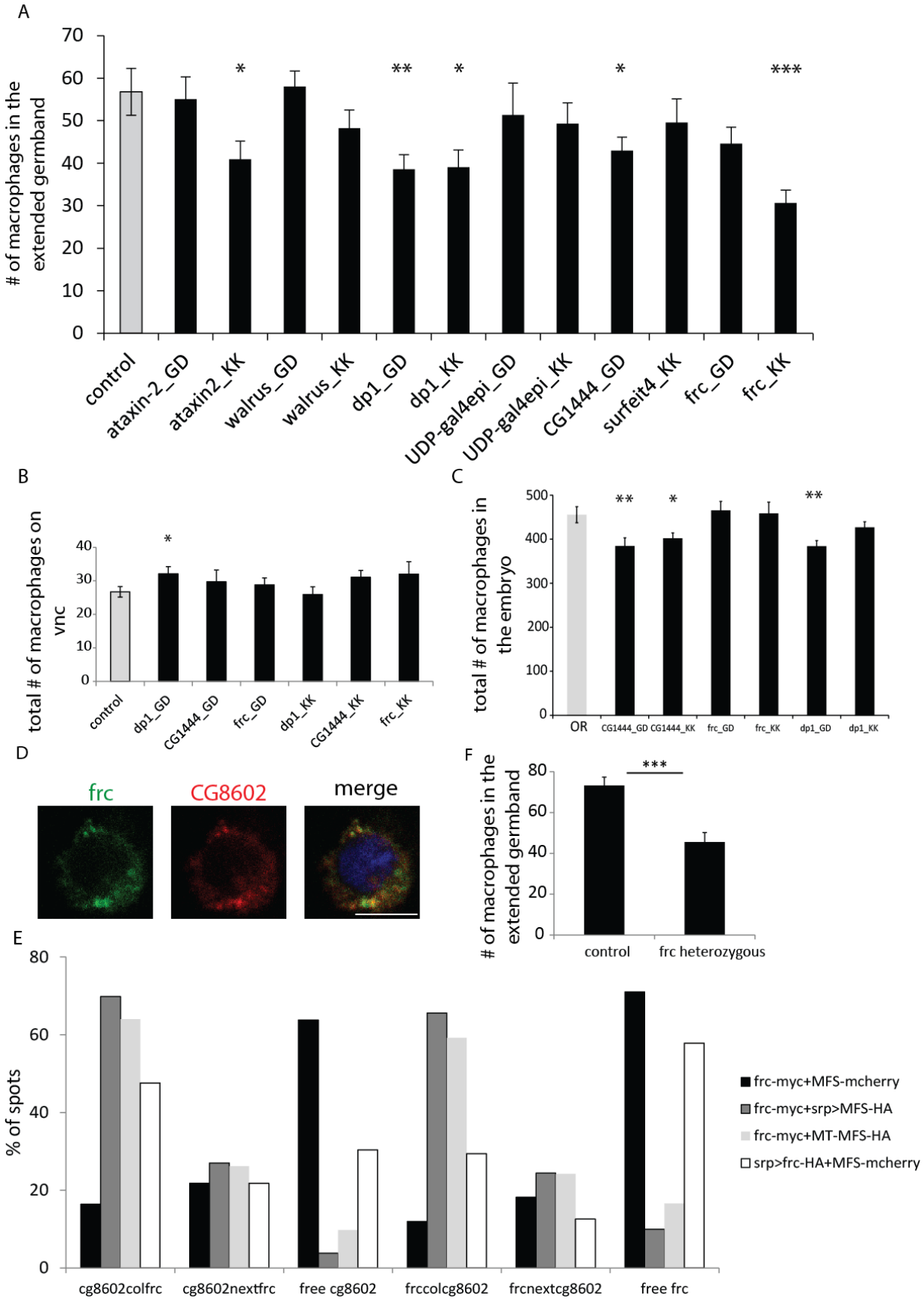
A
# of macrophages in the extended germband
control
ataxin-2_GD
ataxin2_KK
walrus_GD
walrus_KK
dp1_GD
dp1_KK
UDP-gal4epi_GD
UDP-gal4epi_KK
CG1444_GD
surfeit4_KK
frc_GD
frc_KK
B
total # of macrophages on vnc
C
total # of macrophages in the embryo
OR
CG1444_GD
CG1444_KK
frc_GD
frc_KK
dp1_GD
dp1_KK
D
frc
CG8602
merge
F
# of macrophages in the extended germband
control
frc heterozygous
E
% of spots
cg8602colfrc
cg8602nextfrc
free cg8602
frccolcg8602
frcnextcg8602
free frc
frc-myc+MFS-mcherry
frc-myc+srp>MFS-HA
frc-myc+MT-MFS-HA
srp>frc-HA+MFS-mcherry

Figure 2: Fringe connection specifically influences germband invasion and might interact with CG8602
A: RNAi screen of the genes for 7 different proteins (Ataxin-2: v34956 v108843, Walrus: v36076, v103811, Dp1: v37583, v106047, UDP-galactose-4'epimerase: v47408, v106750, CG1444: v40949, v110678, Surfeit-4: v108944, Frc: v47543, v107816) that were pulled down together with CG8602 or were detected in a two-hybrid assay (frc). **B:** The total number of macrophages on the vnc analyzed for 2 RNAi lines of 3 candidates (*frc, dp1 and CG1444*). **C:** Total number of macrophages in the embryo analyzed for 2 RNAi lines of 3 candidates (*frc, dp1 and CG1444*). **D**: A representative image of partial co-localization of CG8602 (red) and Frc (green) in S2 R+ cells **E:** Manual quantification of co-localization of spots of CG8602 and Frc in different combination of constructs **F:** Number of macrophages in the extended germband in control and heterozygous mutant for *frc*.
Scale bar in D is 5µM. Significance in A, B, C, F was analyzed by Student's t-test.

tagged). We co-expressed it with either FLAG-HA tagged (DPiM project) or a 3xmCherry tagged CG8602 (made by Julia Biebl) in S2 R+ cells. We conclude that Fringe connection and CG8602 are partially co-localized (Fig 2D, E). Co-localization and pull down does not definitively indicate a functional interaction, therefore we aimed to perform a genetic interaction test (double heterozygous mutants). Unfortunately, *frc* is haploinsufficient so we could not analyze the potential interaction between these two genes (Fig 2F).

Notch might not play a role in invasive migration

Frc was shown to be important for the proper glycosylation and therefore functionality of Notch (Goto et al., 2001; Selva et al., 2001). Notch was shown before to be a component of the hemocyte differentiation program. Notch promotes crystal cell differentiation, preventing the cells from adopting other cell fates and simultaneously promotes morphological characteristics of crystal cell differentiation (Lebestky et al., 2000; Terriente-Felix et al., 2013). However, one study showed that Notch is neither necessary nor sufficient for crystal cell development in embryos (Bataillé et al., 2005).

We therefore wondered whether CG8602 could influence hemocyte maturation/ differentiation in general on a transcriptional level. To test this, we performed qPCR analysis of a few macrophage-specific genes (*rhoL, PVR, papilin, draper* and srpHemo measured through expression of *mCherry* in *srpHemo-3mCherry* flies) on FACS-sorted macrophages from stage 12 embryos and showed that there is no significant change in expression on the RNA level of any of them (Fig 3A).

notch is not enriched in macrophages compared to other tissues (Fig 3B). However, the question is whether it could function in macrophages in other pathways than only crystal cell differentiation. Staining with a Delta antibody shows the potential ligand to be around macrophages (Fig 3C). To assess the role of Notch in tissue invasion, we performed hemocyte-specific RNAi against *notch* and analyzed the number of macrophages entering the extended germband. We got no significant change in the number of macrophages (Fig 3D). However, this experiment was done using RNAi what brings some limitations, e.g. RNAi not being strong enough to cause the phenotype or produced too late to actually influence migration, especially if assumed that it could function through influencing/modulating differentiation. Therefore, the question of Notch involvement needs to be addressed more carefully to make a firm conclusion.

Figure 3

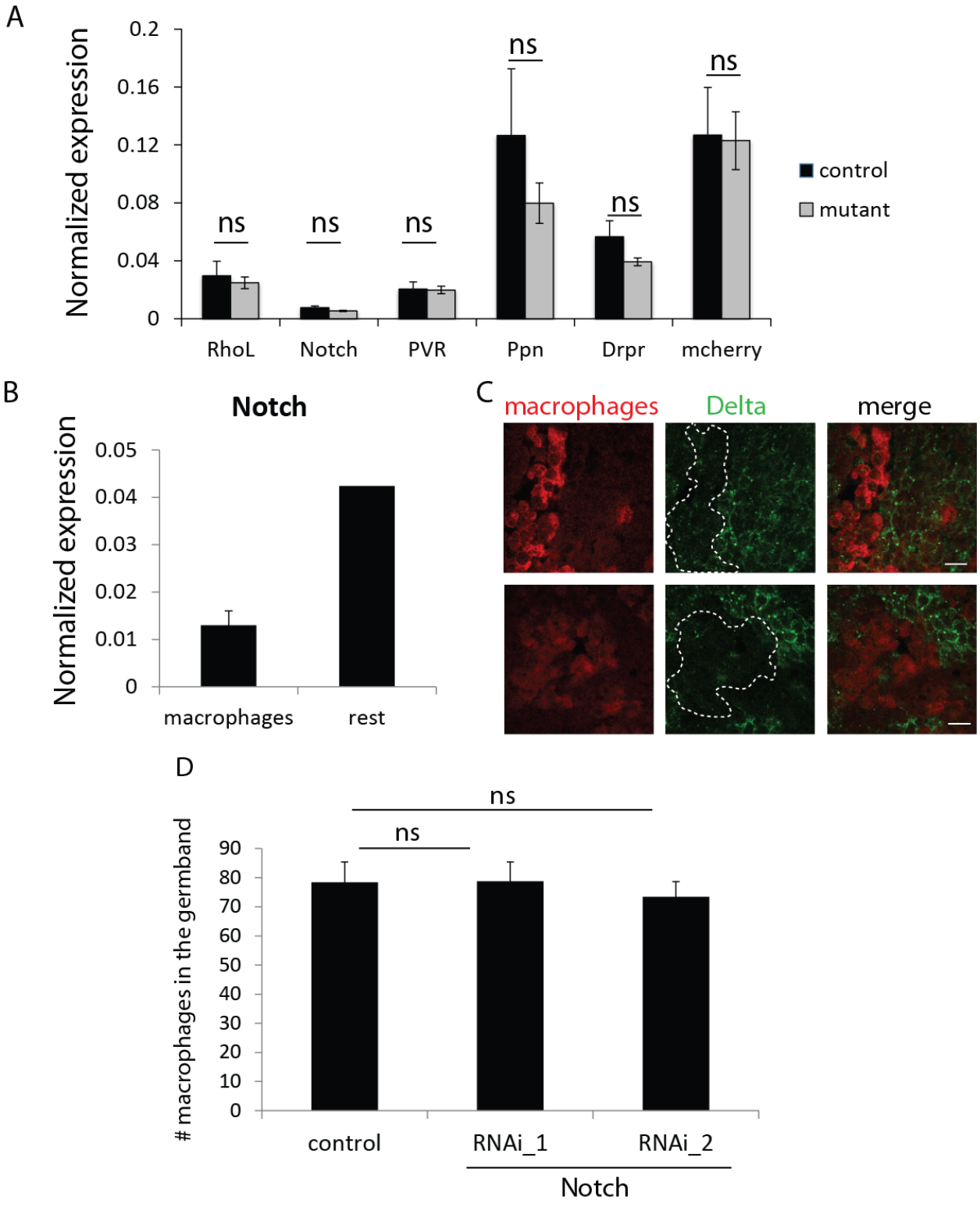

Figure 3: Notch might not play a role in invasive migration of embryonic macrophages

A: Expression of macrophage genes (*rhoL, notch, PVR, ppn, drpr, srpHemo* analyzed by expression of *srpHemo-3xmCherry* construct) normalized to housekeeping gene in the control and *CG8602* mutant. **B:** Expression of Notch in macrophages (mCherry positive cells) and randomly collected non-positive cells (mCherry negative cells from the same embryos, marked as rest) normalized to a housekeeping gene. **C:** Delta staining (green) in the head of early stage 12 embryos . Macrophages are marked with *srpHemo-3xmCherry* (red) **D:** Macrophage-specific RNAi of Notch (v1112, v27229 from VDRC).
Scale bar in C is 10 µm. Significance in A and D is analyzed by Student t-test.

N Cadherin degradation is delayed in CG8602 mutant

CG8602 is co-localized and potentially interacting with a sugar transporter Frc. This raised the possibility that it could play a role in glycosylation (for more details see Chapter 3). One of the important players in cell adhesion that is known to be regulated by glycosylation is Cadherin (Carvalho et al., 2016; Larsen et al., 2017; Xu et al., 2017). We were therefore wondering whether CG8602 could potentially influence cadherins. We stained control and mutant embryos (Fig 4A) with DE-Cad and DN-Cad antibody and detected no obvious change in their staining, localization or morphology of mesoderm and ectoderm in the germband before and at the time of the macrophage entry.

Drosophila macrophages are born in head mesoderm that expresses DN-Cadherin. We therefore checked DN-Cad dynamics in the macrophages anlage. In control embryos, there is strong staining at stage 8 (Fig 4B) that slowly decreases through stage 10. At stage 12, there is very little DN-Cad left (Fig 4B). As a next step, we stained mutant and control embryos with DN-Cadherin antibody. In the *CG8602* mutant, DN-Cadherin downregulation seems to be delayed as there is still a lot of staining on the macrophages that are entering the extended germbad which is not the case for the control (Fig 4C). To confirm this result, we use Imaris to quantify the signal intensity. The result shows an approximately doubling of the signal for DN-Cad staining in the mutant embryos compared to the control (Fig 4D). We therefore conclude that DN-Cadherin downregulation, internalization or degradation is delayed in the $CG8602^{EP3102}$ mutant.

Discussion

In our secondary screen, we identified a potential player in tissue invasion that seems to be specific for this process as it does not influence migration on the vnc or cell proliferation. This protein potentially interacts with a sugar transporter called Fringe connection. As Fringe connection regulates Notch through glycosylation, CG8602 could potentially play a role in this regulation as well. However, Notch RNAi specifically in macrophages does not show a significant change in the number of macrophages in the extended germband therefore the role of Notch in hemocytes outside of differentiation is debatable.

Another option for its function (that is not mutually exclusive with a role in the Notch pathway) is through regulation of DN-Cadherin degradation and or internalization. DN-Cadherin is expressed in the hemocyte anlage as they are of mesodermal origin but when they start to migrate towards the extended germband, it is downregulated. Intriguingly, it stays up in crystal cells that do not migrate out from the head (Fig 4E). We hypothesize that downregulation/ internalization/ degradation of DN-Cadherin is needed for proper migration and that DN-Cadherin on the surface causes macrophages to stay in the head for a longer time, slows macrophages down and/or negatively influences their ability to enter the extended germband.

Figure 4

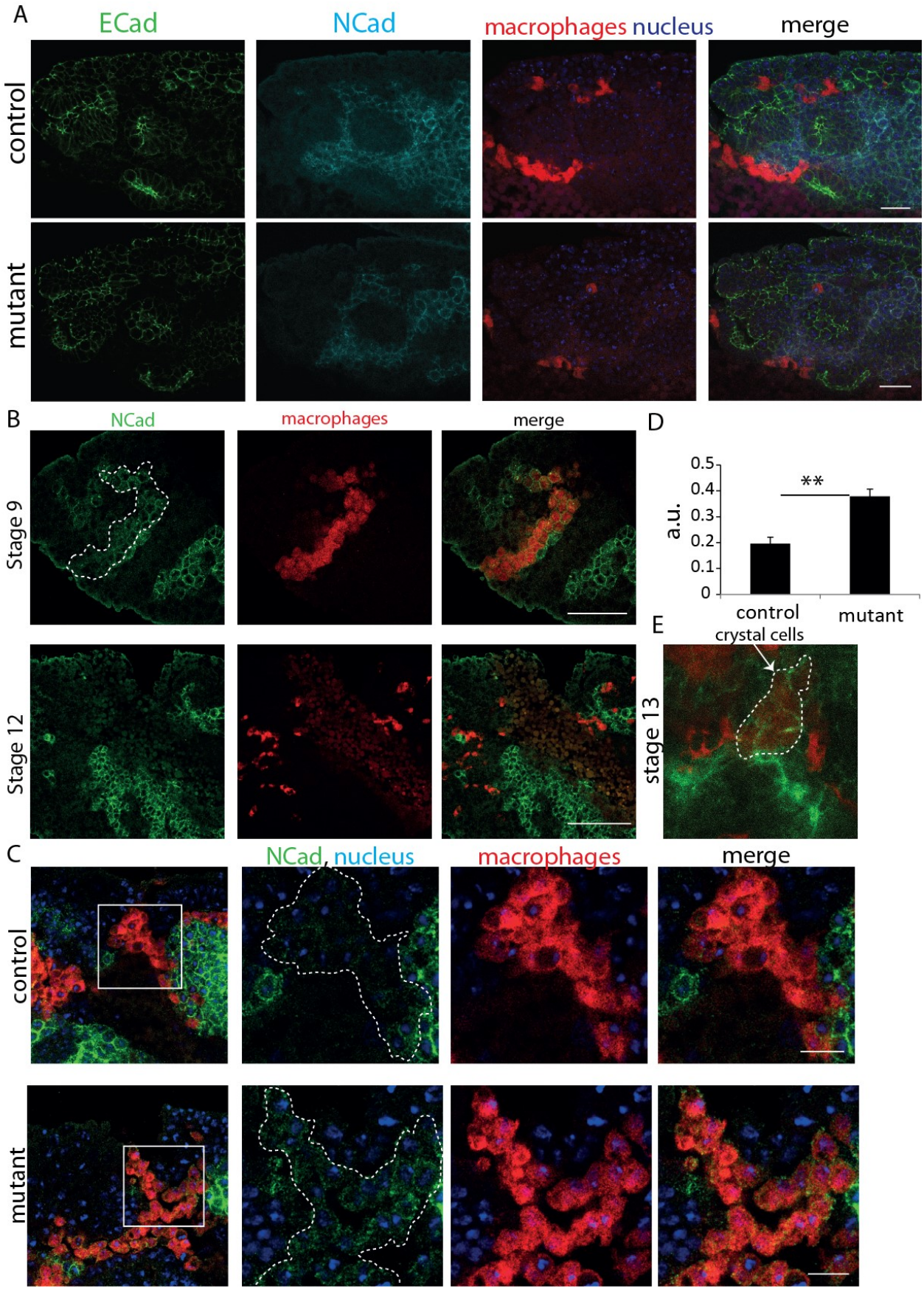
A
ECad
NCad
macrophages nucleus
merge
control
mutant
B
NCad
macrophages
merge
Stage 9
Stage 12
D
a.u.
0.5
0.4
0.3
0.2
0.1
0
**
control
mutant
E
crystal cells
stage 13
C
NCad, nucleus
macrophages
merge
control
mutant

Figure 4: DN-Cadherin degradation is delayed in *CG8602* mutant

A: Confocal images of germband entry in stage 12 control and CG8602 mutant embryos stained with the ectodermal marker (DE-Cadherin, green), the mesodermal marker (DN-Cadherin, cyan) and DAPI (blue) to visualize nuclei. Macrophages are marked by 3xmcherry expression (red). **B:** DN-Cadherin staining (green) in stage 9 (top) and stage 12 (bottom) embryo. Macrophages are marked by 3xmCherry expression (red). White dashed line in stage 9 embryo shows the position of macrophages in the head. C: DN-Cadherin staining (green) in early stage 12 embryo control (top) and *CG8602* mutant (bottom). Macrophages are marked by 3xmCherry expression (red). White dashed line shows the position of macrophages. **D**: Quantification of DN-Cadherin staining in the macrophages normalized to the mesoderm in the germband in the control and *CG8602* mutant. **E**: A confocal image of the head of a stage 13 embryo. The dashed area marks and the arrow points to the probable position of crystal cells.

Scale bar is 20µm in A, 50 µm in B and 10 µm in C. Significance in D was analyzed by Student t-test.

Our current working model is shown in Figure 5. We propose that CG8602 is a Golgi-localized protein that influences the glycosylation of an unknown protein that subsequently localizes to the plasma membrane where it is responsible for the correct timing of DN-Cadherin internalization. In the mutant macrophages, incorrect glycosylation could affect the unknown protein's degradation or its functionality or localization. We hypothesize that DN-Cadherin downregulation/ internalization in macrophages is needed to modulate their migration properties as well as to decrease their binding to the mesoderm in the extended germband which contains a large amount of DN-Cad on its surface. Excessive interaction with DN-Cadherin on the surface of the mesoderm could lead to macrophages being stuck at the entry site or moving slower inside the germband compared to wild-type macrophages.

The model based on DN-Cadherin has an unknown component that needs to be revealed and assumes a role for CG8602 in glycosylation that is described more in detail in Chapter 3.

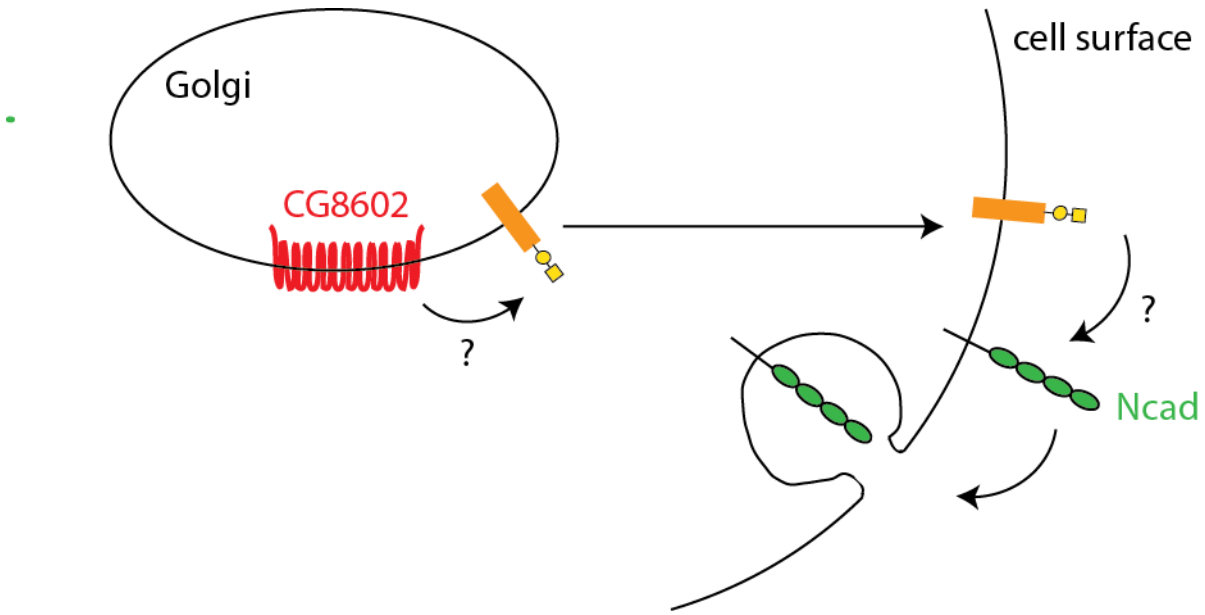

Figure 5: Model

Material and methods

In this section, I describe only material and methods that are not described in Chapter 3

Fly lines

srpHemo-GAL4 was provided by K. Brückner (UCSF, USA) (Brückner et al., 2004). The stocks *w1118; CG8602^{3102}* (BDSC-17262), *w^{-}; P{w[+mC]=UAS-mCherry.NLS}2;MKRS/Tm6b, Tb[1]* (BDSC-38425); *y[1] w[67c23]; P{y[+mDint2] w[BR.E.BR]=SUPor-P}KG05284 ry[506*] (BDSC-13990); *w[1118]; P{w[+mC]=EP}Vha68-2[EP2364]/CyO* (BDSC-17243); *y1 w67c23; P{lacW}l(2)09851k08138/CyO (BDSC-10777)* were obtained from the Bloomington *Drosophila* Stock Centre, Bloomington, USA. The RNAi lines *v106783, v42822, v34956, 108843, v36076, v103811, v37583, v106047, v47408, v106750, v40949, v110678, v108944, v47543, v107816, v1112; v 27229* were obtained from the Vienna *Drosophila* Resource Center (VDRC), Vienna, Austria. Line w*-; P{w[+mC; srpHemo-3xmCherry},* was published previously (Gyoergy et al., 2018).

Exact genotype of Drosophila lines used in Figures:

Figure 1F-I: Contro*l: w-; srpHemo-Gal4 UAS-mCherry::nls; +*. *CG8602* mutant*: w-; srpHemo-Gal4 UAS-mCherry::nls; P{EP}CG8602^{3102}* **Figure 1J-L**: Control: *w-; srpHemo-Gal4 UAS-GFP; +*. *CLN7* mutant*: w-; srpHemo-Gal4 UAS-GFP; P{SUPor-P}KG05284* **Figure 1M-P**: Control: *w-; +*; *srpHemo-Gal4 UAS-GFP UAS-H2A::RFP; vha68-2* mutant: *w-*; P{EP}Vha68-2EP2364; *srpHemo-Gal4 UAS-GFP UAS-H2A::RFP;* **Figure 1Q-R**: Control: *w-; +*; *srpHemo-Gal4 UAS-GFP UAS-H2A::RFP; l(2)09851* mutant: *w-; P P{EPgy2}l(2)09851EY06365*; *srpHemo-Gal4 UAS-GFP UAS-H2A::RFP* **Figure 1S-T**: Control: *w-,UAS-Dcr2/+; +*; *srpHemo-Gal4 UAS-GFP UAS-H2A::RFP/+* RNAi1: : *w-,UAS-Dcr2/+; RNAi cwo (*v106783)/+ ; *srpHemo-Gal4 UAS-GFP UAS-H2A::RFP/+,* RNAi2: : *w-,UAS-Dcr2/+; RNAi cwo (*v42822)/+ ; *srpHemo-Gal4 UAS-GFP UAS-H2A::RFP/+,* **Figure 2 A-C:** Control: *w-,UAS-Dcr2/+; +*; *srpHemo-Gal4 UAS-GFP UAS-H2A::RFP/+, ataxin-2_GD: : w-,UAS-Dcr2/+; +; srpHemo-Gal4 UAS-GFP UAS-H2A::RFP/v34956, ataxin-2_KK: w-,UAS-Dcr2/+; v108843/+; srpHemo-Gal4 UAS-GFP UAS-H2A::RFP/+, walrus_GD: w-,UAS-Dcr2/+; v36076/+; srpHemo-Gal4 UAS-GFP UAS-H2A::RFP/+, walrus_KK: w-,UAS-Dcr2/+; v103811/+; srpHemo-Gal4 UAS-GFP UAS-H2A::RFP/+, dp1_GD: w-,UAS-Dcr2/+; v37583/+; srpHemo-Gal4 UAS-GFP UAS-H2A::RFP/+, dp1_KK: w-,UAS-Dcr2/+; v106047/+; srpHemo-Gal4 UAS-GFP UAS-H2A::RFP/+, UDP_gal4epi_GD: w-,UAS-Dcr2/+; +; srpHemo-Gal4 UAS-GFP UAS-H2A::RFP/v47408, UDP_gal4epi_KK: w-,UAS-Dcr2/+; v106750/+; srpHemo-Gal4 UAS-GFP UAS-H2A::RFP/+, CG1444_GD: w-,UAS-Dcr2/+; v40949/+; srpHemo-Gal4 UAS-GFP UAS-H2A::RFP/+, CG1444_KK: w-,UAS-Dcr2/+; v110678/+; srpHemo-Gal4 UAS-GFP UAS-H2A::RFP/+, surfeit4_KK: w-,UAS-Dcr2/+; v108944/+; srpHemo-Gal4 UAS-GFP UAS-H2A::RFP/+, frc_GD: w-,UAS-Dcr2/+; +; srpHemo-Gal4 UAS-GFP UAS-H2A::RFP/v47543, frc_KK: w-,UAS-Dcr2/+; v107816/+; srpHemo-Gal4 UAS-GFP UAS-H2A::RFP/+,* **Figure 2F***:* Contro*l: w-; srpHemo-Gal4 UAS-mCherry::nls; +*, *frc* heterozygous: *w-; srpHemo-Gal4 UAS-mCherry::nls*; *frc00702P[Bac]/+.* **Figure 3A**: Control: *w-; +, srpHemo-3xmCherry. CG8602* mutant: *w-; +, srpHemo-3xmCherry P{EP}CG8602^{3102}* **Figure 3B**: *w-; +, srpHemo-3xmCherry* **Figure 3C:** Control: *w-; +, srpHemo-3xmCherry. CG8602* mutant: *w-; +, srpHemo-3xmCherry P{EP}CG86023102,* **Figure 3D**: Control: *w-; srpGal4/+; srpHemo-H2A::3xmcherry/+;* RNAi1: *w-; srpGal4/ v1112; srpHemo-H2A::3xmcherry/+* ; RNAi2: *w-; srpGal4/+; srpHemo-H2A::3xmcherry/v 27229.* **Figure**

4A-E: Control: *w-; +, srpHemo-3xmCherry. CG8602* mutant: *w-; +, srpHemo-3xmCherry P{EP}CG86023102*

qPCR

RNA was isolated from approximately 50,000 mCherry positive or mCherry negative FACS sorted macrophages using RNeasy Plus Micro Kit (Qiagen, Hilden, Germany following manufacturer's protocol. Further steps were according to the manufacturers protocol. The resulting RNA was used for cDNA synthesis using Sensiscript RT Kit (Qiagen, Hilden, Germany) and oligo dT primers. A Takyon qPCR Kit (Eurogentec, Liege, Belgium) was used to mix qPCR reactions based on the provided protocol. qPCR was run on a LightCycler 480 (Roche, Basel, Switzerland) and data were analyzed in the LightCycler 480 Software and Prism (GraphPad Software). Data are represented as relative expression to a housekeeping gene ($2^{-\Delta ct}$). Primer sequences utilized for flies were obtained from the FlyPrimerBank http://www.flyrnai.org/FlyPrimerBank).

RhoL fw 5'CCTGAGCTATCCCAGTACCAA
rv 5'ACCACTTGCTTTTCACGTTTTC
Notch fw 5'CGCTTCCTGCACAAGTGTC
rv 5'GCGCAGTAGGTTTTGCCATT
PVR fw 5'GTGACTTTGGTCTGGCTCG
rv 5'GATTCCAGCGCCAGC
Ppn fw 5'GCCTGCGAAGAGATGATCGT
rv 5'CCGGACAGTCTTGGGTGTTG
Drpr fw 5'TCCACCTATCGCATTAAACACC
rv 5'ACAGTCCCTCACAATACGGTT
mCh fw 5'ACATCCCCGACTACTTGAAGC
rv 5'ACCTTGTAGATGAACTCGCCG
RpL32: Fw 5'AGCATACAGGCCCAAGATCG
Rv 5'TGTTGTCGATACCCTTGGGC

Embryo Immunochemistry

For staining, embryos were fixed with 17% formaldehyde/heptane for 20 min followed by ethanol devitellinization (delta staining) or hand devitellinized (DN-Cadherin and DE-Cadherin). Fixed embryos were blocked in BBT (0.1M PBS + 0,1% TritonX-100 + 0,1% BSA) for 2 hours at RT. Antibodies were used at the following dilutions: α-Delta (C594.9B; DSHB; mouse (Qi et al., 1999)) 1:10, α-DN-Cadherin (DN-Ex #8; DSHB; rat (Iwai et al., 1997) 1:10; α-DE-Cadherin (Santa Cruz; rabbit) 1:50 and incubated overnight at 4°C (α-Delta) or room temperature (α-DN-Cadherin, α-DE-Cadherin). Afterwards, embryos were washed in BBT for 2 hours, incubated with secondary antibodies (Thermo Fisher Scientific, Waltham, Massachusetts, USA) at RT for 2 hours, and washed again for 2 hours. Vectashield with DAPI (Vector Laboratories, Burlingame, USA) was then added. After overnight incubation in Vectashield at 4°C, embryos were mounted on a slide and imaged with a Zeiss Inverted LSM700 Confocal Microscope using a Plan-Apochromat 63X/1.4 Oil Objective.

DN-Cadherin quantification

DN-Cadherin staining on macrophages was quantified using Imaris software (Bitplane). The mcherry signal from macrophages was used to set up a mask; signal intensity for the 488 channel in the mask was then measured and normalized to the 488 signal intensity in the mesoderm inside of the extended germband.

Table 1: Proteins pulled-down with CG8602 in S2 R+ cells (Guruharsha et al., 2011)

Number	Name	Description	Expression stage 10-12	Unique peptides
CG7393	p38b	wing morphogenesis,immune response,protein amino acid phosphorylation,,regulation of BMP signaling pathway,response to stress, response to salt stress	11-12: hindgut, faint ubiquitous, trunk mesoderm, midgut	12
CG6214	Multidrug-Resistance like Protein 1	transmembrane transport	no data	7
CG8385	ADP ribosylation factor at 79F	endosome transport,neurotransmitter secretion,cell shape regulation,cell adhesion,protein amino acid ADP-ribosylation,small GTPase signal transduction	ubiquitous	7
CG1444	-	oxidation reduction	9-10: procephalic ectoderm, central brain, VNC, mesoderm, germ cell, 11-12: trunk mesoderm, vent epidermis, muscle sys, midgut, brain, fat body/gonad, VNC	6
CG6701	-	zinc ion binding, RNA interference	no data	6
CG5215	Zinc-finger protein at 72D	phagocytosis, engulfment	ubiquitous	5
CG9012	Clathrin heavy chain	dsRNA transport,vesicle-mediated transport,synaptic vesicle coating,neurotransmitter secretion,sperm individualization,intracellular protein transport	no data	5
CG31729	-	cation transport,phospholipid transport,ATP biosynthetic process	ubiquitous	5

CG8258	-	mitotic spindle organization,protein folding	9-10: endoderm, mesoderm, faint ubiquitous 11-12: hindgut, mesoderm, Malpighian tubule, anal pad, muscle sys, midgut, faint ubiquitous	5
CG13472	-	spliceosome assembly	ubiquitous	4
CG6995	Scaffold attachment factor B	regulation of alternative nuclear mRNA splicing, via spliceosome	ubiquitous	4
CG5170	Dodeca-satellite-binding protein 1	heterochromatin formation,chromosome segregation,chromosome condensation,positive regulation of translation	9-10: endoderm, inclusive hindgut, 11-12: hindgut, mesoderm, midgut,salivary gland body	4
CG3584	Quaking related 58E-3	regulation of alternative nuclear mRNA splicing, via spliceosome,apoptosis	ubiquitous	4
CG6647	Porin	anion transport,transmembrane transport,phototransduction,ion transport,mitochondrial transport	ubiquitous	3
CG43443	Hu li tai shao	spectrosome, centrosome and fusome organization;ocyte fate determination,germ-line cyst formation,cystoblast division,ring canal formation, actin assembly	no data	3
CG12030	UDP-galactose 4'-epimerase	cellular metabolic process,galactose metabolic process	9-10: amnioserosa, yolk nuclei, 11-12: amnioserosa, yolk nuclei, post midgut, plasmatocytes, salivary gland body	3
CG4611	-	-	no data	3
CG5655	Repressor splicing factor 1	negative regulation of nuclear mRNA splicing, via spliceosome	ubiquitous	3
CG14786	-	oxidation reduction	11-12: midgut	3
CG11258	L20	translation	no data	3
CG1341	Regulatory particle triple-A ATPase 1	proteolysis,cellular response to DNA damage stimulus	ubiquitous	3

CG9159	Kruppel homolog 2	-	no data	3
CG4729	-	metabolic process	ubiquitous	2
CG5166	Ataxin-2	bristle development,oocyte differentiation,phagocytosis, engulfment,compound eye development,regulation of actin filament polymerization	ubiquitous	2
CG8996	Walrus	oxidative phosphorylation; morphogenesis of Malpighian tubules,open tracheal, epithelium and ectodermal gut; head involution	ubiquitous	2
CG1483	Microtubule -associated protein 205	microtubule-based process	11-12: trunk mesoderm, dors pharyngeal muscle, visceral muscle, muscle sys, VNC, brain, somatic muscle	2
CG12076	YT521-B	RNA metabolic process	no data	2
CG3689	-	mRNA cleavage	ubiquitous	2
CG10622	Sucb	tricarboxylic acid cycle	11-12: hindgut proper, Malpighian tubule, ant midgut, post midgut	2
CG6643	-	-	no data	2
CG17291	Protein phosphatase 2A at 29B	phagocytosis, engulfment,chromosome segregation,spindle assembly,centrosome cycle,protein amino acid dephosphorylation,mitotic spindle organization	no data	2
CG3458	Topoisomer ase 3β	DNA catabolic process, endonucleolytic,DNA unwinding during replication,DNA topological change	no data	2
CG9366	RhoL	cell migration,ovarian cell and mesoderm development,small GTPase signal transduction,regulation of cell shape,response to DNA damage,cell adhesion	4-10: head mesoderm, 11-12: plasmatocytes	2
CG8231	T-cp1ζ	protein folding,centriole replication,mitotic spindle organization	9-10: post endoderm, germ cell, ant endoderm, mesoderm	2

CG1258	Pavarotti	mitosis and meiosis,smoothened signaling pathway,microtubule-based movement,PNS development, regulation of NFAT protein import into nucleus	11-12: neuroblasts, germ cell, VNC, brain, dorsomedial neurosecretory cell	2
CG9742	SmG	nuclear mRNA splicing, via spliceosome,mitotic spindle organization,spliceosome assembly	ubiquitous	2
CG4199	-	oxidation reduction,cell redox homeostasis	9-10: no staining, 11-12: leading edge cell, ant midgut, post midgut	2
CG11505	-	nucleotide binding; nucleic acid binding	no data	2
CG8309	TANGO7	Golgi organization	ubiquitous	2
CG15098	-	-	11-12: midgut	1
CG5479	L43	translation	11-12: hindgut, trunk mesoderm, ubiquitous, midgut	1
CG13608	S24	translation	no data	1
CG5183	KDEL receptor	intra-Golgi vesicle-mediated transport,retrograde vesicle-mediated transport, Golgi to ER,protein retention in ER lumen	11-12: hindgut, trunk mesoderm, tracheal, foregut, midgut, salivary gland body, fat body/gonad, ubiquitous	1
CG15735	-	Anticodon-binding domain	ubiquitous	1
CG4043	Rrp46	mRNA processing	no data	1
CG11271	Ribosomal protein S12	translation	ubiquitous	1
CG5497	S28	translation	11-12: midgut	1
CG3800	-	zinc ion binding; nucleic acid binding.	ubiquitous	1
CG31363	Jupiter	positive regulation of microtubule polymerization	ubiquitous	1
CG3204	Ras-associated protein 2-like	small GTPase mediated signal transduction,germ-line stem cell maintenance	no data	1
CG11027	ADP ribosylation factor at 102F	small GTPase signal transduction,synaptic vesicle endocytosis,neurotransmitter secretion,protein transport,protein amino acid ADP-ribosylation	ubiquitous	1

CG10849	Sc2	lipid metabolic process	no data	1
CG8427	SmD3	lymph gland, CNS, PNS and muscle development;mitotic spindle organization,nuclear mRNA splicing, neuron differentiation	no data	1
CG11246	Rpb8	transcription from RNA polymerase II promoter	1-10: ubiqiutous, 11-12: midgut	1
CG14981	Maggie	intracellular protein transport.	11-12: trunk mesoderm, dors pharyngeal muscle, muscle sys, midgut, somatic muscle	1
CG42481	-	-	no data	1
CG6202	Surfeit 4	lateral inhibition	9-10: mesoderm, 11-12: trunk mesoderm, muscle sys, salivary gland, plasmatocytes, salivary gland body	1
CG11857	-	vesicle-mediated transport	ubiquitous	1
CG9035	Translocon-associated protein δ	protein retention in ER lumen	9-10: head mesoderm, 11-12: hindgut, trunk mesoderm, garland cell, tracheal, foregut, midgut, salivary gland body, fat body/gonad	1

Chapter 3: A conserved Major Facilitator Superfamily member orchestrates a subset of O-glycosylation to aid macrophage tissue invasion

Katarína Valošková[1§], Julia Biebl[1§], Marko Roblek[1], Shamsi Emtenani[1], Attila Gyoergy[1], Michaela Mišová[1], Aparna Ratheesh[1, 3], Patrícia Reis-Rodrigues[1], Kateryna Shkarina[1,4], Ida S.B. Larsen[2], Sergey Y. Vakhrushev[2] , Henrik Clausen[2], Daria E. Siekhaus[1]

§: These authors contributed equally

1 – Institute of Science and Technology Austria, Am Campus 1, 3400 Klosterneuburg, Austria

2 - Copenhagen Center for Glycomics, Departments of Cellular and Molecular Medicine, Faculty of Health Sciences, University of Copenhagen, Blegdamsvej 3B, DK-2200 Copenhagen N, Denmark

3 – Current address: Centre for Mechanochemical Cell Biology and Division of Biomedical Sciences, Warwick Medical School, University of Warwick, Coventry, United Kingdom

4- Current address: University of Lausanne, Department of Biochemistry, Chemin des Boveresses 155-CP51-CH-1066 Epalinges, Switzerland

For experimental contributions of authors, see the table 3 at the end of this chapter.

Introduction

The set of proteins expressed by a cell defines much of its potential capacities. However, a diverse set of modifications can occur after the protein is produced to alter its function and thus determine the cell's final behavior. One of the most frequent and variable of such alterations is glycosylation, in which sugars are added onto the oxygen (O) of a serine or threonine or onto the nitrogen (N) of an asparagine (Kornfeld and Kornfeld, 1985; Marshall, 1972; Ohtsubo and Marth, 2006). O-linked addition can occur on cytoplasmic and nuclear proteins in eukaryotes (Comer and Hart, 2000; Hart et al., 2011), but the most extensive N- and O- linked glycosylation occurs during the transit of a protein through the secretory pathway. A series of sugar molecules are added starting in the endoplasmic reticulum (ER) or cis-Golgi and continuing to be incorporated and removed until passage through the trans Golgi network is complete (Aebi, 2013; Stanley et al., 2009). N-linked glycosylation is initiated in the ER at consensus NxS/T X≠P site, whereas the most common GalNAc-type O-linked glycosylation is initiated in the early Golgi and glycosites display no clear sequence motifs, apart from a prevalence of neighboring prolines (Bennett et al., 2012; Christlet and Veluraja, 2001). Glycosylation can affect protein folding, stability and localization as well as serve specific roles in fine-tuning protein processing and functions such as protein adhesion and signaling (Goth et al., 2018; Varki, 2017). The basic process by which such glycosylation occurs has been well studied. However our understanding of how specific glycan structures participate in modulating particular cellular functions is still at its beginning.

The need to understand the regulation of O-glycosylation is particularly relevant for cancer (Fu et al., 2016; Häuselmann and Borsig, 2014). The truncated O-glycans called T and Tn antigen are not normally found on most mature human cells (Y Cao et al., 1996) but up to 95% of cells from many cancer types display these at high levels (Boland et al., 1982; Y Cao et al., 1996; Howard and Taylor, 1980; Limas and Lange, 1986; Orntoft et al., 1985; Springer, 1984; Springer

et al., 1975). The T O-glycan structure (Galβ1-3GalNAcα1-O-Ser/Thr) is synthesized by the large family of polypeptide GalNAc-transferases (GalNAc-Ts) that initiate protein O-glycosylation by adding GalNAc to form Tn antigen and the core1 synthase C1GalT1 that adds Gal to the initial GalNAc residues (Tian and Ten Hagen, 2009) to form T antigen (**Figure 1A**). The human C1GalT1 synthase requires a dedicated chaperone, COSMC, for folding and ER exit (Ju and Cummings, 2005). In adult humans these O-glycans are normally capped by sialic acids and/or elongated and branched into complex structures (Tarp and Clausen, 2008). However, in cancer this elongation and branching is reduced or absent and the appearance of these truncated T and Tn O-glycans correlates positively with cancer aggressiveness and negatively with long-term prognoses for many cancers in patients (Baldus et al., 2000; Carrasco et al., 2013; Ferguson et al., 2014; MacLean and Longenecker, 1991; Schindlbeck et al., 2005; Springer, 1997, 1989; Summers et al., 1983; Yu et al., 2007). The molecular basis for the enhanced appearance of T antigen in cancers is not clear (Chia et al., 2016a), although higher Golgi pH in cancer cells correlates with increases in T antigen (Kellokumpu, Sormunen and Kellokumpu, 2002). Interestingly, T antigen is also observed as a transient fetal modification (Barr et al., 1989) and cancer cells frequently recapitulate processes that happened earlier in development (Cofre and Abdelhay, 2017; Pierce, 1974). Identifying new mechanisms that regulate T antigen modifications developmentally has the potential to lead to important insights into cancer biology.

Drosophila as a classic genetic model system is an excellent organism in which to investigate these questions. *Drosophila* displays T antigen as the predominant form of GalNAc-, or mucin-type, O-glycosylation in the embryo with 18% of the T glycans being further elaborated, predominantly by the addition of GlcA (Aoki et al., 2008). As in vertebrates, the GalNAc-T isoenzymes directing the initial step of GalNAc addition to serines and threonines are numerous, with several already known to display conserved substrate specificity *in vitro* with vertebrates (Müller et al., 2005; Schwientek et al., 2002; Ten Hagen et al., 2003b). The *Drosophila* GalNAc-Ts affect extracellular matrix (ECM) secretion, gut acidification and the formation of the respiratory system (Tian and Ten Hagen, 2006; Tran et al., 2012; Zhang et al., 2010). In flies the main enzyme adding Gal to form T antigen is C1GalTA (Müller et al., 2005) whose absence causes defects in ventral nerve cord (vnc) condensation during Stage 17, hematopoetic stem cell maintenance, and neuromuscular junction formation (Fuwa et al., 2015; Itoh et al., 2016; Lin et al., 2008; Yoshida et al., 2008). While orthologous to the vertebrate Core1 synthases, the *Drosophila* C1GALTs differ in not requiring a specific chaperone (Müller et al., 2005). Most interestingly, T antigen is found on embryonic macrophages (Yoshida et al., 2008), a cell type which can penetrate into tissues in a manner akin to metastatic cancer (Ratheesh et al., 2018a; Siekhaus et al., 2010). Macrophage invasion of the germband (**Figure 1B**, arrow in **Figure 1C**) occurs between the closely apposed ectoderm and mesoderm (Ratheesh et al., 2018a; Siekhaus et al., 2010) from late Stage 11 through Stage 12. This invasion occurs as part of the dispersal of macrophages throughout the embryo (**Figure 1C**) along other routes that are mostly noninvasive, such as along the inner ventral nerve cord (vnc) (arrowhead in **Figure 1C**) (Campos-Ortega and Hartenstein, 1997; Evans et al., 2010). Given these potentially related but previously unconsolidated observations, we sought to determine the relationship between the appearance of T antigen and macrophage invasion and to use the genetic power of *Drosophila* to find new pathways by which this glycophenotype is regulated.

Results

T antigen is enriched and required in invading macrophages in Drosophila embryos

To identify glycan structures present on fly embryonic macrophages during invasion we performed a screen examining FITC-labelled lectins (see Methods for abbreviations). Only two lectins had higher staining on macrophages than on surrounding tissues (labeled enriched): PNA, which primarily binds to the core1 T O-glycan, and UEA-I, which can recognize Fucα1-2Galβ1-4GlcNAc(Molin et al., 1986; Natchiar et al., 2007) (Figure 1D, Figure 1-figure supplement 1A-B). Both glycans are associated with the invasive migration of mammalian cancer cells (Agrawal et al., 2017; Hung et al., 2014). SBA, WGA, GS-II, GS-I, ConA, MPA and BPA bound at similar or lower levels on *Drosophila* macrophages compared to flanking tissues (Figure 1D, Figure 1-figure supplement 1C-I). We saw no staining with the sialic acid-recognizing lectin LPA, and none with DBA and HPA, that both recognize α-GalNAc (Piller et al., 1990) (Figure 1D, Figure 1-figure supplement 1J-L). Thus PNA and UEA-I display enriched macrophage binding during their embryonic invasive migration.

To confirm T antigen as the source of the upregulated PNA signal in embryonic macrophages during invasion and to characterize its temporal and spatial enrichment, we used a monoclonal antibody (mAb 3C9) to the T O-glycan structure (Steentoft et al., 2011). Through Stage 10, macrophages displayed very little T antigen staining, similar to other tissues (Figure 1E, F). However, at late Stage 11 (Figure 1-figure supplement 1A) and early Stage 12, when macrophages start to invade the extended germband, T antigen staining began to be enriched on macrophages moving towards and into the germband (Figure 1E-H). Our results are consistent with findings showing T antigen expression in a macrophage-like pattern in late Stage 12 embryos, and on a subset of macrophages at Stage 16 (Yoshida et al., 2008). We knocked down the core1 synthase C1GalTA required for the final step of T antigen synthesis (Figure 1A) (Lin et al., 2008; Müller et al., 2005) using RNAi expression only in macrophages and observed strongly reduced staining (Figure 1I, Figure 1-figure supplement 1M). We conclude that the antibody staining is the result of T antigen produced by macrophages themselves.

To determine if these T O-glycans on macrophages are important for facilitating their germband invasion, we knocked down C1GalTA in macrophages with the RNAi line utilized above as well as one other and used the P element excision allele *C1GalTA[2.1]* which removes conserved sequence motifs required for activity (Lin et al., 2008). We visualized macrophages through specific expression of fluorescent markers and observed a 25 and a 33% decrease in their number in the germband for the RNAis (Figure 1J,K), and a 44% decrease in the *C1GalTA*[2.1] mutant (Figure 1L). When we counted the number of macrophages sitting on the yolk next to the germband in the strongest RNAi we observed an increase (Figure 1-figure supplement 1N) that we also observed in the C1GalT mutant (Figure 1-figure supplement 1O). The sum of the macrophages in the yolk and germband is the same in the control, RNAi knockdown (control 136.5±6.4, RNAi 142.3±6.6, p=0.7) and mutant (control 138.5±4.9, mutant, 142.3±7.4, p=0.87) arguing that macrophages in which C1GalTA levels are reduced cannot enter the germband but are retained on the yolk. We observed no effect on the migration of macrophages on the vnc, a route that does not require tissue invasion (Figure 1-figure

Valoskova et al. Figure 1

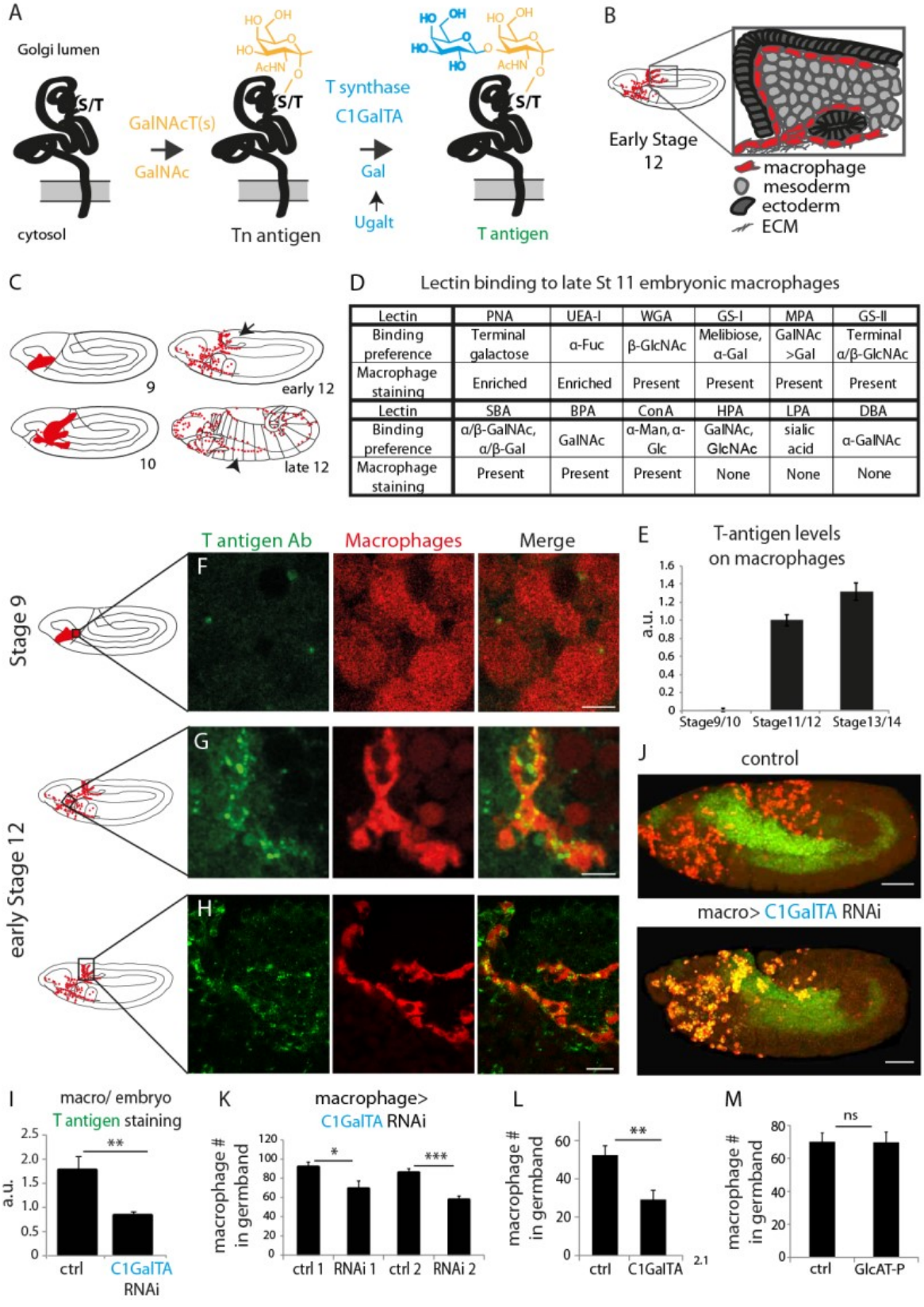

Lectin	PNA	UEA-I	WGA	GS-I	MPA	GS-II
Binding preference	Terminal galactose	α-Fuc	β-GlcNAc	Melibiose, α-Gal	GalNAc >Gal	Terminal α/β-GlcNAc
Macrophage staining	Enriched	Enriched	Present	Present	Present	Present
Lectin	SBA	BPA	ConA	HPA	LPA	DBA
Binding preference	α/β-GalNAc, α/β-Gal	GalNAc	α-Man, α-Glc	GalNAc, GlcNAc	sialic acid	α-GalNAc
Macrophage staining	Present	Present	Present	None	None	None

Figure 1: **T antigen is enriched on *Drosophila* macrophages prior to and during their invasion of the extended germband.** (**A**) Schematic of T antigen modification of serine (S) and threonine (T) on proteins within the Golgi lumen, through successive addition of GalNAc (yellow) by GalNAcTs and Gal (blue) by C1GalTs. Ugalt transports Gal into the Golgi. Glycosylation is shown at a much larger scale than the protein. (**B**) Schematic of an early Stage 12 embryo and a magnification of macrophages (red) entering between the germband ectoderm (dark grey), and mesoderm (light grey). (**C**) Schematic showing macrophages (red) disseminating from the head mesoderm in Stage 9. By Stage 10, they migrate towards the extended germband, the dorsal vessel and along the ventral nerve cord (vnc). At late Stage 11 germband invasion (arrow) begins and continues during germband retraction. Arrowhead highlights migration along the vnc in late Stage 12. (**D**) Table summarizing a screen of glycosylation-binding lectins for staining on macrophages invading the germband in late Stage 11 embryos. The listed binding preferences are abbreviated summaries of the specificities defined with mammalian glycans or simple saccharides which may have only incomplete relevance to insect glycomes. Enrichment was seen for PNA which recognizes T antigen and UEA-I which can recognize fucose. (**E**) Quantification of T antigen fluorescence intensities on wild type embryos shows upregulation on macrophages between Stage 9/10 and Stage 11/12. Arbitrary units (au) normalized to 1 for Stage 11) p <0.0001. (**F-H**) Confocal images of fixed lateral wild type embryos from (**F**) Stage 9 and (**G-H**) early Stage 12 with T antigen visualized by antibody staining (green) and macrophages by *srpHemo-3xmCherry* expression (red). Schematics at left with black boxes showing the imaged regions. (**I**) Quantification of control shows T antigen enrichment on macrophages when normalized to whole embryo. RNAi in macrophages against C1GalTA by *srpHemo(macrophage)>C1GalTA RNAi vdrc2826* significantly decreases this T antigen staining (n=8 embryos, p= 0.011). (**J**) Representative confocal images of Stage 12 embryos from control and the aforementioned C1GalTA RNAi. Macrophages marked with cytoplasmic GFP (red) and nuclear RFP (green). **(K,L)** Quantification of macrophages in the germband in Stage 12 embryos for (**K**) control and two independent RNAis against C1GalTA (*vdrc110406 or vdrc2826*) expressed in macrophages by the *srpHemo-Gal4* driver (n=21-31 embryos, p<0.0001 and 0.017) or (**L**) in control and the *C1GalTA[2.1]* excision mutant (n=23-24, p=0.0006). Macrophages labeled with *srpHemo-H2A::3xmCherry.* The RNAis and the mutant significantly decreased the macrophage number, arguing that T antigen is required in macrophages for germband entry. (**M**) Quantification of germband macrophages in early Stage 12 embryos in control and *GlcAT-P^{MI05251}* embryos shows no defect in macrophage invasion in the mutant (n=17-20, p=0.962). **E** analyzed by Kruskal-Wallis test **I, K-M** analyzed by Student's t-test. ns=p>0.05, * p<0.05; ** p<0.01; *** p<0.001. Scale bars represent 10μm in **F-H,** and 50μm in **J**. See also Figure 1-figure supplement 1.

supplement 1P) (Campos-Ortega and Hartenstein, 1997; Evans et al., 2010). 18% of T antigen in the embryo has been found to be further modified, predominantly by glucoronic-acid (GlcA) (Aoki et al., 2008). Of the three GlcA transferases found in *Drosophila* only GlcAT-P is robustly capable of adding GlcA onto the T O-glycan structure in cells (Breloy et al., 2016a; Itoh et al., 2018; Kim et al., 2003). To examine if the specific defect in germband invasion that we observed by blocking the formation of T antigen is due to the need for a further elaboration by GlcA, we utilized a lethal MI{MIC} transposon insertion mutant in the *GlcAT-P* gene. We observed no change in the numbers of macrophages within the germband in the *GlcAT-P^{MI05251}* mutant (Figure 1M) and a 20% increase in the number of macrophages on the yolk (Figure 1-figure supplement 1Q). Therefore our results strongly suggest that the T antigen we observe being upregulated in macrophages as they move towards and into the germband is itself needed for efficient tissue invasion.

An atypical MFS member acts in macrophages to increase T antigen levels

We sought to determine which proteins could temporally regulate the increase in the appearance of T O-glycans in invading macrophages. We first considered proteins required for synthesizing the core1 structure, namely the T synthase, C1GalTA, and the UDP-Gal sugar transporter, Ugalt (Aumiller and Jarvis, 2002) (Figure 1A). However, q-PCR analysis of FACS sorted macrophages

Valoskova et al Figure S1

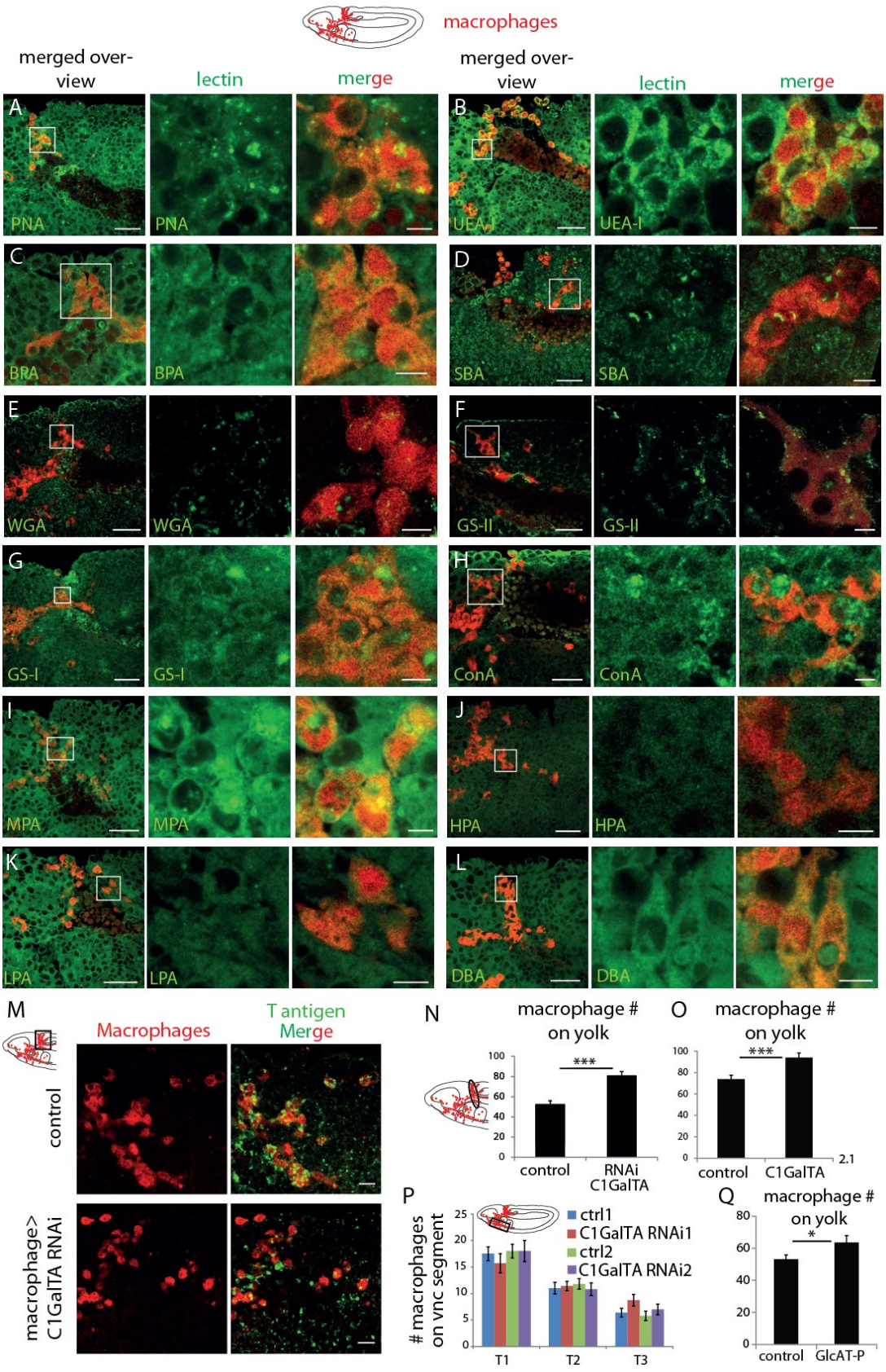

Figure 1-figure supplement 1: Lectin screen reveals enriched staining for PNA and UEA-1 on macrophages
(A-L) Confocal images of fixed late Stage 11/ early Stage 12 wild type embryos schematic above) stained with different lectins (visualized in green) indicated in green type in the lower left corner. Macrophages are detected through srpHemo-3xmCherry expression (red). Boxed area in schematic shows area of merged overview image at left. Boxed area in merged overview corresponds to the images shown magnified at right. **(M)** Confocal images of the germband from fixed early Stage 12 embryos from the control and ones in which UAS-C1GalTA RNAi is expressed in macrophages under srpHemo-GAL4 control. Macrophages visualized with an antibody against GFP expressed in macrophages (srpHemo>GFP) (red) and T antigen by antibody staining (green). Boxed area in schematic at left indicates embryo region imaged. **(N,O)** Quantification of macrophages on the yolk in fixed early Stage 12 embryos in **(N)** srpHemo>UAS-C1GalTA RNAi (vdrc 2826) and **(O)** the C1GalTA[2.1] excision mutant shows an increase in both compared to the control (n=14-24, p=0.00004 for N, p=0.0007 for O). **(P)** Quantification of macrophage number in the vnc segments shown in the schematic in fixed mid Stage 12 embryos detects no significant difference between control and srpHemo>UAS-C1GalTA RNAi embryos (n=10-20). **(Q)** Quantification of macrophages on the yolk in fixed early Stage 12 embryos in GlcAT-PMI05251 shows a 20% increase compared to the control (n=17-20, p=0.04). Significance was assessed by Mann-Whitney test in **N** and Student's t-test in **O-Q,** ns=p>0.05, *=p<0.05, ***=p<0.001. Scale bars are 30μm in overview images and 5μm in magnifications in **A-L**, 10μm in **M**.

from Stage 9-10, Stage 12, and Stage 13-17 show that though both are enriched in macrophages, neither is transcriptionally upregulated before or during Stage 12 (Figure 2A,B). We therefore examined the Bloomington *Drosophila* Genome Project (BDGP) *in situ* database looking for predicted sugar binding proteins expressed in macrophages with similar timing to the observed T antigen increase (Tomancak et al., 2007, 2002). We identified CG8602, a predicted member of the Major Facilitator Superfamily (MFS), a protein group defined by shared structural features, whose members are known to transport a diverse set of molecules across membranes (Yan, 2015). CG8602 contains regions of homology to known sugar responsive proteins and predicted sugar or neurotransmitter transporters (Figure 2C) and in a phylogenetic analysis is on a branch neighboring the SLC29 group shown to be involved in nucleoside transport (Baldwin et al., 2004; Perland et al., 2017). BDGP *in situ* hybridizations (Tomancak et al., 2007, 2002) (http://insitu.fruitfly.org/cgi-bin/ex/report.pl?ftype=10&ftext=FBgn0035763) indicate that CG8602 RNA is maternally depo-sited, with expression throughout the embryo through Stage 4 after which its levels decrease, with weak ubiquitous expression continuing through Stage 9-10. This is followed by strong enrichment in macrophages from Stage 11-12, with apparently equivalent levels of expression in macrophages entering the germband as in those migrating along other routes such as the ventral nerve cord. We confirmed this by q-PCR analysis of FACS sorted macro-phages, which detected seven-fold higher levels of CG8602 RNA in macrophages than in the rest of the embryo by Stage 9-10 and 12-fold by Stage 12 (Figure 2D). These data show that RNA expression of CG8602, an MFS protein with homology to sugar transporters increases in macrophages preceding and during the period of invasion. To determine if CG8602 could affect T antigen levels, we examined a viable P-element insertion mutant in the 5'UTR, $CG8602^{EP3102}$ (Figure 2- figure supplement 1A). This insertion displays strongly reduced CG8602 expression in FACS-sorted macrophages to 15% of wild type levels, as assessed by q-PCR (Figure 2E). We also created an excision allele, Δ33, removing the 5'UTR flanking the P-element, the start methionine, and 914 bp of the ORF (Figure 2- figure supplement 1A). This is a lethal allele, and the line carrying it over a balancer is very weak; exceedingly few embryos are laid and the embryos homozygous for the mutation do not develop past Stage 12. Therefore, we did not continue experiments with this allele, and instead utilized the insertion mutant. This $CG8602^{EP3102}$ P-element mutant displays

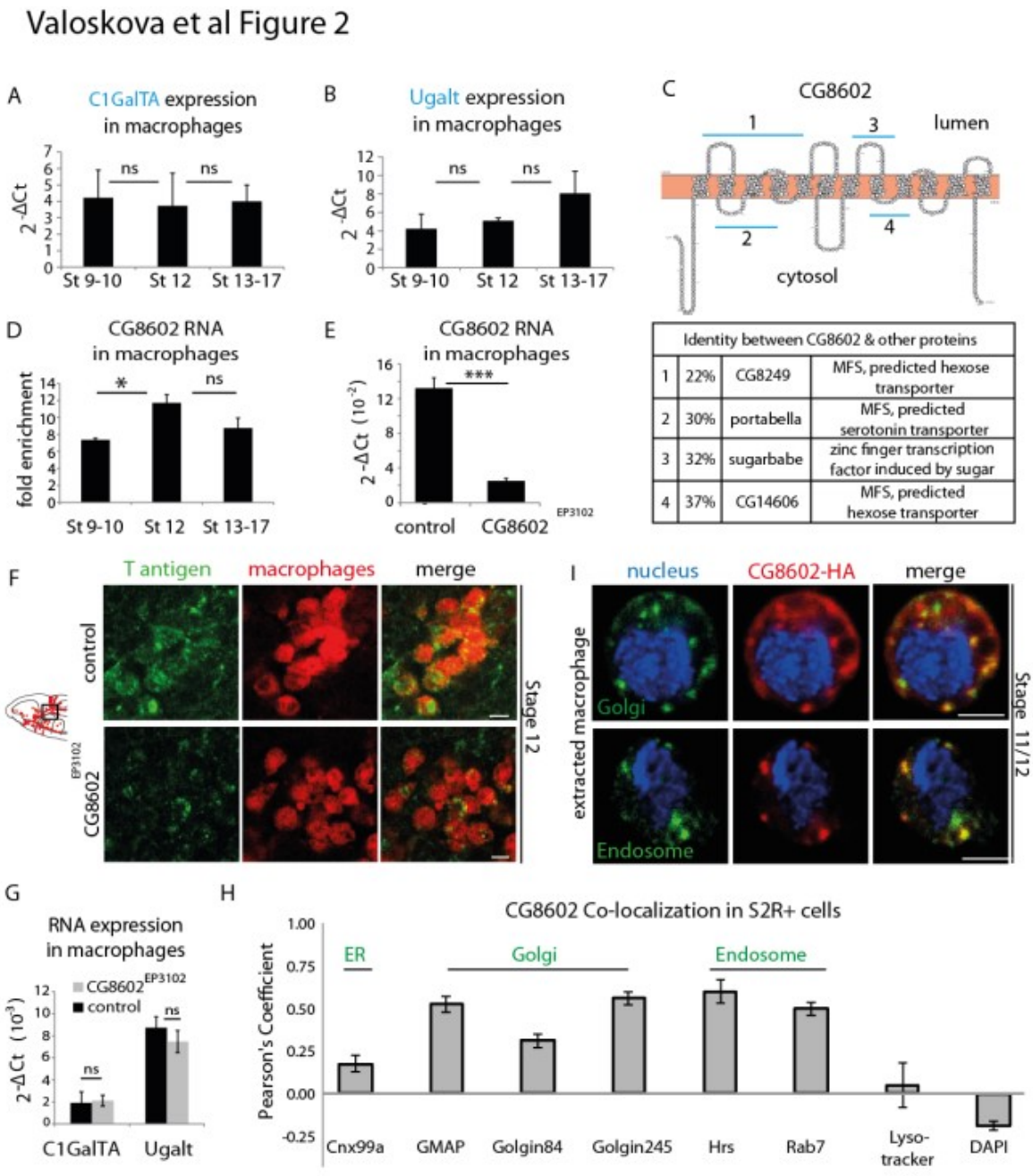

Figure 2: An atypical MFS family member, CG8602, located in the Golgi and endosomes, is required for T antigen enrichment on invading macrophages. (**A,B**) qPCR quantification ($2^{-\Delta Ct}$) of RNA levels in *mCherry+* macrophages FACS sorted from *srpHemo-3xmCherry* wild type embryos reveals no significant change in the expression of (**A**) the C1GalTA galactose transferase or (**B**) the Ugalt Gal transporter during Stage 9-17 (n=7 biological replicates, 3 independent FACS sorts). **(C)** Schematic made with Protter (Omasits et al., 2014) showing the predicted 12 transmembrane domains of CG8602. Blue lines indicate regions displaying higher than 20% identity to the correspondingly numbered *Drosophila* protein indicated below, along with the homologous protein's predicted or determined function. (**D**) Quantification by qPCR of CG8602 RNA levels in FACS sorted *mCherry+* macrophages compared to other *mCherry-* cells obtained from *srpHemo-3xmCherry* wild type embryos at Stage 9-10, Stage 12 and Stage 13-17. CG8602 macrophage expression peaks at Stage 12, during macrophage germband entry (n=3-7 biological replicates, 4 independent FACS sorts, p= 0.036). **(E)** qPCR quantification in FACS sorted *srpHemo-*

3xmCherry labeled macrophages from control and *CG8602*^{EP3102} mutant Stage 12 embryos shows an extremely strong decrease in CG8602 RNA expression in the P element insertion mutant used in this study (n=7 biological replicates, 3 independent FACS sorts, p=0.0024). **(F**) Confocal images of Stage 12 control and *CG8602*^{EP3102} mutant embryos with macrophages (red) visualized by *srpHemo-mCherry* expression and T antigen by antibody staining (green). Schematic at left depicts macrophages (red) entering the germband. Black box indicates the region next to the germband imaged at right. We observe decreased T antigen staining on macrophages in the *CG8602*^{EP3102} mutant compared to the control. **(G)** qPCR quantification ($2^{-\Delta Ct}$) of C1GalTA and Ugalt RNA levels in FACS sorted macrophages from Stage 12 embryos from control and *mrva*^{EP3102} mutant embryos shows no significant change in expression of the Gal transferase, or the Gal and GalNAc transporter in the mutant compared to the control (n=7 biological replicates, 3 independent FACS sorts). (**H**) Quantitation using Fiji of the colocalization of transfected *MT-CG8602::FLAG::HA* in fixed S2R+ cells with markers for the ER (Cnx99a), the Golgi (Golgin 84, Golgin 245, and GMAP), the early endosome (Hrs), the late endosome (Rab7), and live S2R+ cells transfected with *srp-CG8602::3xmCherry* with dyes that mark the lysosome (Lysotracker) and the nucleus (DAPI). Representative images are shown in Figure S2B-J. n=24, 23, 23, 17, 6, 22, 6 and 13 cells analyzed per respective marker. (**I**) Macrophages near the germband extracted from *srpHemo>CG8602-HA* Stage 11/12 embryos show partial colocalization of the HA antibody labeling CG8602 (red) and a Golgin 84 or Hrs antibody marking the Golgi or endosome respectively (green). Nucleus is stained by DAPI (blue). For all qPCR experiments values are normalized to expression of a housekeeping gene RpL32. Scale bars are 5μm in **F,** 3μm in **I**. Significance was assessed by Kruskal-Wallis test in **A, B**, One way Anova in **D** and Student's t-test in **E, G**. ns=p>0.05, * p<0.05, *** p<0.001. See also Figure 2-figure supplement 1.

decreased T antigen staining on macrophages moving towards and entering the germband (Figure 2F) in Stage 11 through late Stage 12. q-PCR analysis on FACS sorted macrophages show that the reduction in T antigen levels in the mutant is not caused by changes in the RNA levels of the T synthase C1GalTA or the Ugalt Gal and GalNAc transporter (Aumiller and Jarvis, 2002; Segawa et al., 2002) (**Figure2G**). These results argue that CG8602 is required for enriched T antigen levels on macrophages.

To assess if CG8602 could directly regulate T antigen addition, we examined if it is found in the Golgi where O-glycosylation is initiated. We first utilized the macrophage-like S2R+ cell line, transfecting a FLAG::HA or 3xmCherry labeled form of CG8602 under *srpHemo* or a copper inducible MT promoter control. We detected significant colocalization with markers for the cis-Golgi marker GMAP, the Trans Golgi Network marker Golgin 245 and the endosome markers Rab7, Rab11 and Hrs (Riedel et al., 2016) (**Figure 2H, Figure 2- figure supplement 1C-G**). We detected no colocalization with markers for the nucleus, ER, peroxisomes, mitochondria or lysosomes (**Figure 2H, Figure 2- figure supplement 1B,H-J)**. We confirmed the presence of CG8602 in the Golgi and endosomes in macrophages from late Stage 11 embryos through colocalization with Golgin 84 and Hrs, using cells extracted from positions in the head adjacent to the germband (**Figure 2I**). We conclude that the T antigen enrichment on macrophages migrating towards and into the germband requires a previously uncharacterized atypical MFS with homology to sugar binding proteins that is localized predominantly to the Golgi and endosomes.

The MFS, Minerva, is required in macrophages for dissemination and germband invasion

We examined if CG8602 affects macrophage invasive migration. The *CG8602*^{EP3102} mutant displayed a 35% reduction in macrophages within the germband at early Stage 12 compared to the control (Figure 3A-B,D, Figure 3- figure supplement 1A). The same decrease is observed when the mutant is placed over the deficiency Df(3L)BSC117 that removes the gene entirely (Figure

Figure S2

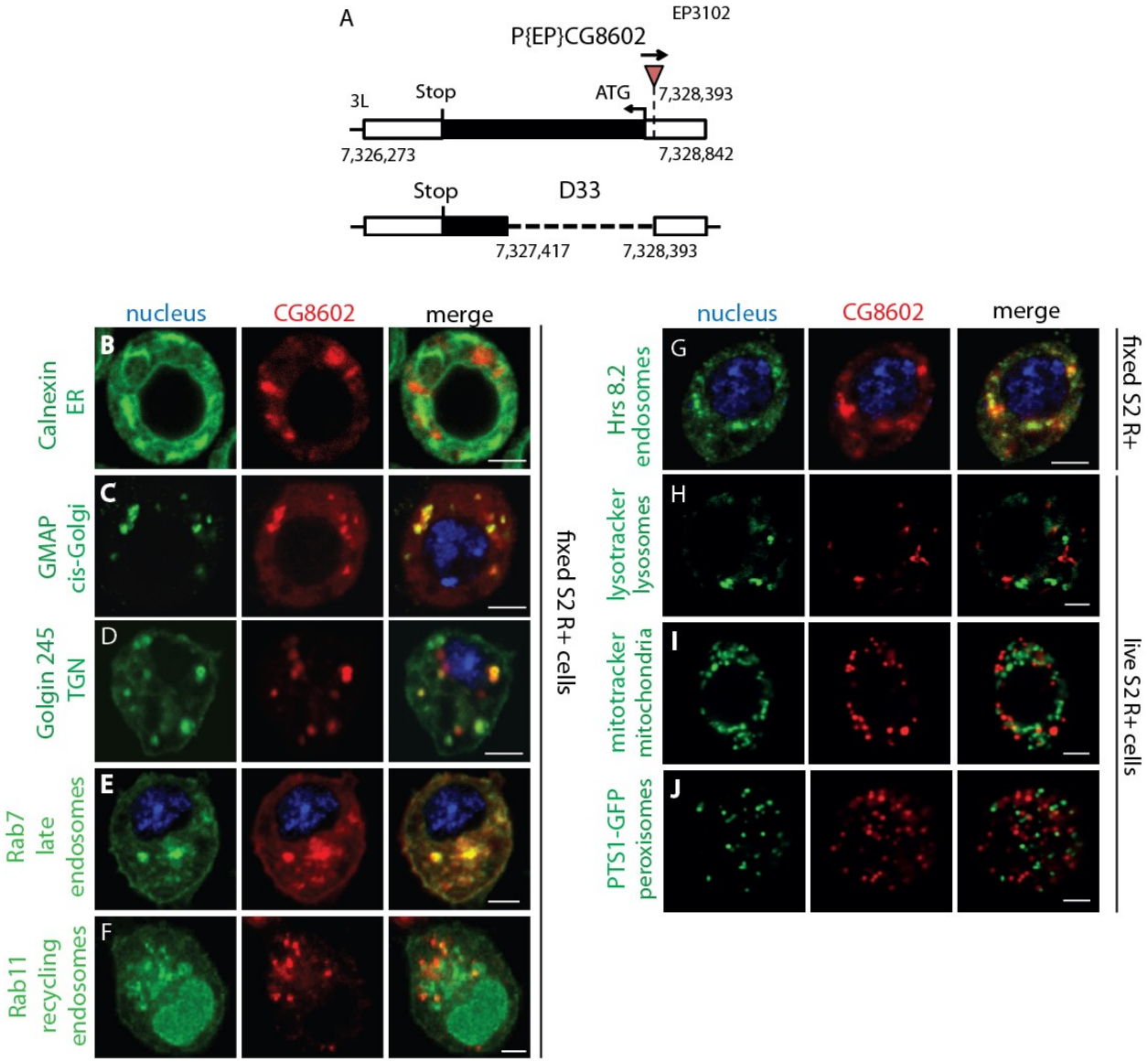

Figure 2-figure supplement 1: CG8602 expression and localization

(A) Schematic depicting the CG8602 gene and the insertion site of the EP3102 P element and the Δ33 excision mutant induced by P element mobilization which removes 914 bp of the ORF. (**B-J**) Confocal images of S2R+ cells transfected with (**B-G**) *MT-CG8602::FLAG::HA,* and then fixed and visualized by HA antibody staining (red) or (**H-J**) *srpHemo-CG8602::3xmCherry (*red*)* with different parts of the endomembrane system visualized by live markers as indicated (green). DAPI (blue) marks the nucleus. CG8602 showed (**B**) no colocalization with the ER marker Calnexin, partial colocalization with the (**C,D**) Golgi markers GMAP and Golgin 245, (**E**) late endosomal marker Rab7, (**F**) recycling endosome marker Rab11-YFP, and (**G**) endosomal marker Hrs8.2, no colocalization with the (**H**) lysosome marker lysotracker, (**I**) mitochondrial marker mitotracker and (**J**) peroxisomal marker PTS1-GFP in fixed (**B-G**) or live (**H-J**) S2R+ cells. Scale bar is 3μm in B-J.

the Ugalt Gal and GalNAc transporter (Aumiller and Jarvis, 2002; Segawa et al., 2002) (**Figure 2G**). These results argue that CG8602 is required for enriched T antigen levels on macrophages.

3D), arguing that *CG8602*^{EP3102} is a genetic null for macrophage germband invasion. The P element transposon insertion itself causes the migration defect because its precise excision restored the number of macrophages in the germband to wild type levels (Figure 3D). Expression of the CG8602 gene in macrophages can rescue the *CG8602*^{EP3102} P element mutant (Figure 3C-D, Figure 3-figure supplement 1A), and RNAi knockdown of CG8602 in macrophages can recapitulate the mutant phenotype (Figure 3E, Figure 3-figure supplement 1B). Our data thus argues that CG8602 is required in macrophages themselves for germband invasion.

Decreased numbers of macrophages in the extended germband could be caused by specific problems entering this region, or by general migratory defects or a decreased total number of macrophages. To examine the migratory step that precedes germband entry, we counted the number of macrophages sitting on the yolk next to the germband in fixed embryos in the *CG8602*^{EP3102} mutant. We observed a 30% decrease compared to the control (**Figure 3F**), suggesting a defect in early dissemination. Entry into the germband by macrophages occurs between the closely apposed DE-Cadherin expressing ectoderm and the mesoderm and is accompanied by deformation of the ectodermal cells (Ratheesh et al., 2018). We tested if reductions in DE-Cadherin could ameliorate the germband phenotype. Indeed, combining the *CG8602*^{EP3102} mutation with *shg*^{P34} which reduces DE-Cadherin expression (Pacquelet and Røth, 1999; Tepass et al., 1996) produced a partial rescue (**Figure 3G**), consistent with CG8602 playing a role in germband entry as well as an earlier migratory step. There was no significant difference in the number of macrophages migrating along the vnc in late Stage 12 compared to the control in fixed embryos (**Figure 3H**) from the *CG8602*^{EP3102} mutant or from a knockdown in macrophages of *CG8602* by RNAi (**Figure 3-figure supplement 1C**), arguing against a general migratory defect. There was also no significant difference in the total number of macrophages in either case (**Figure 3-figure supplement 1D-E).** From analyzing the *CG8602* mutant phenotype in fixed embryos we conclude that CG8602 does not affect later vnc migration but is important for the early steps of dissemination and germband invasion.

To examine the effect of CG8602 on macrophage speed and dynamics, we performed live imaging of macrophages labeled with the nuclear marker *srpHemo-H2A::3xmCherry* in control and *CG8602*^{EP3102} mutant embryos. We first imaged macrophages migrating from their initial position in the delaminated mesoderm up to the germband and detected a 33% decrease in speed (2.46$\pm$0.07 μm/min in the control, 1.66$\pm$0.08 μm/min in the *mrva*^{3102} mutant, p=0.002) (Figure 3I, J) and no significant decrease in persistence (0.43$\pm$0.02 in the control, 0.40$\pm$0.01 in the mutant, p=0.22) (Figure 3-figure supplement 1F). We then examined the initial migration of macrophages into the germband at late Stage 11. We observed a range of phenotypes in the six movies we made of the mutant, with macrophages pausing at the germband edge from twice to six times as long as in the control before invading into the tissue (Figure 3K shows average time for entry). As we observed no change in the timing of the initiation of germband retraction (269.6±9 min in control and 267.1±3 min in mutant, p=-0.75) but did observe a decreased speed of its completion in the mutant (107±12 min from start to end of retraction in control and 133±6 min for mutant p=0.05), we only analyzed macrophages within the germband before its retraction begins. We observed a 43% reduction in macrophage speed within the germband (2.72$\pm$0.32 μm/min in the control and 1.55$\pm$0.04 μm/min in the mutant, p=0.02) (Figure 3L,M). To assess this phenotype's specificity for invasion, we used live imaging of macrophage migration along the inner vnc that occurs during the same time period as germband entry; we observed no

Valoskova et al Figure 3

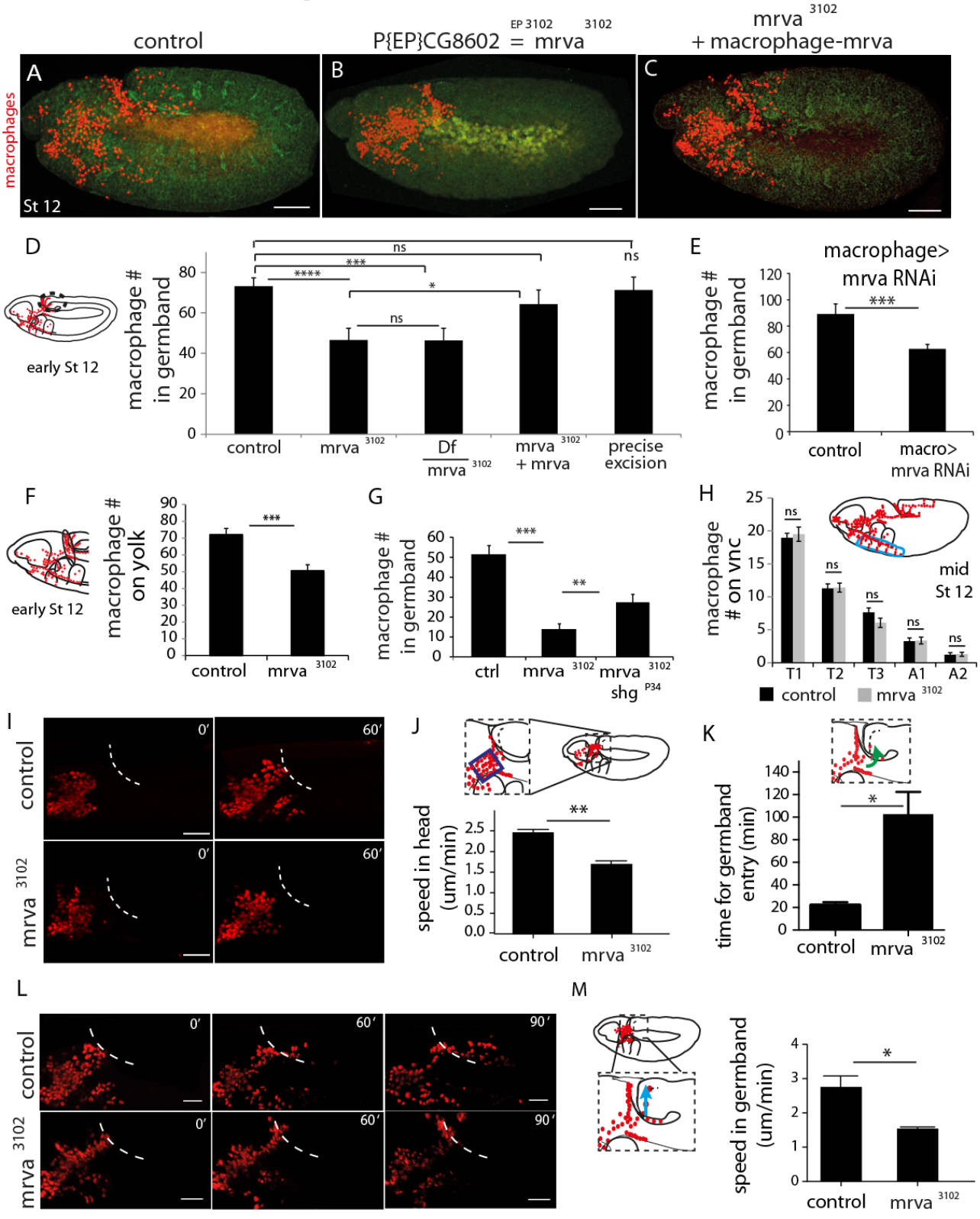

Figure 3: CG8602, which we name Minerva, is required in macrophages for their efficient invasion of the germband

(A-C) Representative confocal images of early Stage 12 embryos from **(A**) control, **(B)** *P{EP}CG8602^{3102}=minerva (mrva)^{3102}* mutant, and (**C)** *mrva^{3102}* mutants with macrophage expression of the gene rescued by *srpHemo(macro)-mrva.* Macrophages express *srpHemo-3XmCherry* (red) and the embryo autofluoresces (green). In the mutant, macrophages remain in the head and fail to enter the germband, hence we name the gene *minerva*. **(D)** Dashed ellipse in schematic at left represents the germband region in which macrophage (red) were counted throughout the study. Comparison of the control (n=38), *mrva^{3102}* mutants (n=37) and *mrva^{3102}* mutant/*Df(3L)BSC117* that removes the gene (n=23) shows that the mutant significantly decreases migration into the extended germband (p<0.0001 for control vs mutant, p=-0002 for control vs Df cross). This defect can be partially rescued by expression in macrophages of *srpHemo>mrva::FLAG::HA* (n=18, p=0.222 for control vs rescue, p=.036 for mutant vs rescue) and completely rescued by precise excision (*mrva$^{\Delta 32}$*) of the P element (n=16, p=0.826). *srpHemo>mCherry-nls* labeled the macrophages. **(E-G)** Macrophage quantification in early Stage 12 embryos. (**E**) Fewer germband macrophages upon expression of *mrva* RNAi *v101575* only in macrophages under the control of *srpHemo* (n=28-35 embryos, p<0.0001). (**F)** Fewer macrophages found on the yolk neighboring the germband (oval in schematic) in the *mrva^{3102}* mutant compared to control embryos (n=14-16 embryos, p=0.0003). (**G**) Increased germband macrophage numbers in *shg^{P34}; mrva^{3102}* compared to the *mrva^{3102}* mutant indicates a partial rescue from reducing DE-Cadherin which is expressed in the germband ectoderm (n=19-29, p<0.0001, p=0.005). **(H**) No significant difference in number of macrophages labeled with *srpHemo-3xmCherry* in vnc segments (area in blue oval in schematic) between control and *mrva^{3102}* mutant embryos in fixed mid Stage 12 embryos (n=23-25, p=0.55). Images from two-photon movies of (**I**) Stage 10 and (**L**) late Stage 11-early Stage 12 embryos in which macrophages (red) are labeled with *srpHemo-H2A::3xmCherry*. (**I**) Stills at 0 and 60 min and (**J**) quantification of macrophage speed reveal 33% slower macrophage migration in the head towards the yolk neighboring the germband in the *mrva^{3102}* mutant compared to the control, n=3 movies for each, #tracks: control=329, mutant=340, p=0.002. Blue box in magnification in schematic indicates region analysed in J. (**K**) The first macrophage in *mrva^{3102}* mutants is much slower to enter the germband after macrophages reach the germband edge (control=22.00±1.53, n=3, *mrva^{3102}* mutant=102.0±20.35, n=4. p-value = 0.021). (**L**) The time when macrophages reached the germband in each genotype was defined as 0'. Stills at 60 and 90 min and (**M**) quantification of macrophage speed reveal 43% slower macrophage migration in the germband in the *mrva^{3102}* mutant compared to the control. Blue arrow in schematic indicates route analyzed. n=3 movies for each, #tracks: control=21, mutant=14, p=0.022. Significance was assessed by Kruskal-Wallis test with Conover post test comparison in D, G, Student's t-test in E, F, H, J-K, M. ns=p> 0.05, * p<0.05, ** p<0.01, *** p<0.001, ***p<0.0001. Scale bars are 50μm in A-C, 40μm in I, 30μm in L. See also Figure 3-figure supplement 1 and Figure 1-video 1-4..

---

significant change in speed (2.41±0.06 μm/min in the control and 2.23±0.01 μm/min in the mutant, p=0.11) or directionality (0.43±0.03 in the control and 0.43±0.02 in the mutant, p=0.9742) (Figure 3-figure supplement 1G). We conclude from the sum of our experiments in fixed and live embryos that CG8602 is important for the initial disseminatory migration out of the head and for invasive migration into and within the germband, but does not alter general migration. We name the gene *minerva (mrva)*, for the Roman goddess who was initially trapped in the head of her father, Jupiter, after he swallowed her pregnant mother who had turned herself into a fly.

Minerva is not required for border cell invasion or germ cell migration

To assess if Minerva only affects macrophage invasion or also other types of tissue penetration in *Drosophila*, we examined the migration of germ cells and border cells. Germ cells move in an Integrin-independent fashion through gaps in the midgut created by ingressing

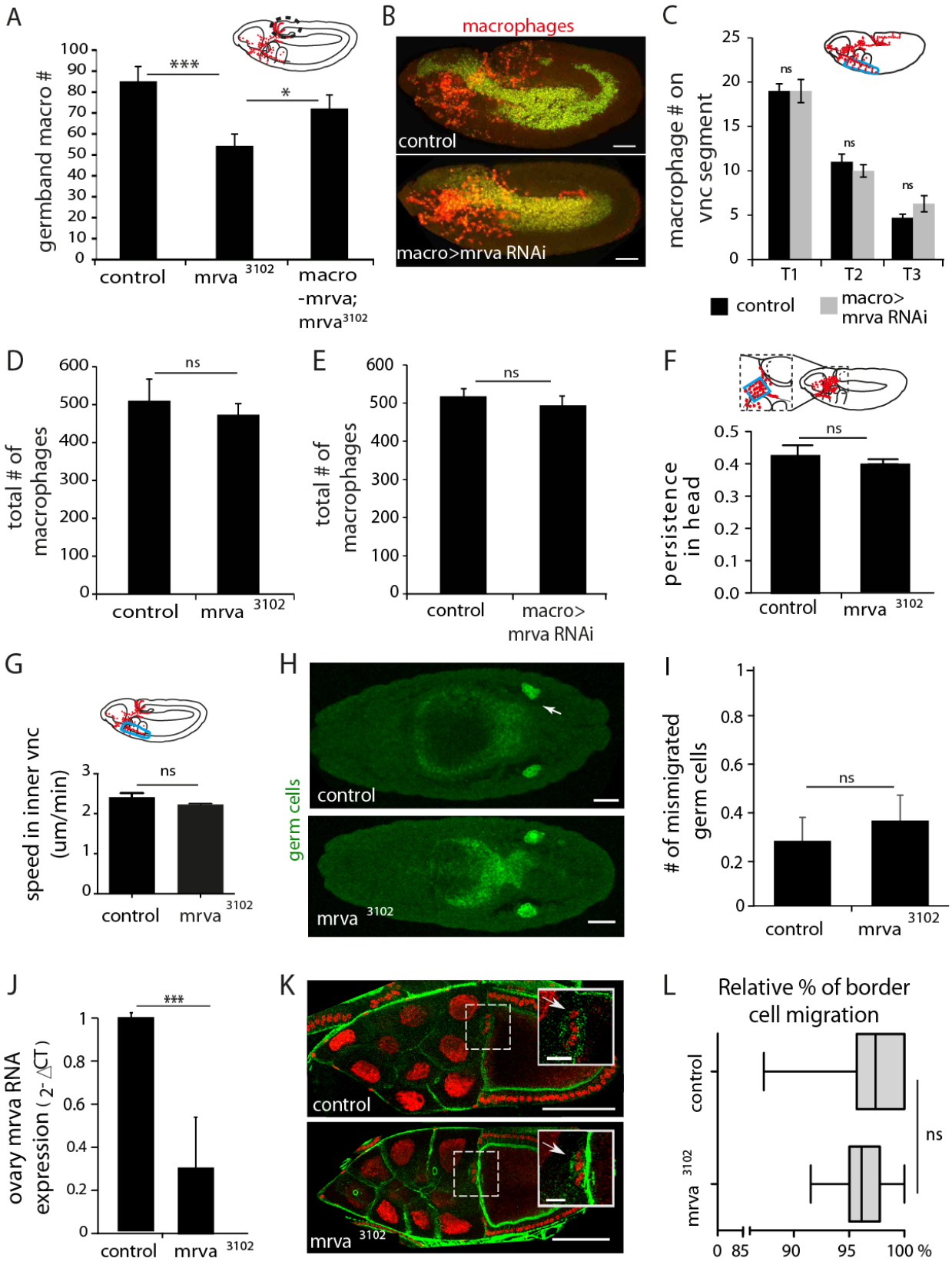
A
germband macro #
***
*
control
mrva 3102
macro -mrva; mrva3102
B
macrophages
control
macro>mrva RNAi
C
macrophage # on vnc segment
ns
T1
T2
T3
control
macro> mrva RNAi
D
total # of macrophages
ns
control
mrva 3102
E
total # of macrophages
ns
control
macro> mrva RNAi
F
persistence in head
ns
control
mrva 3102
G
speed in inner vnc (um/min)
ns
control
mrva 3102
H
germ cells
control
mrva 3102
I
# of mismigrated germ cells
ns
control
mrva 3102
J
ovary mrva RNA expression (2-ΔCT)
***
control
mrva 3102
K
control
mrva 3102
L
Relative % of border cell migration
control
mrva 3102
ns
0 85 90 95 100 %

Figure 3-figure supplement 1: CG8602 (Minerva) affects macrophage migration into the germband but not along the vnc and does not alter border cell or germ cell migration. (A) Quantification of the number of macrophages in the germband (dotted circle in schematic) in embryos from control, *mrva2*^{3102}, and *mrva*^{3102} *srpHemo(macro)-mrva::HA* showing Mrva is required in macrophages for germband invasion. Macrophages visualized by *srpHemo-H2A::3xmCherry*. (n=25-28, p=0.001 for mutant vs control, 0.14 for control vs rescue, 0.05 for mutant vs rescue). (**B**) Representative confocal images of early Stage 12 embryos from control and *srpHemo(macro)-Gal4* driving *UAS-minerva RNAi* (v101575) expression in macrophages labeled by H2A-RFP (green) and cytoplasmic GFP (red). (**C**) Quantification of the number of macrophages in vnc segments (area circled in blue in schematic) reveals no significant difference in macrophage migration along the vnc between control embryos and those expressing an RNAi against *mrva* (v101575) in macrophages under *srpHemo(macro)-GAL4* control (n=19-20, p=0.5). (**D, E**) Quantification of the total number of macrophages visualized with (**D**) *srpHemo>mCherry::nls* or (**E**) *srpHemo>H2A::RFP GFP* reveals no significant difference between (**D**) control and *mrva*^{3102} mutant embryos (n=15, p>0.05) and (**E**) control and *srpHemo(macro)>mrva RNAi* embryos (n=26, p=0.1439). The area analyzed is indicated with the black box in the schematic above**. (F)** Quantification of persistence in the head from 2-photon movies with *srpHemo-H2A::3xmCherry* labeling macrophages shows no change in the *mrva*^{3102} compared to the control. n=3. # tracks: control=329, mutant=340, p=0.2182. The area analyzed is indicated with the blue box in the schematic above**. (G**) Macrophage speed in the inner vnc in early Stage 12 embryos (see area circled in blue in schematic above) shows no significant change in the *mrva*^{3102} compared to the control (n=3 movies for each, #tracks: control=180, mutant=180, p=0.113). (**H**) Dorsal confocal images of representative Stage 14 control and *mrva*^{3102} embryos stained with Vasa antibody to visualize primordial germ cells (PGCs) (green). White arrow in control image indicates one of the two gonads. (**I**) Quantitation of the number of mismigrated PGCs per control and *mrva*^{3102} embryo revealed no significant difference (n=22,28, p=0.57). (**J**) Quantification by qPCR of *mrva* RNA levels in ovaries from *mrva*^{3102} mutant adult females compared to the control (n=3, p=0.0001). (**K**) Representative confocal images of border cells in stage 10 oocytes from control and *mrva*^{3102} adult females. DNA was labeled using DAPI (red) and actin was detected by phalloidin-A488 (green). Insets at upper right show enlargements of the dotted boxed area in the main images. Border cells are indicated with arrows. (**L**) Quantitation of border cell migration in stage 10 oocytes. Box plots show the relative percentages of migration measured for control (n=37) and *mrva*^{3102} (n=40) compared to complete migration to the edge of the oocyte. Whiskers in the box plot represent the distribution maximum and minimum. We observe no significant difference in the mutant (p=0.05).
Significance was assessed by One-way Anova in A and Student's t-test in C-G, I-J, L. ns=p>0.05, * p<0.05, *** p<0.001. Scale bars are 50μm in B,H, 20μm in inset and 100 um in main image in J.

formerly epithelial cells (Devenport and Brown, 2004; Seifert and Lehmann, 2012). We found no defect in germ cell migration when examining control and *mrva*^{3102} embryos stained with the Vasa Ab (Figure 3-figure supplement 1H-I). Border cells are born in the epithelia surrounding the ovary and then delaminate to move invasively between the nurse cells towards the oocyte (Montell, 2003), guided by the same receptor that macrophages use during their embryonic dispersal, PVR (Duchek et al., 2001). They migrate as a tumbling collective, using invadopodia and Cadherin-based adhesion to progress (Cai et al., 2014; Niewiadomska et al., 1999). *mrva* is expressed in dissected control ovaries and the *mrva*^{3102} mutant reduces the levels of *mrva* RNA in the ovary by 70%, similar to the reduction observed in macrophages (Figure 3-figure supplement 1J). We identified border cells by staining with DAPI to detect their clustered nuclei. We observed no change in border cell migration towards the oocyte in the *mrva*^{3102} mutant compared to the control (Figure 3-figure supplement 1K-L). These results support the conclusion that Mrva is not generally required for all migratory cells that move confined through tissues during development, but specifically for the invasion of macrophages, which is an Integrin-dependent process (Siekhaus et al., 2010).

Minerva affects a small fraction of the Drosophila embryonic O-glycoproteome

We set out to determine if Minerva induces T glycoforms on particular proteins. We first conducted a Western Blot with a mAb to T antigen on whole embryo extracts. We used the whole embryo because we were unable to obtain enough protein from FACS sorted macrophages or to isolate CRISPR-induced full knockouts of *minerva* in the S2R+
macrophage-like cell line. We observed that several bands detected with the anti-T mAb were absent or reduced in the *minerva* mutant (Figure 4A), indicating an effect on the T antigen modification of a subset of proteins.

We wished to obtain a more comprehensive view of the proteins affected by Minerva. Since there is little information about *Drosophila* O-glycoproteins and O-glycosites (Schwientek *et al.*, 2007; Aoki and Tiemeyer, 2010), we used lectin-enriched O-glycoproteomics to identify proteins displaying T and Tn glycoforms in Stage 11/12 embryos from wild type and $mrva^{3102}$ mutants (Figure 4-figure supplement 1A). We labeled tryptic digests of embryonic protein extracts from control or mutant embryos with stable dimethyl groups carrying medium ($C_2H_2D_4$) or light (C_2H_6) isotopes respectively to allow each genotype to be identified in mixed samples (Boersema et al., 2009; Schjoldager et al., 2012, 2015). The pooled extracts were passed over a Jacalin column to enrich for T and Tn O-glycopeptides; the eluate was analyzed by mass spectrometry to identify and quantify T and Tn modified glycopeptides in the wild type and the mutant sample through a comparison of the ratio of the light and medium isotope labeling channels for each glycopeptide (see Figure 4-figure supplement 1B-C for example spectra).
In the wild type we identified T and Tn glycopeptides at 936 glycosites derived from 270 proteins (Figure 4B). 62% of the identified O-glycoproteins and 77% of identified glycosites contained only Tn O-glycans. 33% of the identified O-glycoproteins and 23% of glycosites displayed a mixture of T or Tn O-glycans, and 5% of identified O-glycoproteins and 4% of glycosites had solely T O-glycans (Figure 4C). In agreement with previous studies (Steentoft et al., 2013b), only one glycosite was found in most of the identified O-glycoproteins (44%) (Figure 4D). In 20% we found two sites, and some glycoproteins had up to 27 glycosites. The identified O-glycosites were mainly on threonine residues, (78.5%) with some on serines (21.2%) and very few on tyrosines (0.3%) (Figure 4-figure supplement 1D). Metabolism, cuticle development, and receptors were the most common functional assignments for the glycoproteins (Figure 4-figure supplement 1E). We sought to assess the changes in glycosylation in the *mrva* mutant. A majority of the quantifiable Tn and T O-glycoproteome was unaltered between the wild type and the $mrva^{3102}$ mutant, with only 63 proteins (23%) showing more than a three-fold change and 18 (6%) a ten-fold shift (Figure 4F). We observed both increases and decreases in the levels of T and Tn modification on proteins in the mutant (Figure 4F-G, Table 1), but a greater number of proteins showed decreased rather than increased T antigen levels. 67% of the vertebrate orthologs of *Drosophila* proteins displaying shifts in this O-glycosylation have previously been linked to cancer (Figure 4H, Table 1). These proteins were affected at specific sites, with 40% of glycosites on these proteins changed more than three fold and only 14% more than ten fold. The glycosite shifts in T antigen occurred either without significant alterations in Tn (33% of glycosites had only decreased T antigen, 17% of glycosites had only increased T antigen) or with changes in T antigen occurring in the same direction as the changes in Tn (22% of glycosites both Tn and T antigen increased, 22% of glycosites both Tn and T decreased) (Table 1). Only 1% of glycosites displayed decreased T antigen with a significant increase in Tn. Interestingly, a higher proportion of the

Valoskova et al Figure 4

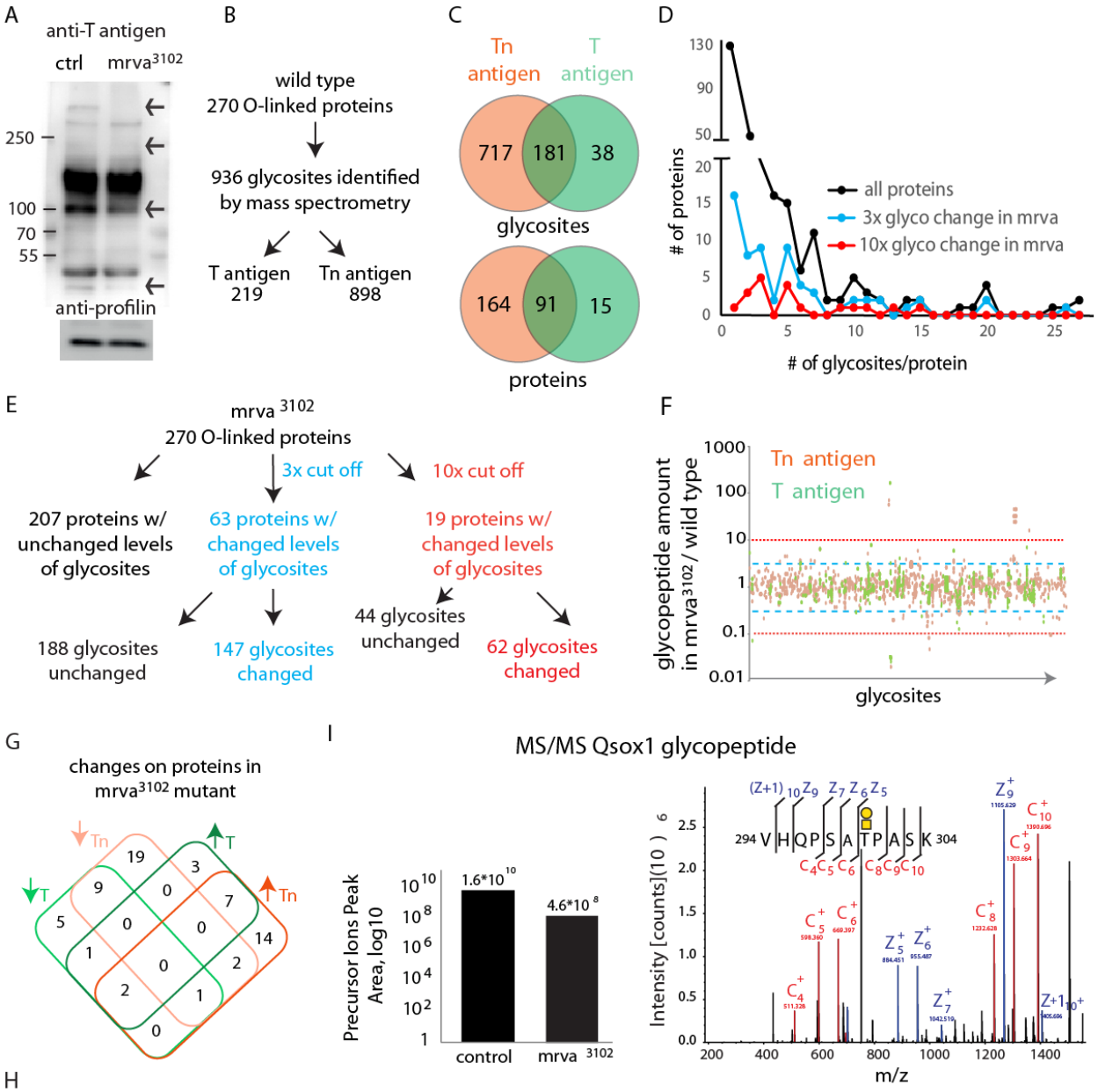

H

Glycosite(s) position	Gene	Function	Subcellular localization	T	Tn (same sites)	Tn (other sites)	Unchanged GS	Human ortholog	Site conserved	Cancer link
294-VHQP S A T PASKI	dQsox1	protein disulfide isomerase	G, ES	52x dec.	43x dec.	no	yes	QSOX1	+	1
321-EAPAK TSTT AG 330-AGPLV T VEPTK S I T EPNEE 431-SNRQA S PTEEP	Dtg	development (dpp target gene)	CS, vesicles	13x dec.	10x dec	4x inc.	yes	no	-	
307-IVA S I T S T AKPVT	CG17667	axonogenesis	ECM	10x dec.	no	4-11x dec.	no	no	-	
903-PVDEI T P T PAE	CG2918	heat-shock protein, chaperone	endo, EC	8x dec.	4-8x dec.	4-8x dec.	no	HYOU1	-	2
126-KVVEG S AIP T PEPKH	CG17660	lung 7TM receptor-like	membrane	6x dec.	no	no	no	TMEM87B	+	3
834-VYVV T PQPRH	CG7884	unknown	unknown	6x dec.	no	15x dec.	no	no	-	
129-KYIK ST T EATTQ	put	receptor, dpp signaling	PM	5x dec.	5x dec.	5x dec.	yes	ACVR2B	-	4
683-VALPA T ASPV S EVPIK	Tango1	Golgi organization, protein secretion	ER exit site, G	5x dec. 6x inc.	5x inc.	no	yes	CTAGE5	-	
30-AQEFL T KAQGD	Nplp2	humoral immune response	ES	5x dec	no	no	no	no	-	
487-TVEH S T LVYER	CG8027	GlcNAc phospho transferase	unknown	5x dec.	no	5x dec.	yes	GNPTAB	+	
371-DAEEA T PPNYD	GCS2beta	Glucose hydrolysis from oligomannosidic N-Glycans	endo	5x dec.	4-7x dec.	7x dec.	yes	Glu2B	-	
169-KAQEP TS HPAEN	GCS2alpha	Glucose hydrolysis from oligomannosidic N-Glycans	endo, EC	4x dec. 50x inc.	no	no	yes	GANAB	+	5
221-ATGLA T PKPTH	CG4194	unknown	unknown	4x dec.	no	no	no	no	-	
1087-VHKLV T LLPVR	CG1273	unknown	unknown	4x dec	no	no	yes	no	-	
42-LPVET T T RSPTK	Gp150	receptor, Notch signaling	PM	4x dec.	no	4x dec.	yes	LRIG1	-	6
1382-PERTI T PPPPF	sas	receptor activity	apical PM	4x dec.	no	no	yes	no	-	

Figure 4: Glycoproteomic analysis reveals Minerva is required for higher levels of T-antigen on a subset of proteins

(A) Representative Western blot of protein extracts from Stage 11/12 control and *mrva*^{3102} mutant embryos probed with T antigen antibody. Arrows indicate decreased/missing bands in the mutant compared to the control. Profilin serves as a loading control (n=10 biological replicates). **(B)** Summary of glycomics results on wild type embryos. **(C)** Venn diagram indicating number of glycosites or proteins found with T, Tn or T and Tn antigen modifications in the wild type**. (D)** Plot showing the number of T and Tn antigen glycosites per protein in the total glycoproteome and on proteins that show three (blue) and ten-fold (red) altered glycopeptides in the *mrva*^{3102} mutant. Proteins strongly affected by Minerva have a higher number of glycosites (p = 0.005). (**E**) Summary of glycomics on *mrva*^{3102} embryos showing the numbers of proteins and glycosites exhibiting three (blue) or ten (red) fold changes in T and Tn antigen levels. (**F**) T antigen (in orange) and Tn antigen (green) occupied glycosites plotted against the ratio of the levels of glycopeptides found for each glycosite in *mrva*^{3102}/control mutant. Higher positions on the plot indicate a lower level of glycosylation in the mutant. Blue dashed line represents the cut off for 3x changes in glycosylation, and the red dotted line the 10x one. (**G**) Venn diagram of the number of proteins with at least 3 fold change in the T antigen (T, green) or Tn antigen (Tn orange) glycosylation in the *mrva*^{3102} mutant. Up arrows denote increase, down arrows indicate decrease in levels. (**H**) Proteins with at least a three fold decrease in T antigen levels in the *mrva*^{3102} mutant. Glycan modified amino acids are highlighted in bold green font. Unchanged/Higher GS column indicates if any other glycosite on the protein is unchanged or increased. Table does not show the two chitin and chorion related genes unlikely to function in macrophages. G: Golgi, ES: Extracellular space, Endo: Endosomes, ER: Endoplasmic reticulum, ECM: Extracellular Matrix, PM: Plasma Membrane, GS: Glycosite. Cancer links as follows. 1) QSOX1: Promotes cancer invasion *in vitro*, overexpression worse patient outcomes (Katchman et al., 2013, 2011). 2) HYOU1: Overexpression associated with vascular invasion, worse patient outcomes (Stojadinovic et al., 2007) (Zhou et al., 2016). 3) TMEM87B: translocation breakpoint in cancer, (Hu et al., 2018). 4) ACVR2B: over expressed in renal cancer (Senanayake et al., 2012). 5) GANAB: inhibits cancer invasion *in vitro* (C. Chiu et al., 2011). 6) LRIG1: inhibits cancer invasion *in vitro*, and in mice (Sheu et al., 2014), (Mao et al., 2018). (**I)** Annotated ETD MS2 spectra of the VHQPSATPASK glycopeptide from Qsox1 with T antigen glycosylation at position T7. See schematic in which the yellow square represents GalNAc and the yellow circle Gal. Assigned fragment ions in MS2 spectra are highlighted by red for "c" type fragments (those retaining the original N terminus) and blue for "z" type fragments (those retaining the original C terminus). The graph at the left shows the relative quantification of the glycopeptide precursor ion's peak area in the control and *mrva*^{3102} mutant plotted on a logarithmic scale. See also Figure 4-figure supplement 1, Figure 4-Dataset 1, Table 1 and 2.

glycoproteins with altered O-glycosylation in the *mrva*^{3102} mutant had multiple glycosites than the general glycoproteome (Figure 4D) (P value=0.005 for ten-fold changes). We conclude that Minerva affects O-glycosylation occupancy on a small subset of O-glycoproteins, many of whose vertebrate orthologs have been linked to cancer, with both T and Tn O-glycopeptides being affected.

Minerva raises T antigen levels on proteins required for invasion

Given that the knockdown of the C1GalTA enzyme which blocks Tn to T conversion produced a germband invasion defect, we examined the known functions of the 18 proteins with lower T antigen in the absence of Minerva to distinguish which processes Minerva could influence to facilitate invasion (Figure 4H). We excluded two proteins involved in eggshell and cuticle production. To spot proteins whose reduced T antigen-containing glycopeptides are caused directly by alterations in glycosylation rather than indirectly by decreased protein expression in the *mrva* mutant, we checked if glycosylation at other identified glycosites was unchanged or increased. We identified ten such proteins, several of which were in pathways that

Valoskova et al Figure 4-figure supplement 1

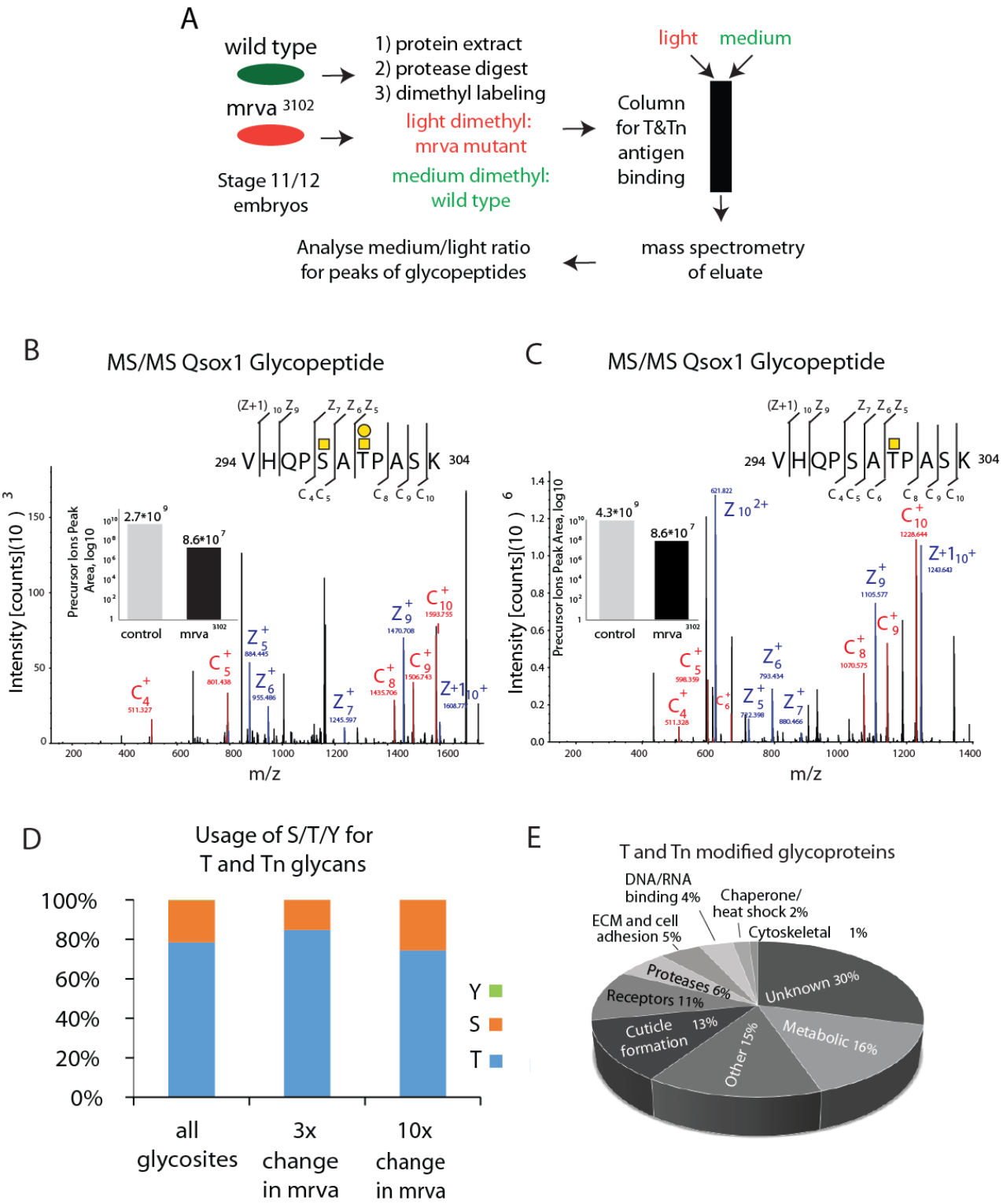

Figure 4-figure supplement 1: Further information on the mass spectrometry results. (A) Work flow for mass spectrometry analysis of T and Tn antigen modifications on proteins in Stage 11/12 control and *mrva*^{3102} mutant embryos. **(B, C)** Annotated ETD MS2 spectra of the VHQPSATPASK glycopeptides from Qsox1 in its different glycosylation forms in the control. Assigned fragment ions in MS2 spectra are highlighted by red for "c" type fragments (those retaining the original N terminus) and blue for "z" type fragments (those retaining the original C terminus). See schematics in upper right in which the yellow squares represent GalNAc and the yellow circles Gal. The insets show the relative quantification, based on the corresponding glycopeptide precursor ion's peak area, in the control and *mrva*^{3102} mutant plotted on a logarithmic scale. (**B**) Glycopeptide with Tn antigen glycosylation at position S5 and T antigen glycosylation at the position T7. **(C)** Glycopeptide with Tn antigen glycosylation at position T7. **(D)** Similar usage of serine (S), threonine (T) and tyrosine (Y) for glycosylation in all modified proteins in the control and at glycosites that showed at least three fold and ten fold changes in the *mrva*^{3102} mutant. **(E)** Analysis of the fractional representation of various functions among all T and Tn antigen modified glycoproteins in Stage 11/12 *Drosophila* embryos.

---

had been previously linked to invasion in vertebrates. Qsoz1, a predicted sulfhydryl oxidase required for the secretion, and thus potential folding of EGF repeats (Tien et al., 2008) showed the strongest alterations of any protein, with a 50-fold decrease in T antigen levels in the *mrva* mutant (Figure 4I). The mammalian ortholog QSOX1 has been shown to affect disulfide bond formation, is overexpressed in some cancers, promotes Matrigel invasion, and can serve as a negative prognostic indicator in human cancer patients (Chakravarthi et al., 2007; Katchman et al., 2011; Lake and Faigel, 2014). Dtg, with a 13-fold reduction in T antigen (Hodar et al., 2014), and Put with a five-fold reduction (Letsou et al., 1995) respond to signaling by the BMP-like ligand, Dpp. Dpp signaling directs histoblast invasion in the fly (Ninov et al., 2010). Gp150 shows a four fold decrease in T antigen and modulates Notch signaling (Fetchko et al., 2002; Li, 2003). Notch and BMP promote invasion and metastasis in mice (Bach et al., 2018; Garcia and Kandel, 2012; Owens et al., 2015; Pickup et al., 2015; Sahlgren et al., 2008; Sonoshita et al., 2011). We conclude that Mrva is required to increase T O-glycans on a subset of the glycosites of selected glycoproteins involved in protein folding, glycosylation and signaling in pathways frequently linked to promoting cancer metastasis. Its strongest effect is on a predicted sulfhydryl oxidase, the *Drosophila* ortholog of the mammalian cancer protein, QSOX1.

We wished to determine how Qsox1 might affect *Drosophila* macrophage germband invasion. Embryos from the KG04615 P element insertion in the 5'UTR of the *qsox1* gene displayed 42% fewer macrophages in the germband compared to the control (Figure 5A,B) with an increase in macrophages remaining on the yolk (Figure 5-figure supplement 1A). We observed a small decrease in migration along the vnc (Figure 5-figure supplement 1B) and no change in total macrophage numbers in these embryos (Figure 5-figure supplement 1C). These migration phenotypes were also observed in embryos in which RNAi line v108288 knocked down *qsox1* only in macrophages (Figure 5C, Figure 5-figure supplement 1D-E). We then conducted live imaging (Figure 5D) to examine how the *qsox1*^{KG04615} mutant affected the dynamics of macrophage migration. During the movement of macrophages labeled with the nuclear marker *srpHemo-H2A::3xmCherry* from their initial position up to the germband we detected an 18% decrease in speed (Figure 5E) (2.46±0.07 μm/min in the control, 2.02±0.03 μm/min in the *qsox1*^{KG046152} mutant, p=0.006, n=3) and no significant decrease in persistence (Figure 5-figure

Valoskova et al Figure 5

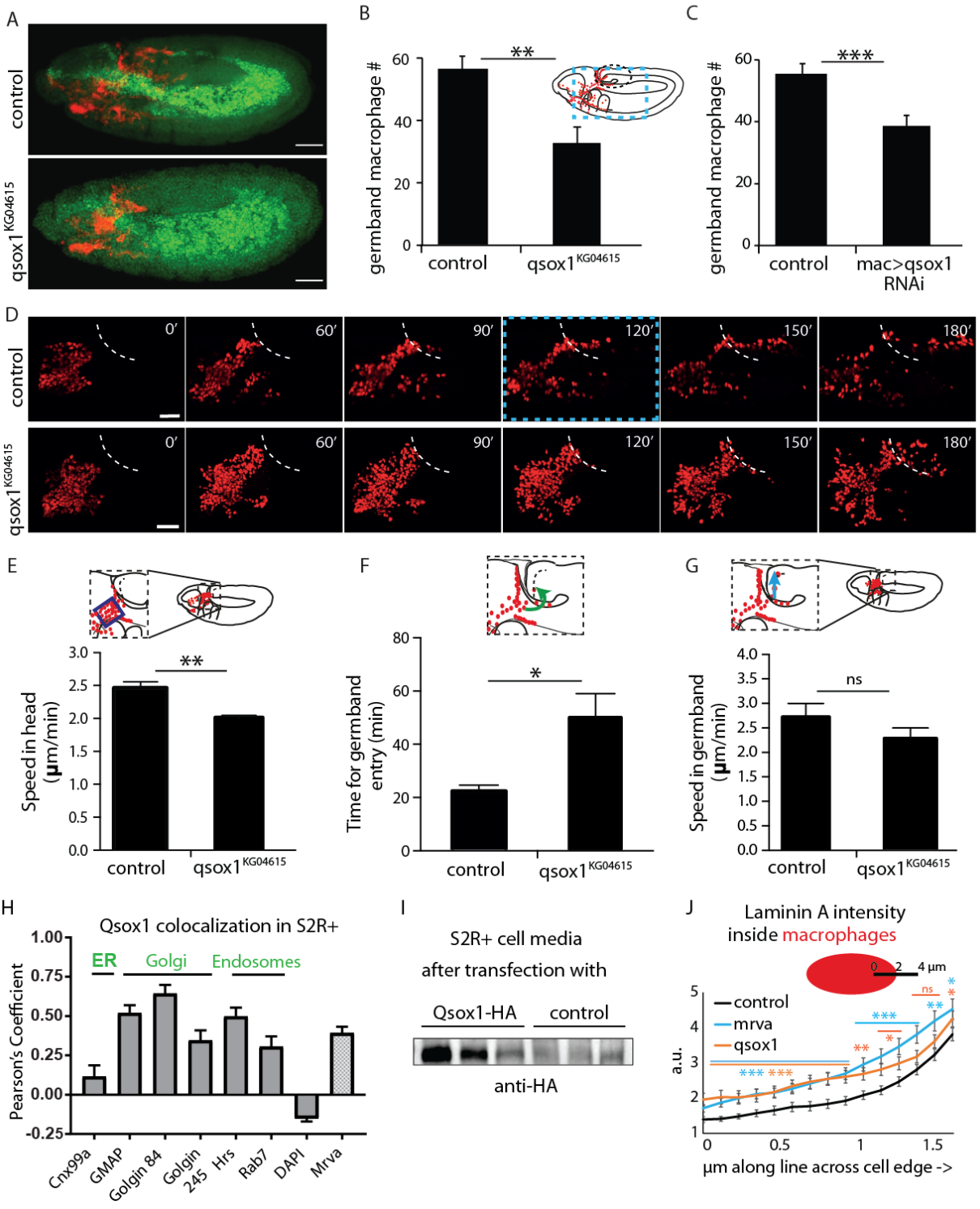

Figure 5: Qsox1 is required for macrophage dissemination and entry into the germband tissue
(A) Representative confocal images of early Stage 12 embryos from control and *P{SUPor-P}Qsox1KG04615* = *qsox1*^{KG04615}. **(B-C)** Quantification in early Stage 12 embryos showing a significant reduction in germband macrophages (**B**) in the P-element mutant *qsox1*^{KG04615} located in the Qsox1 5'UTR (n=18, p=0.0012) and **(C)**

upon the expression in macrophages under *srpHemo-GAL4* control of an RNAi line (v108288) against Qsox1 (n=24, 23 embryos, p= 0.001). **(D)** Images from two-photon movies from control and *qsox1*^{KG04615}. Macrophage nuclei (red) are labeled with *srpHemo-H2A::3xmCherry.* Stills at 0, 60, 90, 120, 150 and 180 minutes. **(E)** Quantification of macrophage speed reveals 18% slower macrophage migration in the head towards the yolk neighboring the germband in the *qsox1*^{KG04615} mutant compared to the control (n=3 movies for each, #tracks: control=329, mutant=396, p=0.0056). **(F)** Quantification of the time required for macrophage entry into the germband in *qsox1*^{KG04615} compared to the control. n=3 movies for each, p=0.043. **(G)** Quantification of macrophage speed in the germband in the *qsox1*^{KG04615} mutant compared to the control (n=3 movies for each, #tracks: control=21, mutant=19, p=0.300). **(H)** Pearson's Coefficient analysis indicating the level of colocalisation of a *MT-Qsox1::FLAG::HA* construct transfected into S2R+ cells visualized with an HA antibody and antibodies against markers for the ER (Cnx99a), the Golgi (Golgin 84, Golgin 245, and GMAP), the early endosome (Hrs), the late endosome (Rab7) and the nucleus (DAPI) (n= 11-15) as well as with a *srpHemo-mrva::3xmCherry* construct (n= 18). (**I**) Western blot of concentrated supernatant collected from S2R+ cells transfected with *srpGal4 UAS-qsox1::FLAG::HA* (first 3 lines) and S2R+ cells that are untransfected. (**J**) Quantification of intracellular LanA intensity along a 4µm line in macrophages (as indicated in schematic) from the control (black), *minerva*^{3102} (blue) and the *qsox1*^{KG04615} mutants (orange) (n=4-5 embryos, 80-100 cells, 240-300 lines). For the whole graph see Figure 5-figure supplement 1G-J. Scale bars 50µm for A, 30µm in D. B-C, E-G and J were analyzed with Student's test. ns=p> 0.05, * p<0.05, ** p<0.01, *** p<0.001. See also Figure 5-figure supplement 1.

---

supplement 1F) (0.43±0.02 in the control, 0.39±0.01 in the mutant, p=0.13). Macrophages in the *qsox1* mutant were delayed twice as long at the germband edge before entering (Figure 5F) (time to entry 22.00±1.53 min in the control and 49.67±9.33 min in the *qsox1*^{KG046152} mutant, n=3). Once in, they moved within the germband with a 17% slower speed, a reduction that was not statistically significant (Figure 5G) (2.72±0.32 µm/min in the control, 2.27±0.20 µm/min in the *qsox1*^{KG046152} mutant, p=0.30, n=3). We conclude that Qsox1
aids the disseminatory migration of macrophages but is most strongly required for their initial invasion into the germband tissues.

We wished to examine how Qsox1 could be exerting this effect on macrophage tissue entry. Vertebrate QSOX1 has been shown to localize to the Golgi and act as a sulfhydryl
oxidase, catalyzing di-sulfide bond formation and protein folding (Alon et al., 2012; Chakravarthi et al., 2007; Heckler et al., 2008; Hoober et al., 1996). The *Drosophila* protein has been shown to be required for the secretion of multimerized EGF domains and was hypothesized to act redundantly with ER oxidoreductin-like-1 to form disulfide bonds (Tien et al., 2008). We found that an HA-tagged form of Qsox1 transfected into the *Drosophila* macrophage like cell line, S2R+, colocalizes little with markers for the ER, and considerably with those for Golgi and endosomes (Figure 5H, Figure 5, figure supplement 1G-I). We also observed significant colocalization with 3xmCherry-tagged Mrva (Figure 5H, Figure 5-figure supplement 1J). Vertebrate QSOX1 can be cleaved from its transmembrane domain to allow secretion (Rudolf et al., 2013), and has been shown *in vitro* to be required extracellularly for the incorporation of laminin produced by fibroblasts into the extracellular matrix (ECM), thereby supporting efficient cancer cell migration (Ilani et al., 2013). *Drosophila* Qsox1 also has a transmembrane domain, yet we detected an HA-tagged form in the media after transfection into S2R+ cells (Figure 5I), indicating that it can be secreted. To examine if *Drosophila* Qsox1 might also affect Laminin, we stained *mrva*^{3102} and *qsox1*^{KG046152} mutant embryos with an antibody against Laminin A (LanA) (Figure 5-figure supplement 1K). In both mutants we observed increased amounts of LanA inside and somewhat

Valoskova et al Figure 5-figure supplement 1

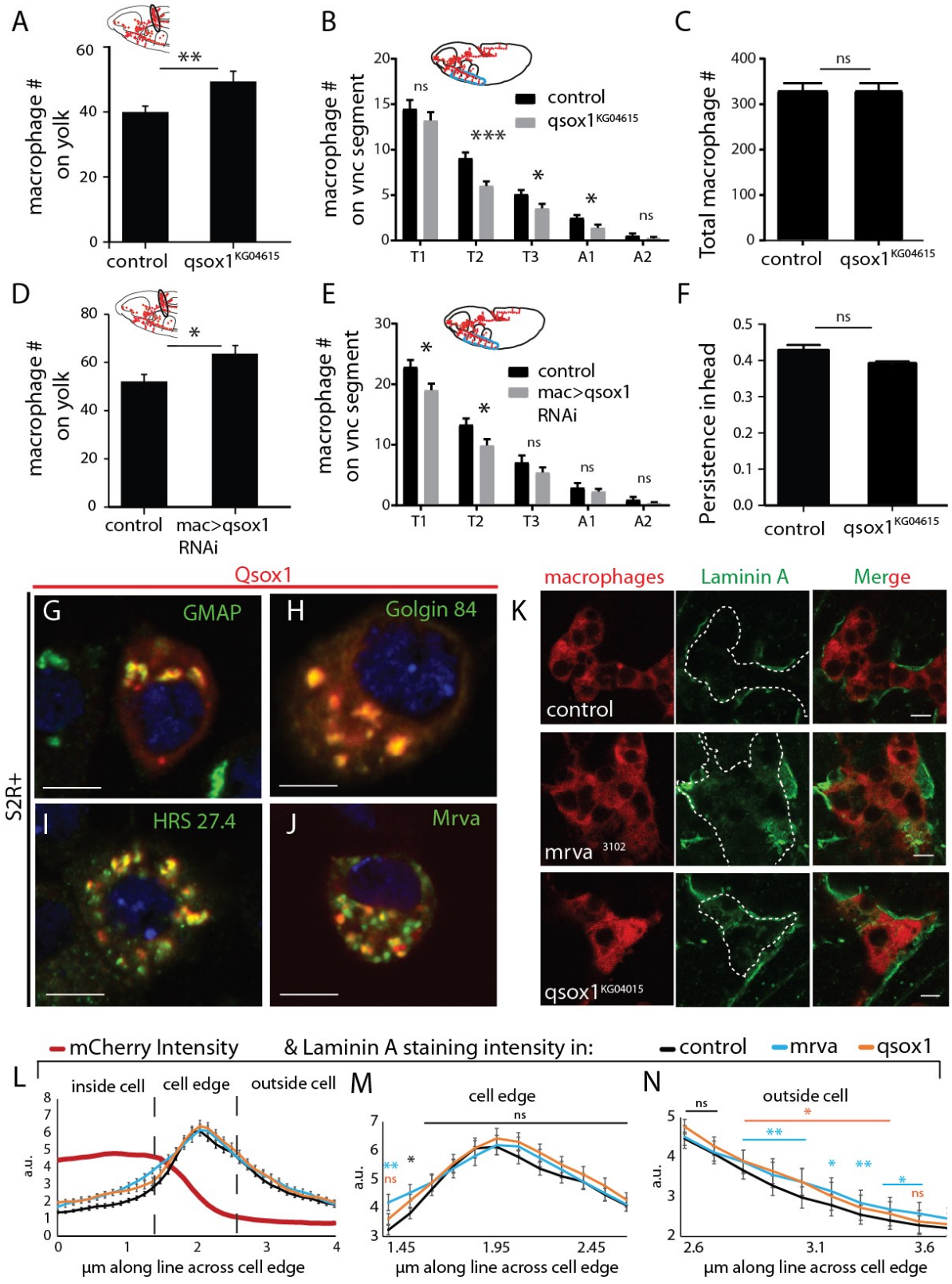

Figure 5-figure supplement 1: Qsox1 affects germband entry and Laminin A.
(**A-B**) Quantification of macrophages in fixed mid-Stage 12 embryos in control and *qsox1*^{KG04615} mutants reveals that in the mutant there are (**A**) increased numbers of macrophages on the yolk neighboring the germband (n=18, p=0.002) and (**B**) reduced numbers on some vnc segments (n= 21; p value T1= 0.357, T2 = 0.0006, T3= 0.031, A1=0.034, A2= 0.329). (**C**) Quantification of macrophages in the whole embryo in the *qsox1* ^{KG04615} mutant compared to the control (n=12-14, p value= 0.999) shows no change. (**D-E**) Quantification of macrophages in fixed mid-Stage 12 embryos from the control and upon knockdown in macrophages of Qsox1 with RNAi (*v108288)* driven by *srpHemo-GAL4* reveals that in the mutant there are (**D**) increased numbers of macrophages on the yolk neighboring the germband (n=23,24, p=0.02) and (**E)** reduced numbers on some vnc segments (n= 13-15; p value T1=0.024, T2=0.030, T3= 0.258, A1=0.445, A2=0.233). (**F**) Analysis of the persistence of macrophages in the head in the *qsox1*^{KG04615} mutant compared to the control shows no significant difference (n=3 movies for each, p=0.126). (**G-J**) Qsox1::FLAG::HA produced from an *MT* promoter visualized by HA-antibody staining (green) with (**G-I**) different parts of the endomembrane system as indicated visualized by antibody staining (green) and (**J**) Mrva::3xmCherry from the *srpHemo* promoter visualized by mCherry fluorescence. (**K**) Confocal images of LanA (green) staining in control, *mrva*^{3102} and *qsox1*^{KG04615} mutant embryos expressing cytoplasmic 3xmCherry (red) in macrophages from the *srpHemo* promoter. Dotted white lines in the LanA channel correspond to an outline traced from the mCherry channel. (**L-N**) Quantification of LanA and mCherry (red) intensity along a 4μm line in macrophages from control (black line), *mrva*^{3102} (blue) and *qsox1*^{KG04615} mutant (orange) (n=4-5 embryos, 80-100 cells, 240-300 lines). (**M-N**) Magnified view of LanA quantification from (**M**) the cell edge and (**N**) outside the cell. Scale bar is 5μm in G-K. A-F and L-N were analyzed with Student's t test. ns=p>0.05, * p<0.05, ** p<0.01, *** p<0.001.

higher levels adjacent to the macrophages, but no significant alteration at the cell edges compared to the control (Figure 5J, Figure 5-figure supplement 1L-N). We conclude that *Drosophila* Qsox1 can be secreted but is also found in the Golgi and endosomes like Mrva, and that both proteins affect LanA, a component of the ECM.

Conservation of Minerva's function in macrophage invasion and T antigen modification by its mammalian ortholog MFSD1

To determine if our studies could ultimately be relevant for mammalian biology and therefore also cancer research, we searched for a mammalian ortholog. MFSD1 from *mus musculus* shows strong sequence similarity with Mrva, with 50% of amino acids displaying identity and 68% conservation (Figure 6A, Figure 6-figure supplement 1A). A transfected C-terminally GFP-tagged form (Figure 6-figure supplement 1B) showed localization to the secretory pathway, colocalizing with the Golgi marker GRASP65 in murine MC-38 colon carcinoma, 4T1 breast cancer cells and LLC1.1 lung cancer (Figure 6B-C, Figure 6-figure supplement 1C-E) and with Golgi and endosomal markers in B16-BL6 melanoma cells (Figure 6C, Figure 6-figure supplement 1F). mmMFSD1 expression in macrophages in *mrva*^{3102} mutant embryos can completely rescue the germband invasion defect (Figure 6D-E). This macrophage-specific expression of MFSD1 also resulted in higher levels of T antigen on macrophages when compared to those in *mrva*^{3102} mutants (Figure 6F-G). Thus MFSD1 not only displays localization in the Golgi apparatus in multiple types of mammalian cancer but can also rescue O-glycosylation and migration defects when expressed in *Drosophila*, arguing that the functions Mrva carries out to promote invasion into the germband are conserved up to mammals.

Valoskova et al Figure 6

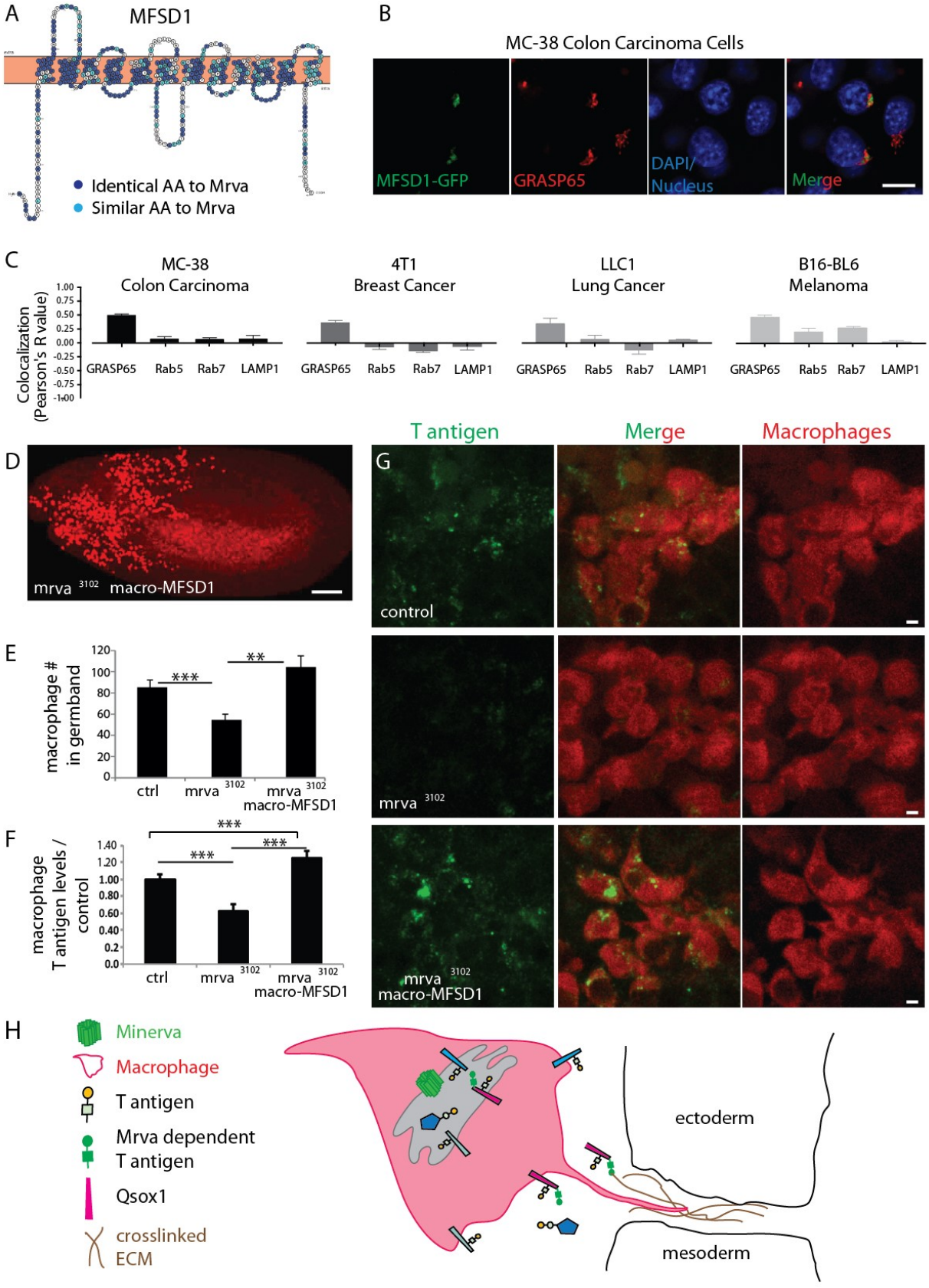

Figure 6: Minerva's murine ortholog, MFSD1, can substitute for Minerva's functions in migration and T-antigen glycosylation

Topology prediction of mouse MFSD1 (NP_080089.1) using the online tools TMPred (Hofman and Stoffel, 1993) and Protter (Omasits et al., 2014). 50% of amino acids are identical between the *M. musculus* MFSD1 and *D. melanogaster* sequence of *mrva (CG8602)* (NP648103.1) and are highlighted in dark blue, similar amino acids are in light blue. (**B**) Confocal images of MC38 colon carcinoma cells showing colocalization of MFSD1-eGFP (green) with the Golgi marker GRASP65 (red). DAPI labels the nucleus (blue). (**C**) Quantitation using Fiji of the colocalization of MFSD1-eGFP with the Golgi marker (GRASP65), early endosome marker (Rab5), late endosome marker (Rab7), and lysosome marker (LAMP1) in MC38 colon carcinoma, B16-BL6 melanoma, LLC1 Lewis lung carcinoma, and 4T1 breast carcinoma cells. Representative images are shown in Figure 6-figure supplement 1C-F (n=8-15, 5-9, 4-9, 5-10 cells per condition within the respective cancer types). (**D**) Confocal image of a Stage 12 fixed embryo showing that expression of *mmMFSD1* in macrophages under the direct control of the *srpHemo(macro)* promoter in the $mrva^{3102}$ mutant can rescue the defect in macrophage migration into the germband. Compare to Figure 3A,B. Macrophages visualized with *srpHemo-H2A::3xmCherry* for D-E. **(E**) Quantitation of the number of macrophages in the germband of early Stage 12 embryos from the control (n=25), $mrva^{3102}$ mutants (n=29), and $mrva^{3102}$ *srpHemo(macro)-mmMFSD1* (n=13, p=0.0005 for mutant vs control, p<0.0001 for mutant vs rescue). (**F**) Quantification of T antigen levels on macrophages in late Stage 11 embryos from control, $mrva^{3102}$mutant and $mrva^{3102}$ *srpHemo(macro)-mmMFSD1* embryos. T antigen levels normalized to those observed in the control (n=8-9 embryos, 280, 333, and 289 cells quantified respectively, p<0.0001 for both). **(G)** Confocal images of macrophages (red) on the germband border stained with T antigen antibody (green) in the control, the $mrva^{3102}$ mutant, and $mrva^{3102}$ *srpHemo(macro)-mmMFSD1* shows that mmMFSD1 expression in macrophages can rescue the decrease of macrophage T antigen observed in the $mrva^{3102}$ mutant. Macrophages visualized with *srpHemo-3xmCherry* for F-G. (**H**) Model for Minerva's function during macrophage invasion based on our findings and the literature: Minerva in the Golgi (grey) leads to increases in T antigen levels on a subset of proteins that aid invasion, including Qsox1 which regulates protein folding through disulfide bond isomerization. We propose that increased T antigen on Qsox1 facilitates its sulfhydryl oxidase activity that aids the formation of a robust crosslinked ECM which macrophages utilize during tissue entry. Significance was assessed by Kruskal-Wallis test with Conover post test analysis in **E,F**. ***p<0.001, ****p<0.0001. Scale bars are 10μm in B, 50μm in D, and 3μm in G. See also Figure 6-figure supplement

Discussion

O-glycosylation is one of the most common posttranslational modifications, yet the intrinsic technical challenges involved in identifying O-glycosites and altered O-glycosylation on a proteome-wide level has hampered the discovery of biological functions (Levery et al., 2015). Here we provide two important new advances for the field. First, we identify a key regulator of this O-glycosylation, Minerva, with an unexpected role for a member of the major facilitator superfamily. Our demonstration that this conserved protein affects invasion and the appearance of the cancer-associated core1 T glycoform on a set of proteins connected to invasion provides a new perspective on T glycoform regulation and may have implications for cancer. Second, we define the GalNAc-type O-glycoproteome of *Drosophila* embryos. As O-glycosites cannot as yet be reliably predicted, our proteomic characterization in a highly genetically accessible organism will permit future studies on how glycosylation affects cell behavior; we highlight T and Tn O-glycosylated receptors in **Table 2** to further this goal.

Valoskova et al Figure 6-figure supplement 1

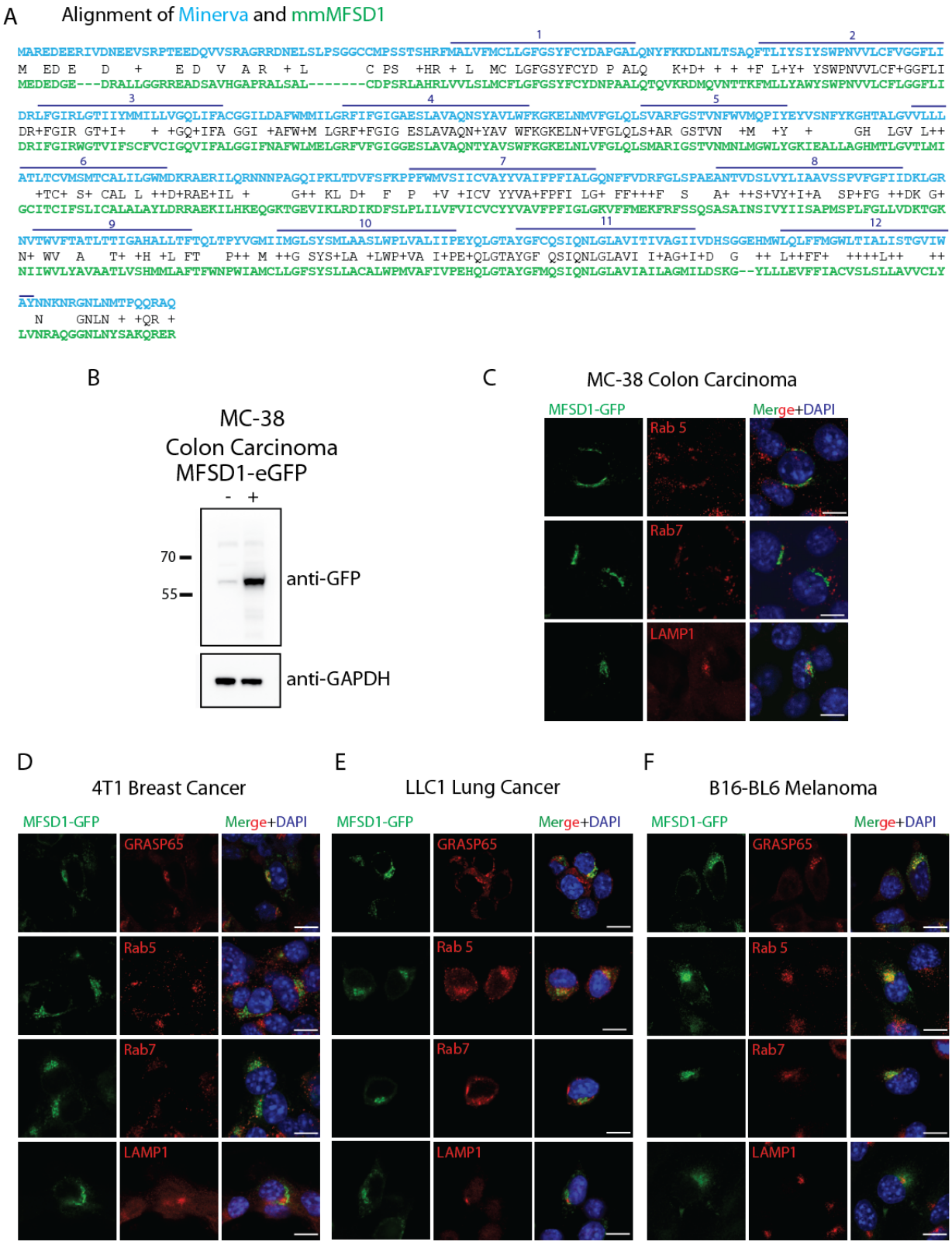

Figure 6-figure supplement 1: MFSD1-eGFP localization in colon carcinoma

(**A**) Alignment of Minerva and mmMFSD1 by BLAST. The first row shows the Minerva sequence in blue type, the second identical (one letter symbol) or similar (+) amino acids in black, and the third the mmMFSD1 sequence in green. Gaps are marked with '-'. The predicted twelve transmembrane domains of Minerva are shown with dark blue lines and numbered above**. (B)** Western blot of control (-) and Doxycycline induced (+) MFSD1-eGFP expression in MC-38 colon carcinoma cells. MFSD1-eGFP was detected with an anti-GFP antibody. GAPDH serves as a loading control. **(C-F)** Representative images from co-immunofluorescence of mouse MFSD1-eGFP (green) and the Golgi marker GRASP65, early endosome marker Rab5 or late endosome marker Rab7 (red) in **(C)** MC-38 colon carcinoma, **(D)** 4T1 breast cancer, **(E)** LLC1 Lewis lung carcinoma, and **(F)** B16 BL6 cells. Nuclei are labeled with DAPI (blue). Scale bars indicate 10μm in C-F.

Modifications of the O-glycoproteome by an MFS family member

Our identification of a MFS family member as a regulator of O-glycosylation is surprising. MFS family members can serve as transporters and shuttle a wide variety of substrates (Quistgaard et al., 2016; Reddy et al., 2012). Minerva displays homology to sugar transporter and is localized to the Golgi and endosomes. Minerva could thus affect O-glycosylation in the Golgi through substrate availability. However, the lower and higher levels of glycosylation in the *mrva*^{3102} mutant we observe are hard to reconcile with this hypothesis. Given that the changes in T antigen on individual glycosites in the *mrva* mutant are found either with no significant change in Tn or with a change in the same direction (**Table 1**), regulation appears to occur at the initial GalNAc addition on the protein subset as well as on further T antigen elaboration. 95% of the proteins with 10-fold altered glycosylation in the *mrva* mutant had multiple O-glycosylation sugar modifications compared to 56% of the general O-glycoproteome. Greatly enhanced glycosylation of protein sequences containing an existing glycan modification is observed for some GalNAc-Ts due to a lectin domain (Hassan et al., 2000; Kubota et al., 2006; Revoredo et al., 2016) and Minerva could theoretically affect such a GalNAc-T in *Drosophila*. Alternatively, Minerva, while in the "outward open" conformation identified for MFS structures (Quistgaard et al., 2016), may itself have a lectin-like interaction with Tn and T glycoforms that have already been added on a loop of particular proteins. Minerva's binding could open up the target protein's conformation to increase or block access to other potential glycosites and thus affect the final glycosylation state on select glycoproteins.

The changes we see in O-glycosylation are also likely due to a combination of Minerva's direct and indirect effects. O-GalNAc modification of vertebrate Notch can affect Notch signaling during development (Boskovski et al., 2015); the *Drosophila* ortholog of the responsible GalNAc transferase is also essential for embryogenesis (Bennett et al., 2010; Schwientek et al., 2002). A GalNAcT in *Xenopus* can glycosylate a peptide corresponding to the ActR IIB receptor and inhibit Activin and BMP type signaling (Herr et al., 2008; Voglmeir et al., 2015). Thus the changed glycosylation we observe on components of the Notch and Dpp pathways could alter transcription (Hamaratoglu et al., 2014; Ntziachristos et al., 2014), shifting protein levels and thereby changing the ratio of some glycopeptides in the *mrva* mutant relative to the wild type. Proteins in which glycosylation at other sites is unchanged or changed in the opposite direction are those most likely to be directly affected by Minerva. Such proteins include ones involved in protein folding and O-glycan addition and removal (**Figure 4H**) (Tien et al., 2008). If changes in the glycosylation of these proteins alters their specificity or activity, some of the shifts we observe in our glycoproteomic analysis could be indirect in a different way; an initial effect of Minerva on

the glycosylation of regulators of protein folding and glycosylation could change how these primary Minerva targets affect the glycosylation of a second wave of proteins.

An invasion program regulated by Minerva

The truncated immature core1 T and Tn O-glycans are not usually present in normal human tissues but exposure of these uncapped glycans has been found on the majority of cancers and serves as a negative indicator of patient outcome (Fu et al., 2016; Springer, 1984)**.** Increases in Tn antigen due to a shift in GalNAcT localization to the ER promote invasion and metastasis (Gill et al., 2013). An antibody against T antigen has decreased the metastatic spread of cancer cells in mice (Heimburg et al., 2006). Here we further strengthen the case for a causative relationship between T antigen modification and the invasive migration that underlies metastasis. The transient appearance of T antigen in human fetuses (Barr et al., 1989) and the conserved function of Minerva lead us to propose that the change in O-glycosylation in cancer represents the reactivation of an ancient developmental program for invasion. Our embryonic glycoproteome analysis identifies 106 T antigen modified proteins, a very large set to investigate. However, the absence of Mrva causes invasion defects and deficits in T antigen modification on only 10-20 proteins; these include components involved in protein folding, glycosylation modification, and the signaling pathways triggered by Notch and the BMP family member, Dpp.

Our working model is that the defect in germband tissue invasion seen in the *mrva* mutant is caused by the absence of T antigen on this group of proteins that act coordinately (**Figure 6H**). 56% of these have vertebrate orthologs, and 55% of those have already been linked to cancer and metastasis. The vertebrate ortholog of Qsox1, the protein with the largest changes in T antigen in the *mrva* mutant, enhances cancer cell invasion in *in vitro* assays and higher levels of the protein predict poor patient outcomes (Katchman et al., 2013, 2011). We find that the strongest effect of *Drosophila* Qsox1 on macrophage migration is to reduce the time by two fold that macrophages take sitting at the germband edge before they successfully begin to invade into the germband tissues. We also observe in *qsox1* and *mrva* mutants that LanA levels are higher within the macrophages and somewhat elevated near but not at the macrophage cell edges. This could be due to some combination of the following shifts in cellular processes: an increase in LanA production, a decrease in its degradation, a slowing of its secretion or a speeding of its diffusion. We base our model on the functions that have been previously defined for the Qsox1 sulfhydryl oxidase family, in integrating laminin into the ECM (Ilani et al., 2013) and aiding secretion of EGF domains (Tien et al., 2008) which are found in *Drosophila* Laminins. If Qsox1 is needed for the efficient secretion and integration of LanA into the ECM, its absence could result in a less robustly cross-linked matrix. ECM crosslinking has been shown to enhance Integrin signaling, focal adhesion formation, and invasion of mammalian tumor cells (Levental et al., 2009). In its absence *Drosophila* macrophages which utilize Integrin during invasion (Siekhaus et al., 2010) and whose invasive migration is accompanied by deformation of the flanking tissue (Ratheesh et al, 2018), could be unable to generate sufficient traction forces to enter. Indeed, mutating another subunit of the *Drosophila* Laminin trimer, LanB1, reduces both normal LanA deposition and germband invasion by macrophages (Matsubayashi et al., 2017; Sánchez-Sánchez et al., 2017). A determination of the effect of Minerva's regulation awaits a characterization of Qsox1 mutated such that it is incapable of being modified by T antigen on the Mrva-dependent sites. Nonetheless, the similarity of the changes in LanA we observe in the $mrva^{3102}$ and

qsox1^{KG046152} mutant supports the conclusion that Mrva dependent T-antigen modification of Qsox1 is necessary for its activity on some substrates. Given that *mrva*^{3102} mutants take even longer than *qsox1*^{KG04615} to enter germband tissue and display much stronger defects thereafter, we propose that T antigen modifications on other proteins are also crucial for tissue entry, and underlie the defect in invasive migration within the germband.

Minerva's vertebrate ortholog, MFSD1, can rescue macrophage migration defects and restores higher T antigen levels. Tagged versions of Minerva's vertebrate ortholog, MFSD1, detected the protein in lysosomes in HeLa and rat liver cells (Chapel et al., 2013; Palmieri et al., 2011). In four metastasizing mouse tumor cell lines we find MFSD1 mainly in the Golgi, where O-glycosylation is known to occur (Bennett et al., 2012). We do not yet know if invasion and metastasis is altered by the absence of MFSD1 but will be testing this in future work. Akin to how kinases add phospho-groups to affect a set of proteins and orchestrate a particular cellular response, we propose that Minerva in *Drosophila* macrophages and its vertebrate ortholog MFSD1 in cancer trigger changes in O-glycosylation that coordinately modulate, activate and inhibit a protein group to affect cellular dissemination and tissue invasion.

Material and Methods

Key resource table

Designation	**Source or reference**	**Identifiers**	**Additional information**
mrva	NA	FlyBase:FBgn0035763	
qsox1	NA	FlyBase: FBgn0033814	
C1GalTA	NA	FlyBase: FBgn0032078	
srp-Gal4	PMID: 15239955		
srp-3xmCherry	PMID: 29321168	RRID:BDSC_78358 and 78359	
srp-H2A::3xmCherry	PMID: 29321168	RRID:BDSC_78360 and 78361	
UAS-CG8602::FLAG::HA	PMID: 22036573		
mrva^{3102}	Bloomington *Drosophila* Stock Center (BDSC), RRID:SCR_006457	RRID:BDSC_17262	

Df(3L)BSC117	BDSC, RRID:SCR_006457	RRID:BDSC_8976	
UAS-mCherry.NLS	BDSC, RRID:SCR_006457	RRID:BDSC_38425	
C1GalTA2.1	BDSC, RRID:SCR_006457	RRID:BDSC_28834	
C1GalTA RNAi 1	Vienna *Drosophila* Resource Centre (VDRC), RRID:SCR_013805	VDRC: 2826	
C1GalTA RNAi 2	VDRC, RRID:SCR_013805	VDRC: 110406	
CG8602 RNAi	VDRC, RRID:SCR_013805	VDRC: 101575	
qsox1RNAi	VDRC, RRID:SCR_013805	VDRC: 108288	
qsox1 KG04615	BDSC, RRID:SCR_006457	RRID:BDSC_13824	
MC-38	Other		Gift from Borsig lab, Univ of Zurich (UZH)
4T1	Other	ATCC Cat# CRL-2539, RRID:CVCL_0125	Gift from Borsig lab, UZH
LLC1	Other	ATCC Cat# CRL-1642, RRID:CVCL_4358	Gift from Borsig lab, UZH
B16-BL6	Other	NCI-DTP Cat# B16BL-6, RRID:CVCL_0157	Gift from Borsig lab, UZH
S2R+	Other		Gift from Frederico Mauri of the Knoblich lab at IMBA, Vienna
srpHemo-CG8602::3xmCherry	this paper		CG8602 amplified from genome

			cloned into DSPL172 (PMID: 29321168)
MT-CG8602::FLAG::HA	*Drosophila* Genomic Resource Center (DGRC), RRID:SCR_002845	DGRC: FMO06045	
MT-Qsox1::FLAG::HA	DGRC, RRID:SCR_002845	DGRC: FMO06379	
PTS1-GFP	Other		Gift from Dr. McNew
MFSD1-eGFP	this paper		MFSD1 amplified from dendritic cell cDNA library, inserted into Doxycycline inducible expression vector pInducer20
anti-GFP clone 2B6	Other		Gift from Ogris lab, MFPL Vienna; (1:100) for WB
anti-GFP clone 5G4	Other		Gift from Ogris lab, MFPL Vienna; (1:50) for immunochemistry
anti-T-antigen (mouse monoclonal)	PMID: 23584533		(1:5 for immunochemistry; 1:10 for WB)
anti-profilin (mouse monoclonal)	Developmental Studies Hybridoma Bank (DSHB), RRID:SCR_013527	DSHB Cat# chi 1J, RRID:AB_528439	(1:50)
anti-GAPDH (rabbit monoclonal)	Abcam, RRID:SCR_012931	Abcam Cat# ab181603, RRID:AB_2687666	(1:10000) for WB

anti-GRASP65 (rabbit polyclonal)	Thermo Fisher Scientific, RRID:SCR_008452	ThermoFischer Cat# PA3-910, RRID:AB_2113207	(1:200) for immunochemistry
anti-Rab5 (rabbit monoclonal)	Cell Signaling Technology (CST), RRID:SCR_004431, Clone C8B1	CST Cat# 3547, RRID:AB_2300649	(1:200) for immunochemistry
anti-Rab7 (rabbit monoclonal)	CST, RRID:SCR_004431, Clone D95F2	CST Cat# 9367, RRID:AB_1904103	(1:200) for immunochemistry
anti-LAMP1 (rabbit polyclonal)	Abcam, RRID:SCR_012931	Abcam Cat# ab24170, RRID:AB_775978	(1:200) for immunochemistry
anti- Cnx99a (mouse monoclonal)	DSHB, RRID:SCR_013527	DSHB Cat# Cnx99A 6-2-1, RRID:AB_2722011	(1:5)
anti- Hrs 27.4 (mouse monoclonal)	DSHB, RRID:SCR_013527	DSHB Cat# Hrs 27-4, RRID:AB_2618261	(1:5)
anti- Golgin 84 (mouse monoclonal)	DSHB, RRID:SCR_013527	DSHB Cat# Golgin84 12-1, RRID:AB_2722113	(1:5)
anti Rab7 (mouse monoclonal)	DSHB, RRID:SCR_013527	DSHB Cat# Rab7, RRID:AB_2722471	(1:5)
anti-GMAP (goat polyclonal)	DSHB, RRID:SCR_013527	DSHB Cat# GMAP, RRID:AB_2618259	(1:50)
anti- Golgin 245 (goat polyclonal)	DSHB, RRID:SCR_013527	DSHB Cat# Golgin245, RRID:AB_2618260	(1:50)
anti- HA (rat monoclonal)	Roche, RRID:SCR_001326	Roche Cat# 3F10, RRID:AB_2314622	(1:50)
anti-LanA (rabbit polyclonal)	PMID:9257722		gift from Stefan Baumgartner
anti-Vasa (rat monoclonal)	DSHB, RRID:SCR_013527	DSHB Cat# anti-vasa, RRID:AB_760351	(1:25)

Alexa 488- or 557- or 633-secondaries	Thermo Fisher Scientific, RRID:SCR_008452		(1:500 for 488 and 557; 1:100 for 633)
goat-anti-rabbit IgG (H+L)-HRP	BioRad	Bio-Rad Cat# 170-6515, RRID:AB_2617112	(1:10000)
goat-anti-mouse IgG (H/L):HRP	BioRad	Bio-Rad Cat# 170-6516, RRID:AB_11125547	(1:10000)
LysoTracker Green DND-26	Invitrogen, RRID:SCR_008410	L7526	75nM
Alexa Fluor 488 Phalloidin	Invitrogen, RRID:SCR_008410	A12379	(1:500)
Vectashield mounting medium	Vector Laboratories, RRID:SCR_000821	VectorLabs: H-1000	
Vectashield mounting medium with DAPI	Vector Laboratories, RRID:SCR_000821	VectorLabs: H-1200	
Halocarbon Oil 27	Sigma-Aldrich, RRID:SCR_008988	Sigma Aldrich: Cat# H8773	
srpHemo-mrva	this paper		CG8602 amplified from genome cloned into srpHemo plasmid
srpHemo-MFSD1	this paper		mmMFSD1 amplified from dendritic cell cDNA library cloned into srpHemo plasmid
Mrva fw	Fly Primer Bank		qPCR; 5'TGTGCTTCGTGGGAGGTTTC
Mrva rv	Fly Primer Bank		qPCR; 5'GCAGGCAAAGATCAACTGACC

C1GalTA fw	Fly Primer Bank		qPCR; 5'TGCCAACAGT CTGCTAGGAAG
C1GalTA rv	Fly Primer Bank		qPCR: 5'CTGTGATGTG CATCGTTCACG
Ugalt fw	Fly Primer Bank		qPCR; 5'GCAAGGATGC CCAGAAGTTTG
Ugalt rv	Fly Primer Bank		qPCR; 5'GATATAGACC AGCGAGGGGAC
RpL32 fw	Fly Primer Bank		qPCR; 5'AGCATACAGG CCCAAGATCG
RpL32 rv	Fly Primer Bank		qPCR; 5'TGTTGTCGAT ACCCTTGGGC
Lectin staining kit #2	EY Laboratories	EYLabs:FLK-002	
FIJI	http://fiji.sc/ RRID:SCR_002285)		
Imaris	http://www.bitplane.com/imaris/imaris, RRID:SCR_007370		
Matlab	https://www.mathworks.com/products/matlab.html, RRID:SCR_001622		
FlowJo	https://www.flowjo.com/RRID:SCR_008520		
LaVision ImSpector	http://www.lavisionbiotec.com/, RRID:SCR_015249		
Proteome Discoverer 1.4	https://www.thermofisher.com/order/catalog/product/OPTON-		

	30795, RRID:SCR_014477		
LightCycler 480 software	https://lifescience.roche.com/en_at/products/lightcycler14301-480-software-version-15.html		
GraphPad Prism	https://www.graphpad.com/scientific-software/prism/ RRID:SCR_002798		

Fly work

Flies were raised on food bought from IMBA (Vienna, Austria) which contained the standard recipe of agar, cornmeal, and molasses with the addition of 1.5% Nipagin. Adults were placed in cages in a Percival DR36VL incubator maintained at 29ºC and 65% humidity; embryos were collected on standard plates prepared in house from apple juice, sugar, agar and Nipagin supplemented with yeast from Lesaffre (Marcq, France) on the plate surface. Embryo collections for fixation (7 hour collection) as well as live imaging (4.5 hour collection) were conducted at 29ºC.

Fly Lines utilized: *srpHemo-GAL4* was provided by K. Brückner (UCSF, USA) (Brückner et al., 2004), *UAS-CG8602::FLAG::HA* (from K. VijayRaghavan National Centre for Biological Sciences, Tata Institute of Fundamental Research) (Guruharsha et al., 2011). The stocks w^{1118}*;* $minerva^{3102}$ (BDSC-17262), (pn^{1};; $ry^{503}Dr^{1}$P[Δ 2-3] (BDSC-1429), *Df(3L)BSC117* (BDSC-8976), *Oregon R* (BDSC-2375), w^{-}*; P{w[+mC]=UAS-mCherry.NLS}2;MKRS/Tm6b, Tb[1]* (BDSC-38425), w^{-}*,P{UAS-Rab11-GFP}2* (BDSC-8506), *y[1] sc[*] v[1]; P{y[+t7.7] v[+t1.8]=TRiP.GL00069}attP2* (BDSC-35195), *y[1] w[*]; Mi{y[+mDint2]=MIC}GlcAT-P[MI05251]/TM3, Sb[1]* (BDSC-40779) were obtained from the Bloomington *Drosophila* Stock Centre, Bloomington, USA. The RNAi lines v60100, v110406, v2826, v101575 were obtained from the Vienna *Drosophila* Resource Center (VDRC), Vienna, Austria. Lines w^{-}; *P{w[+mC*; *srpHemo-3xmCherry}*, w^{-}; *P{w[+mC; srpHemo-H2A::3xmCherry}* were published previously (Gyoergy et al., 2018).

Exact genotype of *Drosophila* lines used in Figures:

Figure 1D-H: *w-; +; srpHemo-3xmCherry.* **I-K**: Control: *w- P(w+)UAS-dicer/w-; P{attP,y[+],w[3`]/+; srpHemo-Gal4 UAS-GFP UAS-H2A::RFP/+.* C1GalTA RNAi: w^{-} *P(w+)UAS-dicer2/w-; RNAi C1GalTA (v110406)/+; srpHemo-Gal4 UAS-GFP UAS-H2A:RFP/+.* **L**: Control: *w-; +; srpHemo-H2A::3xmCherry. C1GalLTA* mutant: *w-;* $C1GalTA^{2.1}$*; srpHemo-H2A::3xmCherry.* **M**: Control: *w-; srpHemo-H2A::3xmCherry. GlcAT-P* mutant: *w-; srpHemo-H2A::3xmCherry, Mi{MIC}GlcAT-PMI05251.* **Figure 1-figure supplement 1A-L***: w-; +; srpHemo-3xmCherry.* **M, N, P**: Control: *w-UAS-Dicer2/w-; P{attP,y[+]w[3`]/+; srpHemo-Gal4 UAS-GFP UAS-H2A::RFP/+ . C1GalTA* RNAi: *w-UAS-Dicer2/ w-; RNAi C1GalTA (v110406)/+; srpHemo-Gal4 UAS-GFP UAS-H2A::RFP/+*. **O:**

Control: *w-; +; srpHemo-H2A::3xmCherry. C1GalTA* mutant: *w-; C1GalTA$^{2.1}$; srpHemo-H2A::3xmCherry*. **P**: Control: *w- UAS-Dicer2/w-; P{attP,y[+]w[3`]/+; srpHemo-Gal4 UAS-GFP UAS-H2A::RFP/+ . C1GalTA* RNAi: *w-UAS-Dicer2/ w-; RNAi C1GalTA (v2826)/+; srpHemo-Gal4 UAS-GFP UAS-H2A::RFP/+*. **Q**: Control: *w-; srpHemo-H2A::3xmCherry. GlcAT*-P mutant: *w-; srpHemo-H2A::3xmCherry; Mi{MIC}GlcAT-PMI05251.*

Figure 2A, B, D: *w-; +; srpHemo-3xmCherry.* **E**, **F, G:** Control: *w-; +; srpHemo-3xmCherry. CG8602* mutant: *w-; +; srpHemo-3xmCherry,P{EP}CG8602^{3102}.* **I:** *w-; srpHemo-Gal4; UAS-CG8602::FLAG::HA.*

Figure 3A: *w-; +; srpHemo-H2A::3xmCherry.* **B:** *w-; +; srpHemo-H2A::3xmCherry, P{EP}CG8602^{3102}.* **C:** *w-; srpHemo-CG8602; srpHemo-H2A::3xmCherry P{EP}CG8602^{3102}*. **D:** Control*: w-; srpHemo-Gal4 UAS-mCherry::nls; +*. CG8602 (Mrva) mutant*: w-; srpHemo-Gal4 UAS-mCherry::nls; P{EP}CG8602^{3102},* Df cross: *w-; srpHemo-Gal4 UAS-mCherry:nls; P{EP}CG8602^{3102}/ Df(3L)BSC117.* Rescue*: w-; srpHemo-Gal4 UAS-mCherry:nls; UAS-CG8602::FLAG::HA P{EP}CG8602^{3102}*. Precise excision: *srpHemo-Gal4 UAS-mCherry:nls; P{EP}CG8602^{3102}Δ32.* **E:** Control: *w^{-} P(w+)UAS-dicer/+; +; srpHemo-Gal4 UAS-GFP UAS-H2A:RFP/+*. Mrva RNAi: *w- UAS-dicer2/w-; RNAi CG8602 (v101575)/+; srpHemo-Gal4 UAS-GFP UAS-H2A:RFP/+*. **F**: Control: *w-; srpHemo-Gal4 UAS-mCherry::nls; +*. *mrva* mutant: *w-; srpHemo-Gal4 UAS-mCherry::nls; P{EP}CG8602^{3102}* .**G**: Control: *w-; +; srpHemo-3xmCherry.* Mrva mutant: *w-; +; srpHemo-3xmCherry P{EP}CG8602^{3102}. cadherin mrva* double mutant: *w-; shg^{P34}; srpHemo-3xmCherry P{EP}CG8602^{3102}.* **H**: Control: *w-; +; srpHemo-3xmCherry. mrva* mutant: *w-; +; srpHemo-3xmCherry P{EP}CG8602^{3102}* **I-M**: Control: *w-; +; srpHemo-H2A::3xmCherry. mrva* mutant: *w-; +; srpHemo-H2A::3xmCherry P{EP}CG8602^{3102}.*

Figure 3-figure supplement 1A: Control: *w-; +; srpHemo-H2A::3xmCherry. mrva* mutant: *w-; +; srpHemo-H2A::3xmCherry P{EP}CG8602^{3102}.* Rescue: *w-; srp-CG8602; srpHemo-H2A::3xmCherry P{EP}CG8602^{3102}.* **B, C, E:** Control: *w-; +; srpHemo-Gal4 UAS-GFP UAS-H2A:RFP/+. mrva* RNAi: *w-; RNAi CG8602 (v101575)/+; srpHemo-Gal4 UAS-GFP UAS-H2A::RFP/+.* **D, F-G**: Control: *w-; +; srpHemo-H2A::3xmCherry. mrva* mutant: *w-; +; srpHemo-H2A::3xmCherry P{EP}CG8602^{3102}.* **H-L*:*** **Control:** *w-; +; srpHemo-3xmCherry. mrva* mutant: *w-; +; srpHemo-3xmCherry P{EP}CG8602^{3102}*

Figure 4A-I: Control: *w-; +, srpHemo-3xmCherry*. *mrva* mutant: *w-; +, srpHemo-3xmCherry P{EP}CG8602^{3102} .*

Figure 5A-B: Control: *w-; +; srpHemo-3xmCherry. qsox1* mutant: *w-;P{SUPor-P}Qsox1KG04615; srpHemo-3xmCherry.* **C**: *w/ y,w[1118]; P{attP,y[+],w[3`]}/srpHemo-Gal4; srpHemo-H2A::3xmCherry/+. qsox1* RNAI: *w-/ y,w[1118]; v108288/srpHemo-Gal4; srpHemo-H2A::3xmCherry/+.* **D-G**: Control: *w-; +; srpHemo-H2A::3xmCherry. qsox1* mutant: *w-;P{SUPor-P}Qsox1KG04615; srpHemo-H2A::3xmCherry*. **J**: Control: *w-; +; srpHemo-3xmCherry.* Mrva mutant: *w-; +; srpHemo-3xmCherry P{EP}CG8602^{3102}. qsox1* mutant: *w-; P{SUPor-P}Qsox1KG04615;srpHemo-3xmCherry.*

Figure 5-figure supplement 1A-B*:* Control: *w-; +; srpHemo-3xmCherry. qsox1* mutant: *w-;P{SUPor-P}Qsox1KG04615; srpHemo-3xmCherry.* **C, F**: *w-; +; srpHemo-H2A::3xmCherry, w-; P{SUPor-P}Qsox1KG04615; srpHemo-H2A::3xmCherry.* **D-E**: Control: *w-/ y,w[1118]; P{attP,y[+],w[3`]}/srpHemo-Gal4; srpHemo-H2A::3xmCherry/+. qsox1* RNAi: *w-/ y,w[1118]; v108288/srpHemo-Gal4; srpHemo-H2A::3xmCherry/+.* **K-N:** Control: *w-; +; srpHemo-3xmCherry.* Mrva mutant: *w-; +; srpHemo-3xmCherry P{EP}CG8602^{3102}, qsox1* mutant: *w-; P{SUPor-P}Qsox1KG04615; srpHemo-3xmCherry.*

Fig**ure 6D**: *w-; srpHemo-MFSD1; srpHemo-H2A::3xmCherry P{EP}CG8602^{3102}.* **E**: Control: *w-; +; srpHemo-H2A::3xmCherry. mrva* mutant: *w-; +; srpHemo-H2A::3xmCherry P{EP}CG8602^{3102}.* MFSD1 rescue*: w-; srpHemo-MFSD1; srpHemo-H2A::3xmCherry P{EP}CG8602^{3102}.* **F, G**: Control: *w-; +; srpHemo-3xmCherry. mrva* mutant: *w-; +; srpHemo-3xmCherry P{EP}CG8602^{3102}.* MFSD1 rescue*: w-; srpHemo-MFSD1; srpHemo-3xmCherry P{EP}CG8602^{3102}*.

Embryo Fixation and Immunohistochemistry

Embryos were collected on apple juice plates from between 6 and 8.5 hours at 29°C. Embryos were incubated in 50% Chlorox (DanClorix) for 5 min and washed. Embryos were fixed with 17% formaldehyde/heptane for 20 min followed by methanol or ethanol devitellinization except for T antigen analysis, when embryos were fixed in 4% paraformaldehyde/heptane. Fixed embryos were blocked in BBT (0.1M PBS + 0,1% TritonX-100 + 0,1% BSA) for 2 hours at RT. Antibodies were used at the following dilutions: α-T antigen (Steentoft et al., 2011) 1:5, α-GFP (Aves Labs Inc., Tigard, Oregon) 1:500; α-LanA (Kumagai C, et al., 1997) (a gift from Stefan Baumgartner) 1:500; α-Vasa (Aruna et al., 2009) (DSHB, deposited by A. Sprading/ D. Williams) 1:25; and incubated overnight at 4°C (GFP) or room temperature (T antigen, LanA). Afterwards, embryos were washed in BBT for 2 hours, incubated with secondary antibodies (Thermo Fisher Scientific, Waltham, Massachusetts, USA) at RT for 2 hours, and washed again for 2 hours. Vectashield (Vector Laboratories, Burlingame, USA) was then added. After overnight incubation in Vectashield at 4°C, embryos were mounted on a slide and imaged with a Zeiss Inverted LSM700 Confocal Microscope using a Plan-Apochromat 20X/0.8 Air Objective or a Plan-Apochromat 63X/1.4 Oil Objective.

Ovary dissection and immunostaining

3-5 day old females were fed with yeast for 2 days at 25°C. For ovary dissection, females were anesthetized using the FlyNap anesthetic kit (Carolina, Burlington, NC, USA) and further transferred to ice cold PBS in which ovaries were extracted with pre-cleaned forceps. Individual ovaries were fixed in 4% Paraformaldehyde/PBS at room temperature (RT) for 20 minutes with agitation. Three wash steps with PBS at RT for 10 minutes were performed and individual ovaries were incubated in PBS supplemented with 0.1% of Triton X-100 (PBT) for 10 minutes at RT to allow permeabilization of the tissue. Ovaries were incubated in phalloidin-A488 (Thermo Fisher) diluted in PBT (1:300) overnight at 4°C. After being washed with PBT and PBS, ovaries were mounted in Vectashield+DAPI (LifeTechnologies, Carlsbad, USA).

Fixed ovary image analysis for border cell migration

Ovaries were imaged as a Z-series (1µm apart) with a Plan-Apochromat 20X/0.8 Air Objective on a Zeiss LSM700 inverted microscope. Images were acquired from stage 10 oocytes and maximum-intensity projections were created using ImageJ (NHI, USA). Border cells were identified by the clustered nuclei and their enriched actin staining. Border cell migration was quantified in the DAPI images as the percentage observed relative to the expected migration to the edge of the oocyte for these cells in stage 10 oocytes. Measurements were performed using ImageJ software (NIH, USA).

Lectin staining

Embryos were fixed with 10% formaldehyde/heptane and devitellinized with Ethanol. Blocking was conducted in BBT for 2 hours at room temperature. A FITC-labeled lectin kit #2 (EY laboratories, San Mateo, CA, USA) was utilized (table below summarizes abbrevations of used lectins). Each lectin was diluted to 1:25 and incubated with fixed embryos overnight at room temperature (RT). Embryos were washed in BBT for 2 hours at RT and Vectashield was added. After overnight incubation at 4°C, embryos were mounted on a slide and imaged with a Zeiss Inverted LSM700 Confocal Microscope using a Plan-Apochromat 63X/1.4 Oil Objective. Macrophages in late Stage 11 embryos were imaged at germband entry and evaluated by eye for enriched staining on macrophages compared to other tissues.

Lectin	**peanut agglutinin**	**Ulex europaeus agglutinin**	**Wheat germ agglutinin**	**Griffonia simplicifolia agglutinin I**	**Maclura pomifera agglutinin**	**Griffonia simplicifolia agglutinin II**
Abbreviation	PNA	UEA-I	WGA	GS-I	MPA	GS-II
Lectin	**Soybean agglutinin**	**Dolichos biflorus agglutinin**	**Concanavalin A**	**Helix pomatia agglutinin**	**Limulus poly-phenus agglutinin**	**Bauhinia purpurea agglutinin**
Abbreviation	SBA	DBA	ConA	HPA	LPA	BPA

Macrophage extraction

Embryos were bleached in 50% Chlorox in water for 5 minutes at RT. Stage late 11/early 12 embryos were lined up and then glued to 50 mm Dish No. 0 Coverslip, 14 mm Glass Diameter, Uncoated dish (Zeiss, Germany). Cells from the germband margin were extracted using a ES Blastocyte Injection Pipet (spiked, 20µm inner diameter, 55mm length; BioMedical Instruments, Germany). Extracted cells were placed in Schneider's medium (Gibco, Dublin, Ireland) supplemented with 20% FBS (Sigma-Aldrich, Saint Louis, Missouri, USA).

Immunohistochemistry of extracted macrophages

Extracted macrophages were collected by centrifugation at 500g for 5 min at room temperature. The cell pellet was resuspended in a small volume of Phospho-buffered saline (PBS) and smeared on a cover slip. The cell suspension was left to dry before cells were fixed with 4% paraformaldehyde in 0.1M Phosphate Buffer for 20 min at room temperature. Cells were washed 3 times in 0.1M PBS and permeabilized in 0.5% Triton-X 100 in PBS. Cells were blocked for 1 hour at room temperature in 20% Fetal Bovine Serum + 0.25% Triton X-100 in PBS. Primary antibodies were diluted in blocking buffer: anti-HA (Roche, Basel, Switzerland) 1:50, anti-Golgin 84, 1:25, anti-Calnexin 99a 1:25, anti-Hrs.8.2 1:25 or anti-Rab7 1:25 all from DSHB (Riedel et al., 2016), and incubated for 1 hour at room temperature. Cells were then washed 5 times in blocking buffer. Secondary antibodies were diluted in blocking buffer: anti-rat 633 1:300, anti-mouse 488 1:300 (both from ThermoFisher Scientific, Waltham, Massachusetts, USA). Secondary antibodies were incubated for 1 hour at room temperature. Cells were washed 5 times in PBS + 0.1% Triton X-100 and mounted in VectaShield+DAPI (LifeTechnologies, Carlsbad, USA) utilized at 1:75.

S2 cell work

S2R+ cells (a gift from Frederico Mauri of the Knoblich laboratory at IMBA, Vienna) were grown in Schneider's medium (Gibco) supplemented with 10% FBS (Gibco) and transfected with PTS1-GFP (a gift from Dr. McNew) and/or the *srpHemo-CG8602::3xmCherry* construct using Effectene Tranfection Reagent (Qiagen, Hilden, Germany) following the manufacturer's protocol. Transfected S2R+ cells were grown on Poly-L-Lysine coated coverslips (ThermoFisher Scientific, Waltham, Massachusetts, USA) in complete Schneider's medium (Gibco) supplemented with 10% FBS (Sigma-Aldrich, Saint Louis, Missouri, USA) and 1% Pen/Strep (Gibco) to a confluency of 60%. To visualize lysosomes, cells were incubated with Lysotracker 75nM Green DND-26 (Invitrogen) in complete Schneider's medium for 30 minutes at 25°C. Cells were washed in complete Schneider's medium 3 times before imaging on an inverted LSM-700 (Zeiss). To visualize mitochondria, mitotracker Green FM (Invitrogen, Carlsbad, CA, USA) was diluted in prewarmed Schneider's medium supplemented with 1% Pen/Strep to a concentration of 250nM. Cells were incubated in the Mitotracker solution for 45 minutes at 25°C. Cells were then washed 3 times in complete Schneider's medium before imaging.

To visualize Golgi, ER, early and late endosomes as well as the nucleus, S2R+ cells were transfected with MT-CG8602::FLAG::HA (DGRC: FMO06045) or MT-Qsox1::FLAG::HA (DGRC: FMO06379) with Effectene Tranfection Reagent (Qiagen) following the manufacturer's protocol. 24 hours after transfection gene expression was induced by addition of 1mM Cu2SO4 (Sigma) and cells were incubated for an additional 24 hours. Cells were then fixed in 4% PFA (Sigma) in 0.1M PB for 20 min at room temperature, permeabilized in 0.5% Triton X-100 (Sigma) in PBS for 15 min and blocked for 2 hours in 20% FBS (Sigma), 0.25% Triton X-100 in PBS at room temperature.

Cells were then stained with anti-HA antibody 1:50 (Roche) and either anti-Cnx99a (1:5), anti-Hrs 8.2 (1:5), anti- Golgin 84 (1:5), anti-Rab7 (1:5), anti- GMAP (1:50) or anti- Golgin 245 (1:50) (all antibodies from DSHB) (Riedel et al. 2011). Cells were washed in 20% FBS (Sigma), 0.25% Triton X-100 in PBS 5 times and then incubated with anti-rat Alexa Fluor 633 1:50 and either anti- mouse Alexa Fluor 488 or anti-goat Alexa Fluor 488 1:100 (Thermo Fisher) for 2 hours at room temperature. Cells were washed again 5 times and then mounted in Vectashield Mounting Medium + DAPI (Vector Laboratories) and imaged with Zeiss LSM 700 or 800 confocal microscopes. Quantitation of colocalization was performed as indicated below.
The cell line was routinely tested for Mycoplasm infection and found to be negative.

DNA Isolation from Single Flies

Single male flies were frozen for at least 3 hours before grinding them in 100mM Tris-HCl, 100mM EDTA, 100mM NaCL and 0.5% SDS. Lysates were incubated at 65°C for 30 minutes. Then 5M KAc and 6M LiCl were added at a ratio of 1:2.5 and lysates were incubated on ice for 10 min. Lysates were centrifuged for 15 minutes at 20,000xg, supernatant was isolated and mixed with Isopropanol. Lysates were centrifuged again for 15 minutes at 20.000xg, supernatant was discarded and the DNA pellet was washed in 70% EtOH and subsequently dissolved in ddH20.

FACS sorting

Embryos were collected for 1 hour and aged for an additional 5 hours, all at 29°C. Embryos collected from w- flies were processed in parallel and served as a negative control. Embryos were

dissociated as described previously (Gyoergy et al., 2018). The cells were sorted using a FACS Aria III (BD) flow cytometer. Emission filters were 600LP, 610/20 and 502 LP, 510/50. Data was analyzed with FlowJo software (Tree Star). The cells from the dissociated negative control *w*$^{-}$ embryos were sorted to set a baseline plot.

qPCR

RNA was isolated from approximately 50,000 mCherry positive or mCherry negative FACS sorted macrophages using RNeasy Plus Micro Kit (Qiagen, Hilden, Germany following manufacturer's protocol. RNA was also isolated from 50-100 mg of ovaries (about 15-20 pairs of ovaries extracted as indicated above). Ovaries were homogenized with a pellet homogenizer (VWR, Radnor, USA) and plastic pestles (VWR, Radnor, USA) in 1ml of Trizol (Thermo Fisher Scientific, Waltham, MA, USA) and centrifuged at 12,000xg for 5 min at 4°C. Further steps were according to the manufacturers protocol. The resulting RNA was used for cDNA synthesis using Sensiscript RT Kit (macrophages) or Omniscript (ovaries) (Qiagen, Hilden, Germany) and oligo dT primers. A Takyon qPCR Kit (Eurogentec, Liege, Belgium) was used to mix qPCR reactions based on the provided protocol. qPCR was run on a LightCycler 480 (Roche, Basel, Switzerland) and data were analyzed in the LightCycler 480 Software and Prism (GraphPad Software). Data are represented as relative expression to a housekeeping gene ($2^{-\Delta ct}$) or fold change in expression ($2^{-\Delta\Delta ct}$). Primer sequences utilized for flies were obtained from the FlyPrimerBank (http://www.flyrnai.org/FlyPrimerBank). Minerva/CG8602: Fw pr TGTGCTTCGTGGGAGGTTTC, Rv pr GCAGGCAAAGATCAACTGACC. C1GalTA: Fw pr TGCCAACAGTCTGCTAGGAAG, Rv pr CTGTGATGTGCATCGTTCACG. Ugalt: Fw pr GCAAGGATGCCCAGAAGTTTG, Rv pr GATATAGACCAGCGAGGGGAC. RpL32: Fw pr AGCATACAGGCCCAAGATCG, Rv pr TGTTGTCGATACCCTTGGGC

Protein preps from embryos for Western

Embryos were collected for 7 hours at 29ºC, bleached and hand-picked for the correct Stage. 50-200 embryos were smashed in RIPA buffer (150mM NaCl, 0,5% Sodiumdeoxychalat, 0,1% SDS, 50mM Tris, pH 8) with Protease inhibitor (Complete Mini, EDTA free, Roche, Basel, Switzerland) using a pellet homogenizer (VWR, Radnor, USA) and plastic pestles (VWR, Radnor, USA) and incubated on ice for 30 min. Afterwards, samples were centrifuged at 4ºC, 16,000g for 30 min and the supernatant was collected and used for experiments. The protein concentration was quantified using the Pierce BCA Protein Assay Kit (ThermoFisher Scientific).

Western Blots

30 µg of protein samples were loaded on a 4-15% Mini-PROTEAN TGX Precast Protein Gel (Bio-Rad, Hercules, USA) and run at 100V for 80 min in 1x running buffer (25mM Tris Base, 190mM glycine and 0.1%SDS) followed by transfer onto Amersham Protran Premium 0.45 µm NC (GE Healthcare Lifescience, Little Chalfont, UK) or Amersham Hybond Low Fluorescence 0.2 µm PVDF (GE Healthcare Lifescience, Little Chalfont, UK) membrane using a wet transfer protocol with 25mM Tris Base, 190 mM Glycine + 20% MeOH at either 100 Volts for 60 min or 200mA for 90 min at Mini Trans-Blot Cell Module (Bio-Rad, Hercules, USA). Membranes were blocked in PBS-T (0.1% Triton X-100 in PBS) containing 2% BSA or Pierce Clear Milk Blocking Buffer (ThermoFisher Scientific) for 1 hour at RT. Primary antibodies were incubated overnight at 4ºC at the following concentrations: α-T antigen (Copenhagen) 1:10, α-profilin (Verheyen and Cooley, 1994, DSHB)

1:50, anti-GFP (clone 2B6, Ogris lab, MFPL), anti-GAPDH (ab181603, Abcam, Cambridge, UK). Afterwards, blots were washed 3x for 5 min in blocking solution and incubated with Goat anti Mouse IgG (H/L):HRP (Bio-Rad, Hercules, USA) or goat-anti-rabbit IgG (H+L)-HRP (Bio-Rad, Hercules, USA) at 1:5 000 - 10,000 for 1-2 hours at room temperature. Blots were washed 2x 5 min in blocking solution and 1x 5 min with PBS-T. Blots were developed using SuperSignal West Femto Maximum Sensitivity Substrate (ThermoFisher Scientific, Waltham, Massachusetts, USA) according to manufacturer's instructions. Chemiluminescent signal was detected using the Amersham Imager 600 (GE Healthcare Lifescience) or VersaDoc (Bio-Rad). Images were processed with ImageJ.

Western Blot analysis of S2R+ supernatant

S2R+ cells were transfected as described previously with srpGal4 UAS-Qsox1::FLAG::HA. 2 days post-transfection, medium was removed and cells were washed with PBS. Afterwards, serum-free S2 medium was added and incubated for approximately 40 hours. Afterwards, supernatant was collected and concentrated using Amicon Ultra-4 10K Centrifugal Filter Device (Merck, Kenilworth, New Jersey, United States) to gain 80µl of concentrated supernatant. 20µl of supernatant was loaded on gel and analyzed by anti-HA (1:200, Roche). Images were processed with ImageJ.

Time-lapse imaging, tracking, speed, persistence and germband entry analysis

Embryos were dechorionated in 50% bleach for 5 min, washed with water, and mounted in halocarbon oil 27 (Sigma-Aldrich, Saint Louis, Missouri, USA) between a coverslip and an oxygen permeable membrane (YSI). The anterior dorsolateral region of the embryo was imaged on an inverted multiphoton microscope (TrimScope II, LaVision) equipped with a W Plan-Apochromat 40X/1.4 oil immersion objective (Olympus). mCherry was imaged at 1100 nm excitation wavelengths, using a Ti-Sapphire femtosecond laser system (Coherent Chameleon Ultra) combined with optical parametric oscillator technology (Coherent Chameleon Compact OPO). Excitation intensity profiles were adjusted to tissue penetration depth and Z-sectioning for imaging was set at 1µm for tracking and segmentation respectively. For long-term imaging, movies were acquired for 132 - 277 min with a frame rate of 40 sec. All embryos were imaged with a temperature control unit set to 28.5°C.

Images acquired from multiphoton microscopy were initially processed with InSpector software (LaVision Bio Tec) to compile channels from the imaging data, and the exported files were further processed using Imaris software (Bitplane) to visualize the recorded channels in 3D. Macrophage speed and persistence were calculated by using embryos in which the macrophage nuclei were labeled with *srpHemo-H2A::3XmCherry* (Gyoergy et al., 2018). The movie from each imaged embryo was rotated and aligned along the AP axis for tracking analysis. Increasing the gain allowed determination of germband position from the autofluorescence of the yolk. Movies for vnc analysis were analyzed for 2 hours from the time point that cells started to dive into the channels to reach the outer vnc. Macrophage nuclei were extracted using the spot detection function and nuclei positions in xyz-dimensions were determined for each time point and used for further quantitative analysis. Cell speeds and directionalities were calculated in Matlab (The MathWorks Inc., Natick, Massachusetts, USA) from single cell positions in 3D for each time frame measured in Imaris (Bitplane). Instantaneous velocities from single cell trajectories were

averaged to obtain a mean instantaneous velocity value over the course of measurement. To calculate directionality values, single cell trajectories were split into segments of equal length (10 frames) and calculated via a sliding window as the ratio of the distance between the macrophage start-to-end location over the entire summed distance covered by the macrophage between successive frames in a segment. Calculated directionality values were averaged over all segments in a single trajectory and all trajectories were averaged to obtain a mean directionality value for the duration of measurement, with 0 being the lowest and 1 the maximum directionality. T**o** estimate the time for entry into the germband, we increased the gain to visualize the germband position from the autofluorescence of the yolk. We assessed the time point when the first macrophage nucleus reached the edge of the germband (taken as T0) and the time point when the first cell nucleus was just within the germband (taken as T1). T1-T0 was defined as the time for macrophage entry.

Fixed embryo image analysis for T antigen levels

Embryos were imaged with Plan-Apochromat 63X/1.4 Oil Objective on a Zeiss LSM700 inverted. 10µm stacks (0.5µm intervals) were taken for properly staged and oriented embryos, starting 10µm deep in the tissue. These images were converted into Z-stacks in Fiji. ROIs were drawn around macrophages (signal), copied to tissue close by without macrophages (background) and the average intensity in the green channel of each ROI was measured. For each pair of ROIs background was subtracted from signal individually. The average signal from control ROIs from one imaging day and staining was calculated and all data point from control, mutant and rescue from the same set was divided by this value. This way we introduced an artificial value called Arbitrary Unit (AU) that makes it possible to compare all the data with each other, even if they come from different imaging days when the imaging laser may have a different strength or from different sets of staining. Analysis was done on anonymized samples.

Macrophage cell counting

Transmitted light images of the embryos were used to measure the position of the germband to determine the stages for analysis. The extent of germband retraction away from the anterior along with the presence of segmentation was used to classify embryos. Embryos with germband retraction of between 29-31% were assigned to late Stage 11. Those with 29-41% retraction for all experiments except the *punt* RNAi (Figure 4J) in which 35-45% was used (both early Stage 12) were analyzed for the number of macrophages that had entered the germband and those with 50-75% retraction (late Stage 12) for the number along the ventral nerve cord (vnc), and in the whole embryo. Macrophages were visualized using confocal microscopy with a Z-resolution of 3µm and the number of macrophages within the germband or the segments of vnc was calculated in individual slices (and then aggregated) using the Cell Counter plugin in FIJI.

To check that this staging allows embryos from the control and *mrva*^{3102} mutant to be from the same time during development, embryos were collected for 30 minutes and then imaged for a further 10 hours using a Nikon-Eclipse Wide field microscope with a Plan-Apochromat 20X/ 0.5 DIC water Immersion Objective. Bright field images were taken every 5 minutes, and the timing of the start of the movies was aligned based on when cellularization occurred. We found no significant difference in when germband retraction begins (269.6±9 min in control and 267.1±3 min in *mrva*^{3102}, p=0.75) or in when the germband retracts to 41% (300±9

min for control, 311±5 min in *mrva*^{3102}, p=0.23) , or in when the germband retraction is complete (386.5±10 min for control, 401.6±8 min for *mrva*^{3102}, p=0.75). n=10 embryos for control and 25 embryos for *mrva*^{3102}.

Cloning

Standard molecular biology methods were used and all constructs were sequenced by Eurofins before injection into flies. Restriction enzymes *BSi*WI, and *Asc*I were obtained from New England Biolabs, Ipswich, Massasuchetts, USA (Frankfurt, Germany). PCR amplifications were performed with GoTaq G2 DNA polymerase (Promega, Madison, USA) using a peqSTAR 2X PCR machine from PEQLAB, (Erlangen, Germany). All Infusion cloning was conducted using an Infusion HD Cloning kit obtained from Clontech's European distributor (see above); relevant oligos were chosen using the Infusion primer Tool at the Clontech website.

Construction of *srpHemo*-minerva: A 1467 bp fragment containing the Minerva (CG8602) ORF was amplified from the UAS-CG8602:FLAG:HA construct (DGRC) using primers Fw GAAGCTTCTGCAAGGATGGCGCGCGAGGACGAGGAAC, Rv CGGTGCCTAGGCGCGCTATTCAAAGTTCTGATAATTCTCG. The fragment was cloned into the srpHemo plasmid (a gift from Katja Brückner, (Brückner et al., 2004)) after its linearization with AscI, using an Infusion HD cloning kit.

Construction of *srpHemo-MFSD1:* A 1765 bp fragment containing the MFSD1 ORF was amplified from cDNA prepared from dendritic cells (a gift from M. Sixt lab) with Fw primer TAGAAGCTTCTGCAACTTTGCTTCCTGCTCCGTTC, Rv primer ATGTGCCTAGGCGCGAAGGAAAGGCTTCATCCGCA). The fragment was cloned into the srpHemo plasmid (a gift from Katja Brückner, (Brückner et al., 2004)]) using an Infusion HD cloning kit (Clontech) after its linearization with AscI (NEB).

Construction of *srpHemo-mrva::3xmCherry*: Minerva (CG8602) was amplified from a DNA prep from Oregon flies (Fw primer: AGAGAAGCTTCGTACGCGACAACCCTGCTCTACAGAG; Rv primer CGACCTGCAGCGTACGACCCGATCCTTCAAAGTTCTG). The vector, PCasper4 containing a 3xmCherry construct under the control of the srpHemo promoter (Gyoergy et al., 2018), was digested with BsiWI according to the manufacturer's protocol. The vector and insert were homologously recombined using the In-Fusion HD Cloning Kit.

Generation of pInducer20-MFSD1-eGFP constructs: For C-terminal tagging MFSD1 was PCR amplified from cDNA prepared from dendritic cells (a gift from M. Sixt lab) with the following primers; fw: GATCTCGAGATGGAGGACGAGGATG; rev: CGACCGGTAACTCTGGATGAGAGAGC and digested with XhoI and AgeI (both New England Biolabs, Ipswich, Massasuchetts, USA). This MFSD1 fragment was cloned into XhoI/AgeI digested peGFP-N1 (Addgene, Cambridge, Massachusetts, USA). C-terminally eGFP tagged MFSD1 was further PCR amplified with following primers; fw: GGGGACAAGTTTGTACAAAAAAGCAGGCTTAATGGAGGACGAGGAT; rev: GGGGACCACTTTGTACAAGAAAGCTGGGTATTACTTGTACAGCTC. This fragment was cloned using Gateway BP Clonase II Enzyme mix and Gateway LR Clonase II Enzyme Mix (ThermoFisher Scientific, Waltham, Massachusetts, USA) via donor vector pDonR211 into the final Doxycyclin inducible expression vector pInducer20 (Meerbrey et al., 2011) according to manufacturer's instructions. pInducer20-MFSD1-eGFP was amplified in stbl3 bacteria (ThermoFisher Scientific, Waltham, Massachusetts, USA).

Precise excision

mrva^{3102} flies which contain the 3102 P element insert in the 5' region of CG8602 were crossed to a line expressing transposase (BL-1429 (*pn*^{1}; *ry*^{503}*Dr*^{1}P[Δ 2-3]). To allow excision of the P Element, males from the F1 generation containing both the P element and the transposase, were crossed to virgins with the genotype Sp/Cyo; PrDr/TM3Ser (gift from Lehmann lab). In the F2 generation white eyed males were picked and singly crossed to Sp/Cyo; PrDr/TM3Ser virgins.

LanA quantification

Images were taken with a Z-resolution of 0.5µm from the head of late stage 12 embryos using a Zeiss LSM800 confocal microscope and a 40x/1.4 Oil DIC objective. A 4µm long line was drawn over a macrophage with the middle of the line located approximately at the edge of the cell. mCherry and LanA (488) intensities were measured using the Multichannel Plot Profile Plugin in Fiji. Three lines were drawn on each cell to catch the variability of secretion. Only cells standing alone or in small groups that have at least some small visible amount of extracellular LanA analyzed. From each embryo, 20 cells were analyzed. Images were anonymized before quantification.

Mammalian cell culture

MC-38 colon carcinoma cells, 4T1 breast carcinoma (ATCC, CRL-2539), Lewis Lung carcinoma LLC1 (ATCC, CRL-1642) and B16-BL6 melanoma (NCI-DTP; B16BL-6) (all gifts from the Borsig lab) were kept in DMEM supplemented with 10% FCS (Sigma-Aldrich, Saint Louis, Missouri, USA), Non-essential Amino Acids, and Na-Pyruvate (Thermo Fisher Scientific, Waltham, Massachusetts, USA). All cells were kept in a humidified incubator at 37°C with 5% CO2. Cells were infected with lentiviral particles containing pInducer20-MFSD1-eGFP. Expression of MFSD1-eGFP was induced with 20ng/ml (for MC-38) and 100ng/ml (for 4T1, LLC, B16-BL6) of Doxycycline for 24 hours prior subsequent analysis. Cell lines were routinely tested for Mycoplasm infection and found to be negative. The identity of the cell lines was confirmed by STR analysis by the cell bank from which they were obtained.

Mammalian Cell lysis

Cells were lysed in lysis buffer (25mM Tris, 150mM NaCl, 1mM EDTA, 1% Triton X-100) supplemented with protease inhibitor cocktail (Complete, Roche, Basel, Switzerland) for 20 min on ice, followed by centrifugation at 14,000x g, 4°C for 5 min. The protein lysates were stored at -80°C. Protein concentration was determined with the Pierce BCA Protein Assay Kit (Thermo Fisher Scientific).

Mammalian Cell Immunofluorescence

Cells were fixed with 4% formaldehyde (Thermo Fisher Scientific) in PBS for 15 minutes at room-temperature. Cells were washed three times with PBS followed by blocking and permeabilization with 1% BSA (Sigma-Aldrich, Saint Louis, Missouri, USA)/0.3% Triton X-100 in PBS for 1 hour. Antibodies were diluted in blocking/permeabilization buffer and incubated for 2 hours at room temperature. Primary antibodies used were: anti-GFP (clone 5G4, Ogris lab, MFPL), anti-GRASP65 (Thermo Fisher, PA3-910), anti-Rab5 (Cell Signaling Technology, #C8B1), anti-Rab7 (Cell Signaling Technology, #D95F2) and anti-LAMP1 (Abcam, Cambridge, UK, #ab24170). Cells were washed

three times with PBS-Tween20 (0.05%) for 5 minutes each, followed by secondary antibody incubation in blocking/permeabilization buffer for 1 hour at room-temperature. Secondary antibodies used were: goat anti-mouse IgG (H+L) Alexa Fluor 488 (Thermo Fisher A11001), goat anti-rabbit IgG (H+L) Alexa Fluor 555 (Thermo Fisher, A21428), Cells were counterstained with DAPI (Thermo Fisher) for 10 minutes in PBS. Cells were mounted with ProLong Gold Antifade Mountant (Thermo Fisher #P36930). Images were acquired using a Plan-Apochromat 40x/1.4 Oil DIC objective M27 on a Zeiss LSM880 confocal microscope. Pictures were processed with ImageJ.

Quantification of Secretory Pathway Marker Colocalization with Mrva, MFSD1 and Qsox1

Colocalization analysis was performed by ImageJ's (NIH) Coloc 2 plugin and determined with the pixel intensity spatial correlation analysis (Pearson's correlation coefficient).

Embryonic Protein Prep for Glycoproteomics

150 mg fly embryos were homogenized in 2 ml 0.1% RapiGest, 50mM ammonium bicarbonate using a dounce homogenizer. The lysed material was left on ice for 40 min with occasional vortexing followed by probe sonication (5 sec sonication, 5 sec pause, 6 cycles at 60% amplitude). The lysate was cleared by centrifugation (1,000× g for 10 min). The cleared lysate was heated at 80°C, 10 min followed by reduction with 5mM dithiothreitol (DTT) at 60°C, 30 min and alkylation with 10mM iodoacetamide at room temperature (RT) for 30 min before overnight (ON) digestion at 37°C with 25µg trypsin (Roche). The tryptic digests were labeled with dimethyl stable isotopes as described (Boersema et al., 2009). The digests were acidified with 12µL trifluoroacetic acid (TFA), 37°C, 20 min and cleared by centrifugation at 10,000g, 10 min. The cleared acidified digests were loaded onto equilibrated SepPak C18 cartridges (Waters) followed by 3× CV 0.1% TFA wash. Digests were labeled on column by adding 5 mL 30 mM $NaBH_3CN$ and 0.2% formaldehyde (COH_2) in 50mM sodium phosphate buffer pH 7.5 (Light, *mrva*^{3102}), or 30mM $NaBH_3CN$ and 0.2% deuterated formaldehyde (COD_2) in 50mM sodium phosphate buffer pH 7.5 (Medium, control). Columns were washed using 3 CV 0.1% FA and eluted with 0.5 mL 50% MeOH in 0.1% FA. The eluates were mixed in 1:1 ratio, concentrated by evaporation, and resuspended in Jacalin loading buffer (175mM Tris-HCl, pH 7.4) Glycopeptides were separated from non-glycosylated peptides by Lectin Weak Affinity Chromatography (LWAC) using a 2.8 m column packed in-house with Jacalin-conjugated agarose beads. The column was washed with 10 CVs Jacalin loading buffer (100 µL/min) before elution with Jacalin elution buffer (175mM Tris- HCl, pH 7.4, 0.8M galactose) 4 CVs, 1 mL fractions. The glycopeptide-containing fractions were purified by in-house packed Stage tips (Empore disk-C18, 3M).

Quantitative O-glycoproteomic Strategy

The glycopeptide quantification based on M/L isotope labeled doublet ratios was evaluated to estimate a meaningful cut-off ratio for substantial changes (Schjoldager et al., 2015). The labeled glycopeptides produced doublets with varying ratios of the isotopic ions as well as a significant number of single precursor ions without evidence of ion pairs. Labeled samples from control *srpHemo-3xmCherry* embryos and *mrva*^{3102} *srpHemo-3xmCherry* mutant embryos were mixed 1:1 and subjected to LWAC glycopeptide enrichment. The distribution of labeled peptides from the LWAC flow-through showed that the quantitated peptide M/L ratios were normally

distributed with 99.7% falling within +/-0.55 (Log_{10}). We selected doublets with less/more than +/-0.55(Log_{10}) value as candidates for isoform-specific O-glycosylation events.

Mass spectrometry

EASY-nLC 1000 UHPLC (Thermo Scientific) interfaced via nanoSpray Flex ion source to an -Orbitrap Fusion mass spectrometer (Thermo Scientific) was used for the glycoproteomic study. A precursor MS1 scan (m/z 350–1,700) of intact peptides was acquired in the Orbitrap at a nominal resolution setting of 120,000. The five most abundant multiply charged precursor ions in the MS1 spectrum at a minimum MS1 signal threshold of 50,000 were triggered for sequential Orbitrap HCD-MS2 and ETD-MS2 (m/z of 100–2,000). MS2 spectra were acquired at a resolution of 50,000. Activation times were 30 and 200 ms for HCD and ETD fragmentation, respectively; isolation width was 4 mass units, and 1 microscan was collected for each spectrum. Automatic gain control targets were 1,000,000 ions for Orbitrap MS1 and 100,000 for MS2 scans. Supplemental activation (20 %) of the charge-reduced species was used in the ETD analysis to improve fragmentation. Dynamic exclusion for 60 s was used to prevent repeated analysis of the same components. Polysiloxane ions at *m/z* 445.12003 were used as a lock mass in all runs. The mass spectrometry glycoproteomics data have been deposited to the ProteomeXchange Consortium (Vizcaino et al., 2016) via the PRIDE partner repository with the dataset identifier PXD011045.

Mass spectrometry Data analysis

Data processing was performed using Proteome Discoverer 1.4 software (Thermo Scientific) using Sequest HT Node as previously described (Schjoldager et al., 2015).

Briefly, all spectra were initially searched with full cleavage specificity, filtered according to the confidence level (medium, low and unassigned) and further searched with the semi-specific enzymatic cleavage. In all cases the precursor mass tolerance was set to 6 ppm and fragment ion mass tolerance to 20 mmu. Carbamidomethylation on cysteine residues was used as a fixed modification. Methionine oxidation as well as HexNAc and HexHexNAc attachment to serine, threonine and tyrosine were used as variable modifications for MS2 data. All spectra were searched against a concatenated forward/reverse *Drosophila melanogaster*-specific database (UniProt, March 2018, containing 39034 entries with 3494 canonical reviewed entries) using a target false discovery rate (FDR) of 1%. FDR was calculated using target decoy PSM validator node. The resulting list was filtered to include only peptides with glycosylation as a modification. Glycopeptide M/L ratios were determined using dimethyl 2plex method as previously described (Schjoldager et al., 2015)

Statistics and Repeatability

Statistical tests as well as the number of embryos/ cells assessed are listed in the Figureure legends. All statistical analyses were performed using GraphPad Prism and significance was determined using a 95% confidence interval. Data points from individual experiments / embryos were pooled to estimate mean and standard error of the mean. Sample size refers to biological replicates. No statistical method was used to predetermine sample size and the experiments were not randomized. For major questions, data were collected and analyzed masked. Normality was evaluated by D'Agostino & Pearson or Shapiro-Wilk normality test. Unpaired t-test or Mann-

Whitney test was used to calculate the significance in differences between two groups and One-Way Anova followed by Tukey post-test or Kruskal-Wallis test followed by Conover or Dunn's post-test for multiple comparisons.

All measurements were performed in 3-38 embryos and at least 37 oocytes. Representative images shown in Figure 1E-G, I, Figure 2F, I, I Figure 3A-C Figure 5A, Figure 5B, D and G and Supplementary Figureures S2B-J, S3B,G,J, S5G-K were from separate experiments repeated 3 to 6 times. The stainings underlying Figure S1A-M, Figure 2H and S6 C-F are from separate experiments that were repeated at least twice. Stills shown in Figure 3I, K and Figure 5D are representative images from two-photon movies, which were repeated at least 3 times.

Tables

Table 1 (see Appendix 1): All candidate proteins from the O-glycoproteome with at least 3-fold changes in T and Tn antigen in the *mrva*^{3102} mutant. Columns list the gene name, the predicted or known function of the gene, if other T or Tn glycosites on the protein are unchanged or changed in the opposite direction, any known human ortholog (identified by BLAST), the precise site altered, the T and Tn antigen changes observed at a particular glycosylation site, the number of glycosites on the peptide, the peptide sequence and if the glycosylation site is conserved. The site is considered conserved if the human ortholog has a serine or threonine +/- 5 amino acids from the *Drosophila* glycosite.

Table 2: T or Tn antigen modified receptors from the wild-type St 11-12 *Drosophila melanogaster* embryo O-glycoproteome. Columns list the gene name for the receptor, its reported function, what kind of glycosylation we identified to be present on the receptors in the wild type sample, and what kind of glycosylation change we observed in the *mrva*^{3102} mutant.

Receptor	Function	Glycosylation	Changes in *mrva*^{3102}
Babo	Activin signaling	2 glyco sites, T antigen only	no
Boi	Regulation of Hh-dependent processes	3 glyco sites, Tn antigen only	no
CG12121	Unknown	3 glyco sites, Tn antigen only	no
CG15765	Carbohydrate binding, nervous system development	1 glycosite, T antigen	no
CG5888	Unknown	1 glyco site, T or Tn antigen	no
CG9095	Carbohydrate binding	1 glyco site, Tn antigen	no
Cirl	Calcium independent receptor for a-latrotoxin, adult locomotory behavior	1 glyco site, T or Tn antigen	no
Crb	epithelial morphogenesis, apico-basal cell polarity, negative regulator of Notch activity	1 glyco site, Tn antigen	no
Dg	non-integrin ECM receptor, connects ECM to the actin cytoskeleton	1 glycosite, T or Tn antigen	no
Drl	axon guidance through Wnt5	1 glyco site, T or Tn antigen	no
Hbs	Muscle cell fusion	2 glycosites, T and Tn antigen	no

Hmu	Hydrolase activity	15 glycosites, both T and Tn antigen	Tn inc.
LpR1	Regulation of immune responses	2 glycosites, Tn antigen	Tn inc.
LpR2	Cellular uptake of neutral lipids	3 sites, T and Tn antigen	T & Tn inc.
LRP1	LDL receptor, works with megalin	4 glycosites, T and Tn antigen	no
Mgl	Lipid regulation	2 glycosites, Tn antigen	Tn dec.
Mthl5	GPCR, heart morphogenesis	1 glyco site, T or Tn antigen	no
NimB2	Defense response to bacterium	1 glycosite, Tn antigen	no
NimC4	Recognition and engulfment of apoptotic cells during development	1 glycosite, T or Tn antigen	no
Nrx-IV	Septate junction formation, glial neural interaction	1 glyco site, Tn antigen	no
PlexB	Axon guidance	1 glyco site, Tn antigen	no
Put	Dpp signaling	5 glyco sites, T and Tn antigen	T&Tn dec.
Sas	Pathfinding, glial neuron interaction		T dec.
Sdc	Robo neural pathfinding, synapse at neuromascular junction	1 glyco site, Tn antigen	no
Sema-1b	Neural pathfinding	1 glyco site, Tn antigen	no
Sli	Neural pathfinding, robo interaction	2 glyco sites, T and Tn antigen	T & Tn inc.
Sr-CII	Scavenger receptor, immune response	6 glyco sites, T and Tn antigen	no
Syb	Synaptic vesicle, SNAP receptor activity	1 glyco site, T or Tn antigen	no
Tequila	Scavenger receptor, serine protease, glucose homeostasis, long and short term memory	5 glycosite, Tn antigen	no
Unc-5	Neural pathfinding, netrin receptor	1 glycosite, Tn antigen	no
Verm	Cuticle development and tracheal tube size control	1 glycosite, T or Tn antigen	T & Tn inc.

Table 3: Summary of contribution of authors based on type of experiment and figure panels that represent the data (KV: Katarína Valošková, JB: Julia Biebl, MR: Marko Roblek, SE: Shamsi Emtenani, MM: Michaela Mišová, AR: Aparna Ratheesh, PRR: Patrícia Reis-Rodrigues, ISBL: Ida S.B. Larsen, SYV: Sergey Y. Vakhrushev, HC: Henrik Clausen, DES: Daria E. Siekhaus)

Experiment	**Figure panels**	**Work done by**
Lectin screen	Fig 1D, Fig1-S1A-L	Staining and imaging: KV, MM; Analysis: KV
T antigen changes during development	Fig 1E-H	Staining and imaging: KV, JB; Quantification: JB
C1GalTA downregulation	Fig 1I-L; Fig 1-S1 M-P	RNAi: KV Null mutant: JB
GlcAT-P downregulation	Fig 1M, Fig1-S1Q	KV

qPCR (C1GAlTA, Ugalt, CG8602)	Fig 2A,B,D,E,G	FACS, cDNA synthesis, qPCR, analysis: KV RNA extraction: MR
T antigen staining on the *CG8602* mutant	Fig 2F	KV
Mrva co-localization	Fig 2I,H, Fig 2-S1B-J	S2 cells: KV, JB; Extracted hemocytes: JB
Mrva phenotype – fixed embryos	Fig 3A-F, H; Fig 3-S1A-E	KV
Shg rescue	Fig 3G	KV
Mrva phenotype – live embryos	Fig 3I-M, Fig 3-S1F,G	Movies: JB, KV; Analysis: AR, SE
PGCs migration	Fig 3-S1 H-I	KV
Border cell migration	Fig 3-S1J-L	PRR
T antigen WB	Fig 4A	KV, except blotting: JB
Glycoproteomics	Fig 4AB-I, Fig 4-S1A-E	Sample collection and freezing: KV, JB Glycoproteomics: ISBL, SYV Data analysis and statistics: SYV Data interpretation: KV, DES, HC
Qsox1 phenotype-fixed	Fig5 A-C, Fig5-S1A-E	JB
Qsox1 phenotype-live	Fig 5D-G, Fig 5-S1F	Movies:JB; Analysis: SE
Qsox1 co-localization	Fig 5H; Fig 5-S1G-J	JB
Qsox1 secretion	Fig 5I	KV, except blotting: JB
LamininA quantification	Fig 5J, Fig 5-S1K-N	KV
MFSD1 co-localization in cancer cells	Fig 6B,C; Fig 6-S1B-F	MR
MFSD1 rescue	Fig 6D-G	Migration phenotype: KV; Glycosylation phenotype:JB

Developmental movies	n.a., numbers in text	KV

Chapter 4: Future directions

The above described research provokes many interesting questions. In the following chapter, I will discuss some of them, including some spin-off projects that are already running in our lab and topics being investigated by my colleagues.

Minerva's molecular function

Although we show in our work that Minerva influences migration, probably by regulating the whole set of other molecules such as LanA, Qsox1 or NCad, we do not actually uncover what Minerva is doing on the molecular level. We work with a few different hypotheses that needs to be tested:

Is Minerva a transporter?

Based on predictions, Minerva belongs to the MFS which is a big family consisting of transporters (Griffith et al., 1992; Pao et al., 1998). Therefore from the beginning, we've approached Minerva as a transporter and have been trying to figure out the transported material. As we found out, it is localized in Golgi so our collaborators (group of Mariusz Olczak, University of Wrocław, Poland) attempted to test whether it could transport UDP-GlcNAc, UDP-Gal, UDP-GlcA or UDP-GalNAc. However, the constructs made in our lab (prepared by Julia Biebl) killed the yeast. Therefore only mouse MFSD1 (made by Marko Roblek) was tested, with negative results for all of these substances (unpublished data, Olczak lab). This argues against the direct influence on O-GalNAc glycosylation through transported material but does not mean that Minerva is not acting as a transporter when regulating tissue invasion.

MFS transporters are known to be symporters or antiporters, often anti/symporting H+ which could influence pH homeostasis. As Minerva seems to have quite a broad localization, this could have an extensive effect on protein modifications, transport and localization. In mammals, it was shown that even a slight but significant change in the medial/trans Golgi pH is a marker of cancer cells and increase in pH Golgi is associated with massive T antigen expression on the cell surface (Rivinoja et al., 2006). Therefore we hypothesize that Minerva could transiently modify the pH of Golgi or other parts of the protein sorting system in order to correctly time the whole process of initial migration and invasion into the extended germband. To test it, we would need to construct and optimize a Golgi-localized pH sensor and measure, preferably in live cells whether there are changes in the control compare to the mutant macrophages as well whether there is potentially a temporal change in the pH to allow invasive migration.

Potential lectin-like function

When small parts of Minerva sequences were BLASTed (mainly those predicted to form a translocone, based on InterPro prediction) against the *Drosophila* genome, many of them carried similarities to sugar transporters or sugar binding proteins. Although a sugar-transporting function related to O-GalNAc glycosylation was not confirmed (but cannot be fully excluded), we hypothesize that Minerva instead of having a function as a transporter, could use the ability to bind some sugar structure and therefore having lectin-like function: allowing formation of local and transient protein interactions between modified proteins and transferase(s) to allow or

prevent modification on some sites. Interestingly, glycoproteomic analysis showed that the majority of the candidates have more glycosylation sites compared to the whole set (where the most common number of glycosites is 1, see figure 4, Chapter 3). At the same time, many of the candidates have some glycosites differently modified and some of them not changed at all (see tables, Chapter 3). Transporters were previously shown to interact with lectins to influence transporter function or conformation (Fernández-Calotti et al., 2016; Molnár et al., 2009). However, to my knowledge, there is no previous study showing a predicted (sugar) transporter functioning as a lectin instead of a transporter.

Direct/indirect influence on GalNAc-Ts

Minerva has predicted long C- and N-terminal tails (Figure 1, Chapter 2) that could fulfill an anchoring function. For some glycosylation enzymes, it was shown that sequential acting medial-Golgi enzymes form pH-sensitive heterodimers (Hassinen and Kellokumpu, 2014; Kellokumpu et al., 2016). Although the existence of such complexes for O-GalNAc glycosylation related enzymes in *Drosophila* was not shown before, we hypothesize that these quite prevalent complexes could exist in *Drosophila* and Minerva could potentially play a role in their formation, maintenance or trafficking. Our analysis of T and Tn antigen in the embryos shows that there is only a subgroup of proteins changed and only some glycosites on these glycoproteins show a significant change. As it was demonstrated before that some glycosyltransferases are site-specific and need a presence of another occupied glycosite for their activity (Hassan et al., 2000; Kubota et al., 2006; Revoredo et al., 2016), modulation of transferase activity through complex formation thanks to the anchoring function of Minerva or indirectly by transiently influencing conditions in the Golgi through the transported material would fit our results.

Glycosylation-related questions

Our work identifies not only a role of Minerva in tissue invasion but also proves that short forms of O-GalNAc glycosylation are needed for proper tissue invasion. This fits very well with short forms of O-GalNAc glycosylation being known for a long time to be associated with metastasis and being considered a bad prognosis marker (Yi Cao et al., 1996). However, as the presence of Tn and T on the surface of tumors seems to be independently regulated as well as tumor specific (Chia et al., 2016b; Fu et al., 2016; Nguyen et al., 2017), the important questions are related to the function of each short form of O-GalNAc glycosylation as we see the whole set of changes in our glycoproteomic analysis of the control and mutant embryos (see Chapter 3 for more details)

Which glycosylation step is actually needed?

The short forms of O-GalNAc glycosylation were previously associated with the higher invasiveness of some types of tumors ((Fu et al., 2016; Hua et al., 2012; Hung et al., 2014)). It includes Tn and T antigen, as well as their sialylated versions (Fu et al., 2016; Springer, 1984). In *Drosophila*, except in a few very specific neurons, sialylation does not occur during embryonic development (Islam et al., 2013; Repnikova et al., 2010). Instead T and Tn antigen can be futher modified by glucuronylation, a sugar moiety with similar properties to sialic acid. Therefore GlcA addition could be considered as an insect replacement for sialyation, although some

glucuronylated proteins were detected in a context/function where sialylated proteins were never present therefore GlcA should not be seen as only replacement of sialic acid (Aoki and Tiemeyer, 2010a). We tested a mutant in a transferase GlcAT-P that is known to glucuronylate T antigen (Breloy et al., 2016a) and which is expressed in macrophages. We showed that this enzyme is not needed for tissue invasion (see Figure 1, Chapter 3). However, missing tools to analyze glucuronylation did not allow us to test whether the mutant we used fully removed glucuronylation from the embryo. As there are 2 other enzymes that are able to add glucuronic acid (Kim et al., 2003), although with at least 12fold lower expression in macrophages that GlcAT-P (unpublished data, V Belyaeva), deeper analysis (preferentially including null mutants for all 3 enzymes) would be needed.

Are T and Tn needed for different steps (initiation vs. invasion)?

The glycoproteomics results showed that *minerva* mutant has changes both in Tn and T antigen. Analysis of fixed embryos showed that downregulating C1GalTA strongly reduces T antigen staining on macrophages and leads to results in impaired migration into the extended germband without obvious deficits in migration towards the extended germband (Figure 1, Chapter 3). We therefore hypothesize that T antigen is needed for proper invasive migration. However, a proper live imaging could shed more light on the whole process and point out the exact step(s) that are regulated by T antigen (or theoretically glucuronylated version) modified proteins.

Minerva seems to affect more processes than just invasion into the extended germband. These processes could be on the one side dependent on the glycosylation unrelated functions we propose, such as the regulation of trafficking or related to other types of glycosylation influenced by its potential interaction with Frc (for more details, see Chapter 2). However, the other option would be a role for Tn antigen in initiating migration and regulating its early steps. To test this hypothesis, we first have to figure out which GalNAc-Ts are functional in macrophages by conducting macrophage-specific RNAi on the candidates whose RNA we have found expressed in macrophages. Afterwards, a deeper live imaging analysis could dissect the role of Tn antigen and different GalNAc-Ts (as some could be very specific for one or few proteins).

Glycoproteomics showed both increase and decrease in Tn antigen. Whether early migration requires higher or lower Tn antigen could be tested by downregulation or overexpression of some of the GalNAc-Ts (the ones that were detected before to be functional in the process) in the background of the *minerva* mutant.

What are the targets?

While Minerva is localized to the secretory pathway we never detected it on the surface of S2 cells or migrating macrophages. Minerva thus must function through some targets, possibly some indirectly affected in what we call a ‘second wave’. This fits also with the whole range of effects Minerva has not only on macrophage migration but also on development in general as well as lower movement of larvae and adults and reduced fertility that we noticed while propagating our flies. In this part, I will talk about our analysis of potential targets – both tested with preliminary results as well as those planned to be tested.

Interaction with Qsox1

As described in Chapter 3, the strongest target from the glycoproteomics is Qsox1. We confirmed that *qsox1* mutant partly phenocopies *minerva* phenotype in migration into the germband as well as in its effect on LanA. However, *qsox1* mutant does not show the exactly same phenotype as *minerva* mutant (see the vnc analysis and live imaging of the *qsox1* mutant, Figure 5, Chapter 3) therefore the question of the direct interaction of these proteins is still opened. A genetic test is not possible, as *qsox1* is haploinsufficient (only 41-50 macrophages in the germband compared to around 70 in the control). In any case, the difference could be caused by the fact that the *qosx1* mutant has low/no expression of normally glycosylated Qsox1 while in *minerva* mutant, Qsox1 is present but incorrectly glycosylated what could change the substrate specificity or efficiency of the protein.

We propose to more deeply test whether the defect in the molecular function of Qsox1 is repeated in the *minerva* mutant. It was shown before that in S2 cells, Qsox1 influences the proper folding of EGF domains (Tien et al., 2008). We want to test whether *minerva* RNAi in S2 cells shows the same phenotype as was described for *qsox1* RNAi and therefore if Minerva could influence the proper folding of EGF domains. As we detected LanA as one of potential effectors of the migration phenotype, we hypothesize that improper folding of its EGF domains could result in problems with its incorporation into the ECM and therefore observed upregulation of LanA production as a result of a feedback loop.

On the hunt for the mysterious band on T antigen Western blot

In Figure 4 in Chapter 3, we show a T antigen Western blot that displays decreases in few different bands with the strongest effect on a high molecular weight band that is almost fully missing on a majority of the western blots from mutant embryos that we did (and also on the *qsox1* western blot although we know that the band is not Qsox1 itself, Figure 1A, done by Julia Biebl). In order to discover which high molecular weight protein it is, we took a few different approaches that helped us to exclude some candidates:

1. We tested by Western blot the whole set of proteins potentially involved in the migration that could be differently glycosylated in the mutant, e.g. DN-Cadherin, Notch, Integrin; with no positive results (Fig 1B-D)
2. We did a mass spectrometry analysis of the high molecular band cut from a gel run with samples from the control and *mrva* mutant (work done by Julia Biebl and Marko Roblek). The analysis revealed a whole set of candidates (see Table 1) from which we directly tested few candidates for which antibodies existed (Dhc64c, Shot, GP210, Tango, Fig 1E-H) and indirectly tested some candidates using RNAi in macrophages (done by Julia Biebl, Michaela Misova and Shamsi Emtenani). RNAi in macrophages did not confirm any of the tested candidates. However, the Western blot based analysis pointed to an unexpected result. Dynein heavy chain 64c (Dhc64c) that is known to be a subunit of the dynein motor complex (Hays et al., 1994) is increased in the mutant compared to the control (Fig 1E). Dhc64c is a protein localized to the cytoplasm which excludes the option of it being directly regulated by Minerva and O-GalNAc glycosylation. The detected difference (both in the mass spectrometry and confirmed by Western blot) could be a result of a 'second wave' or a feedback compensation, however it is intriguing and would deserve proper characterization of potential defects in vesicular trafficking, especially in the light of results on delayed DN-Cadherin degradation and

increased LanA staining inside of macrophages, as a change in the amount of the motor protein could move the balance of trafficking and therefore slow down secretion of the protein or their internalization.

3. As glycoproteomic approach gave us more than 60 candidates which we plan to test, including 14 those that have decreased T antigen (see Fig 4, Chapter 3). This could tell us whether these candidates could be considered as an invasive program that is triggered by Minerva's increasing T antigen modification on them.

Based on our results with LanA (see Fig 5, Chapter 3), we currently guess that the high molecular weight missing band is a component of the ECM. To test this, we need to do T antigen Western blot on null mutants/deficiency lines of candidate ECM components such as LanA, LanB1, LanB2 or Collagen IV.

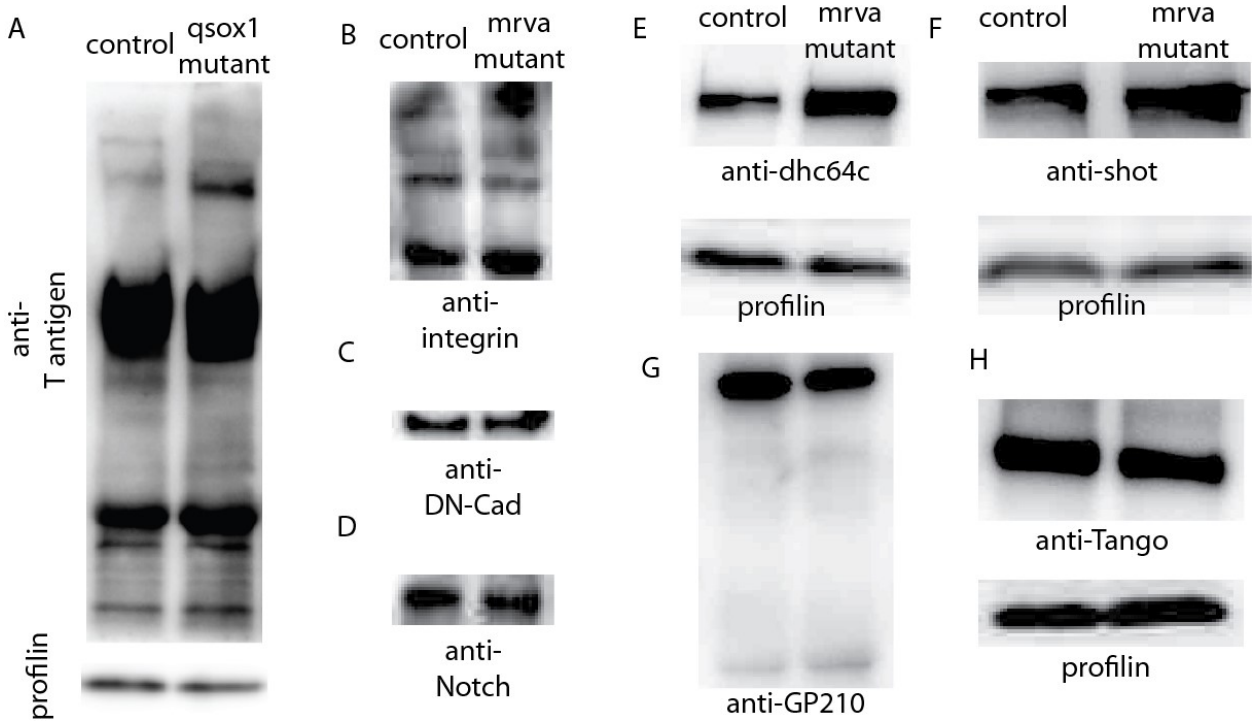

Figure 1: Western blot analysis of potential candidates for the missing high-molecular weight band
A: Anti-T antigen WB on control and qsox1 mutant embryos stage early 12 **B-H:** WB on control and mrva mutant embryos stage early 12 probed against (**B**) Integrin, (**C**) DN-Cadherin, (**D**) Notch, (**E**) Dhc64c, (**F**) Shot, (**G**) GP210 and (**H**) Tango. In A, E, F and H Profilin is used as a loading control.

Conservation of Minerva function

As shown in Figure 6, Chapter 3, mouse MFSD1 can fully rescue the phenotype. This result is very interesting suggests that we can use our results from flies to gain insight into mammals. However, to prove that our system is a good way to uncover regulators and components of tissue invasion, we still need to better characterize the rescue itself as well as the function of mammalian MFSD1. These questions are already being analyzed by my colleagues.

Where is the rescue of Minerva mutant happening?

In *Drosophila* macrophages, Minerva is quite broadly localized into the main parts of the secretory system (except ER, see Chapter 3). However, as shown in Fig6 in Chapter 3, MFSD1 seems to be more strictly localized and its localization depends on the cell type. Therefore, we would like to determine where the MFSD1 which is rescuing the *minerva* mutant phenotype, is localized. The current version of the rescue construct is not tagged and we do not have a good antibody that could detect mouse MFSD1 in *Drosophila* embryos. To test it, a new line with a tagged version of MFSD1 has to be made and tested for its ability to rescue the mutant phenotype, followed by a localization study.

Is MFSD1 functioning in immune cells of mammals the same way as of flies? Is MFSD1 important for invasion/metastasis?

If the results from our work will get confirmed in mammals, MFSD1 could become an interesting target for cancer treatment or the prevention of metastasis. However, this part of the project is being addressed by my colleagues who might make the whole project into the realm of medical relevance.

Table 1: Candidate from mass spectrometric analysis of the missing high-molecular weight protein. Red highlights proteins that are increased in the mutant, blue those that are decreased

Name	Mol. weight [kDa]	Unique peptides	Ratio mutant/ control
Shot	989.5	48	5.81
CG13185	631.3	11	1.30
spen	593.5	47	1.69
kis	593.4	120	0.90
poe	590.7	87	0.85
CG8184	553.1	92	13.99
Bruce	537.9	27	1.00
Dhc64C	530.8	28	0.80
CG32113	445.0	13	1.68
Nipped-A	429.9	4	0.80
mv	399.9	6	1.51
CG42232	378.6	80	0.29
Vps13	374.5	18	0.98
Rfabg	372.7	120	1.02
pcx	365.3	1	0.68
rg	358.6	7	0.40
tefu	318.0	3	1.33
faf	309.9	3	0.85
Ppn	299.5	5	6.31
Nup358	296.4	6	1.10
CG17514	293.9	26	1.20
Piezo	288.3	2	0.63
CG43367	286.5	3	0.73

Tor	281.2	1	0.00
Prp8	279.6	12	1.16
FASN1	266.4	2	0.89
Mtor	262.4	1	0.69
Not1	249.8	2	1.61
CG5205	249.0	20	0.99
Ubr3	247.0	11	0.78
l(3)72Ab	244.5	48	0.94
rod	239.7	19	0.94
CG14215	235.2	9	0.72
Nup205	232.7	12	1.15
shtd	227.3	10	2.25
zip	226.8	4	0.67
ana3	225.6	1	1.00
PlexA	216.4	5	1.13
yl	215.0	9	3.93
sti	211.3	40	0.64
CG8771	210.3	3	1.69
Gp210	209.8	36	1.20
gig	203.8	6	0.75
Mcr	202.8	4	1.31

References

Abramson J, Smirnova I, Kasho V, Verner G, Kaback HR, Iwata S. 2003. Structure and Mechanism of the Lactose Permease of Escherichia coli. Science (80-) 301:610–615. doi:10.1126/science.1088196

Acar M, Jafar-Nejad H, Takeuchi H, Rajan A, Ibrani D, Rana NA, Pan H, Haltiwanger RS, Bellen HJ.2008. Rumi is a CAP10 domain glycosyltransferase that modifies Notch and is required for Notch signaling. *Cell*. **132**(2):247-58. doi: 10.1016/j.cell.2007.12.016.

Aebi M. 2013. N-linked protein glycosylation in the ER. Biochim Biophys Acta - Mol Cell Res 1833:2430–2437. doi:10.1016/j.bbamcr.2013.04.001

Agrawal P, Fontanals-Cirera B, Sokolova E, Jacob S, Vaiana CA, Argibay D, Davalos V, McDermott M, Nayak S, Darvishian F, Castillo M, Ueberheide B, Osman I, Fenyö D, Mahal LK, Hernando E. 2017. A Systems Biology Approach Identifies FUT8 as a Driver of Melanoma Metastasis. Cancer Cell 31:804–819.e7. doi:10.1016/j.ccell.2017.05.007

Allan AK, Du J, Davies SA, Dow JAT. 2005. Genome-wide survey of V-ATPase genes in Drosophila reveals a conserved renal phenotype for lethal alleles. Physiol Genomics 22:128–138. doi:10.1152/physiolgenomics.00233.2004

Alfonso TB, Jones BW. 2002. gcm2 promotes glial cell differentiation and is required with glial cells missing for macrophage development in *Drosophila*. *Dev Biol.* **248**(2):369-83.

Alon A, Grossman I, Gat Y, Kodali VK, DiMaio F, Mehlman T, Haran G, Baker D, Thorpe C, Fass D. 2012. The dynamic disulphide relay of quiescin sulphydryl oxidase. Nature 488:414–8.

doi:10.1038/nature11267
Aoki K, Porterfield M, Lee SS, Dong B, Nguyen K, McGlamry KH, Tiemeyer M. 2008. The diversity of O-linked glycans expressed during *Drosophila melanogaster* development reflects stage- and tissue-specific requirements for cell signaling. J Biol Chem 283:30385–30400. doi:10.1074/jbc.M804925200
Aoki K, Tiemeyer M. 2010a. The Glycomics of Glycan Glucuronylation in *Drosophila melanogaster*Methods in Enzymology. pp. 297–321. doi:10.1016/S0076-6879(10)80014-X
Aoki K, Tiemeyer M. 2010b. The glycomics of glycan glucuronylation in *Drosophila melanogaster*, 1st ed, Methods in Enzymology. Elsevier Inc. doi:10.1016/S0076-6879(10)80014-X
Ashida M, Brey PT. 1995. Role of the integument in insect defense: pro-phenol oxidase cascade in the cuticular matrix. Proc Natl Acad Sci U S A 92:10698–702.
Aumailley M, Battaglia C, Mayer U, Reinhardt D, Nischt R, Timpl R, Fox JW. 1993. Nidogen mediates the formation of ternary complexes of basement membrane components. Kidney Int 43:7–12.
Aumiller JJ, Jarvis DL. 2002. Expression and functional characterization of a nucleotide sugar transporter from *Drosophila melanogaster*: relevance to protein glycosylation in insect cell expression systems. Protein Expr Purif 26:438–48.
Aviezer D, Hecht D, Safran M, Eisinger M, David G, Yayon A. 1994. Perlecan, basal lamina proteoglycan, promotes basic fibroblast growth factor-receptor binding, mitogenesis, and angiogenesis. Cell 79:1005–13.
Bach D-H, Park HJ, Lee SK. 2018. The Dual Role of Bone Morphogenetic Proteins in Cancer. Mol Ther oncolytics 8:1–13. doi:10.1016/j.omto.2017.10.002
Baldus SE, Zirbes TK, Hanisch F, Ph D, Kunze D, Shafizadeh ST, Nolden S, Mo SP, Karsten U, Ph D, Thiele J, Ho AH. 2000. Thomsen-Friedenreich Antigen Presents as a Prognostic Factor in Colorectal Carcinoma A Clinicopathologic Study of 264 Patients. Cancer 88:1536–1543.
Baldwin SA, Beal PR, Yao SYM, King AE, Cass CE, Young JD. 2004. The equilibrative nucleoside transporter family, SLC29. Pflugers Arch 447:735–43. doi:10.1007/s00424-003-1103-2
Barczyk M, Carracedo S, Gullberg D. 2010. Integrins. Cell Tissue Res 339:269–80. doi:10.1007/s00441-009-0834-6
Barr N, Taylor CR, Young T, Springer GF. 1989. Are pancarcinoma T and Tn differentiation antigens? Cancer 64:834–41.
Bataillé L, Augé B, Ferjoux G, Haenlin M, Waltzer L. 2005. Resolving embryonic blood cell fate choice in Drosophila: interplay of GCM and RUNX factors. Development 132:4635–4644. doi:10.1242/dev.02034
Bennett EP, Chen YW, Schwientek T, Mandel U, Schjoldager KTBG, Cohen SM, Clausen H. 2010. Rescue of *Drosophila Melanogaster* l(2)35Aa lethality is only mediated by polypeptide GalNAc-transferase pgant35A, but not by the evolutionary conserved human ortholog GalNAc-transferase-T11. Glycoconj J 27:435–444. doi:10.1007/s10719-010-9290-5
Bennett EP, Mandel U, Clausen H, Gerken TA, Fritz TA, Tabak LA. 2012. Control of mucin-type O-glycosylation: a classification of the polypeptide GalNAc-transferase gene family. Glycobiology 22:736–56. doi:10.1093/glycob/cwr182
Bergwitz C, Rasmussen MD, DeRobertis C, Wee MJ, Sinha S, Chen HH, Huang J, Perrimon N. 2012. Roles of major facilitator superfamily transporters in phosphate response in

Drosophila. PLoS One 7:1–10. doi:10.1371/journal.pone.0031730
Bernardoni R, Vivancos V, Giangrande A. 1997. glide/gcm is expressed and required in the scavenger cell lineage. Dev Biol 191:118–30.
Bhagavan NV. 2002. Carbohydrate Metabolism III: Glycoproteins, Glycolipids, GPI Anchors, Proteoglycans, and Peptidoglycans. Med Biochem 307–330. doi:10.1016/B978-012095440-7/50018-4
Bhattacharya R, Gonzalez AM, Debiase PJ, Trejo HE, Goldman RD, Flitney FW, Jones JCR. 2009. Recruitment of vimentin to the cell surface by beta3 integrin and plectin mediates adhesion strength. J Cell Sci 122:1390–400. doi:10.1242/jcs.043042
Bian B, Mongrain S, Cagnol S, Langlois M-J, Boulanger J, Bernatchez G, Carrier JC, Boudreau F, Rivard N. 2016. Cathepsin B promotes colorectal tumorigenesis, cell invasion, and metastasis. Mol Carcinog 55:671–87. doi:10.1002/mc.22312
Boersema PJ, Raijmakers R, Lemeer S, Mohammed S, Heck AJR. 2009. Multiplex peptide stable isotope dimethyl labeling for quantitative proteomics. Nat Protoc 4:484–494. doi:10.1038/nprot.2009.21
Bogaert T, Brown N, Wilcox M. 1987. The *Drosophila* PS2 antigen is an invertebrate integrin that, like the fibronectin receptor, becomes localized to muscle attachments. Cell 51:929–40.
Boland CR, Montgomery CK, Kim YS. 1982. Alterations in human colonic mucin occurring with cellular differentiation and malignant transformation. Proc Natl Acad Sci U S A 79:2051–5.
Boskovski MT, Yuan S, Borbye Pedersen N, Knak Goth C, Makova S, Clausen H, Brueckner M, Khokha MF. 2015. The heterotaxy gene, GALNT11, glycosylates Notch to orchestrate cilia type and laterality. Anal Chem 25:368–379. doi:10.1016/j.cogdev.2010.08.003.Personal
Brabant MC, Fristrom D, Bunch TA, Brower DL. 1996. Distinct spatial and temporal functions for PS integrins during *Drosophila* wing morphogenesis. Development 122:3307–17.
Breloy I, Schwientek T, Althoff D, Holz M, Koppen T, Krupa A, Hanisch F-G. 2016a. Functional Analysis of the Glucuronyltransferases GlcAT-P and GlcAT-S of *Drosophila melanogaster*: Distinct Activities towards the O-linked T-antigen. Biomolecules 6:8. doi:10.3390/biom6010008
Breloy I, Schwientek T, Althoff D, Holz M, Koppen T, Krupa A, Hanisch FG. 2016b. Functional analysis of the glucuronyltransferases GlcAT-P and GlcAT-S of *Drosophila melanogaster*: Distinct activities towards the O-linked T-antigen. Biomolecules 6:2–17. doi:10.3390/biom6010008
Brockhausen I, Yang JM, Burchell J, Whitehouse C, Taylor-Papadimitriou J. 1995. Mechanisms underlying aberrant glycosylation of MUC1 mucin in breast cancer cells. Eur J Biochem. 233(2):607-17.
Brückner K, Kockel L, Duchek P, Luque CM, Rørth P, Perrimon N. 2004. The PDGF / VEGF Receptor Controls Blood Cell Survival in *Drosophila* 77 Avenue Louis Pasteur 7:73–84.
Brückner K, Perez L, Clausen H, Cohen S. 2000. Glycosyltransferase activity of Fringe modulates Notch-Delta interactions. *Nature*. **406**(6794):411-5.
Bunch TA, Salatino R, Engelsgjerd MC, Mukai L, West RF, Brower DL. 1992. Characterization of mutant alleles of myospheroid, the gene encoding the beta subunit of the *Drosophila* PS integrins. Genetics 132:519–28.
Bunt S, Hooley C, Hu N, Scahill C, Weavers H, Skaer H. 2010. Hemocyte-secreted type IV

collagen enhances BMP signaling to guide renal tubule morphogenesis in *Drosophila*. Dev Cell 19:296–306. doi:10.1016/j.devcel.2010.07.019
Burda P, Aebi M. 1999. The dolichol pathway of N-linked glycosylation. Biochim Biophys Acta 1426:239–57.
Cai D, Chen SC, Prasad M, He L, Wang X, Choesmel-Cadamuro V, Sawyer JK, Danuser G, Montell DJ. 2014. Mechanical feedback through E-cadherin promotes direction sensing during collective cell migration. Cell 157:1146–1159. doi:10.1016/j.cell.2014.03.045
Campbell ID, Humphries MJ. 2011. Integrin structure, activation, and interactions. Cold Spring Harb Perspect Biol 3:a004994–a004994. doi:10.1101/cshperspect.a004994
Campos-Ortega JA, Hartenstein V. 1997. The Embryonic Development of *Drosophila melanogaster*. Berlin, Heidelberg: Springer Berlin Heidelberg. doi:10.1007/978-3-662-22489-2
Cao B, Yang L, Rong W, Feng L, Han N, Zhang K, Cheng S, Wu J, Xiao T, Gao Y. 2015. Latent transforming growth factor-beta binding protein-1 in circulating plasma as a novel biomarker for early detection of hepatocellular carcinoma. Int J Clin Exp Pathol 8:16046–54.
Cao Y, Stosiek P, Springer GF, Karsten U. 1996. Thomsen-Friedenreich-related carbohydrate antigens in normal adult human tissues: a systematic and comparative study. Histochem Cell Biol 106:197–207.
Cao Y, Stosiek P, Springer GF, Karsten U. 1996. Thomsen-Friedenreich-related carbohydrate antigens in normal adult human tissues: a systematic and comparative study. Histochem Cell Biol 106:197–207. doi:10.1007/BF02484401
Carman C V, Springer TA. 2008. Trans-cellular migration: cell-cell contacts get intimate. Curr Opin Cell Biol 20:533–40. doi:10.1016/j.ceb.2008.05.007
Carrasco C, Gilhooly NS, Dillingham MS, Moreno-Herrero F. 2013. On the mechanism of recombination hotspot scanning during double-stranded DNA break resection. Proc Natl Acad Sci U S A 110:E2562-71. doi:10.1073/pnas.1303035110
Carvalho S, Reis CA, Pinho SS. 2016. Cadherins Glycans in Cancer: Sweet Players in a Bitter Process. Trends in Cancer 2:519–531. doi:10.1016/j.trecan.2016.08.003
Cawthorn TR, Moreno JC, Dharsee M, Tran-Thanh D, Ackloo S, Zhu PH, Sardana G, Chen J, Kupchak P, Jacks LM, Miller NA, Youngson BJ, Iakovlev V, Guidos CJ, Vallis KA, Evans KR, McCready D, Leong WL, Done SJ. 2012. Proteomic analyses reveal high expression of decorin and endoplasmin (HSP90B1) are associated with breast cancer metastasis and decreased survival. PLoS One 7:e30992. doi:10.1371/journal.pone.0030992
Chakravarthi S, Jessop CE, Willer M, Stirling CJ, Bulleid NJ. 2007. Intracellular catalysis of disulfide bond formation by the human sulfhydryl oxidase, QSOX1. Biochem J 404:403–411. doi:10.1042/BJ20061510
Chambers AF, Groom AC, MacDonald IC. 2002. Dissemination and growth of cancer cells in metastatic sites. Nat Rev Cancer 2:563–72. doi:10.1038/nrc865
Chapel A, Kieffer-Jaquinod S, Sagné C, Verdon Q, Ivaldi C, Mellal M, Thirion J, Jadot M, Bruley C, Garin J, Gasnier B, Journet A. 2013. An Extended Proteome Map of the Lysosomal Membrane Reveals Novel Potential Transporters. Mol Cell Proteomics 12:1572–1588. doi:10.1074/mcp.M112.021980
Chia J, Goh G, Bard F. 2016a. Short O-GalNAc glycans: regulation and role in tumor

development and clinical perspectives. Biochim Biophys Acta - Gen Subj 1860:1623–1639. doi:10.1016/J.BBAGEN.2016.03.008
Chia J, Goh G, Bard F. 2016b. Short O-GalNAc glycans: Regulation and role in tumor development and clinical perspectives. Biochim Biophys Acta - Gen Subj 1860:1623–1639. doi:10.1016/j.bbagen.2016.03.008
Chia J, Tham KM, Gill DJ, Bard-Chapeau EA, Bard FA. 2014. ERK8 is a negative regulator of O-GalNAc glycosylation and cell migration. Elife 2014:1–22. doi:10.7554/eLife.01828
Chiu C-C, Lin C-Y, Lee L-Y, Chen Y-J, Lu Y-C, Wang H-M, Liao C-T, Chang JT-C, Cheng A-J. 2011. Molecular chaperones as a common set of proteins that regulate the invasion phenotype of head and neck cancer. Clin Cancer Res 17:4629–41. doi:10.1158/1078-0432.CCR-10-2107
Chiu C, Lin C, Lee L, Chen Y, Lu Y, Wang H. 2011. Molecular Chaperones as a Common Set of Proteins That Regulate the Invasion Phenotype of Head and Neck Cancer. Clin Cancer Res 17:1–14. doi:10.1158/1078-0432.CCR-10-2107
Cho NK, Keyes L, Johnson E, Heller J, Ryner L, Karim F, Krasnow MA. 2002. Developmental control of blood cell migration by the *Drosophila* VEGF pathway. Cell 108:865–76. doi:S0092867402006761 [pii]
Christlet HT, Veluraja K. 2001. Database Analysis of O-Glycosylation Sites in Proteins. Biophys J 80:952–960. doi:10.1016/S0006-3495(01)76074-2
Chung C-Y, Majewska NI, Wang Q, Paul JT, Betenbaugh MJ. 2017. SnapShot: N-Glycosylation Processing Pathways across Kingdoms. Cell 171:258–258.e1. doi:10.1016/j.cell.2017.09.014
Cofre J, Abdelhay E. 2017. Cancer Is to Embryology as Mutation Is to Genetics : Hypothesis of the Cancer as Embryological Phenomenon 2017. doi:10.1155/2017/3578090
Comber K, Huelsmann S, Evans I, Sanchez-Sanchez BJ, Chalmers A, Reuter R, Wood W, Martin-Bermudo MD. 2013. A dual role for the PS integrin myospheroid in mediating *Drosophila* embryonic macrophage migration. J Cell Sci 126:3475–3484. doi:10.1242/jcs.129700
Comer FI, Hart GW. 2000. O-glycosylation of nuclear and cytosolic proteins. Dynamic interplay between O-GlcNAc and O-phosphate. J Biol Chem 275:29179–29182. doi:10.1074/jbc.R000010200
Copeland RJ, Han G, Hart GW. 2013. O-GlcNAcomics--Revealing roles of O-GlcNAcylation in disease mechanisms and development of potential diagnostics. Proteomics Clin Appl 7:597–606. doi:10.1002/prca.201300001
Correia T, Papayannopoulos V, Panin V, Woronoff P, Jiang J, Vogt TF, Irvine KD. 2003. Molecular genetic analysis of the glycosyltransferase Fringe in *Drosophila*. Proc Natl Acad Sci 100:6404–6409. doi:10.1073/pnas.1131007100
Crozatier M, Meister M. 2007. *Drosophila* haematopoiesis. Cell Microbiol 9:1117–26. doi:10.1111/j.1462-5822.2007.00930.x
Dalziel M, Whitehouse C, Mcfarlane I, Brockhausen I, Gschmeissner S, Schwientek T, Clausen H, Burchell JM, Taylor-papadimitriou J. 2001. The Relative Activities of the C2GnT1 and ST3Gal-I Glycosyltransferases Determine O -Glycan Structure and Expression of a Tumor-associated Epitope on MUC1 * 276:11007–11015. doi:10.1074/jbc.M006523200
Dennis J, Waller C, Timpl R, Schirrmacher V.1982. Surface sialic acid reduces attachment of metastatic tumour cells to collagen type IV and fibronectin. Nature. 300(5889):274-6

Desgrosellier JS, Cheresh DA. 2010. Integrins in cancer: biological implications and therapeutic opportunities. Nat Rev Cancer 10:9–22. doi:10.1038/nrc2748

Devenport D, Brown NH. 2004. Morphogenesis in the absence of integrins: mutation of both *Drosophila* beta subunits prevents midgut migration. Development 131:5405–15. doi:10.1242/dev.01427

Díaz de la Loza MC, Díaz-Torres A, Zurita F, Rosales-Nieves AE, Moeendarbary E, Franze K, Martín-Bermudo MD, González-Reyes A. 2017. Laminin Levels Regulate Tissue Migration and Anterior-Posterior Polarity during Egg Morphogenesis in *Drosophila*. Cell Rep 20:211–223. doi:10.1016/j.celrep.2017.06.031

Dinkins MB, Fratto VM, Lemosy EK. 2008. Integrin alpha chains exhibit distinct temporal and spatial localization patterns in epithelial cells of the *Drosophila* ovary. Dev Dyn 237:3927–39. doi:10.1002/dvdy.21802

Dragojlovic-Munther M, Martinez-Agosto JA. 2013. Extracellular matrix-modulated Heartless signaling in *Drosophila* blood progenitors regulates their differentiation via a Ras/ETS/FOG pathway and target of rapamycin function. Dev Biol 384:313–30. doi:10.1016/j.ydbio.2013.04.004

Dustin ML, Springer TA. 1988. Lymphocyte function-associated antigen-1 (LFA-1) interaction with intercellular adhesion molecule-1 (ICAM-1) is one of at least three mechanisms for lymphocyte adhesion to cultured endothelial cells. J Cell Biol 107:321–31.

Evans CJ, Hartenstein V, Banerjee U. 2003. Thicker than blood: Conserved mechanisms in *Drosophila* and vertebrate hematopoiesis. Dev Cell 5:673–690. doi:10.1016/S1534-5807(03)00335-6

Evans IR, Hu N, Skaer H, Wood W. 2010. Interdependence of macrophage migration and ventral nerve cord development in *Drosophila* embryos. Development 137:1625–1633. doi:10.1242/dev.046797

Fabini G, Freilinger A, Altmann F, Wilson IB. 2001. Identification of core alpha 1,3-fucosylated glycans and cloning of the requisite fucosyltransferase cDNA from *Drosophila melanogaster*. Potential basis of the neural anti-horseadish peroxidase epitope. J Biol Chem 276:28058–67. doi:10.1074/jbc.M100573200

Fan X, Wang C, Song X, Liu H, Li X, Zhang Y. 2018. Elevated Cathepsin K potentiates metastasis of epithelial ovarian cancer. Histol Histopathol 33:673–680. doi:10.14670/HH-11-960

Ferguson K, Yadav A, Morey S, Abdullah J, Hrysenko G, Eng JY, Sajjad M, Koury S. 2014. Preclinical studies with JAA - F11 anti - Thomsen-Friedenreich monoclonal antibody for human breast cancer 10:385–399.

Fernández-Calotti P, Casulleras O, Antolin M, Guarner F, Pastor-Anglada M. 2016. Galectin-4 interacts with the drug transporter human concentrative nucleoside transporter 3 to regulate its function. FASEB J 30:544–54. doi:10.1096/fj.15-272773

Fessler JH, Fessler LI. 1989. *Drosophila* extracellular matrix. Annu Rev Cell Biol 5:309–39. doi:10.1146/annurev.cb.05.110189.001521

Fessler LI, Campbell AG, Duncan KG, Fessler JH. 1987. *Drosophila* laminin: characterization and localization. J Cell Biol 105:2383–91.

Fetchko M, Huang W, Li Y, Lai ZC. 2002. *Drosophila* Gp150 is required for early ommatidial development through modulation of Notch signaling. EMBO J 21:1074–1083. doi:10.1093/emboj/21.5.1074

Fischer KR, Durrans A, Lee S, Sheng J, Li F, Wong STC, Choi H, El Rayes T, Ryu S, Troeger J, Schwabe RF, Vahdat LT, Altorki NK, Mittal V, Gao D. 2015. Epithelial-to-mesenchymal transition is not required for lung metastasis but contributes to chemoresistance. Nature 527:472–6. doi:10.1038/nature15748

Fogerty FJ, Fessler LI, Bunch TA, Yaron Y, Parker CG, Nelson RE, Brower DL, Gullberg D, Fessler JH. 1994. Tiggrin, a novel *Drosophila* extracellular matrix protein that functions as a ligand for *Drosophila* alpha PS2 beta PS integrins. Development 120:1747–58.

Fossett N, Tevosian SG, Gajewski K, Zhang Q, Orkin SH, Schulz RA. 2001. The Friend of GATA proteins U-shaped, FOG-1, and FOG-2 function as negative regulators of blood, heart, and eye development in *Drosophila*. *Proc Natl Acad Sci USA* **98:**7342–7. doi:10.1073/pnas.131215798

Fossett N, Hyman K, Gajewski K, Orkin S.H, Schulz R.A. 2003. Combinatorial interactions of serpent, lozenge, and U-shaped regulate crystal cell lineage commitment during Drosophila hematopoiesis. *Proc. Natl. Acad. Sci. USA.* **100**: 11451-11456

Franc NC, Dimarcq JL, Lagueux M, Hoffmann J, Ezekowitz RAB. 1996. Croquemort, a novel *Drosophila* hemocyte/macrophage receptor that recognizes apoptotic cells. Immunity 4:431–443. doi:10.1016/S1074-7613(00)80410-0

Fu C, Zhao H, Wang Y, Cai H, Xiao Y, Zeng Y, Chen H. 2016. Tumor-associated antigens: Tn antigen, sTn antigen, and T antigen. Hla 88:275–286. doi:10.1111/tan.12900

Fuwa TJ, Kinoshita T, Nishida H, Nishihara S. 2015. Reduction of T antigen causes loss of hematopoietic progenitors in *Drosophila* through the inhibition of fi lopodial extensions from the hematopoietic niche. Dev Biol 401:206–219. doi:10.1016/j.ydbio.2015.03.003

Gahmberg CG, Fagerholm SC, Nurmi SM, Chavakis T, Marchesan S, Grönholm M. 2009. Regulation of integrin activity and signalling. Biochim Biophys Acta 1790:431–44. doi:10.1016/j.bbagen.2009.03.007

García-Alonso L, Fetter RD, Goodman CS. 1996. Genetic analysis of Laminin A in *Drosophila*: extracellular matrix containing laminin A is required for ocellar axon pathfinding. Development 122:2611–21.

Garcia A, Kandel JJ. 2012. Notch: a key regulator of tumor angiogenesis and metastasis. Histol Histopathol 27:151–6. doi:10.14670/HH-27.151

Garrison K, MacKrell AJ, Fessler JH. 1991. *Drosophila* laminin A chain sequence, interspecies comparison, and domain structure of a major carboxyl portion. J Biol Chem 266:22899–904.

Geiger B, Spatz JP, Bershadsky AD. 2009. Environmental sensing through focal adhesions. Nat Rev Mol Cell Biol 10:21–33. doi:10.1038/nrm2593

Ghosh S. 2018. Sialylation and sialyltransferase in insects. Glycoconj J 35:433–441. doi:10.1007/s10719-018-9835-6

Gill DJ, Tham KM, Chia J, Wang SC, Steentoft C, Clausen H, Bard-Chapeau EA, Bard FA. 2013. Initiation of GalNAc-type O-glycosylation in the endoplasmic reticulum promotes cancer cell invasiveness. Proc Natl Acad Sci 110:E3152–E3161. doi:10.1073/pnas.1305269110

Ginsberg MH. 2014. Integrin activation. BMB Rep 47:655–9.

Giot L, Bader JS, Brouwer C, Chaudhuri A, Kuang B, Li Y, Hao YL, Ooi CE, Godwin B, Vitols E, Vijayadamodar G, Pochart P, Machineni H, Welsh M, Kong Y, Zerhusen B, Malcolm R, Varrone Z, Collis A, Minto M, Burgess S, McDaniel L, Stimpson E, Spriggs F, Williams J,

Neurath K, Ioime N, Agee M, Voss E, Furtak K, Renzulli R, Aanensen N, Carrolla S, Bickelhaupt E, Lazovatsky Y, DaSilva A, Zhong J, Stanyon CA, Finley RL, White KP, Braverman M, Jarvie T, Gold S, Leach M, Knight J, Shimkets RA, McKenna MP, Chant J, Rothberg JM. 2003. A protein interaction map of *Drosophila melanogaster*. Science 302:1727–36. doi:10.1126/science.1090289

Glinsky V V, Huflejt ME, Glinsky G V, Deutscher SL, Quinn TP. 2000. Effects of Thomsen-Friedenreich antigen-specific peptide P-30 on beta-galactoside-mediated homotypic aggregation and adhesion to the endothelium of MDA-MB-435 human breast carcinoma cells. Cancer Res 60:2584–8.

Gohrig A, Detjen KM, Hilfenhaus G, Korner JL, Welzel M, Arsenic R, Schmuck R, Bahra M, Wu JY, Wiedenmann B, Fischer C. 2014. Axon Guidance Factor SLIT2 Inhibits Neural Invasion and Metastasis in Pancreatic Cancer. Cancer Res 74:1529–1540. doi:10.1158/0008-5472.CAN-13-1012

Gold KS, Brückner K. 2015. Macrophages and cellular immunity in *Drosophila melanogaster*. Semin Immunol 27:357–368. doi:10.1016/j.smim.2016.03.010

Gonias SL, Karimi-Mostowfi N, Murray SS, Mantuano E, Gilder AS. 2017. Expression of LDL receptor-related proteins (LRPs) in common solid malignancies correlates with patient survival. PLoS One 12:e0186649. doi:10.1371/journal.pone.0186649

Goth CK, Vakhrushev SY, Joshi HJ, Clausen H, Schjoldager KT. 2018. Fine-Tuning Limited Proteolysis: A Major Role for Regulated Site-Specific O-Glycosylation. Trends Biochem Sci 43:269–284. doi:10.1016/j.tibs.2018.02.005

Goto S, Taniguchi M, Muraoka M, Toyoda H, Sado Y, Kawakita M, Hayashi S. 2001. UDP-sugar transporter implicated in glycosylation and processing of Notch. Nat Cell Biol 3:816–822. doi:10.1038/ncb0901-816

Gotwals PJ, Fessler LI, Wehrli M, Hynes RO. 1994a. *Drosophila* PS1 integrin is a laminin receptor and differs in ligand specificity from PS2. Proc Natl Acad Sci U S A 91:11447–51.

Gotwals PJ, Fessler LI, Wehrli M, Hynes RO. 1994b. *Drosophila* PS1 integrin is a laminin receptor and differs in ligand specificity from PS2. Proc Natl Acad Sci U S A 91:11447–51.

Griffith JK, Baker ME, Rouch DA, Page MGP, Skurray RA, Paulsen IT, Chater KF, Baldwin SA, Henderson PJF. 1992. Membrane transport proteins: implications of sequence comparisons. Curr Opin Cell Biol 4:684–695. doi:10.1016/0955-0674(92)90090-Y

Grigorian M, Liu T, Banerjee U, Hartenstein V. 2013. The proteoglycan Trol controls the architecture of the extracellular matrix and balances proliferation and differentiation of blood progenitors in the *Drosophila* lymph gland. Dev Biol 384:301–12. doi:10.1016/j.ydbio.2013.03.007

Grotewiel MS, Beck CD, Wu KH, Zhu XR, Davis RL. 1998. Integrin-mediated short-term memory in *Drosophila*. Nature 391:455–60. doi:10.1038/35079

Guruharsha KG, Rual JF, Zhai B, Mintseris J, Vaidya P, Vaidya N, Beekman C, Wong C, Rhee DY, Cenaj O, McKillip E, Shah S, Stapleton M, Wan KH, Yu C, Parsa B, Carlson JW, Chen X, Kapadia B, Vijayraghavan K, Gygi SP, Celniker SE, Obar RA, Artavanis-Tsakonas S. 2011. A protein complex network of *Drosophila melanogaster*. Cell 147:690–703. doi:10.1016/j.cell.2011.08.047

Gyoergy A, Roblek M, Ratheesh A, Valoskova K, Belyaeva V, Wachner S, Matsubayashi Y, Sánchez-Sánchez BJ, Stramer B, Siekhaus DE. 2018. Tools Allowing Independent

Visualization and Genetic Manipulation of *Drosophila melanogaster* Macrophages and Surrounding Tissues. G3 (Bethesda) 8:845–857. doi:10.1534/g3.117.300452
Hallmann R, Zhang X, Di Russo J, Li L, Song J, Hannocks M-J, Sorokin L. 2015. The regulation of immune cell trafficking by the extracellular matrix. Curr Opin Cell Biol 36:54–61. doi:10.1016/j.ceb.2015.06.006
Hamaratoglu F, Affolter M, Pyrowolakis G. 2014. Dpp/BMP signaling in flies: From molecules to biology. Semin Cell Dev Biol 32:128–136. doi:10.1016/j.semcdb.2014.04.036
Harpaz N, Ordan E, Ocorr K, Bodmer R, Volk T. 2013. Multiplexin promotes heart but not aorta morphogenesis by polarized enhancement of slit/robo activity at the heart lumen. PLoS Genet 9:e1003597. doi:10.1371/journal.pgen.1003597
Hart GW, Slawson C, Ramirez-Correa G, Lagerlof O. 2011. Cross talk between O-GlcNAcylation and phosphorylation: roles in signaling, transcription, and chronic disease. Annu Rev Biochem 80:825–58. doi:10.1146/annurev-biochem-060608-102511
Hassan H, Reis CA, Bennett EP, Mirgorodskaya E, Roepstorff P, Hollingsworth MA, Burchell J, Taylor-Papadimitriou J, Clausen H. 2000. The lectin domain of UDP-N-acetyl-D-galactosamine: polypeptide N-acetylgalactosaminyltransferase-T4 directs its glycopeptide specificities. J Biol Chem 275:38197–205. doi:10.1074/jbc.M005783200
Hassinen A, Kellokumpu S. 2014. Organizational interplay of Golgi N-glycosyltransferases involves organelle microenvironment-dependent transitions between enzyme homo- and heteromers. J Biol Chem 289:26937–48. doi:10.1074/jbc.M114.595058
Hattrup CL, Gendler SJ. 2008. Structure and function of the cell surface (tethered) mucins. Annu Rev Physiol. 70:431-57
Häuselmann I, Borsig L. 2014. Altered tumor-cell glycosylation promotes metastasis. Front Oncol 4:1–15. doi:10.3389/fonc.2014.00028
Hays TS, Porter ME, McGrail M, Grissom P, Gosch P, Fuller MT, McIntosh JR. 1994. A cytoplasmic dynein motor in *Drosophila*: identification and localization during embryogenesis. J Cell Sci 107 (Pt 6):1557–69.
Heckler EJ, Alon A, Fass D, Thorpe C. 2008. Human quiescin-sulfhydryl oxidase, QSOX1: probing internal redox steps by mutagenesis. Biochemistry 47:4955–63. doi:10.1021/bi702522q
Heimburg J, Yan J, Morey S, Glinskii O V., Huxley VH, Wild L, Klick R, Roy R, Glinsky V V., Rittenhouse-Olson K. 2006. Inhibition of Spontaneous Breast Cancer Metastasis by Anti—Thomsen-Friedenreich Antigen Monoclonal Antibody JAA-F11. Neoplasia 8:939–948. doi:10.1593/neo.06493
Herr P, Korniychuk G, Yamamoto Y, Grubisic K, Oelgeschläger M. 2008. Regulation of TGF-(beta) signalling by N-acetylgalactosaminyltransferase-like 1. Development 135:1813–22. doi:10.1242/dev.019323
Higashi N, Fujioka K, Denda-Nagai K, Hashimoto S-I, Nagai S, Sato T, Fujita Y, Morikawa A, Tsuiji M, Miyata-Takeuchi M, Sano Y, Suzuki N, Yamamoto K, Matsushima K, Irimura T. 2002. The macrophage C-type lectin specific for galactose/N-acetylgalactosamine is an endocytic receptor expressed on monocyte-derived immature dendritic cells. J Biol Chem 277:20686–93. doi:10.1074/jbc.M202104200
Hodar C, Zuñiga A, Pulgar R, Travisany D, Chacon C, Pino M, Maass A, Cambiazo V. 2014. Comparative gene expression analysis of Dtg, a novel target gene of Dpp signaling pathway in the early *Drosophila melanogaster* embryo. Gene 535:210–217.

doi:10.1016/j.gene.2013.11.032
Hofman K, Stoffel W. 1993. TMbase-A database of membrane spanning proteins segments. BiolChem 374:166.
Hollfelder D, Frasch M, Reim I. 2014. Distinct functions of the laminin β LN domain and collagen IV during cardiac extracellular matrix formation and stabilization of alary muscle attachments revealed by EMS mutagenesis in *Drosophila*. BMC Dev Biol 14:26. doi:10.1186/1471-213X-14-26
Hollingsworth MA, Swanson BJ. 2004. Mucins in cancer: protection and control of the cell surface. Nat Rev Cancer. 4(1):45-60.
Holz A, Bossinger B, Strasser T, Janning W, Klapper R. 2003. The two origins of hemocytes in *Drosophila*. Development 130:4955–62. doi:10.1242/dev.00702
Honti V, Csordás G, Kurucz É, Márkus R, Andó I. 2014. The cell-mediated immunity of *Drosophila melanogaster*: hemocyte lineages, immune compartments, microanatomy and regulation. Dev Comp Immunol 42:47–56. doi:10.1016/j.dci.2013.06.005
Hoober KL, Joneja B, White HB, Thorpe C. 1996. A sulfhydryl oxidase from chicken egg white. J Biol Chem 271:30510–6.
Hori K, Sen A, Artavanis-Tsakonas S. 2013. Notch signaling at a glance. *J Cell Sci*. **126**(Pt 10):2135-40. doi: 10.1242/jcs.127308.
Howard DR, Taylor CR. 1980. An antitumor antibody in normal human serum: reaction of anti-T with breast carcinoma cells. Oncology 37:142–8. doi:10.1159/000225423
Hu X, Wang Q, Tang M, Barthel F, Amin S, Yoshihara K, Lang FM, Martinez-ledesma E, Lee SH, Zheng S, Verhaak RGW. 2018. TumorFusions : an integrative resource for cancer-associated transcript fusions. Nucleic Acids Res 46:1144–1149. doi:10.1093/nar/gkx1018
Hua D, Shen L, Xu L, Jiang Z, Zhou Y, Yue A, Zou S, Cheng Z, Wu S. 2012. Polypeptide N-acetylgalactosaminyltransferase 2 regulates cellular metastasis-associated behavior in gastric cancer. Int J Mol Med 30:1267–74. doi:10.3892/ijmm.2012.1130
Huang X, Jin M, Chen Y-X, Wang J, Zhai K, Chang Y, Yuan Q, Yao K-T, Ji G. 2016. ERP44 inhibits human lung cancer cell migration mainly via IP3R2. Aging (Albany NY) 8:1276–86. doi:10.18632/aging.100984
Huang Z, Yazdani U, Thompson-Peer KL, Kolodkin AL, Terman JR. 2007. Crk-associated substrate (Cas) signaling protein functions with integrins to specify axon guidance during development. Development 134:2337–47. doi:10.1242/dev.004242
Hung J-S, Huang J, Lin Y-C, Huang M-J, Lee P-H, Lai H-S, Liang J-T, Huang M-C. 2014. C1GALT1 overexpression promotes the invasive behavior of colon cancer cells through modifying O-glycosylation of FGFR2. Oncotarget 5:2096–106. doi:10.18632/oncotarget.1815
Ilani T, Alon A, Grossman I, Horowitz B, Kartvelishvily E, Cohen SR, Fass D. 2013. A secreted disulfide catalyst controls extracellular matrix composition and function. Science 341:74–6. doi:10.1126/science.1238279
Inoue M, Ton SM, Ogawa H, Tanizawa O. 1991. Expression of Tn and sialyl-Tn antigens in tumor tissues of the ovary. Am J Clin Pathol 96:711–6.
Inoue Y, Hayashi S. 2007. Tissue-specific laminin expression facilitates integrin-dependent association of the embryonic wing disc with the trachea in *Drosophila*. Dev Biol 304:90–101. doi:10.1016/j.ydbio.2006.12.022
Irvine KD, Wieschaus E. 1994. fringe, a Boundary-specific signaling molecule, mediates

interactions between dorsal and ventral cells during *Drosophila* wing development. Cell 79:595–606.

Islam R, Nakamura M, Scott H, Repnikova E, Carnahan M, Pandey D, Caster C, Khan S, Zimmermann T, Zoran MJ, Panin VM. 2013. The Role of *Drosophila* Cytidine Monophosphate-Sialic Acid Synthetase in the Nervous System. J Neurosci 33:12306–12315. doi:10.1523/JNEUROSCI.5220-12.2013

Itoh K, Akimoto Y, Fuwa TJ, Sato C, Komatsu A. 2016. Mucin-type core 1 glycans regulate the localization of neuromuscular junctions and establishment of muscle cell architecture in *Drosophila*. Dev Biol 412:114–127. doi:10.1016/j.ydbio.2016.01.032

Itoh K, Akimoto Y, Kondo S, Ichimiya T, Aoki K. 2018. Glucuronylated core 1 glycans are required for precise localization of neuromuscular junctions and normal formation of basement membranes on *Drosophila* muscles. Dev Biol 436:108–124. doi:10.1016/j.ydbio.2018.02.017

Itzkowitz SH, Yuan M, Montgomery CK, Kjeldsen T, Takahashi HK, Bigbee WL, Kim YS. 1989. Expression of Tn, sialosyl-Tn, and T antigens in human colon cancer. Cancer Res 49:197–204.

Iwai Y, Usui T, Hirano S, Steward R, Takeichi M, Uemura T. 1997. Axon patterning requires DN-cadherin, a novel neuronal adhesion receptor, in the *Drosophila* embryonic CNS. Neuron 19:77–89.

Jacquemet G, Hamidi H, Ivaska J. 2015. Filopodia in cell adhesion, 3D migration and cancer cell invasion. Curr Opin Cell Biol 36:23–31. doi:10.1016/j.ceb.2015.06.007

Jain BP, Pandey S. 2018. WD40 Repeat Proteins: Signalling Scaffold with Diverse Functions. Protein J 37:391–406. doi:10.1007/s10930-018-9785-7

Jattani R, Patel U, Kerman B, Myat MM. 2009. Deficiency screen identifies a novel role for beta 2 tubulin in salivary gland and myoblast migration in the *Drosophila* embryo. Dev Dyn 238:853–63. doi:10.1002/dvdy.21899

Joshi HJ, Narimatsu Y, Schjoldager KT, Tytgat HLP, Aebi M, Clausen H, Halim A. 2018. SnapShot: O-Glycosylation Pathways across Kingdoms. Cell. doi:10.1016/j.cell.2018.01.016

Ju T, Brewer K, D'Souza A, Cummings RD, Canfield WM. 2002a. Cloning and Expression of Human Core 1 β1,3-Galactosyltransferase. J Biol Chem 277:178–186. doi:10.1074/jbc.M109060200

Ju T, Cummings RD. 2005. Protein glycosylation: Chaperone mutation in Tn syndrome. Nature 437:1252–1252. doi:10.1038/4371252a

Ju T, Cummings RD. 2002. A unique molecular chaperone Cosmc required for activity of the mammalian core 1 beta 3-galactosyltransferase. Proc Natl Acad Sci U S A 99:16613–8. doi:10.1073/pnas.262438199

Ju T, Cummings RD, Canfield WM. 2002b. Purification, characterization, and subunit structure of rat core 1 Beta1,3-galactosyltransferase. J Biol Chem 277:169–77. doi:10.1074/jbc.M109056200

Ju T, Lanneau GS, Gautam T, Wang Y, Xia B, Stowell SR, Willard MT, Wang W, Xia JY, Zuna RE, Laszik Z, Benbrook DM, Hanigan MH, Cummings RD. 2008. Human tumor antigens Tn and sialyl Tn arise from mutations in Cosmc. Cancer Res 68:1636–46. doi:10.1158/0008-5472.CAN-07-2345

Kadener S, Stoleru D, McDonald M, Nawathean P, Rosbash M. 2007. Clockwork Orange is a

transcriptional repressor and a new *Drosophila* circadian pacemaker component. Genes Dev 21:1675–1686. doi:10.1101/gad.1552607

Katchman BA, Antwi K, Hostetter G, Demeure MJ, Watanabe A, Decker GA, Miller LJ, Von Hoff DD, Lake DF. 2011. Quiescin sulfhydryl oxidase 1 promotes invasion of pancreatic tumor cells mediated by matrix metalloproteinases. Mol Cancer Res 9:1621–31. doi:10.1158/1541-7786.MCR-11-0018

Katchman BA, Ocal IT, Cunliffe HE, Chang Y, Hostetter G, Watanabe A, Lobello J, Lake DF. 2013. Expression of quiescin sulfhydryl oxidase 1 is associated with a highly invasive phenotype and correlates with a poor prognosis in Luminal B breast cancer Expression of quiescin sulfhydryl oxidase 1 is associated with a highly invasive phenotype and corre. Breast Cancer Res 15:R28. doi:10.1186/bcr3407

Kelemen-Valkony I, Kiss M, Csiha J, Kiss A, Bircher U, Szidonya J, Maróy P, Juhász G, Komonyi O, Csiszár K, Mink M. 2012. *Drosophila* basement membrane collagen col4a1 mutations cause severe myopathy. Matrix Biol 31:29–37. doi:10.1016/j.matbio.2011.09.004

Kellokumpu S, Hassinen A, Glumoff T. 2016. Glycosyltransferase complexes in eukaryotes: Long-known, prevalent but still unrecognized. Cell Mol Life Sci 73:305–325. doi:10.1007/s00018-015-2066-0

Kellokumpu S, Sormunen R, Kellokumpu I. 2002. Abnormal glycosylation and altered Golgi structure in colorectal cancer: dependence on intra-Golgi pH. FEBS Lett 516:217–24.

Kiermaier E, Moussion C, Veldkamp CT, Gerardy-Schahn R, de Vries I, Williams LG, Chaffee GR, Phillips AJ, Freiberger F, Imre R, Taleski D, Payne RJ, Braun A, Förster R, Mechtler K, Mühlenhoff M, Volkman BF,Sixt M. 2016.Polysialylation controls dendritic cell trafficking by regulating chemokine recognition. Science. 351(6269):186-90. doi: 10.1126/science.aad0512.

Kim B-T, Tsuchida K, Lincecum J, Kitagawa H, Bernfield M, Sugahara K. 2003. Identification and characterization of three *Drosophila melanogaster* glucuronyltransferases responsible for the synthesis of the conserved glycosaminoglycan-protein linkage region of proteoglycans. Two novel homologs exhibit broad specificity toward oligosaccharides from proteoglycans, glycoproteins, and glycosphingolipids. J Biol Chem 278:9116–24. doi:10.1074/jbc.M209344200

Kókai E, Páldy FS, Somogyi K, Chougule A, Pál M, Kerekes É, Deák P, Friedrich P, Dombrádi V, Ádám G. 2012. CalpB modulates border cell migration in *Drosophila* egg chambers. BMC Dev Biol 12:20. doi:10.1186/1471-213X-12-20

Kornfeld R, Kornfeld S. 1985. Assembly of asparagine-linked oligosaccharides. Annu Rev Biochem 54:631–64. doi:10.1146/annurev.bi.54.070185.003215

Krakhmal N V, Zavyalova M V, Denisov E V, Vtorushin S V, Perelmuter VM. 2015. Cancer Invasion: Patterns and Mechanisms. Acta Naturae 7:17–28.

Kraynov VS, Chamberlain C, Bokoch GM, Schwartz MA, Slabaugh S, Hahn KM. 2000. Localized Rac activation dynamics visualized in living cells. Science 290:333–7.

Kubota T, Shiba T, Sugioka S, Furukawa S, Sawaki H, Kato R, Wakatsuki S, Narimatsu H. 2006. Structural basis of carbohydrate transfer activity by human UDP-GalNAc: polypeptide alpha-N-acetylgalactosaminyltransferase (pp-GalNAc-T10). J Mol Biol 359:708–27. doi:10.1016/j.jmb.2006.03.061

Kumagai C, Kadowaki T, Kitagawa Y. 1997. Disulfide-bonding between *Drosophila* laminin β and

γ chains is essential for α chain to form αβγ trimer. FEBS Lett 412:211–216. doi:10.1016/S0014-5793(97)00780-1

Kunkel EJ, Ley K. 1996. Distinct phenotype of E-selectin-deficient mice. E-selectin is required for slow leukocyte rolling in vivo. Circ Res 79:1196–204.

Kusche-Gullberg M, Garrison K, MacKrell AJ, Fessler LI, Fessler JH. 1992. Laminin A chain: expression during *Drosophila* development and genomic sequence. EMBO J 11:4519–27.

Kuwabara H, Uda H, Takenaka I. 1997. Immunohistochemical detection of sialosyl-Tn antigen in carcinoma of the prostate. Br J Urol 80:456–9.

Lafite P, Daniellou R. 2012. Rare and unusual glycosylation of peptides and proteins. Nat Prod Rep 29:729. doi:10.1039/c2np20030a

Lake DF, Faigel DO. 2014. The Emerging Role of QSOX1 in Cancer. Antioxid Redox Signal 21:485–496. doi:10.1089/ars.2013.5572

Larsen ISB, Narimatsu Y, Joshi HJ, Siukstaite L, Harrison OJ, Brasch J, Goodman KM, Hansen L, Shapiro L, Honig B, Vakhrushev SY, Clausen H, Halim A. 2017. Discovery of an O-mannosylation pathway selectively serving cadherins and protocadherins. *Proc Natl Acad Sci* **114**:201708319. doi:10.1073/pnas.1708319114

Lauffenburger DA, Horwitz AF. 1996. Cell migration: a physically integrated molecular process. Cell **84**:359–69.

Lebestky, T., Chang, T., Hartenstein, V., Banerjee, U. 2000. Specification of *Drosophila* hematopoietic lineage by conserved transcription factors. *Science.* **288**(5463): 146--149.

Lee TV, Sethi MK, Leonardi J, Rana NA, Buettner FF, Haltiwanger RS, Bakker H, Jafar-Nejad H. 2013. Negative regulation of notch signaling by xylose. *PLoS Genet*. **9**(6):e1003547. doi: 10.1371/journal.pgen.1003547.

Letsou A, Arora K, Wrana JL, Simin K, Twombly V, Jamal J, Staehling-Hampton K, Hoffmann FM, Gelbart WM, Massagué J, O'Connor MB. 1995. *Drosophila* Dpp signaling is mediated by the punt gene product: A dual ligand-binding type II receptor of the TGFβ receptor family. Cell 80:899–908. doi:10.1016/0092-8674(95)90293-7

Levery SB, Steentoft C, Halim A, Narimatsu Y, Clausen H, Vakhrushev SY. 2015. Advances in mass spectrometry driven O-glycoproteomics. Biochim Biophys Acta - Gen Subj 1850:33–42. doi:10.1016/j.bbagen.2014.09.026

Levi BP, Ghabrial AS, Krasnow MA. 2006. *Drosophila* talin and integrin genes are required for maintenance of tracheal terminal branches and luminal organization. Development 133:2383–93. doi:10.1242/dev.02404

Li S, Liu P, Xi L, Jiang X, Wu M, Deng D, Wei J, Zhu T, Zhou L, Wang S, Xu G, Meng L, Zhou J, Ma D. 2008. Expression of TMEM87B interacting with the human papillomavirus type 18 E6 oncogene in the Hela cDNA library by a yeast two-hybrid system. Oncol Rep 20:421–7.

Li Y. 2003. Scabrous and Gp150 are endosomal proteins that regulate Notch activity. Development 130:2819–2827. doi:10.1242/dev.00495

Li Y, Bharti A, Chen D, Gong J, Kufe D. 1998. Interaction of glycogen synthase kinase 3beta with the DF3/MUC1 carcinoma-associated antigen and beta-catenin. *Mol Cell Biol.* **18**(12):7216-24.

Lim C, Chung BY, Pitman JL, McGill JJ, Pradhan S, Lee J, Keegan KP, Choe J, Allada R. 2007. Clockwork orange encodes a transcriptional repressor important for circadian-clock amplitude in *Drosophila*. Curr Biol 17:1082–9. doi:10.1016/j.cub.2007.05.039

Limas C, Lange P. 1986. T-antigen in normal and neoplastic urothelium. Cancer 58:1236–45.
Lin G, Zhang X, Ren J, Pang Z, Wang C, Xu N, Xi R. 2013. Integrin signaling is required for maintenance and proliferation of intestinal stem cells in *Drosophila*. Dev Biol 377:177–87. doi:10.1016/j.ydbio.2013.01.032
Lin YR, Reddy BVVG, Irvine KD. 2008. Requirement for a core 1 galactosyltransferase in the *Drosophila* nervous system. Dev Dyn 237:3703–3714. doi:10.1002/dvdy.21775
Linton KM, Hey Y, Saunders E, Jeziorska M, Denton J, Wilson CL, Swindell R, Dibben S, Miller CJ, Pepper SD, Radford JA, Freemont AJ. 2008. Acquisition of biologically relevant gene expression data by Affymetrix microarray analysis of archival formalin-fixed paraffin-embedded tumours. Br J Cancer 98:1403–14. doi:10.1038/sj.bjc.6604316
Ma L, Rohatgi R, Kirschner MW. 1998. The Arp2/3 complex mediates actin polymerization induced by the small GTP-binding protein Cdc42. Proc Natl Acad Sci U S A 95:15362–7.
Machesky LM, Insall RH. 1998. Scar1 and the related Wiskott-Aldrich syndrome protein, WASP, regulate the actin cytoskeleton through the Arp2/3 complex. Curr Biol 8:1347–56.
MacLean GD, Longenecker BM. 1991. Clinical significance of the Thomsen-Friedenreich antigen. Semin Cancer Biol 2:433–9.
Madej MG, Kaback HR. 2013. Evolutionary mix-and-match with MFS transporters II. Proc Natl Acad Sci 110:E4831–E4838. doi:10.1073/pnas.1319754110
Mak M, Spill F, Kamm RD, Zaman MH. 2016. Single-Cell Migration in Complex Microenvironments: Mechanics and Signaling Dynamics. J Biomech Eng 138:021004. doi:10.1115/1.4032188
Makki R, Meister M, Pennetier D, Ubeda J-M, Braun A, Daburon V, Krzemień J, Bourbon H-M, Zhou R, Vincent A, Crozatier M. 2010. A short receptor downregulates JAK/STAT signalling to control the *Drosophila* cellular immune response. PLoS Biol 8:e1000441. doi:10.1371/journal.pbio.1000441
Mao F, Holmlund C, Faraz M, Wang W, Bergenheim T, Kvarnbrink S, Johansson M, Henriksson R, Hedman H. 2018. Lrig1 is a haploinsuf fi cient tumor suppressor gene in malignant glioma. Oncogenesis 7:1–12. doi:10.1038/s41389-017-0012-8
Marshall R. 1972. Glycoproteins. Annu Rev Biochem 41:673–702.
Marshansky V, Futai M. 2008. The V-type H+-ATPase in vesicular trafficking: targeting, regulation and function. Curr Opin Cell Biol 20:415–26. doi:10.1016/j.ceb.2008.03.015
Martin D, Zusman S, Li X, Williams EL, Khare N, DaRocha S, Chiquet-Ehrismann R, Baumgartner S. 1999. wing blister, a new *Drosophila* laminin alpha chain required for cell adhesion and migration during embryonic and imaginal development. J Cell Biol 145:191–201.
Matos LL, Suarez ER, Theodoro TR, Trufelli DC, Melo CM, Garcia LF, Oliveira OCG, Matos MGL, Kanda JL, Nader HB, Martins JRM, Pinhal MAS. 2015. The Profile of Heparanase Expression Distinguishes Differentiated Thyroid Carcinoma from Benign Neoplasms. PLoS One 10:e0141139. doi:10.1371/journal.pone.0141139
Matsubayashi Y, Louani A, Dragu A, Sánchez-Sánchez BJ, Serna-Morales E, Yolland L, Gyoergy A, Vizcay G, Fleck RA, Heddleston JM, Chew TL, Siekhaus DE, Stramer BM. 2017. A Moving Source of Matrix Components Is Essential for De Novo Basement Membrane Formation. Curr Biol 27. doi:10.1016/j.cub.2017.10.001
Matsumoto A, Ukai-Tadenuma M, Yamada RG, Houl J, Uno KD, Kasukawa T, Dauwalder B, Itoh TQ, Takahashi K, Ueda R, Hardin PE, Tanimura T, Ueda HR. 2007. A functional genomics

strategy reveals clockwork orange as a transcriptional regulator in the *Drosophila* circadian clock. Genes Dev 21:1687–700. doi:10.1101/gad.1552207
McEver RP. 2015. Selectins: initiators of leucocyte adhesion and signalling at the vascular wall. Cardiovasc Res 107:331–9. doi:10.1093/cvr/cvv154
Meerbrey KL, Hu G, Kessler JD, Roarty K, Li MZ, Fang JE, Herschkowitz JI, Burrows AE, Ciccia A, Sun T, Schmitt EM, Bernardi RJ, Fu X, Bland CS, Cooper TA, Schiff R, Rosen JM, Westbrook TF, Elledge SJ. 2011. The pINDUCER lentiviral toolkit for inducible RNA interference in vitro and in vivo. Proc Natl Acad Sci 108:3665–3670. doi:10.1073/pnas.1019736108
Mohammed A, O'Hare MB, Warley A, Tear G, Tuxworth RI. 2017. in vivo localization of the neuronal ceroid lipofuscinosis proteins, CLN3 and CLN7, at endogenous expression levels. Neurobiol Dis 103:123–132. doi:10.1016/J.NBD.2017.03.015
Molin K, Fredman P, Svennerholm L. 1986. Binding specificities of the lectins PNA, WGA and UEA I to polyvinylchloride-adsorbed glycosphingolipids. FEBS Lett 205:51–55. doi:10.1016/0014-5793(86)80864-X
Molnár J, Kars MD, Gündüz U, Engi H, Schumacher U, Van Damme EJ, Peumans WJ, Makovitzky J, Gyémánt N, Molnár P. 2009. Interaction of tomato lectin with ABC transporter in cancer cells: glycosylation confers functional conformation of P-gp. Acta Histochem 111:329–33. doi:10.1016/j.acthis.2008.11.010
Moloney DJ, Panin VM, Johnston SH, Chen J, Shao L, Wilson R, Wang Y, Stanley P, Irvine KD, Haltiwanger RS, Vogt TF. 2000. Fringe is a glycosyltransferase that modifies Notch. Nature 406:369–75. doi:10.1038/35019000
Momota R, Naito I, Ninomiya Y, Ohtsuka A. 2011. *Drosophila* type XV/XVIII collagen, Mp, is involved in Wingless distribution. Matrix Biol 30:258–66. doi:10.1016/j.matbio.2011.03.008
Monson JM, Natzle J, Friedman J, McCarthy BJ. 1982. Expression and novel structure of a collagen gene in *Drosophila*. Proc Natl Acad Sci U S A 79:1761–5.
Montell DJ. 2003. Border-cell migration: the race is on. Nat Rev Mol Cell Biol 4:13–24. doi:10.1038/nrm1006
Montell DJ, Goodman CS. 1989. *Drosophila* laminin: sequence of B2 subunit and expression of all three subunits during embryogenesis. J Cell Biol 109:2441–53.
Montell DJ, Goodman CS. 1988. *Drosophila* substrate adhesion molecule: sequence of laminin B1 chain reveals domains of homology with mouse. Cell 53:463–73.
Mouw JK, Ou G, Weaver VM. 2014. Extracellular matrix assembly: a multiscale deconstruction. Nat Rev Mol Cell Biol 15:771–85. doi:10.1038/nrm3902
Müller R, Hülsmeier AJ, Altmann F, Ten Hagen K, Tiemeyer M, Hennet T. 2005. Characterization of mucin-type core-1 β1-3 galactosyltransferase homologous enzymes in *Drosophila melanogaster*. FEBS J 272:4295–4305. doi:10.1111/j.1742-4658.2005.04838.x
Muller WA. 2013. Getting leukocytes to the site of inflammation. Vet Pathol 50:7–22. doi:10.1177/0300985812469883
Mullins RD, Heuser JA, Pollard TD. 1998. The interaction of Arp2/3 complex with actin: nucleation, high affinity pointed end capping, and formation of branching networks of filaments. Proc Natl Acad Sci U S A 95:6181–6.
Naba A, Clauser KR, Hoersch S, Liu H, Carr SA, Hynes RO. 2012. The matrisome: in silico definition and in vivo characterization by proteomics of normal and tumor extracellular

matrices. Mol Cell Proteomics 11:M111.014647. doi:10.1074/mcp.M111.014647
Nagaosa K, Okada R, Nonaka S, Takeuchi K, Fujita Y, Miyasaka T, Manaka J, Ando I, Nakanishi Y. 2011. Integrin βv-mediated phagocytosis of apoptotic cells in *Drosophila* embryos. J Biol Chem 286:25770–7. doi:10.1074/jbc.M110.204503
Napoletano C, Rughetti A, Agervig Tarp MP, Coleman J, Bennett EP, Picco G, Sale P, Denda-Nagai K, Irimura T, Mandel U, Clausen H, Frati L, Taylor-Papadimitriou J, Burchell J, Nuti M. 2007. Tumor-associated Tn-MUC1 glycoform is internalized through the macrophage galactose-type C-type lectin and delivered to the HLA class I and II compartments in dendritic cells. Cancer Res 67:8358–67. doi:10.1158/0008-5472.CAN-07-1035
Narimatsu Y, Joshi HJ, Yang Z, Gomes C, Chen YH, Lorenzetti FC, Furukawa S, Schjoldager KT, Hansen L, Clausen H, Bennett EP, Wandall HH. 2018. A validated gRNA library for CRISPR/Cas9 targeting of the human glycosyltransferase genome. Glycobiology 28. doi:10.1093/glycob/cwx101
Nasdala I, Wolburg-Buchholz K, Wolburg H, Kuhn A, Ebnet K, Brachtendorf G, Samulowitz U, Kuster B, Engelhardt B, Vestweber D, Butz S. 2002. A transmembrane tight junction protein selectively expressed on endothelial cells and platelets. J Biol Chem 277:16294–303. doi:10.1074/jbc.M111999200
Natchiar SK, Suguna K, Surolia A, Vijayan M. 2007. Peanut agglutinin, a lectin with an unusual quaternary structure and interesting ligand binding properties. Crystallogr Rev 13:3–28. doi:10.1080/08893110701382087
Nath S, Daneshvar K, Roy LD, Grover P, Kidiyoor A, Mosley L, Sahraei M, Mukherjee P.2013. MUC1 induces drug resistance in pancreatic cancer cells via upregulation of multidrug resistance genes. *Oncogenesis*. **2**:e51. doi: 10.1038/oncsis.2013.16.
Nath S, Mukherjee P. 2014. MUC1: a multifaceted oncoprotein with a key role in cancer progression. Trends Mol Med 20:332–42. doi:10.1016/j.molmed.2014.02.007
Nelson RE, Fessler LI, Takagi Y, Blumberg B, Keene DR, Olson PF, Parker CG, Fessler JH. 1994. Peroxidasin: a novel enzyme-matrix protein of *Drosophila* development. *EMBO J* **13**:3438–47.
Nguyen AT, Chia J, Ros M, Hui KM, Saltel F, Bard F. 2017. Organelle Specific O-Glycosylation Drives MMP14 Activation, Tumor Growth, and Metastasis. *Cancer Cell* **32**:639–653.e6. doi:10.1016/j.ccell.2017.10.001
Nieto MA, Huang RY-J, Jackson RA, Thiery JP. 2016. EMT: 2016. *Cell* **166**:21–45. doi:10.1016/j.cell.2016.06.028
Niewiadomska P, Godt D, Tepass U. 1999. DE-Cadherin is required for intercellular motility during *Drosophila* oogenesis. *J Cell Biol* **144**:533–47.
Ninov N, Menezes-Cabral S, Prat-Rojo C, Manjón C, Weiss A, Pyrowolakis G, Affolter M, Martín-Blanco E. 2010. Dpp signaling directs cell motility and invasiveness during epithelial morphogenesis. *Curr Biol* **20**:513–20. doi:10.1016/j.cub.2010.01.063
Nonaka S, Nagaosa K, Mori T, Shiratsuchi A, Nakanishi Y. 2013. Integrin αPS3/βv-mediated phagocytosis of apoptotic cells and bacteria in *Drosophila*. *J Biol Chem* **288**:10374–80. doi:10.1074/jbc.M113.451427
Noonan DM, Fulle A, Valente P, Cai S, Horigan E, Sasaki M, Yamada Y, Hassell JR. 1991. The complete sequence of perlecan, a basement membrane heparan sulfate proteoglycan, reveals extensive similarity with laminin A chain, low density lipoprotein-receptor, and the

neural cell adhesion molecule. *J Biol Chem* **266**:22939–47.
Ntziachristos P, Lim JS, Sage J, Aifantis I. 2014. From Fly Wings to Targeted Cancer Therapies: A Centennial for Notch Signaling. *Cancer Cell* **25**:318–334. doi:10.1016/j.ccr.2014.02.018
Ohtsubo K, Marth JD. 2006. Glycosylation in cellular mechanisms of health and disease. *Cell* **126**:855–67. doi:10.1016/j.cell.2006.08.019
Okajima T, Irvine KD. 2002. Regulation of notch signaling by o-linked fucose. *Cell*. **111**(6):893-904.
Olofsson B, Page DT. 2005. Condensation of the central nervous system in embryonic *Drosophila* is inhibited by blocking hemocyte migration or neural activity. *Dev Biol* **279**:233–243. doi:10.1016/j.ydbio.2004.12.020
Omasits U, Ahrens CH, Müller S, Wollscheid B. 2014. Protter: Interactive protein feature visualization and integration with experimental proteomic data. *Bioinformatics* **30**:884–886. doi:10.1093/bioinformatics/btt607
Orntoft TF, Mors NP, Eriksen G, Jacobsen NO, Poulsen HS. 1985. Comparative immunoperoxidase demonstration of T-antigens in human colorectal carcinomas and morphologically abnormal mucosa. *Cancer Res* **45**:447–52.
Owens P, Pickup MW, Novitskiy S V, Giltnane JM, Gorska AE, Hopkins CR, Hong CC, Moses HL. 2015. Inhibition of BMP signaling suppresses metastasis in mammary cancer. *Oncogene* **34**:2437–49. doi:10.1038/onc.2014.189
Pacquelet A, Røth P. 1999. Regulatory mechanisms required for DE-cadherin function in cell migration and other types of adhesion. *J Cell Biol* **170**:803–812. doi:10.1083/jcb.200506131
Palmieri M, Impey S, Kang H, di Ronza A, Pelz C, Sardiello M, Ballabio A. 2011. Characterization of the CLEAR network reveals an integrated control of cellular clearance pathways. *Hum Mol Genet* **20**:3852–3866. doi:10.1093/hmg/ddr306
Panin VM, Papayannopoulos V, Wilson R, Irvine KD.1997. Fringe modulates Notch-ligand interactions. *Nature*. **387**(6636):908-12.
Pankov R, Endo Y, Even-Ram S, Araki M, Clark K, Cukierman E, Matsumoto K, Yamada KM. 2005. A Rac switch regulates random versus directionally persistent cell migration. *J Cell Biol* **170**:793–802. doi:10.1083/jcb.200503152
Pao SS, Paulsen IT, Saier MH. 1998. Major facilitator superfamily. *Microbiol Mol Biol Rev* **62**:1–34.
Parsons B, Foley E. 2016. Cellular immune defenses of *Drosophila* melanogaster. *Dev Comp Immunol* **58**. doi:10.1016/j.dci.2015.12.019
Patel U, Myat MM. 2013. Receptor guanylyl cyclase Gyc76C is required for invagination, collective migration and lumen shape in the *Drosophila* embryonic salivary gland. *Biol Open* **2**:711–7. doi:10.1242/bio.20134887
Pérez-Moreno JJ, Espina-Zambrano AG, García-Calderón CB, Estrada B. 2017. Kon-tiki enhances PS2 integrin adhesion and localizes its ligand, Thrombospondin, in the myotendinous junction. *J Cell Sci* **130**:950–962. doi:10.1242/jcs.197459
Perland E, Hellsten S V., Lekholm E, Eriksson MM, Arapi V, Fredriksson R. 2017. The Novel Membrane-Bound Proteins MFSD1 and MFSD3 are Putative SLC Transporters Affected by Altered Nutrient Intake. *J Mol Neurosci* **61**:199–214. doi:10.1007/s12031-016-0867-8
Petrie RJ, Yamada KM. 2016. Multiple mechanisms of 3D migration: the origins of plasticity.

Curr Opin Cell Biol **42**:7–12. doi:10.1016/j.ceb.2016.03.025
Picco G, Julien S, Brockhausen I, Beatson R, Antonopoulos A, Haslam S, Mandel U, Dell A, Pinder S, Taylor-Papadimitriou J, Burchell J.2010. Over-expression of ST3Gal-I promotes mammary tumorigenesis. *Glycobiology*. **20**(10):1241-50. doi: 10.1093/glycob/cwq085.
Pickup MW, Hover LD, Guo Y, Gorska AE, Chytil A, Novitskiy S V, Moses HL, Owens P. 2015. Deletion of the BMP receptor BMPR1a impairs mammary tumor formation and metastasis. *Oncotarget* **6**:22890–904. doi:10.18632/oncotarget.4413
Pierce GB. 1974. Neoplasms, differentiations and mutations. *Am J Pathol* **77**:103–118.
Piller V, Piller F, Cartron J. 1990. Comparison of the carbohydrate-binding specificities of seven N-acetyl-D-galactosamine-recognizing lectins. *Eur J Biochem* **191**:461–466. doi:10.1111/j.1432-1033.1990.tb19144.x
Plow EF, Haas TA, Zhang L, Loftus J, Smith JW. 2000. Ligand binding to integrins. *J Biol Chem* **275**:21785–8. doi:10.1074/jbc.R000003200
Qi H, Rand MD, Wu X, Sestan N, Wang W, Rakic P, Xu T, Artavanis-Tsakonas S. 1999. Processing of the notch ligand delta by the metalloprotease Kuzbanian. *Science* **283**:91–4.
Quistgaard EM, Löw C, Guettou F, Nordlund P. 2016. Understanding transport by the major facilitator superfamily (MFS): structures pave the way. *Nat Rev Mol Cell Biol* **17**:123–132. doi:10.1038/nrm.2015.25
Radhakrishnan P, Dabelsteen S, Madsen FB, Francavilla C, Kopp KL, Steentoft C, Vakhrushev SY, Olsen J V., Hansen L, Bennett EP, Woetmann A, Yin G, Chen L, Song H, Bak M, Hlady RA, Peters SL, Opavsky R, Thode C, Qvortrup K, Schjoldager KT-BG, Clausen H, Hollingsworth MA, Wandall HH. 2014. Immature truncated O-glycophenotype of cancer directly induces oncogenic features. *Proc Natl Acad Sci* **111**:E4066–E4075. doi:10.1073/pnas.1406619111
Ratheesh A, Belyaeva V, Siekhaus DE. 2015. *Drosophila* immune cell migration and adhesion during embryonic development and larval immune responses. *Curr Opin Cell Biol*. doi:10.1016/j.ceb.2015.07.003
Ratheesh A, Biebl J, Vesela J, Smutny M, Papusheva E, Krens SFG, Kaufmann W, Gyoergy A, Casano AM, Siekhaus DE. 2018. *Drosophila* TNF Modulates Tissue Tension in the Embryo to Facilitate Macrophage Invasive Migration. *Dev Cell* **45**:331–346.e7. doi:10.1016/j.devcel.2018.04.002
Reddy VS, Shlykov MA, Castillo R, Sun EI, Saier MH. 2012. The major facilitator superfamily (MFS) revisited. *FEBS J* **279**:2022–2035. doi:10.1111/j.1742-4658.2012.08588.x
Rehorn KP, Thelen H, Michelson a M, Reuter R. 1996. A molecular aspect of hematopoiesis and endoderm development common to vertebrates and *Drosophila*. *Development* **122**:4023–4031.
Repnikova E, Koles K, Nakamura M, Pitts J, Li H, Ambavane A, Zoran MJ, Panin VM. 2010. Sialyltransferase Regulates Nervous System Function in *Drosophila*. *J Neurosci* **30**:6466–6476. doi:10.1523/JNEUROSCI.5253-09.2010
Revoredo L, Wang S, Bennett EP, Clausen H, Moremen KW, Jarvis DL, Ten Hagen KG, Tabak LA, Gerken TA. 2016. Mucin-type o-glycosylation is controlled by short- And long-range glycopeptide substrate recognition that varies among members of the polypeptide GalNAc transferase family. *Glycobiology* **26**:360–376. doi:10.1093/glycob/cwv108
Richier B, Michard-Vanhée C, Lamouroux A, Papin C, Rouyer F. 2008. The clockwork orange *Drosophila* protein functions as both an activator and a repressor of clock gene expression.

J Biol Rhythms **23**:103–16. doi:10.1177/0748730407313817
Riedel F, Gillingham AK, Rosa-Ferreira C, Galindo A, Munro S. 2016. An antibody toolkit for the study of membrane traffic in *Drosophila melanogaster*. *Biol Open* **5**:987–992. doi:10.1242/bio.018937
Rivinoja A, Kokkonen N, Kellokumpu I, Kellokumpu S. 2006. Elevated Golgi pH in breast and colorectal cancer cells correlates with the expression of oncofetal carbohydrate T-antigen. *J Cell Physiol* **208**:167–174. doi:10.1002/jcp.20653
Rizki MT, Rizki RM. 1959. Functional significance of the crystal cells in the larva of *Drosophila* melanogaster. *J Biophys Biochem Cytol* **5**:235–40.
Rizki TM, Rizki RM. 1992. Lamellocyte differentiation in *Drosophila* larvae parasitized by Leptopilina. *Dev Comp Immunol* **16**:103–10.
Rodrigues JG, Balmaña M, Macedo JA, Poças J, Fernandes Â, de-Freitas-Junior JCM, Pinho SS, Gomes J, Magalhães A, Gomes C, Mereiter S, Reis CA. 2018. Glycosylation in cancer: Selected roles in tumor progression, immune modulation and metastasis. *Cell Immunol*. **333**:46-57. doi: 10.1016/j.cellimm.2018.03.007
Rohrbough J, Grotewiel MS, Davis RL, Broadie K. 2000. Integrin-mediated regulation of synaptic morphology, transmission, and plasticity. *J Neurosci* **20**:6868–78.
Rørth P. 2009. Collective cell migration. *Annu Rev Cell Dev Biol* **25**:407–29. doi:10.1146/annurev.cellbio.042308.113231
Roth J. 1984. Cytochemical localization of terminal N-acetyl-D-galactosamine residues in cellular compartments of intestinal goblet cells: implications for the topology of O-glycosylation. *J Cell Biol* **98**:399–406.
Rudolf J, Pringle MA, Bulleid NJ. 2013. Proteolytic processing of QSOX1A ensures efficient secretion of a potent disulfide catalyst. *Biochem J* **454**:181–90. doi:10.1042/BJ20130360
Saeland E, van Vliet SJ, Bäckström M, van den Berg VCM, Geijtenbeek TBH, Meijer GA, van Kooyk Y. 2007. The C-type lectin MGL expressed by dendritic cells detects glycan changes on MUC1 in colon carcinoma. *Cancer Immunol Immunother* **56**:1225–36. doi:10.1007/s00262-006-0274-z
Sahlgren C, Gustafsson M V, Jin S, Poellinger L, Lendahl U. 2008. Notch signaling mediates hypoxia-induced tumor cell migration and invasion. *Proc Natl Acad Sci U S A* **105**:6392–7. doi:10.1073/pnas.0802047105
Salker MS, Singh Y, Zeng N, Chen H, Zhang S, Umbach AT, Fakhri H, Kohlhofer U, Quintanilla-Martinez L, Durairaj RRP, Barros FS V., Vrljicak P, Ott S, Brucker SY, Wallwiener D, Vrhovac Madunić I, Breljak D, Sabolić I, Koepsell H, Brosens JJ, Lang F. 2017. Loss of Endometrial Sodium Glucose Cotransporter SGLT1 is Detrimental to Embryo Survival and Fetal Growth in Pregnancy. *Sci Rep* **7**:12612. doi:10.1038/s41598-017-11674-3
Sánchez-Sánchez BJ, Urbano JM, Comber K, Dragu A, Wood W, Stramer B, Martín-Bermudo MD. 2017. *Drosophila* Embryonic Hemocytes Produce Laminins to Strengthen Migratory Response. *Cell Rep* **21**:1461–1470. doi:10.1016/j.celrep.2017.10.047
Schenkel AR, Mamdouh Z, Chen X, Liebman RM, Muller WA. 2002. CD99 plays a major role in the migration of monocytes through endothelial junctions. *Nat Immunol* **3**:143–50. doi:10.1038/ni749
Schiller B, Hykollari A, Yan S, Paschinger K, Wilson IBH. 2012. Complicated N-linked glycans in simple organisms. *Biol Chem* **393**:661–73. doi:10.1515/hsz-2012-0150

Schindlbeck C, Jeschke U, Schulze S, Karsten U, Janni W, Rack B, Sommer H, Friese K. 2005. Characterisation of disseminated tumor cells in the bone marrow of breast cancer patients by the Thomsen–Friedenreich tumor antigen. *Histochem Cell Biol* **123**:631–637. doi:10.1007/s00418-005-0781-6

Schjoldager KT-BG, Vakhrushev SY, Kong Y, Steentoft C, Nudelman AS, Pedersen NB, Wandall HH, Mandel U, Bennett EP, Levery SB, Clausen H. 2012. Probing isoform-specific functions of polypeptide GalNAc-transferases using zinc finger nuclease glycoengineered SimpleCells. *Proc Natl Acad Sci* **109**:9893–9898. doi:10.1073/pnas.1203563109

Schjoldager KT, Joshi HJ, Kong Y, Goth CK, King SL, Wandall HH, Bennett EP, Vakhrushev SY, Clausen H. 2015. Deconstruction of O-glycosylation--GalNAc-T isoforms direct distinct subsets of the O-glycoproteome. *EMBO Rep* **16**:1713–1722. doi:10.15252/embr.201540796

Schöck F, Perrimon N. 2003. Retraction of the *Drosophila* germ band requires cell-matrix interaction. *Genes Dev* **17**:597–602. doi:10.1101/gad.1068403

Schwientek T, Bennett EP, Flores C, Thacker J, Hollmann M, Reis CA, Behrens J, Mandel U, Keck B, Mireille A, Schäfer, Haselmann K, Zubarev R, Roepstorff P, Burchell JM, Taylor-Papadimitriou J, Hollingsworth MA, Clausena H. 2002. Functional conservation of subfamilies of putative UDP-N-acetylgalactosamine:Polypeptide N-acetylgalactosaminyltransferases in *Drosophila*, Caenorhabditis elegans, and mammals. One subfamily composed of l(2)35Aa is essential in *Drosophila*. *J Biol Chem* **277**:22623–22638. doi:10.1074/jbc.M202684200

Schwientek T, Mandel U, Roth U, Müller S, Hanisch FG. 2007. A serial lectin approach to the mucin-type O-glycoproteome of *Drosophila* melanogaster S2 cells. *Proteomics* **7**:3264–3277. doi:10.1002/pmic.200600793

Seales EC, Jurado GA, Brunson BA, Wakefield JK, Frost AR, Bellis SL.2005. Hypersialylation of beta1 integrins, observed in colon adenocarcinoma, may contribute to cancer progression by up-regulating cell motility. *Cancer Res*. **65(**11):4645-52.

Sears HC. 2003. Macrophage-mediated corpse engulfment is required for normal *Drosophila* CNS morphogenesis. *Development* **130**:3557–3565. doi:10.1242/dev.00586

Segawa H, Kawakita M, Ishida N. 2002. Human and *Drosophila* UDP-galactose transporters transport UDP-N-acetylgalactosamine in addition to UDP-galactose. *Eur J Biochem* **269**:128–38.

Seifert JRK, Lehmann R. 2012. *Drosophila* primordial germ cell migration requires epithelial remodeling of the endoderm. *Development* **139**:2101–6. doi:10.1242/dev.078949

Selva EM, Hong K, Baeg GH, Beverley SM, Turco SJ, Perrimon N, Häcker U. 2001. Dual role of the fringe connection gene in both heparan sulphate and fringe-dependent signalling events. *Nat Cell Biol* **3**:809–815. doi:10.1038/ncb0901-809

Senanayake U, Das S, Vesely P, Alzoughbi W, Frohlich LF, Chowdhury P, Leuschner I, Hoefler G, Guertl B. 2012. miR-192, miR-194, miR-215, miR-200c and miR-141 are downregulated and their common target ACVR2B is strongly expressed in renal childhood neoplasms. *Carcinogenesis* **33**:1014–1021. doi:10.1093/carcin/bgs126

Shattil SJ, Kim C, Ginsberg MH. 2010. The final steps of integrin activation: the end game. *Nat Rev Mol Cell Biol* **11**:288–300. doi:10.1038/nrm2871

Shaw SK, Bamba PS, Perkins BN, Luscinskas FW. 2001. Real-time imaging of vascular

endothelial-cadherin during leukocyte transmigration across endothelium. *J Immunol* **167**:2323–30.

Sheu JJ-C, Lee C-C, Hua C-H, Li C-I, Lai M-T, Lee S-C, Cheng J, Chen C-M, Chan C, Chao SC-C, Chen J-Y, Chang J-Y, Lee C-H. 2014. LRIG1 modulates aggressiveness of head and neck cancers by regulating EGFR-MAPK-SPHK1 signaling and extracellular matrix remodeling. *Oncogene* **33**:1375–1384. doi:10.1038/onc.2013.98

Siekhaus D, Haesemeyer M, Moffitt O, Lehmann R. 2010. RhoL controls invasion and Rap1 localization during immune cell transmigration in *Drosophila*. *Nat Cell Biol* **12**:605–610. doi:10.1038/ncb2063

Smith AN, Lovering RC, Futai M, Takeda J, Brown D, Karet FE. 2003. Revised nomenclature for mammalian vacuolar-type H+ -ATPase subunit genes. *Mol Cell* **12**:801–3. doi:10.1016/S1097-2765(03)00397-6

Sonoshita M, Aoki M, Fuwa H, Aoki K, Hosogi H, Sakai Y, Hashida H, Takabayashi A, Sasaki M, Robine S, Itoh K, Yoshioka K, Kakizaki F, Kitamura T, Oshima M, Taketo MM. 2011. Suppression of colon cancer metastasis by Aes through inhibition of Notch signaling. *Cancer Cell* **19**:125–37. doi:10.1016/j.ccr.2010.11.008

Sorrosal G, Pérez L, Herranz H, Milán M. 2010. Scarface, a secreted serine protease-like protein, regulates polarized localization of laminin A at the basement membrane of the *Drosophila* embryo. *EMBO Rep* **11**:373–9. doi:10.1038/embor.2010.43

Springer GF. 1997. Immunoreactive T and Tn epitopes in cancer diagnosis , prognosis , and immunotherapy 594–602.

Springer GF. 1989. Tn epitope (N-acetyl-D-galactosamine alpha-O-serine/threonine) density in primary breast carcinoma: a functional predictor of aggressiveness. *Mol Immunol* **26**:1–5.

Springer GF. 1984. T and Tn , General Carcinoma Autoantigens. *Science (80-)* **224**:1198–1206.

Springer GF, Desai PR, Banatwala I. 1975. Blood group MN antigens and precursors in normal and malignant human breast glandular tissue. *J Natl Cancer Inst* **54**:335–9.

Springer GF, Desai PR, Banatwala I. 1974. Blood group MN specific substances and precursors in normal and malignant human breast tissues. *Naturwissenschaften* **61**:457–8.

Stanley P, Schachter H, Taniguchi N. 2009. N-Glycans, Essentials of Glycobiology. Cold Spring Harbor Laboratory Press.

Stark KA, Yee GH, Roote CE, Williams EL, Zusman S, Hynes RO. 1997. A novel alpha integrin subunit associates with betaPS and functions in tissue morphogenesis and movement during *Drosophila* development. *Development* **124**:4583–94.

Steen P Van den, Rudd PM, Dwek RA, Opdenakker G. 1998. Concepts and Principles of O-Linked Glycosylation. *Crit Rev Biochem Mol Biol* **33**:151–208. doi:10.1080/10409239891204198

Steentoft C, Vakhrushev SY, Joshi HJ, Kong Y, Vester-Christensen MB, Schjoldager KT-BG, Lavrsen K, Dabelsteen S, Pedersen NB, Marcos-Silva L, Gupta R, Bennett EP, Mandel U, Brunak S, Wandall HH, Levery SB, Clausen H. 2013a. Precision mapping of the human O-GalNAc glycoproteome through SimpleCell technology. *EMBO J* **32**:1478–88. doi:10.1038/emboj.2013.79

Steentoft C, Vakhrushev SY, Joshi HJ, Kong Y, Vester-Christensen MB, Schjoldager KTBG, Lavrsen K, Dabelsteen S, Pedersen NB, Marcos-Silva L, Gupta R, Paul Bennett E, Mandel U, Brunak S, Wandall HH, Levery SB, Clausen H. 2013b. Precision mapping of the human O-GalNAc glycoproteome through SimpleCell technology. *EMBO J* **32**:1478–1488.

doi:10.1038/emboj.2013.79
Steentoft C, Vakhrushev SY, Vester-Christensen MB, Schjoldager KT-BG, Kong Y, Bennett EP, Mandel U, Wandall H, Levery SB, Clausen H. 2011. Mining the O-glycoproteome using zinc-finger nuclease–glycoengineered SimpleCell lines. *Nat Methods* **8**:977–982. doi:10.1038/nmeth.1731
Stevens A, Jacobs JR. 2002. Integrins regulate responsiveness to slit repellent signals. *J Neurosci* **22**:4448–55. doi:20026413
Stojadinovic A, Hooke JA, Shriver CD, Nissan A, Kovatich AJ, Kao T-C, Ponniah S, Peoples GE, Moroni M. 2007. HYOU1 / Orp150 expression in breast cancer. *Med Sci Monit* **13**:231–239.
Sugiura M, Kawasaki T, Yamashina I. 1982. Purification and characterization of UDP-GalNAc:polypeptide N-acetylgalactosamine transferase from an ascites hepatoma, AH 66. *J Biol Chem* **257**:9501–7.
Summers JL, Coon JS, Ward RM, Falor WH, Miller AW, Weinstein RS. 1983. Prognosis in carcinoma of the urinary bladder based upon tissue blood group abh and Thomsen-Friedenreich antigen status and karyotype of the initial tumor. *Cancer Res* **43**:934–9.
Takeuchi H, Haltiwanger RS.2014. Significance of glycosylation in Notch signaling. *Biochem Biophys Res Commun.* **453**(2):235-42. doi: 10.1016/j.bbrc.2014.05.115.
Tamkun JW, DeSimone DW, Fonda D, Patel RS, Buck C, Horwitz AF, Hynes RO. 1986. Structure of integrin, a glycoprotein involved in the transmembrane linkage between fibronectin and actin. *Cell* **46**:271–82.
Tarp MA, Clausen H. 2008. Mucin-type O-glycosylation and its potential use in drug and vaccine development. *Biochim Biophys Acta* **1780**:546–63. doi:10.1016/j.bbagen.2007.09.010
Ten Hagen KG, Fritz TA, Tabak LA. 2003a. All in the family: The UDP-GalNAc:polypeptide N-acetylgalactosaminyltransferases. *Glycobiology* **13**:1–16. doi:10.1093/glycob/cwg007
Ten Hagen KG, Tran DT, Gerken TA, Stein DS, Zhang Z. 2003b. Functional characterization and expression analysis of members of the UDP-GalNAc:polypeptide N-acetylgalactosaminyltransferase family from *Drosophila* melanogaster. *J Biol Chem* **278**:35039–35048. doi:10.1074/jbc.M303836200
Tenno M, Ohtsubo K, Hagen FK, Ditto D, Zarbock A, Schaerli P, von Andrian UH, Ley K, Le D, Tabak LA, Marth JD. 2007. Initiation of protein O glycosylation by the polypeptide GalNAcT-1 in vascular biology and humoral immunity. *Mol Cell Biol* **27**:8783–96. doi:10.1128/MCB.01204-07
Tepass U, Eileen G, F D, Haag A, Omatyar L, Trk T. 1996. shotgun encodes *Drosophila* E-cadherin and is preferentially , required during cell rearrangement in the neurectoderm and other morphogenetically active epithelia 672–685.
Tepass U, Fessler LI, Aziz a, Hartenstein V. 1994. Embryonic origin of hemocytes and their relationship to cell death in *Drosophila*. *Development* **120**:1829–1837. doi:8223268
Terriente-Felix A, Li J, Collins S, Mulligan A, Reekie I, Bernard F, Krejci A, Bray S. 2013. Notch cooperates with Lozenge/Runx to lock haemocytes into a differentiation programme. *Development* **140**:926–937. doi:10.1242/dev.086785
Tian E, Ten Hagen KG. 2009. Recent insights into the biological roles of mucin-type O-glycosylation. *Glycoconj J* **26**:325–34. doi:10.1007/s10719-008-9162-4
Tian E, Ten Hagen KG. 2006. Expression of the UDP-GalNAc: Polypeptide N-acetylgalactosaminyltransferase family is spatially and temporally regulated during

Drosophila development. *Glycobiology* **16**:83–95. doi:10.1093/glycob/cwj051
Tien AC, Rajan A, Schulze KL, Hyung DR, Acar M, Steller H, Bellen HJ. 2008. Ero1L, a thiol oxidase, is required for Notch signaling through cysteine bridge formation of the Lin12-Notch repeats in *Drosophila* melanogaster. *J Cell Biol* **182**:1113–1125. doi:10.1083/jcb.200805001
Tomancak P, Beaton A, Weiszmann R, Kwan E, Shu S, Lewis SE, Richards S, Ashburner M, Hartenstein V, Celniker SE, Rubin GM. 2002. Systematic determination of patterns of gene expression during *Drosophila* embryogenesis. *Genome Biol* **3**:RESEARCH0088. doi:10.1186/gb-2002-3-12-research0088
Tomancak P, Berman BP, Beaton A, Weiszmann R, Kwan E, Hartenstein V, Celniker SE, Rubin GM. 2007. Global analysis of patterns of gene expression during *Drosophila* embryogenesis **8**:1–24. doi:10.1186/gb-2007-8-7-r145
Tran DT, Zhang L, Zhang Y, Tian E, Earl LA, Ten Hagen KG. 2012. Multiple members of the UDP-GalNAc: Polypeptide N- acetylgalactosaminyltransferase family are essential for viability in *Drosophila*. *J Biol Chem* **287**:5243–5252. doi:10.1074/jbc.M111.306159
Urbano JM, Domínguez-Giménez P, Estrada B, Martín-Bermudo MD. 2011. PS integrins and laminins: key regulators of cell migration during *Drosophila* embryogenesis. *PLoS One* **6**:e23893. doi:10.1371/journal.pone.0023893
Urbano JM, Torgler CN, Molnar C, Tepass U, López-Varea A, Brown NH, de Celis JF, Martín-Bermudo MD. 2009. *Drosophila* laminins act as key regulators of basement membrane assembly and morphogenesis. *Development* **136**:4165–76. doi:10.1242/dev.044263
Vakhrushev SY, Steentoft C, Vester-Christensen MB, Bennett EP, Clausen H, Levery SB. 2013. Enhanced mass spectrometric mapping of the human GalNAc-type O-glycoproteome with SimpleCells. *Mol Cell Proteomics* **12**:932–44. doi:10.1074/mcp.O112.021972
van Vliet SJ, Vuist IM, Lenos K, Tefsen B, Kalay H, García-Vallejo JJ, van Kooyk Y. 2013. Human T cell activation results in extracellular signal-regulated kinase (ERK)-calcineurin-dependent exposure of Tn antigen on the cell surface and binding of the macrophage galactose-type lectin (MGL). *J Biol Chem* **288**:27519–32. doi:10.1074/jbc.M113.471045
van Zijl F, Krupitza G, Mikulits W. 2011. Initial steps of metastasis: cell invasion and endothelial transmigration. *Mutat Res* **728**:23–34. doi:10.1016/j.mrrev.2011.05.002
Varki A. 2017. Biological roles of glycans. *Glycobiology* **27**:3–49. doi:10.1093/glycob/cww086
Verheyen EM, Cooley L. 1994. Profilin mutations disrupt multiple actin-dependent processes during *Drosophila* development. *Development* **120**:717–28.
Vestweber D. 2015. How leukocytes cross the vascular endothelium. *Nat Rev Immunol*. doi:10.1038/nri3908
Vizcaino JA, Deutch EW, Wang R, Csordas A, Raisinger F, Rios D, Dianes JA, Sun Z, Farrah T, Bandeira N, Binz P-A, Xenarios I, Eisenacher M, Mayer G, Gatto L, Campos A, Chalkley RJ, Kraus H-J, Albar PJ, Martinez-Bartolome S, Apweiler R, Omenn GS, Martens L, Jones AR, Hermjakob H. 2016. ProteomeXchange provides globally co-ordinated proteomics data submission and dissemination Juan **10**:1939–1947. doi:10.1038/nprot.2015.121.Human
Voglmeir J, Laurent N, Flitsch SL, Oelgeschläger M, Wilson IBH. 2015. Biological and biochemical properties of two Xenopus laevis N-acetylgalactosaminyltransferases with contrasting roles in embryogenesis. *Comp Biochem Physiol Part B Biochem Mol Biol* **180**:40–47. doi:10.1016/j.cbpb.2014.10.003

Voigt A, Pflanz R, Schäfer U, Jäckle H. 2002. Perlecan participates in proliferation activation of quiescent *Drosophila* neuroblasts. *Dev Dyn* **224**:403–12. doi:10.1002/dvdy.10120

Voisin M-B, Woodfin A, Nourshargh S. 2009. Monocytes and neutrophils exhibit both distinct and common mechanisms in penetrating the vascular basement membrane in vivo. *Arterioscler Thromb Vasc Biol* **29**:1193–9. doi:10.1161/ATVBAHA.109.187450

Walls G V, Stevenson M, Lines KE, Newey PJ, Reed AAC, Bowl MR, Jeyabalan J, Harding B, Bradley KJ, Manek S, Chen J, Wang P, Williams BO, Teh BT, Thakker R V. 2017. Mice deleted for cell division cycle 73 gene develop parathyroid and uterine tumours: model for the hyperparathyroidism-jaw tumour syndrome. *Oncogene* **36**:4025–4036. doi:10.1038/onc.2017.43

Waltzer L, Bataille L, Peyrefitte S, Haenlin M. Two isoforms of Serpent containing either one or two GATA zinc fingers have different roles in *Drosophila* haematopoiesis. The EMBO journal. 2002; **21:**5477–5486.

Waltzer L, Ferjoux G, Bataillé L, Haenlin M. 2003. Cooperation between the GATA and RUNX factors Serpent and Lozenge during *Drosophila* hematopoiesis. *EMBO J* **22**:6516–25. doi:10.1093/emboj/cdg622

Wang Q, Han TH, Nguyen P, Jarnik M, Serpe M. 2018. Tenectin recruits integrin to stabilize bouton architecture and regulate vesicle release at the *Drosophila* neuromuscular junction. *Elife* **7**. doi:10.7554/eLife.35518

Wang S, Voisin M-B, Larbi KY, Dangerfield J, Scheiermann C, Tran M, Maxwell PH, Sorokin L, Nourshargh S. 2006. Venular basement membranes contain specific matrix protein low expression regions that act as exit points for emigrating neutrophils. *J Exp Med* **203**:1519–32. doi:10.1084/jem.20051210

Wang Y, Ju T, Ding X, Xia B, Wang W, Xia L, He M, Cummings RD. 2010. Cosmc is an essential chaperone for correct protein O-glycosylation. *Proc Natl Acad Sci U S A* **107**:9228–33. doi:10.1073/pnas.0914004107

Wang, Y., Shao, L., Shi, S., Harris, R.J., Spellman, M.W., Stanley, P., Haltiwanger, R.S. 2001. Modification of Epidermal growth factor-like repeats with O-fucose. Molecular cloning and expression of a novel GDP-fucose protein O-fucosyltransferase. *J. Biol. Chem.* **276**(43): 40338--40345.

Webb DJ, Nguyen DH, Sankovic M, Gonias SL. 1999. The very low density lipoprotein receptor regulates urokinase receptor catabolism and breast cancer cell motility in vitro. *J Biol Chem* **274**:7412–20.

Whitehouse C, Burchell J, Gschmeissner S, Brockhausen I, Lloyd KO, Taylor-Papadimitriou J.1997. A transfected sialyltransferase that is elevated in breast cancer and localizes to the medial/trans-Golgi apparatus inhibits the development of core-2-based O-glycans. *J Cell Biol*. **137**(6):1229-41.

Williamson WR, Wang D, Haberman AS, Hiesinger PR. 2010. A dual function of V0-ATPase a1 provides an endolysosomal degradation mechanism in *Drosophila* melanogaster photoreceptors. *J Cell Biol* **189**:885–899. doi:10.1083/jcb.201003062

Wolf K, Mazo I, Leung H, Engelke K, von Andrian UH, Deryugina EI, Strongin AY, Bröcker E-B, Friedl P. 2003. Compensation mechanism in tumor cell migration: mesenchymal-amoeboid transition after blocking of pericellular proteolysis. *J Cell Biol* **160**:267–77. doi:10.1083/jcb.200209006

Wolfstetter G, Dahlitz I, Pfeifer K, Töpfer U, Alt JA, Pfeifer DC, Lakes-Harlan R, Baumgartner S, Palmer RH, Holz A. 2019. Characterization of *Drosophila* Nidogen/entactin reveals roles in basement membrane stability, barrier function and nervous system patterning. *Development* **146**:dev168948. doi:10.1242/dev.168948

Wolfstetter G, Holz A. 2012. The role of LamininB2 (LanB2) during mesoderm differentiation in *Drosophila*. *Cell Mol Life Sci* **69**:267–82. doi:10.1007/s00018-011-0652-3

Woodfin A, Voisin M-B, Beyrau M, Colom B, Caille D, Diapouli F-M, Nash GB, Chavakis T, Albelda SM, Rainger GE, Meda P, Imhof BA, Nourshargh S. 2011. The junctional adhesion molecule JAM-C regulates polarized transendothelial migration of neutrophils in vivo. *Nat Immunol* **12**:761–9. doi:10.1038/ni.2062

Woodfin A, Voisin M-B, Imhof BA, Dejana E, Engelhardt B, Nourshargh S. 2009. Endothelial cell activation leads to neutrophil transmigration as supported by the sequential roles of ICAM-2, JAM-A, and PECAM-1. *Blood* **113**:6246–57. doi:10.1182/blood-2008-11-188375

Xu A, Haines N, Dlugosz M, Rana NA, Takeuchi H, Haltiwanger RS, Irvine KD.2007. In vitro reconstitution of the modulation of Drosophila Notch-ligand binding by Fringe. *J Biol Chem*. **282**(48):35153-62.

Xu Y, Chang R, Xu F, Gao Y, Yang F, Wang C, Xiao J, Su Z, Bi Y, Wang L, Zha X. 2017. N-Glycosylation at Asn 402 Stabilizes N-Cadherin and Promotes Cell-Cell Adhesion of Glioma Cells. *J Cell Biochem* **118**:1423–1431. doi:10.1002/jcb.25801

Yamamoto-Hino M, Abe M, Shibano T, Setoguchi Y, Awano W, Ueda R, Okano H, Goto S. 2012. Cisterna-specific localization of glycosylation-related proteins to the Golgi apparatus. *Cell Struct Funct* **37**:55–63.

Yan N. 2015. Structural Biology of the Major Facilitator Superfamily Transporters. *Annu Rev Biophys* **44**:257–283. doi:10.1146/annurev-biophys-060414-033901

Yano H, Yamamoto-Hino M, Abe M, Kuwahara R, Haraguchi S, Kusaka I, Awano W, Kinoshita-Toyoda A, Toyoda H, Goto S. 2005. Distinct functional units of the Golgi complex in *Drosophila* cells. *Proc Natl Acad Sci U S A* **102**:13467–13472. doi:10.1073/pnas.0506681102

Yarnitzky T, Volk T. 1995. Laminin is required for heart, somatic muscles, and gut development in the *Drosophila* embryo. *Dev Biol* **169**:609–18. doi:10.1006/dbio.1995.1173

Yasothornsrikul S, Davis WJ, Cramer G, Kimbrell DA, Dearolf CR. 1997. viking: identification and characterization of a second type IV collagen in *Drosophila*. *Gene* **198**:17–25.

Yee GH, Hynes RO. 1993. A novel, tissue-specific integrin subunit, beta nu, expressed in the midgut of *Drosophila* melanogaster. *Development* **118**:845–58.

Yilmaz M, Christofori G. 2010. Mechanisms of motility in metastasizing cells. *Mol Cancer Res* **8**:629–42. doi:10.1158/1541-7786.MCR-10-0139

Yin Y, Jensen MØ, Tajkhorshid E, Schulten K. 2006. Sugar Binding and Protein Conformational Changes in Lactose Permease. *Biophys J* **91**:3972–3985. doi:10.1529/biophysj.106.085993

Yokdang N, Hatakeyama J, Wald JH, Simion C, Tellez JD, Chang DZ, Swamynathan MM, Chen M, Murphy WJ, Carraway Iii KL, Sweeney C. 2016. LRIG1 opposes epithelial-to-mesenchymal transition and inhibits invasion of basal-like breast cancer cells. *Oncogene* **35**:2932–47. doi:10.1038/onc.2015.345

Yoshida H, Fuwa TJ, Arima M, Hamamoto H, Sasaki N, Ichimiya T, Osawa KI, Ueda R, Nishihara S. 2008. Identification of the *Drosophila* core 1 β1,3-galactosyltransferase gene that

synthesizes T antigen in the embryonic central nervous system and hemocytes. *Glycobiology* **18**:1094–1104. doi:10.1093/glycob/cwn094

You J, Zhang Y, Li Z, Lou Z, Jin L, Lin X. 2014. *Drosophila* perlecan regulates intestinal stem cell activity via cell-matrix attachment. *Stem cell reports* **2**:761–9. doi:10.1016/j.stemcr.2014.04.007

Yu LG, Andrews N, Zhao Q, McKean D, Williams JF, Connor LJ, Gerasimenko O V., Hilkens J, Hirabayashi J, Kasai K, Rhodes JM. 2007. Galectin-3 interaction with Thomsen-Friedenreich disaccharide on cancer-associated MUC1 causes increased cancer cell endothelial adhesion. *J Biol Chem* **282**:773–781. doi:10.1074/jbc.M606862200

Yurchenco PD. 2011. Basement membranes: cell scaffoldings and signaling platforms. *Cold Spring Harb Perspect Biol* **3**:a004911–a004911. doi:10.1101/cshperspect.a004911

Zhang L, Tran DT, Ten Hagen KG. 2010. An O-glycosyltransferase promotes cell adhesion during development by influencing secretion of an extracellular matrix integrin ligand. *J Biol Chem* **285**:19491–19501. doi:10.1074/jbc.M109.098145

Zhang Y, Ran Y, Xiong Y, Zhong Z-B, Wang Z-H, Fan X-L, Ye Q-F. 2016. Effects of TMEM9 gene on cell progression in hepatocellular carcinoma by RNA interference. *Oncol Rep* **36**:299–305. doi:10.3892/or.2016.4821

Zheng X, Carstens JL, Kim J, Scheible M, Kaye J, Sugimoto H, Wu C-C, LeBleu VS, Kalluri R. 2015. Epithelial-to-mesenchymal transition is dispensable for metastasis but induces chemoresistance in pancreatic cancer. *Nature* **527**:525–530. doi:10.1038/nature16064

Zhou Y, Liao Q, Li X, Wang H, Wei F, Chen J, Yang J. 2016. HYOU1 , Regulated by LPLUNC1 , Is Up-Regulated in Nasopharyngeal Carcinoma and Associated with Poor Prognosis. *J Cancer* **7**:367–367. doi:10.7150/jca.13695

Zhou Y, Zhu Y, Fan X, Zhang C, Wang Y, Zhang L, Zhang H, Wen T, Zhang K, Huo X, Jiang X, Bu Y, Zhang Y. 2017. NID1, a new regulator of EMT required for metastasis and chemoresistance of ovarian cancer cells. *Oncotarget* **8**:33110–33121. doi:10.18632/oncotarget.16145

Zoncu R, Bar-Peled L, Efeyan A, Wang S, Sancak Y, Sabatini DM. 2011. mTORC1 senses lysosomal amino acids through an inside-out mechanism that requires the vacuolar H+-ATPase. *Science (80-)* **334**:678–683. doi:10.1126/science.1207056

Apendix 1

Increased T antigen									
Protein	**Function**	**Unchanged GS**	**Human ortholog**	**Site**	**T change**	**Tn change**	**# Sites on peptide**	**Peptide sequence**	**Site conservation**
Sli	Cue for migration and differentiation	no	SLIT2	S1908	4x inc.	4x inc.	2	1903-TSAGK**S**SPVAS	no
				S1909	4x inc.	4x inc.	2	1904-SAGKS**S**PVAST	no
26-29kD-proteinase	cysteine-type endopeptidase, proteolysis	no	CTSK	T315	18x inc.	4x inc.	1	310-SGIYN**T**GKPFP	yes
CG14834	unknown	yes	no	T40	not present	5x inc.	3	35-TKPPS**T**LATST	no
				T43	not present	5-9x inc.	3	38-PSTLA**T**STKAS	no
				S44	9x inc.	not changed	3	39-STLAT**S**TKASR	no
				T45	not present	5-9x inc.	3	40-TLATS**T**KASRN	no
Cp1	cysteine-type endopeptidase	no	CTSV	T266	6x inc.	4x inc.	1	261- TDRGF**T**DIPQG	yes
LpR2	LDL receptor, positive regulation of lipid transport	yes	VLDLR	S234	not present	12x inc.	1	233-CKFTE**S**TCSQE	yes
				S274	4x inc.	4-5x inc.	1	269-TSQCR**S**HTCSP	no
				T276	4x inc.	4x inc.	1	271-QCRSH**T**CSPEE	yes
				S278	not present	5x inc.	1	273-RSHTC**S**PEEFAC	no
LpR1	LDL receptor, necrotic clearence from hemolymph	no	VLDLR	T70	5x inc.	4-7x inc.	1	66-FIEA**T**CSSDQ	no
				S73	not present	4x inc.	1	68-EATCS**S**DQFR	yes
Tango1	Golgi organization, protein secretion	yes	CTAGE8	T688	5xdec.	5x inc.	1	683-VALPA**T**ASPVS	no
				S693	6x inc.	5x inc.	2	688-TASPV**S**EVPIK	no
GCS2alpha	hydrolyse activity (O-glycosyl components)	no	GANAB	T175	42x inc., 4x dec.	not changed	1	171-AQEPT**S**HPAEN	yes
				S176	4x dec.	not changed	1	170-KAQEP**T**SHPAE	no
CG9911	protein disulfide isomerase	yes	ERP44	T350	5x inc.	not changed	1	345-HTGKG**T**SPPE	yes

	activity, ER stress			T346	5x inc.	not changed	1	341-EPDPHTGKGTS	no
				S337	4x inc.	not present	1	332-YGPDPSNDIEP	yes
CG10217	wound healing	no	no	T433	4x inc.	not changed	1	428-LGGVTLSPRP	no
Increased Tn antigen without changes in T antigen									
Protein	**Function**	**Unchanged GS**	**Human ortholog**	**Site**	**T change**	**Tn change**	**# Sites on peptide**	**Peptide sequence**	**Conservation of the site**
Scaf	proteolysis, regulation of development	yes	no	T331	not present	20x inc.	1	326-PQIFPTPQPAN	no
Hmu	hydrolase activity on ester bonds, receptor	yes	APMAP	S398	not present	4x inc.	2	393-IGVPPSKATPK	no
				T401	not present	4x inc.	2	396-PPSKATPKPK	no
				T430	not present	4x dec., 29x inc.	1, 2	425-PKPKKTTTPTT	no
				T431	not present	29x inc.	2	426-KPKKTTTPTTP	no
				T436	not present	4-29x inc.	1, 2	431-TTPTTPTPEP	no
				T438	not present	29x inc.	2	433-TPTTPTPEPSK	no
CG14309	hydrolase activity on glycan bonds	yes	HPSE2	T609	not present	6x inc.	1	604-EIPTYTRLPEG	no
Gp93	heat shock protein, unfolded protein binding	yes	HSP90B1	T26	not changed	5x inc.	2	21-DDEAATTETID	no
				T27	not present	5x inc.	2	22-DEAATTETIDL	no
Fon	hemolymph coagulation, metamorphosis	yes	no	T258	not present	8x inc.	1	253-IVEQPTQVTQT	no
				T261	not present	4x inc.	1	256-QPTQVTQTVPV	
Dpy	ECM, transcription factor activity	yes	LTBP1	T11724	not present	4x inc.	2	11719-TNDNTTPSPA	no
				T11725	not present	4xinc.	2	11720-NDNTTPSPAP	no
Hyx	transcription factor binding	no	CDC73	S129	not present	182x inc.	2	124-AEGEPSSVEVA	no

				S130	not present	182x inc.	2	125-EGEPSSVEVAA	no
ImpL1	unknown	yes	no	T310	not present	22-216x inc.	1	305-MPLKDTPTPKP	no
				T312	not present	22-143x inc.	1	307-LKDTPTPKPLE	
CG6409	unknown	yes	no	T46	not present	6x inc.	1	41-VDPKPTAKVVL	no
				T298	not present	10x inc.	1	293-DIPVPTQTKAT	
				T300	not present	21x inc.	2	295-PVPTQTKATTT	
CG7453	unknown	yes	C11orf 24	T183	not present	4x inc.	3	178- TATTKTVNSTI	no
				S186	not present	4x inc.	3	181-TKTVNSTIIAT	no
				T187	not present	4x inc.	3	182-KTVNSTIIATT	no
CG32241	unknown	yes	no	T149	not present	4-6x inc.	2	144-KKVIYTPPPPP	no
				T156	not present	7x inc.	1	151-PPPPPPTKKVVY	
CG12964	unknown	yes	no	Y221	not present	4x inc.	1	216-EEVIQYPVTPL	no
CG15022	unknown	yes	no	S112	not present	6x dec	1	107-LPPKVSLPPPP	no
				S152	not present	18x dec.	1	147-PKVAPSLPPPP	
				S205	not present	21x dec., 4x inc.	1	199-PKVAPSLPPPP	

Decreased Tn antigen without changes in T antigen

Protein	Function	Unchanged GS	Human ortholog	Site	T change	Tn change	# Sites on peptide	Peptide sequence	Conservation of the site
Ndg	cell-matrix adhesion	no	NID1	S656	not present	4x dec.	1	651-PTSEPSPNPSP	no
CG8399	ferric-chelate reductase activity	no	FRRS1	T192	not changed	4x dec.	3	187-APPLPTQSPSA	yes
				T201	not changed	4x dec.	3	196-SAPAGTTR	yes
				T202	not changed	4x dec.	3	197-APAGTTR	no
CG2145	endoribonuclease activity	yes	ENDOU	T84	not changed	6x dec.	1	80-VVVTPTAANKP	no

				S95	not present	6x dec.	1	87-PPLVI**S**HAPLM	no
CG6357	cysteine-type endopeptidase	yes	CTSB	S223	not present	4x dec.	2	218-TIEER**S**SPAPE	no
				S224	not present	4x dec.	2	219-IEERS**S**PAPEI	no
				S26	not present	4-5x dec.	2	20-LGVPV**S**TSSPA	no
				S27	not present	4-5x dec.	2	21-GVPVS**T**SSPAT	no
Neo	regulation of embryonic cell shape	yes	no	T64	not present	4-6x dec.	3	58-PGAKE**T**STEIN	no
				T66	not present	4-6x dec.	3	60-GAKETS**T**EINRT	
				T71	not present	4-6x dec.	3	66-TEINR**T**ERPVE	
CG8420	unknown	no	no	T212	not changed	6x dec.	2	217-GEAKV**T**TEYIH	no
				T213	not changed	6x dec.	2	E218AKVT**T**EYIHN	
CG12213	unknown	yes	RNF214	S299	not changed	5x dec.	1	293-DAPNA**S**VAPK	yes
CG13159	unknown	no	no	T53	not present	4x dec.	5	48-PTYTY**T**TDTTT	no
				T54	not present	4x dec.	5	49-TYTYT**T**DTTTT	
				T56	not present	4x dec.	5	51-TYTTD**T**TTTKP	
				T57	not present	4x dec.	5	52-YTTDT**T**TTKPI	
				T58	not present	4 dec.	5	53-TTDTT**T**TKPIK	
CG12991	unknown	no	no	T218	not present	13x dec.	3	213-AKVLA**T**SPAAA	no
				T225	not present	13x dec.	3	220-PAAAI**T**PRAGG	
				S219	not present	13x dec.	3	214-KVLAT**S**PAAAIT	
CG13722	unknown	yes	no	T265	not present	6x dec.	1	260-YVPPP**T**PTYIP	no
CG15225	unknown	no	no	T74	not present	27x dec.	6	69-VSFPQ**T**TTTTTK	no
				T75	not present	27x dec.	6	70-SFPQT**T**TTTTKK	
				T76	not present	27x dec.	6	71-FPQTT**T**TTTKK	
				T77	not present	27x dec.	6	72-PQTTT**T**TTKKK	

				T78	not present	27x dec.	6	73-QTTTTTTKKKS	
				T79	not present	27x dec.	6	74-TTTTTTKKKSK	
CG1161	unknown	no	TMEM 9	S66	not present	4x dec.	1	61-LAKQVSAPTAA	no
CG12011	unknown	no	no	T301	not changed	4x dec.	1	296-LPNPFTDFPKV	no
CG13992	unknown	no	no	S145	not present	7x dec.	1	140-AFEGGSYPQQP	no
CG32694	unknown	no	no	T179	not present	10x dec.	1	174-KIDLPTFAPQS	no
CG15239	unknown	yes	no	T440	not present	5x dec.	2	435-VAAAVTPATTA	no
				T444	not present	5x dec.	2	439-VTPATTAAADE	
				S451	not present	5x dec.	2	446-AADEDSTTPK	
				T452	not present	5x dec.	2	447-ADEDSTTPK	
Hmu	hydrolase activity on ester bonds, receptor	yes	APMAP	S398	not present	4x inc.	2	393-IGVPPSKATPK	no
				T401	not present	4x inc.	2	396-PPSKATPKPK	no
				T430	not present	4x dec., 29x inc.	1, 2	425-PKPKKTTTPTT	no
				T431	not present	29x inc.	2	426-KPKKTTTPTTP	no
				T436	not present	4-29x inc.	1, 2	431-TTPTTPTPEP	no
				T438	not present	29x inc.	2	433-TPTTPTPEPSK	no
CG15022	unknown	yes	no	S112	not present	6x dec	1	107-LPPKVSLPPPP	no
				S152	not present	18x dec.	1	147-PKVAPSLPPPP	
				S205	not present	21x dec., 4x inc.	1	199-PKVAPSLPPPP	
Gbp1	cytokine	yes	no	T85	not present	4x dec.	2	80-LVNENTTVLPV	no
				T86	not present	4x dec.	2	81-VNENTTVLPVI	
Mgl	regulation of endocytosis, cuticule development	yes	LRP2	Y2864	not present	4x dec.	1	2859-PNYCAYHSCSP	yes
Decreased T antigen									

Protein	Function	Unchanged GS	Human ortholog	Site	T change	Tn change	# Sites on peptide	Peptide sequence	Conservation of the site
CG4670	protein disulfide isomerase	yes	QSOX1	S298	52x dec.	43x dec.	1	294-VHQP**S**ATPA	yes
				T300	12-52x dec.	43x dec.	1	296-QPSA**T**PASKI	yes
Dtg	development (dpp target gene)	yes	no	T326	13x dec.	4-7x dec.	1, 3, 4	321-EAPAK**T**STTAG	no
				S327	4-7x dec.	4-7x dec.	3, 4	322-APAKT**S**TTAGP	
				T328	4x dec.	4-7x dec.	3, 4	323-PAKTS**T**TAGPL	
				T329	8x dec.	7x dec.	1, 4	324-AKTST**T**AGPLV	
				T335	7x dec.	4-9x dec.	4, 1	330-AGPLV**T**VEPTK	
				S341	not present	4x inc.	1	336-VEPTK**S**ITEPN	
				T343	not changed	4x inc.	1	338-PTKSI**T**EPNEE	
				S437	7x dec.	not changed	1	432-SNRQA**S**PTEEP	
				T439	not changed	6x dec.	1	434-RQASP**T**EEPIK	
CG17667	axonogenesis	no	no	S292	not present	11x dec.	1	287-TPFNG**S**LIYPT	no
				T297	not present	4x dec.	1	292-SLIYP**T**EPPLK	
				S312	not present	10x dec.	4	307-PPIVA**S**ITSTA	
				T314	10x dec.	not changed	4	309-IVASI**T**STAKP	
				S315	not changed	10x dec.	4	310-VASIT**S**TAKPV	
				T316	10x dec.	not changed	4	311-ASITS**T**AKPVT	
CG2918	heat-shock protein, chaperone	no	HYOU1	T908	8x dec.	4-8x dec.	2	903-PVDEI**T**PTPAE	no
				T910	not present	4-8x dec.	2	905-DEITP**T**PAEEE	no
CG17660	lung 7TM receptor-like	no	TMEM 87B	S131	6x dec.	not present	1	126-KVVEG**S**AIPTP	yes
				T135	4x dec.	not changed	1	130-GSAIP**T**PEPKH	yes

CG7884	unknown	no	no	T838	5x dec.	not present	1	834-KVYVV**T**PQPRH	no
				T879	not changed	15x dec.	1	876-PRMRP**T**PAGEV	
GCS2beta	N-glycan processing	yes	GLU2B	T321	not changed	7x dec.	2	316-QQPEV**T**TESIQ	no
				T322	not changed	7x dec.	2	317-QPEVT**T**ESIQP	no
				T376	5x dec.	4-7x dec.	1	371-DAEEA**T**PPNYD	no
Put	receptor, dpp signaling	yes	ACVR2B	S129	5x dec.	not changed	2	124-QKYIK**S**TTEAT	no
				T130	5x dec.	5x dec.	2	125-KYIKS**T**TEATT	no
				T131	not changed	5x dec.	2	126-YIKST**T**EATTQ	no
Nplp2	humoral immune response	no	no	T35	5x dec.	not present	1	30-AQEFL**T**KAQGD	no
CG8027	transferase activity	yes	GNPTAB	S492	not present	5x dec.	2	487-DTVEH**S**TLVYER	yes
				T493	5x dec.	not changed	2	488-TVEHS**T**LVYER	yes
CG4194	unknown	no	no	T226	4x dec.	not present	1	221-ATGLA**T**PKPTH	no
CG1273	unknown	yes	no	T1089	4-6x dec.	not changed	1	1084-VHKLV**T**LLPVR	no
Gp150	regulates Notch signaling	yes	LRIG1	T47	not changed	4x dec.	2	42-LPVET**T**TRSPTK	no
				T48	4x dec.	not changed	2	43-LPVETT**T**RSPTKK	no
Sas	receptor activity	yes	no	T1387	4x dec.	not changed	1	1382-PERTI**T**PPPPF	no
Chitin and Chorion Proteins									
Protein	**Function**	**Unchanged GS**	**Human ortholog**	**Site**	**T change**	**Tn change**	**# Sites on peptide**	**Peptide sequence**	**Conservation of the site**
Cpr49Ah	chitin-based cuticule development	yes	no	T113	not present	10x dec.	1	108-GDHIP**T**PPAIP	no
Cpr49Aa	chitin-based cuticule development	no	no	T127	not present	6x dec.	1	122-LAYLA**T**APPPP	no

Cht6	chitinase activity, chitin catabolic process	yes	CHIA	T3542	not present	10x dec.	3	3537-TKAPL**T**FSTSR	no
				T3545	not present	10x dec.	3	3540-PLTFS**T**SRPTA	no
				T3549	not present	10x dec.	3	3544-STSRP**T**AKFVR	no
				T3986	not present	4x inc.	1	3981-TVRLYP**T**IQTEV	no
Verm	chitin deacetylase, cuticle development	no	no	T103	4x inc., 4x dec.	4-5x inc.	1	98-KPILK**T**DEPIC	no
Cp7Fb	chorion-containing eggshell formation	yes	no	T48	4x inc.	8-14x inc.	1	43-LNVPN**T**PKPKK	no
				Y41	4x inc.	not changed	1	36-CPTQLG**Y**QLNVP	
Serp	chitin deacetylase	no	no	T120	5-9x inc.	not changed	1	115-PLLLH**T**DEPLC	no
Cpr67B	chitin-based cuticule development	no	no	T159	not present	4-6x inc.	1	154-LKLPA**T**KTPAV	no
Cpr31A	chitin-based cuticule development	no	no	T325	not present	5x inc.	7	320-PEASS**T**TTTAA	no
				T326	not present	5x inc.	7	321-EASST**T**TTAAP	
				T327	not present	5x inc.	7	322-ASSTT**T**TAAPV	
				T328	not present	5x inc.	7	323-SSTTT**T**AAPVT	
				T333	not present	5x inc.	7	328-TAAPV**T**EENKK	
				S323	not present	5x inc.	7	318-SAPEA**S**STTTT	
				S324	not present	5x inc.	7	319-APEAS**S**TTTTA	